

Structure and Bonding 151

Series Editor: D.M.P. Mingos

Suojiang Zhang · Jianji Wang
Xingmei Lu · Qing Zhou *Editors*

Structures and Interactions of Ionic Liquids



Springer

151

Structure and Bonding

Series Editor:

D.M.P. Mingos, Oxford, United Kingdom

Editorial Board:

F.A. Armstrong, Oxford, United Kingdom

X. Duan, Beijing, China

L.H. Gade, Heidelberg, Germany

K.R. Poeppelmeier, Evanston, IL, USA

G. Parkin, New York, USA

M. Takano, Kyoto, Japan

Aims and Scope

The series *Structure and Bonding* publishes critical reviews on topics of research concerned with chemical structure and bonding. The scope of the series spans the entire Periodic Table and addresses structure and bonding issues associated with all of the elements. It also focuses attention on new and developing areas of modern structural and theoretical chemistry such as nanostructures, molecular electronics, designed molecular solids, surfaces, metal clusters and supramolecular structures. Physical and spectroscopic techniques used to determine, examine and model structures fall within the purview of *Structure and Bonding* to the extent that the focus is on the scientific results obtained and not on specialist information concerning the techniques themselves. Issues associated with the development of bonding models and generalizations that illuminate the reactivity pathways and rates of chemical processes are also relevant.

The individual volumes in the series are thematic. The goal of each volume is to give the reader, whether at a university or in industry, a comprehensive overview of an area where new insights are emerging that are of interest to a larger scientific audience. Thus each review within the volume critically surveys one aspect of that topic and places it within the context of the volume as a whole. The most significant developments of the last 5 to 10 years should be presented using selected examples to illustrate the principles discussed. A description of the physical basis of the experimental techniques that have been used to provide the primary data may also be appropriate, if it has not been covered in detail elsewhere. The coverage need not be exhaustive in data, but should rather be conceptual, concentrating on the new principles being developed that will allow the reader, who is not a specialist in the area covered, to understand the data presented. Discussion of possible future research directions in the area is welcomed.

Review articles for the individual volumes are invited by the volume editors.

In references *Structure and Bonding* is abbreviated *Struct Bond* and is cited as a journal.

Suojiang Zhang • Jianji Wang • Xingmei Lu •
Qing Zhou

Editors

Structures and Interactions of Ionic Liquids

With contributions by

K. Dong • G. Gurau • B. Han • Y. Hu • H. Li • X. Lu •
T. Mu • X. Peng • R.D. Rogers • Hui Wang •
Huiyong Wang • J. Wang • Q. Wang • S. Zhang • Q. Zhou



Springer

Editors

Suojiang Zhang
Beijing Key Laboratory of Ionic
Liquids Clean Process,
Key Laboratory of Green
Process and Engineering,
State Key Laboratory of
Multiphase Complex System
Institute of Process Engineering,
Chinese Academy of Sciences
Beijing
China

Jianji Wang
School of Chemistry and Chemical
Engineering, Key Laboratory of Green
Chemical Media and Reactions,
Ministry of Education
Henan Normal University
Xinxiang
China

Xingmei Lu
Beijing Key Laboratory of Ionic Liquids
Clean Process, Key Laboratory
of Green Process and Engineering
Institute of Process Engineering,
Chinese Academy of Sciences
Beijing
China

Qing Zhou
Beijing Key Laboratory of Ionic Liquids Clean
Process, Key Laboratory of
Green Process and Engineering
Institute of Process Engineering,
Chinese Academy of Sciences
Beijing
China

ISSN 0081-5993

ISSN 1616-8550 (electronic)

ISBN 978-3-642-38618-3

ISBN 978-3-642-38619-0 (eBook)

DOI 10.1007/978-3-642-38619-0

Springer Heidelberg New York Dordrecht London

Library of Congress Control Number: 2013954551

© Springer-Verlag Berlin Heidelberg 2014

This work is subject to copyright. All rights are reserved by the Publisher, whether the whole or part of the material is concerned, specifically the rights of translation, reprinting, reuse of illustrations, recitation, broadcasting, reproduction on microfilms or in any other physical way, and transmission or information storage and retrieval, electronic adaptation, computer software, or by similar or dissimilar methodology now known or hereafter developed. Exempted from this legal reservation are brief excerpts in connection with reviews or scholarly analysis or material supplied specifically for the purpose of being entered and executed on a computer system, for exclusive use by the purchaser of the work. Duplication of this publication or parts thereof is permitted only under the provisions of the Copyright Law of the Publisher's location, in its current version, and permission for use must always be obtained from Springer. Permissions for use may be obtained through RightsLink at the Copyright Clearance Center. Violations are liable to prosecution under the respective Copyright Law.

The use of general descriptive names, registered names, trademarks, service marks, etc. in this publication does not imply, even in the absence of a specific statement, that such names are exempt from the relevant protective laws and regulations and therefore free for general use.

While the advice and information in this book are believed to be true and accurate at the date of publication, neither the authors nor the editors nor the publisher can accept any legal responsibility for any errors or omissions that may be made. The publisher makes no warranty, express or implied, with respect to the material contained herein.

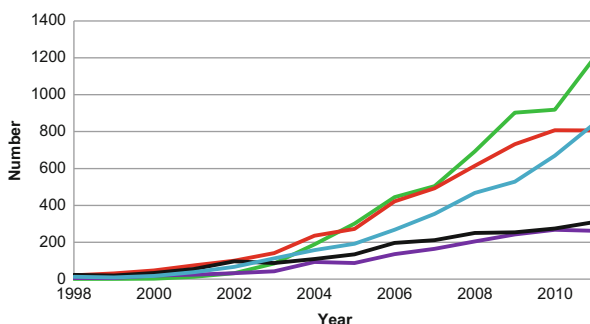
Printed on acid-free paper

Springer is part of Springer Science+Business Media (www.springer.com)

Preface

It is always an honour to be asked to write a Preface to a volume, and doubly so when the editor is so distinguished. Prof. Suojiang Zhang (Institute of Process Engineering, Chinese Academy of Sciences, Beijing) is one of the most respected chemists/chemical engineers in China, and has a long term interest in ionic liquids, having already published a book (Zhang S, Lu X, Zhou Q, Li X, Zhang X, Li S. *Ionic Liquids: Physicochemical Properties*. Elsevier, Amsterdam, 2009) on their physical properties.

Top four regions for producing ionic liquid primary publications (1998–2011). China (*green*), Europe (*red*), Japan (*purple*), USA (*black*), the rest of the world (*light blue*) (M. Deetlefs, M. Faselow and K.R. Seddon, to be published)



In a burgeoning market, with the frequent arrival of new books on ionic liquids (of variable quality), one has to examine the unique features of each volume. Here the answer is clear; the numbers of papers from different regions of the world are illustrated in the figure. In 2000, no papers had ever been published from China on ionic liquids; by 2011, more papers were being published from China than from any other geographical region. This book, with five of the six chapters being authored from within China, gives the rest of the world a chance to see, appreciate, and evaluate the Chinese contribution to this remarkable field, with special emphasis on the structure of ionic liquids and the influence of hydrogen bonding and aggregation

upon their physicochemical properties, thermodynamics, and spectroscopy. This is a book that no practitioner of the science, engineering, and art of ionic liquids should fail to have on their shelves.

A handwritten signature in black ink, appearing to read 'K. Seddon', written over a horizontal line.

Belfast, UK

Kenneth R. Seddon

Contents

Structure, Interaction and Hydrogen Bond	1
Kun Dong, Qian Wang, Xingmei Lu, Qing Zhou, and Suojiang Zhang	
Aggregation in Systems of Ionic Liquids	39
Jianji Wang and Huiyong Wang	
Dissolution of Biomass Using Ionic Liquids	79
Hui Wang, Gabriela Gurau, and Robin D. Rogers	
Structures and Thermodynamic Properties of Ionic Liquids	107
Tiancheng Mu and Buxing Han	
Effect of the Structures of Ionic Liquids on Their Physical Chemical Properties	141
Yufeng Hu and Xiaoming Peng	
Microstructure Study of Ionic Liquids by Spectroscopy	175
Haoran Li	
Index	195

Structure, Interaction and Hydrogen Bond

Kun Dong, Qian Wang, Xingmei Lu, Qing Zhou, and Suojiang Zhang

Abstract Ionic liquids (ILs), as green solvents, have attracted amazing interest and their potential applications have prompted a large amount of research and investment, and some of the results have been inspiring. In recent years, in combination with cations and anions, some new ILs have been synthesized in the laboratory. However, compared with simple solid salts, the structures of ILs are complicated and their properties vary considerably. It is thus very time consuming to explore ILs experimentally when facing the huge number of ionic combinations. A molecular-based understanding can reveal the quantitative correlation between structures and properties, and is thus an important subject in the study of ILs. The unusual complexity of ionic interactions renders molecular-based interpretations difficult and gives rise to controversies about the structure of the ILs. Herein we discuss the ion-pair, cluster and X-ray crystals structures and their relationship with the properties of many typical ILs, especially imidazolium-based. In the ILs, apart from the strong electrostatic forces, non-covalent H-bonds and van der Waals (dispersion, induce forces) are examined and are shown to have a decisive effect on the properties of ILs.

Keywords Ionic liquid • Structure • Interaction • Property • Application

Beijing Key Laboratory of Ionic Liquids Clean Process, Key Laboratory of Green Process and Engineering, State Key Laboratory of Multiphase Complex System, Institute of Process Engineering, Chinese Academy of Sciences, Beijing 100190, PR China.

K. Dong • Q. Wang • X. Lu (✉) • Q. Zhou • S. Zhang (✉)
Institute of Process Engineering, Chinese Academy of Sciences, P.O. Box 353,
Beijing 100190, China
e-mail: sjzhang@home.ipe.ac.cn; xmlu@home.ipe.ac.cn

1 Short Review of Ionic Liquids (ILs)

1.1 Synthesized ILs

Room temperature ionic liquids (RTILs) have been paid close attention by academia and the industries due to their environment-friendly properties, and particularly their potential in green chemistry. It is nearly 100 years since an IL, $[\text{EtNH}_3][\text{NO}_3]$, which has a melting point of 12°C , was first reported in 1914 [1]. Then research on RTILs renewed with the discovery of alkyipyridinium or 1,3-dialkylimidazolium haloaluminate salts by groups at the Air Force Academy in the mid-1970s. These salts were formed by mixing aluminum halides with the corresponding imidazolium or pyridinium halides [2]. Unfortunately, these haloaluminate ILs are highly sensitive to atmospheric moisture. In the 1990s, these salts with imidazolium-based cations incorporated with tetrafluoroborate or hexafluorophosphate anions were stable in the atmosphere and were regarded as a significant milestone in the development of ILs [3, 4]. By careful choice of the combination of these cations and anions it was possible to synthesize a large variety of ILs. Since 2000, more than 6,000 papers related to ILs have been published, with more than 1,000 in 2004, 1,300 in 2005, and nearly 1,900 in 2006 [5].

Non-haloaluminate RTILs share a common general structure of a bulky unsymmetrical “onium” organic cation associated with a weakly coordinating inorganic anion. So far, the most popular cations are 1,3-dialkylimidazolium-, N,N -dialkylpyrrolidinium-, N,N,N,N -tetraalkylammonium-, and N -alkylpyridinium-based. Concerning their anionic counterparts, tetrafluoroborate ($[\text{BF}_4]^-$), hexafluorophosphate ($[\text{PF}_6]^-$), bis(trifluoromethylsulfonyl)amide ($[\text{NTf}_2]^-$), and triflate ($[\text{OTf}]^-$) are the most common. Figure 1 shows some cations and anions commonly used for the preparation of RTILs [6, 7].

RTILs have been attracting interest because of the many unique properties they are supposed to have. RTILs have negligible vapor pressure and are thus nonflammable and nonvolatile, largely decreasing the chance for fugitive emissions. They show high thermal stability, with decomposition temperatures around $300\text{--}500^\circ\text{C}$. They are able to solvate a large variety of organic and inorganic compounds, either polar or nonpolar. They are generally regarded as polar yet noncoordinating solvents. They display a good intrinsic conductivity and are extremely redox-robust. Actually, as a result of the intense research dealing with their physicochemical properties, it has become clear that the above-mentioned properties cannot be considered as generic properties for these media. For instance, it has been shown that many ILs decompose above $80\text{--}90^\circ\text{C}$.

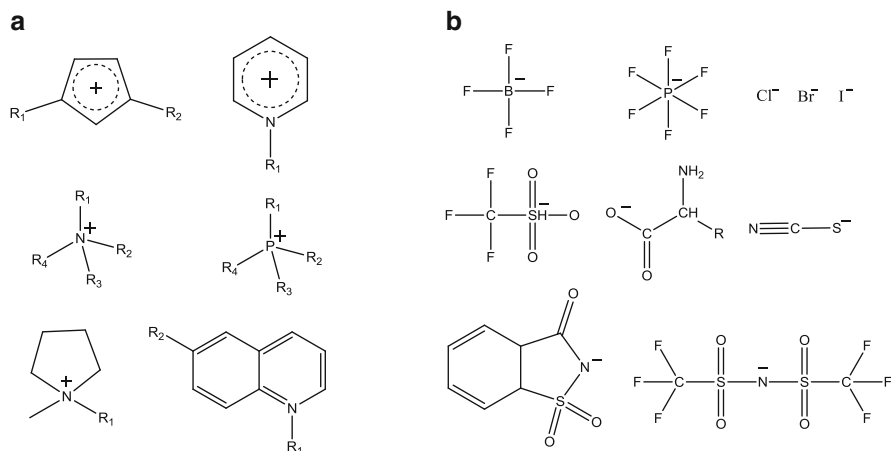


Fig. 1 Cations and anions studied: (a) cations; (b) anions

1.2 Relationship between Properties and Structures of ILs

Melting Points (T_m). Many properties of ILs are special and show prospects for applications. ILs are completely composed of ions, but the unusually low melting points exceed expectations. Melting points of many ILs are lower than 0°C ; even the melting point of [Emim][N(SO₂CF₃)₂] is -16°C [8]. The low melting points are related to the structures and molecular packing of ions. An increase in size, anisotropy, and internal flexibility of the ions should lower the melting point, as shown in Table 1. The symmetry and length of alkyl chain of cations also influence the melting point, and the short *N*-alkyl chains and higher molecular symmetry can frequently increase the melting point. The melting point of [Mmim]Cl IL is 124.5°C and of [Bmim]Cl is 65°C . A simple rule is that cations with short *N*-alkyl chains ($C_n \leq 3$) form crystalline phases with high melting points, and ILs with 4 ~ 10 *N*-alkyl chains exhibit a broad liquid range with low melting points and a remarkable tendency to supercool. When the n in C_n is larger than 10, the salts show a complex phase behavior [10].

Viscosity (η). RTILs are viscous liquids, their viscosities being one to three orders of magnitude higher than those of conventional solvents [11]; obviously that is not very helpful for some applications and it may exert a strong effect on the rate of mass transport within solution and on the conductivity of the salts. The viscosity of the RTILs strongly depends on the nature of the anion [12–14]. ILs containing [NTf₂][−] anion present the lower viscosity, for instance, the viscosity of [Emim][NTf₂] IL is 25 mPa·S as shown in Table 1, but viscosity is higher for RTILs containing [PF₆][−] nonplanar symmetric anions, and the viscosity of [Bmim][PF₆] IL is 308 mPa·S [15]. It has been suggested that the size, shape, and molar mass of the anion contribute to the viscosity with smaller, lighter, and more symmetric anions leading to more viscous RTILs [16]. Additionally, the relative basicity of the

Table 1 Properties of the typical 1-ethyl-3-methylimidazolium-based ILs

Anion	Melting point (°C)	Viscosity (mPa·S)	Conductivity (S·m ⁻¹)	Enthalpy of Vap. (298.15 K, kJ·mol ⁻¹)
Cl ⁻	87			196.1 (363.15 K) [9]
[BF ₄] ⁻	11	37–66.5	1.58–1.38	182.2
[PF ₆] ⁻	62		0.52	189.0
[TfO] ⁻	-9	45	0.86	
[NTf ₂] ⁻	-16	25–34	0.91	135.0

anions and their ability to form H-bonds or to allow van der Waals attractions also have a pronounced effect on viscosity. The fluorinated anions such as [BF₄]⁻, [PF₆]⁻, or [BETI]⁻ form ILs with higher viscosity due to the formation of H-bonds or stronger van der Waals forces, but salts with [N(CN)₂]⁻ and [C(CN)₃]⁻ anions exhibit low viscosity. Compared to anions, cations have secondary effects on the viscosities of ILs. For any of the cation types, increasing the length of alkyl chains results in higher viscosities because of stronger van der Waals interactions between larger cations [17, 18].

Temperature has a remarkable effect on the viscosity of ILs. Okoturo et al. found that the viscosity decreases when the temperature increases. The correlation can be described by the Vogel-Tammann-Fulchers equation:

$$\ln \eta = \ln \eta_{\infty} + \frac{E_{\eta}}{RT} \quad (1)$$

where η_{∞} is the viscosity of infinite high temperature E_{η} is the energetic barrier of ionic motion.

Conductivity (Λ). Conductivity is a property of primary importance and most electrochemical processes are related to the conductivity of the ILs. Being composed of ions, ILs are supposed to be among the most concentrated electrolytes with many charge carriers per unit volume. Some ILs exhibit higher conductivity, and the order of 10 mS·cm⁻¹ can be found in the imidazolium family (Table 1). However, quaternary ammonium ILs exhibit lower conductivity, and the highest conductivity is 2 mS·cm⁻¹, found in *N,N*-dialkylpyrrolidinium bis(trifluoromethylsulfonyl)amide.

As mentioned previously, the high viscosity of RTILs has a major impact on the conductivity because the conductivity is inversely linked to the viscosity [16, 18, 19]. The less viscous [NTf₂]⁻ salts usually exhibit among the highest conductivities [20]. However, quantitative correlations have not been observed between viscosity and conductivity in most ILs. For instance, [Emim][TfO] and [Bmim][NTf₂] display similar viscosities and densities, but the conductivity of [Emim][TfO] is 0.29 mS·cm⁻¹ and [Bmim][NTf₂] is 0.91 mS·cm⁻¹, and their conductivities differ by a factor of 2. Many others factors also influence the conductivity, such as ion size and aggregation, anionic charge delocalization, and correlated ionic motions

[13, 16, 21]. The Nernst-Einstein equation relates the molar conductivity to the self-diffusion coefficients of ions. However, the values predicted by

$$\Lambda = \frac{F^2}{RT} (D_{\text{cation}} + D_{\text{anion}}) \quad (2)$$

are not in good agreement with experimental measurements, and experimental values are smaller than the theoretical values, which can be rationalized by a coupled and clustered aggregation motion of cations and anions in electrically neutral configuration, but the neutral species cannot contribute to the ionic conductivity. On the other hand, increasing the length of the *N*-alkyl chains of cation results in a higher viscosity and a lower conductivity.

Enthalpy of Vaporization (ΔH). An important property of ILs is nonvolatility such that the ILs are green and able to substitute for environmentally contaminating volatile organic chemicals (VOCs). However, Earle et al. [22] found that many RTILs can be distilled and not decomposed at higher temperature and lower pressure. Owing to the strong ionic interactions, the molar enthalpies of vaporization of the ILs are by almost an order of magnitude higher than for typical molecular liquids, as shown in Table 1. The anionic symmetry has the obvious effect on the vaporization of IL, and the ILs with more symmetric anions, Cl^- , $[\text{BF}_4]^-$, and $[\text{PF}_6]^-$, have higher enthalpy of vaporization than $[\text{NTf}_2]^-$ salt. However, these ILs can decompose in the gas phase, for example, $[\text{Emim}]\text{Cl}$ thermally decomposes when heated to 190°C in vacuum. The volatile decomposition products are 1-methylimidazole, 1-ethylimidazole, chloromethane, chloroethane, ethane, and hydrogen chloride species, but the $[\text{NTf}_2]^-$ anionic salts are thermally stable and may be heated to 600 K. Thus most vapor measurements have been carried out on ILs by different methods (isothermogravimetry, Knudsen-type effusion, surface tension, etc.). In such studies it was found that increasing the length of alkyl chains of cation leads to a larger enthalpy of vaporization, the enthalpy values being 135, 155, 173, and $192 \text{ kJ}\cdot\text{mol}^{-1}$ for $[\text{C}_2\text{mim}][\text{NTf}_2]$, $[\text{C}_4\text{mim}][\text{NTf}_2]$, $[\text{C}_6\text{mim}][\text{NTf}_2]$, and $[\text{C}_8\text{mim}][\text{NTf}_2]$, which indicates the long alkyl chain leads to stronger interactions between cations and anions [23, 24].

1.3 *Hydrophilic and Hydrophobic*

The presence of water in ILs can greatly influence the quality of ILs, including viscosity, polarity, and conductivity, and can also influence the solubility of other substance in RTILs. For example, the presence of water in $[\text{Bmim}][\text{PF}_6]$ IL has resulted in the underestimation of the solubility of CO_2 in the ionic liquid [25]. These imidazolium-based ILs present different hydrophilicities. Anions such as halide, pseudo-halide, $[\text{BF}_4]^-$, methyl sulfate, $[\text{NO}_3]^-$, and $[\text{ClO}_4]^-$ are

hydrophilic, which significantly limits their usages, while ionic liquids with anions such as $[\text{PF}_6]^-$, $[\text{SbF}_6]^-$, $[\text{OSO}_2\text{CF}_3]^-$, $[\text{OCOCF}_3]^-$, etc. are hydrophobic and have potential in some industrial applications. However, it is also clear that the commonly called “hydrophobic” ILs are actually hygroscopic and can absorb a certain amount of water from the air [17].

T. Welton et al. have investigated the state of water in many imidazolium-based ILs by ATR and transmission IR spectroscopy [26]. They found that anions are mainly responsible for the solubility of water. In these ILs, the water is not associated together but bound by H-bonds with anions with concentrations of dissolved water in the range $0.2 \pm 0.1 \text{ mol} \cdot \text{dm}^{-3}$. The water molecules at these concentrations exist in symmetric 1:2 type H-bonded complexes: anion...H–O–H...anion. Additional evidence can be seen from Table 2 that the shifts of antisymmetric ν_3 and symmetric ν_1 bands of water molecules in the listed ILs roughly follow the relationship of $\Delta\nu_3 = 1.17\Delta\nu_1 - 0.60$. The strength of H-bonds between the H_2O molecule and anions can be estimated from the wave number shift ($\Delta\nu$) between ν_3 of water in vapor phase and that dissolved in ionic liquids by Eq. 3 [27]:

$$\Delta H = -80(\nu_3^{\text{vapor}} - \nu_3^{\text{IL}}) / \nu_3^{\text{vapor}} \quad (3)$$

(where ΔH is the enthalpy of H-bond, KJ/mol). It can be seen that the different anion can interact with water by the different strength of H-bonds as listed in Table 2. In addition, the water contents absorbed from the open air have a consistent trend with the strength of the H-bonds; for example, the contents of water in $[\text{Bmim}][\text{PF}_6]$, $[\text{Bmim}][\text{BF}_4]$, and $[\text{Bmim}][(\text{CF}_3\text{SO}_3)_2\text{N}]$ increase by the order of 2,640, 19,500, and 33,090 ppm by Karl-Fischer at relative humidity 59 % [26]. It implies that the H-bond play an important role for the solubility of water in ILs.

Although the cation plays a secondary role for the solubility of water in bulk ILs, at the vapor-liquid surface the water mainly interacts with the imidazolium cations. The hydrophobic ILs display a dramatic reorientation at the gas-liquid interface as water contacts the surface. It had been shown by sum frequency generation (SFG) of the C–H stretching mode that C–H groups, especially the C_2 –H group in ring contact with water by C–H...O H-bond interaction, produces a tilting of the cation on the surface. Where the plane of the ring will be, either parallel or perpendicular to the alkyl chain, is dependent on the protonation or methylation of the C_2 position [28, 29].

Generally speaking, the properties presented are important for the application of ILs, especially basic scientific data; however some data are difficult to measure directly. However, the properties of ILs strongly depend on the structures and anion–cation combination styles, and understanding of the structures and the ionic interaction will provide a more convenient way to estimate thermodynamic data prior to practical process design.

Table 2 The shifts of the ν_3 and ν_1 (cm^{-1}) of water in different ionic liquids (with [Bmim]⁺ cation) compared with the corresponding water bands in vapor and the enthalpies of H-bonding [26]

Anion	$\Delta\nu_3$	$\Delta\nu_1$	$-\Delta H$ ($\text{kJ}\cdot\text{mol}^{-1}$)
[PF ₆] [−]	84	62	7.5
[SbF ₆] [−]	93	77	8.3
[BF ₄] [−]	116	97	9.6
[(CF ₃ SO ₂) ₂ N] [−]	119	97	10.5
[ClO ₄] [−]	143	117	12.5
[(CF ₃ SO ₂) ₂ N] [−]	151	113	13.4
[CF ₃ SO ₃] [−]	181	151	15.9
[NO ₃] [−]	236	207	20.1

2 Structures of ILs

In recent years, some new ILs were synthesized in the laboratory, and the number of possible cation and anion combinations has increased significantly such that researchers believe the one trillion RTIL could possibly be prepared [30]. The synthetic problem of being able to design RTILs rationally through variation of the anion and cation still remains to be thoroughly investigated, despite attempts to correlate structures with properties. It is thus essential to develop a systematic method of selectively choosing a given ion pair to be used as a predictive tool in the rational design of new ILs.

A structurally based understanding is a great challenge because the molecular and electronic structure, charge distribution, and orbital overlap of ions, give rise to complex interactions and forces involved in the electrostatic, hydrogen bonds, and van de Waals interactions. Currently there has been substantial growth in the number of theoretical investigations pertaining to ILs, whereby scientists are attempting to predict many of the physical properties and have produced results agreeing with experimental values. Many quantitative correlations have also been established to help predict physic-chemical properties and accelerate the exploration for new ILs [31].

2.1 Dialkylimidazolium-Based Halides ILs

Unlike ionic solid materials, for example NaCl, in which the molecules and ions can be packed close to each other, leading to high lattice energy, the halide anionic ILs are liquid state at ambient temperature, although the strong electrostatic interaction – the bulkiness of both the cation and anion – prevents such packing, thereby lowering the lattice energy.

Halide anionic ILs have already been studied and the anions were found mainly to involve chloride, bromide, and iodide. However, a fatal defect of the class of ILs is their moisture problems in the atmosphere; thus their applications are very limited. In recent years, ILs (1-ethyl-3-methylimidazolium halides ([Emim]X, X = Cl or Br)) have been mixed with the corresponding aluminum(III) halide (AlX₃, X = Cl or Br) to produce the halogenoaluminate ILs, in which the anions

Table 3 Crystallographic data of 1-ethyl-3-methylimidazoium halides ILs [32, 33]

ILs	[Emim]Cl	[Emim]Br	[Emim]I
Chemical formula	C ₆ H ₁₁ ClN ₂	C ₆ H ₁₁ BrN ₂	C ₆ H ₁₁ IN ₂
M	146.62	191.1	238.07
Space group	<i>P2₁2₁2₁</i>	<i>P2₁/c</i>	<i>P2₁/c</i>
Crystal system	Orthorhombic	Monoclinic	Monoclinic
a/nm	1.0087	0.8749	0.8789
b/nm	1.1179	0.7999	0.8130
c/nm	2.8733	1.2662	1.3364
V/nm ³	3.240	0.8332	0.9117
D/g · cm ⁻³	1.204	1.520	1.730

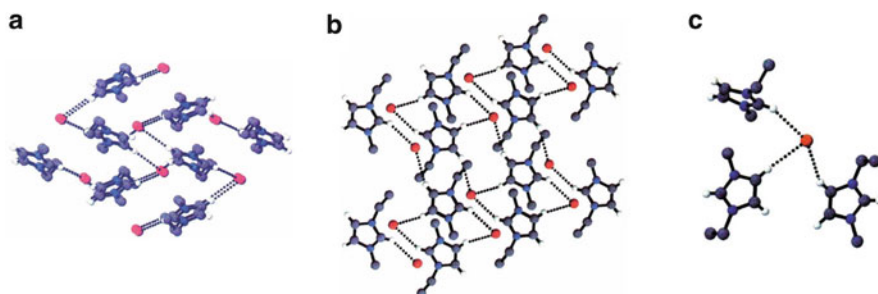


Fig. 2 The packing of ions in solid [Emim]Br (a) and [Emim]I (b), and the local ionic structure (c) [32]. The *dashed lines* showed the H-bonded interactions

exist as $[AlX_4]^-$ and $[Al_2X_7]^-$. Halogenoaluminate(III)-based ionic liquids, which may be used to investigate a wide range of industrially important chemistry, have been of particular interest [32].

The ILs are solid at ambient temperature and their crystallographic data are collected in Table 3. The [Emim]Cl IL is an orthorhombic crystal system, but similar solid structures were found in [Emim]Br and [Emim]I. Starting with the coordinates from the iodide structure, refinement by full-matrix least squares, with non-hydrogen anisotropic atoms and hydrogen isotropic atoms, was used to solve the structure.

Figure 2 shows the packing of ions and local structures in the crystals of [Emim]Br and [Emim]I. The structures consist of different layers of anions and cations which are interconnected by the extensive H-bonds (Fig. 2a, b). Each cation is hydrogen bonded to three anions and each anion is hydrogen bonded to three cations (Fig. 2c). The local structure around the cation is superficially similar to that observed for [Emim]Cl, but the overall morphology of the crystals is somewhat different.

Figure 3 shows the pairwise molecular structures of 1-ethyl-3-methylimidazolium and 1-butyl-3-methylimidazolium halides salts from ab initio calculations with the lowest interactive energies [34]. [Emim]Cl has four different ionic structures (Fig. 3), and the chloride ion with coplanar structures is more stable. Chloride ion, found in the plane of the ring, is associated with the hydrogen of C2 of

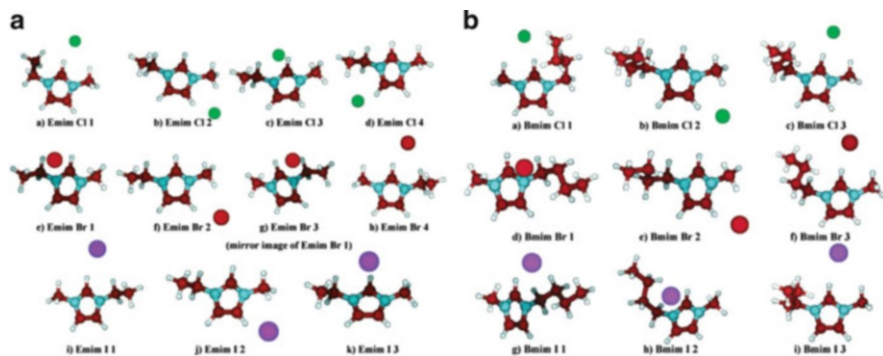


Fig. 3 1-Ethyl-3-methylimidazolium (a) and 1-butyl-3-methylimidazolium (b) halide ion pair structures with lowest interactive energies by ab initio calculations [34]

the ring, positioned closer to the methyl substituent as opposed to the ethyl substituent, which is agreeable with crystal structure. [Emim]Br has three different ionic structures (Fig. 3). The first (Emim Br 1 in Fig. 3) was found to be the most stable structure, and the third (Emim Br 3 in Fig. 3) coalesced with the first at the MP2 levels. Unlike the chloride system, where the chloride was found to be coplanar with the ring, the bromide of the most stable structure was found to be above the ring plane, which was a significant difference with respect to the position of the bromide in the crystal structure and the crystal structure indicates that the bromide resides in the ring plane (Fig. 3). The [Emim]I have two different structures, wherein the anion is within the plane of the ring. The first is the most stable structure (Emim I 1 in Fig. 3), agreeing with the crystal structure. The H-bond distance in the calculated structure (0.285 nm) was found to agree with the literature (0.293 nm).

Gross trends relating interaction energies and melting points were found within the chloride, bromide, and iodide series (see Fig. 4). From the figure it can be seen that the iodide series with the different chain lengths exhibit a “linear” trend, in which the melting points were found to decrease with increasing chain length, and this was associated with a decrease in the magnitude of interaction energy. In the cases of the chloride and bromide anions, the melting points of the [Pmim]⁺ analogue were significantly lower than those of the [Emim]⁺ and [Bmim]⁺ analogues, although the interaction was found to increase in magnitude with increasing alkyl chain length. For the bromides, the structures were different, which introduces some scatter in the results. A trend was also found to exist in the [Bmim]⁺ halide series, where the melting point increase between [Bmim]Cl and [Bmim]Br was associated with an increase in magnitude of the interaction. The melting point was then found to decrease significantly between [Bmim]Br and [Bmim]I, and this was associated with a significant decrease in magnitude of the interaction.

The preliminary investigation of a series of three imidazolium-based cations paired with three halide anions provides some initial hints as to the relationship

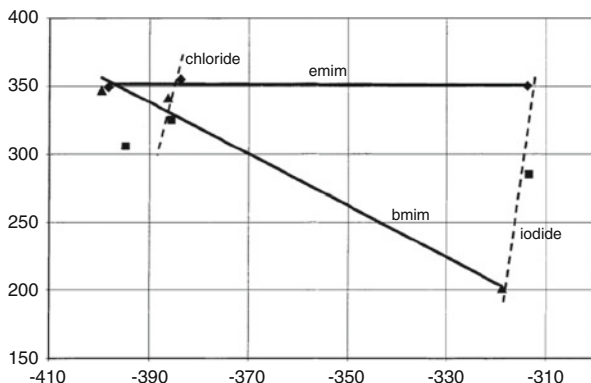


Fig. 4 Correlation between melting points and the binding energies for halide-based ionic liquids: [Emim]⁺ (filled diamonds); [Pmim]⁺ (filled squares); [Bmim]⁺ (filled triangles) [34]

between the interaction energies and the melting points. The result suggests that there is more than one factor contributing to the melting point behavior of ILs. It is possible that for certain systems the melting point is governed more strongly by the cation than the anion and vice versa, with a balance between Coulombic attractions of oppositely charged ions and Van der Waals repulsions of the alkyl chains on the imidazolium cation.

2.2 Fluoro-Anion-Based ILs

The main defect of these halide ILs is that they are very sensitive to the water in air, which prohibits development of further applications. The fluoro-anion ILs (e.g., anion = [BF₄]⁻, [PF₆]⁻, [(FH)_nF]⁻, [AsF₆]⁻, [OCOCF₃]⁻, [OSO₂CF₃]⁻, etc.) are typically air-stable and have a greater potential in many chemical processes.

2.2.1 X-ray Diffraction Single-Crystal Structures

1. ILs with Cations of Different Alkyl Lengths

ILs have shifted the conventional view on ionic molten salts because of their liquid state at room temperature. Coulombic attractive forces in ILs must be diffuse to inhibit or suppress crystallization. Varying the length or degree of branching of the alkyl chains of imidazolium cations can dramatically change their melting points. This has attributed to variations in the rotational freedom of the alkyl chains of the cations and the ability of the cations to pack efficiently (or not) within the crystalline cell. Branching in alkyl substituents can similarly lead to increases in

melting point through restriction of rotational freedom, but can also, conversely, reduce melting points when branching results in enantiomeric mixtures.

Reichert et al. have examined the structure of the solid state imidazonium hexafluorophosphate ([Dmim][PF₆]) ILs with different *N*-alkyl chains by X-ray crystallographic analyses [35]. Figure 5 presents the local structures and ion packing in the crystal structures, in which [PF₆][−] anions contact with imidazolium cation via the H-bonds; however, the length of the *N*-alkyl chains have a remarkable effect on the packing of the ions. When the *N*-alkyl chains are short, $C_n \leq 4$, the [PF₆][−] anions contact not only with the heads (ring) of the cation, but also with the tails (alkyl chains), as shown in Fig. 4a–i. As shown in Fig. 4j–l, [PF₆][−] anions make contact with only the heads of the cation when the chains are longer ($C_n > 4$). From the side views of the cations presented in Fig. 5, it is found that there were several locations of the [PF₆][−] anions above and below the imidazolium heads and in close contact with the C and N atoms of the rings. The direct interactions between the delocalized positive charge of the imidazolium ring and the anion is further indication of the Coulombic nature of ILs based on these ions. Although the electrostatic forces are dominant between cations and anions, the close contacts with a wide angular distribution indicates the C–H...F H-bonded interaction. However, as Reichert et al. said, the H-bonded interactions were weak and more Coulombic in nature. Thus, the interactions that are present in the crystal structures of the short chained salts suggest that the forces responsible for packing in a crystalline lattice are predominantly electrostatic or Coulombic in origin. This also suggests that lattice energies can be described by Eq. 4:

$$U_L = 2I \left[\frac{\alpha}{\sqrt[3]{V}} + \beta \right] \quad (4)$$

I is the ionic strength (=1), V is the molecular volume (in nm³) of the lattice, which is equal to the sum of the individual cation (V_+) and anion (V_-) volumes, and α and β are empirically derived parameters.

2. ILs with different anions

The ILs containing fluoroanions are air-stable, with a consequent greater potential application in chemical processes. Except for the common ILs with [BF₄][−] or [PF₆][−], some other ILs containing fluoroanions have been reviewed in recent papers by Matsumoto and Xue et al. [36, 37]. The melting points of these fluoroanionic ILs are around freezing point, and thus the solid state structures are important to the understanding of the ILs' behavior. Table 4 lists the crystal structural parameters for the fluoro-containing ILs with typical 1-ethyl-3-methylimidazolium ([Emim]⁺) cation.

In the crystal, the [Emim][FHF] is layered and it contains the smallest fluorocomplex anion [FHF][−] in the series. The flat imidazolium rings are stacked and arranged in parallel with the interlayer distance of 3.376 Å. In each layer, very short hydrogen bond distances between the H atom of the cation ring and the F

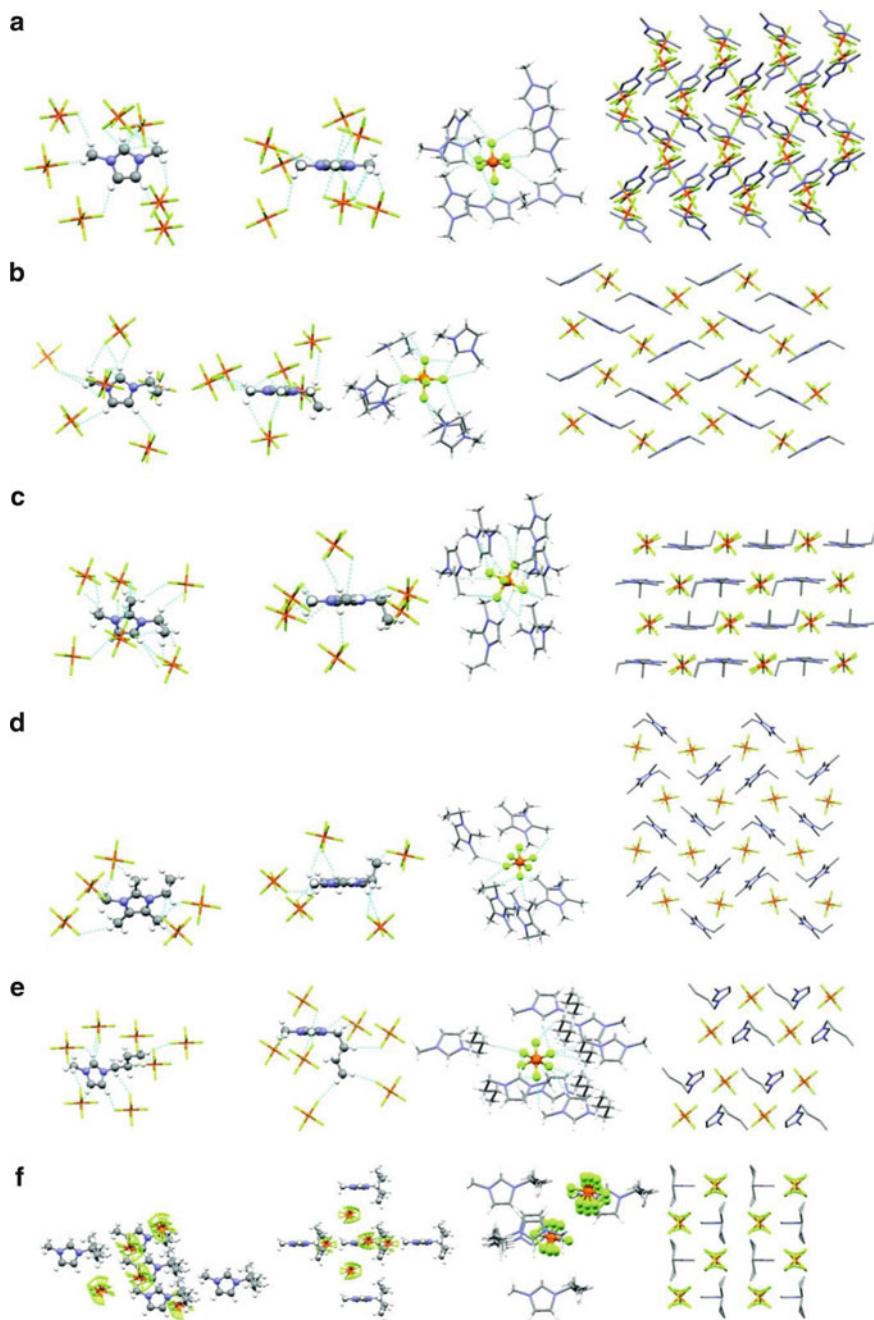


Fig. 5 (continued)

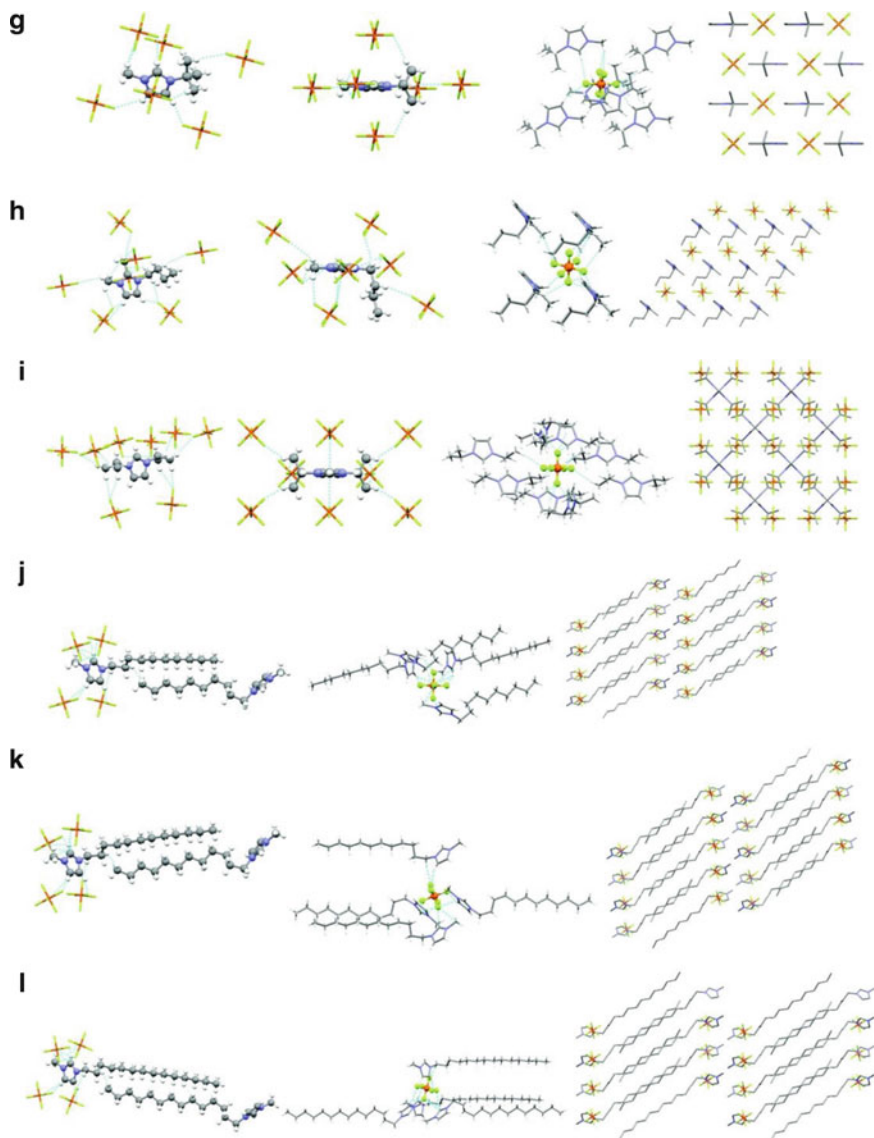


Fig. 5 Local structures and ions packing diagrams of (a) $[C_1mim][PF_6]$, (b) $[C_2mim][PF_6]$, (c) $[C_2dmim][PF_6]$, (d) $[C_2tmim][PF_6]$, (e) $[C_4mim][PF_6]$, (f) $[secC_4mim][PF_6]$, (g) $[terrC_4mim][PF_6]$, (h) $[C_4dmim][PF_6]$, (i) $[isoC_3_2mim][PF_6]$, (j) $[C_{10}mim][PF_6]$, (k) $[C_{12}mim][PF_6]$, and (l) $[C_{14}mim][PF_6]$. The dashed lines show the close contacts and H-bonded interactions [35]

Table 4 Cell parameters and melting points of 1-ethyl-3-methylimidazolium ILs with fluoroanions [36]

ILs	Space group	$V(\text{nm}^3)$	Z	$D(\text{g}\cdot\text{cm}^{-3})$	$T(\text{K})$
[Emim][BF ₄]	$P2_1/c$	0.9068	4	1.450	288
[Emim][FHF]	$P2_1/m$	0.3951	2	1.262	298
[Emim][PF ₆]	$P2_1/c$	1.0920	4	1.558	333
[Emim][AsF ₆]	$P2_1/c$	1.1234	4	1.775	326
[Emim][SbF ₆]	$P2_1/c$	1.1388	4	2.024	283
[Emim][NbF ₆]	$P2_12_12_1$	1.1240	4	1.880	272
[Emim][TFSI]-C ₆ H ₆	$P2_1/n$	1.9896	4	1.567	288

atoms of the anion (1.951, 2.166, and 2.226 Å) are observed [38]. In the [Emim][BF₄] IL, [Emim]⁺ cations form a pillar with the β-carbon of the ethyl group sticking out of the imidazolium-ring plane [39, 40]. The H(methylene)-π interaction sustains the cation–cation interactions with a distance of about 2.86 Å between the H atom in methylene group and the imidazolium ring centroid. [Emim][AsF₆] and [Emim][SbF₆] are isostructural with [Emim][PF₆], whereas [Emim][NbF₆] exhibit a different structure [3, 41]. Figure 6 shows the ion packings in [Emim][AsF₆] and [Emim][NbF₆]. In the [Emim][AsF₆] structure, [Emim]⁺ cations and [AsF₆][−] anions stack alternately along the β-axis to form pillars. On the other hand, in the [Emim][NbF₆] structure, the anion appears in a zigzag arrangement along the α-axis where the nearest fluorine atoms have a distance of 3.441 Å and the cations adopt a pillar-like stacking along the same axis. H-bonds often play an important role in the melting points of ionic compounds. For salts with fluorocomplex anions, in spite of closer H...F contacts in [Emim][NbF₆] than those in [EMIm][PF₆], [EMIm][AsF₆], and [EMIm][SbF₆], the melting points of the former two compounds are much lower than those of the latter three compounds. [Emim][BF₄] also exhibits a low melting point despite relatively strong H-bonds in its lattice. These observations suggest that the strength of hydrogen-bonding is not always a decisive factor in their melting points.

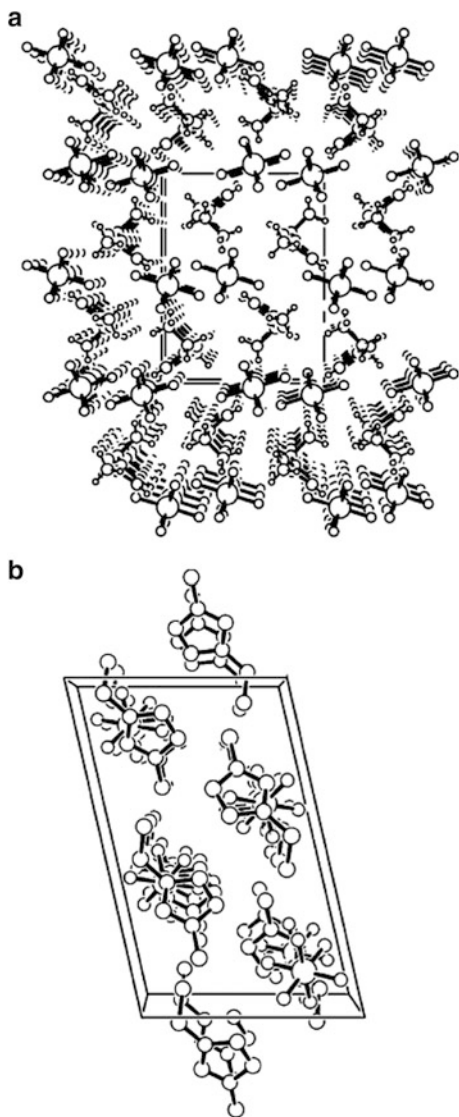
2.2.2 The Structures of Ion Pair and Ion Cluster

1. The Structure of the Ion Pair

It has been verified experimentally that the ions are pairwise in the gas phase [43, 44]. Although in liquid state, the ions are not strictly composed of ion pairs; cations and anions can contact closely due to strong electrostatic attraction. Theoretical calculations have been performed in an attempt to understand the structure of ion pairs and interaction between cation and anion [10, 45].

We have investigated in detail the ion-pair structures of the two typical ILs, [Emim][BF₄] and [Bmim][PF₆], by ab initio DFT calculations [46]. In the [Emim][BF₄] ion pair, [BF₄][−] anion can locate at five positions of cation as shown in Fig. 7. Then the five structures of ethyl-front, methyl-back, back, methyl-front and ethyl-back

Fig. 6 Ions packing in solid
 (a) [Emim][NbF₆] and
 (b) [Emim][AsF₆] ILs [42]



as initial configurations were optimized at B3LYP/6-31++G** theory level. Finally, the three lowest energy geometries were obtained. The [Emim][BF₄](I) was obtained from the ethyl-front, methyl-back, and back configurations, in which [BF₄]⁻ anion moved to the upper part of the ring from the lateral part and located near to the C₂-H group. The [Emim][BF₄](II) was obtained from the methyl-front configuration and [BF₄]⁻ anion also moved to the upper part of the ring. [Emim][BF₄](III) was obtained from the ethyl-back conformer, but [BF₄]⁻ anion did not move and only localized near to the C₅-H group.

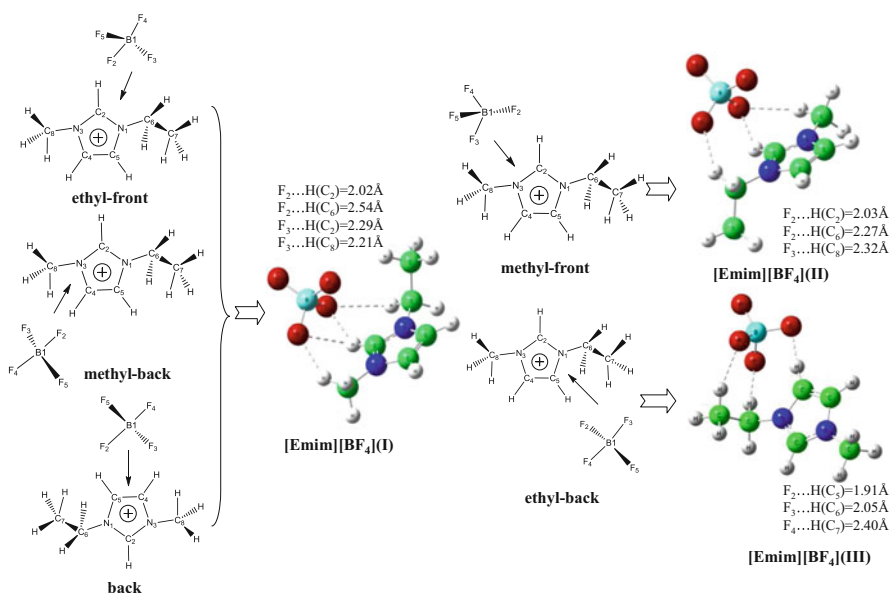


Fig. 7 The optimized structures of [Emim][BF₄] ion-pair when anions are located at five different positions of cation. The *arrows* indicate the initial locations of the anion. The *dashed lines* indicate the H-bonds in these ion pairs

A shallow potential energy well was present when the [BF₄]⁻ anion localized at the back and the methyl-front of imidazolium ring and experienced the minimal electrostatic attraction to the significant stronger electrostatic attraction due to the essential neutral charge distribution on the C_{4/5} atoms and the positive charge on the C₂ atom. However, when localizing at the ethyl back of imidazolium ring as shown in Fig. 7, it is difficult for the [BF₄]⁻ anion to move due to steric exclusion derived from the ethyl side chain and the electron repulsion derived from the π -bond between the C₄ and C₅ atoms.

To date, many researchers have discussed the possible interactions between cation and anion and proposed that H-bonds also widely exist in ILs and represent the most explicit interaction besides electrostatic attraction [47–51]. According to the criterion for forming an H-bond – that the distance between H on donor atom and basic acceptor atom, R_{H...A}, is less than the sum of their respective van der Waals radii – herein the van der Waals distance is 2.670 Å [36]. There are four F...H H-Bonds to form in [Emim][BF₄](I) as drawn by dashed lines in the right of Fig. 4. Two H-bonds form between the F atoms labeled F₂ and H(C₂) atoms of the ring, and H(C₆) atom of the alkyl chain. The distances are 2.02 and 2.54 Å, respectively. The other two occur between the F₃ atom and H(C₂) atom of the ring, and H(C₈) atom of the alkyl chain. The distances are 2.29 and 2.21 Å, respectively. A very similar H-bonded structure can be found in [Emim][BF₄](II), but there is no H-bond between F₃ atom and H(C₂) atom. When [BF₄]⁻ anion locates at the ethyl back of imidazolium ring as [Emim][BF₄](III), shown in Fig. 4,

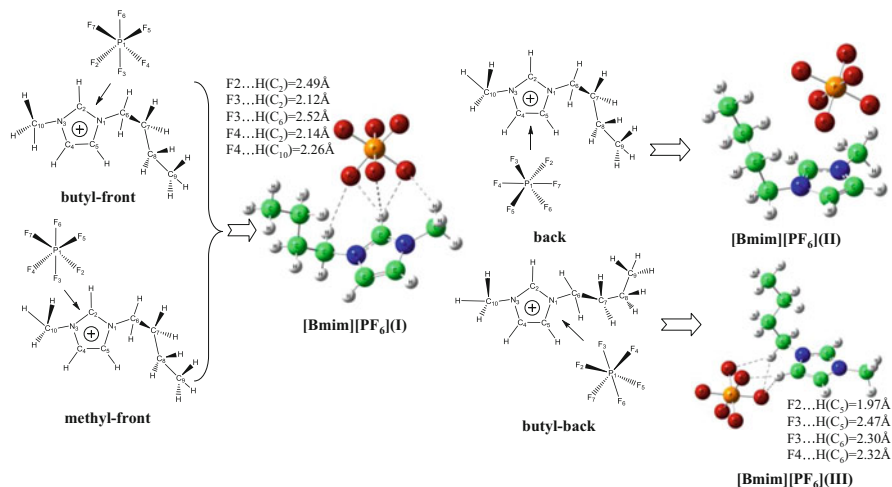


Fig. 8 The optimized structures of [Bmim][PF₆] ion pair with anions located at the five possible different positions around the cation. The *arrows* represent the initial locations. The *dashed lines* indicate the H-bonds in these ion pairs

only two H-bonds form, and one is between the F₂ atom and H(C₂) atom of the ring, and another is between the F₃ atom and H(C₆) atom of the alkyl chain. Their distances are 1.91 and 2.05 Å, respectively.

For the [Bmim][PF₆] ion pair, the similar five initial configurations, butyl-front, methyl-back, back, methyl-front and butyl-back, were optimized at the B3LYP/6-31++G** level. The three lowest energy structures were obtained as shown in Fig. 8. [Bmim][PF₆](I) was obtained from the butyl-front and the methyl-front configurations. [Bmim][PF₆](II) and [Bmim][PF₆](III) were obtained from the back and the butyl-back conformers, respectively. However, no stable point was found at the potential energy surface for the methyl-back configuration. For the back configuration, the [PF₆]⁻ anion moves above the imidazolium ring and the steric exclusion of the long butyl chain is responsible for the location compared with the shorter ethyl chain on the [Emim]⁺ cation.

There are five H-bonds in the [Bmim][PF₆](I) ion-pair. One is between the F atom labeled as F₂ of [PF₆]⁻ anion and the H(C₂) atom of imidazolium ring and the distance is 2.49 Å. Two are between the F₃ atoms and the H(C₂) atom, and the H(C₆) atom of alkyl chain. The distances are 2.12 and 2.52 Å, respectively. The other two are between the F₄ and H(C₂) atoms, and the H(C₁₀) atom of the alkyl chain. The distances are 2.14 and 2.26 Å, respectively. When the [PF₆]⁻ anion locates at butyl-back, there are four H-bonds as [Bmim][PF₆](III) in Fig. 8. One H-bond can form between the F₂ atom and the H(C₅) of ring, and the distance of 1.97 Å is the shortest. The other three are between two F atoms and H(C₅) and H(C₆) of the alkyl chain, and the distances are 2.47, 2.30, and 2.32 Å, respectively. However, when the [PF₆]⁻ anion locates at the back of imidazolium ring, the [PF₆]⁻ anion moves above imidazolium ring to form the [Bmim][PF₆](II) and there is no H-bond to form.

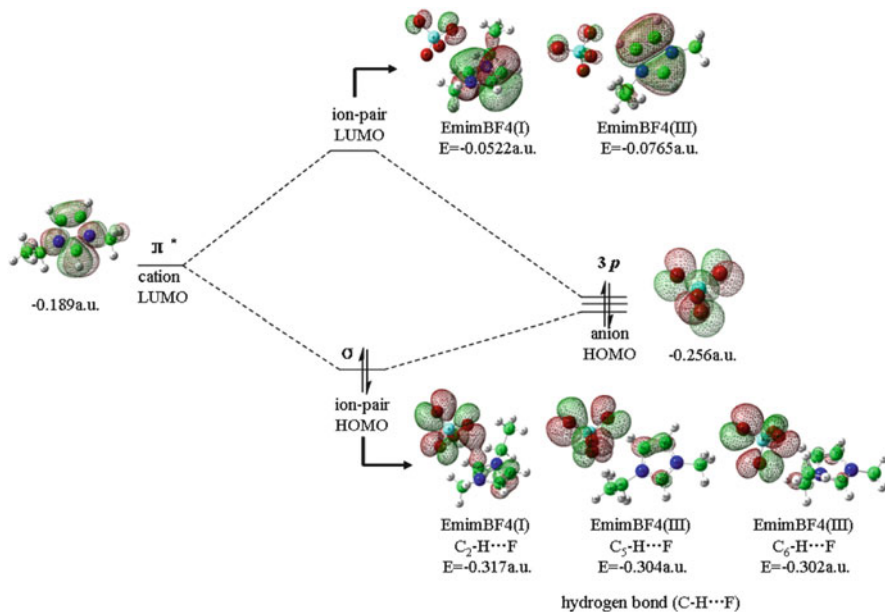
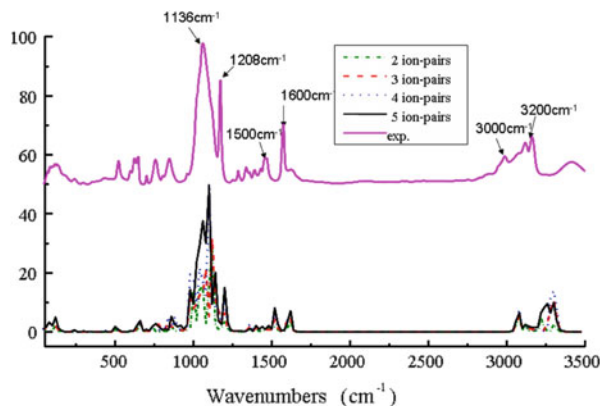


Fig. 9 The orbitals and energies diagram for [Emim][BF₄] ion-pairs. (Due to the same orbital diagram with [Emim][BF₄](I) ion-pair, the [Emim][BF₄](II) ion-pair were not drawn)

2. Understanding the Interaction at Electronic Level

By NBO analysis it was found that in [Emim][BF₄] ion-pairs the occupation on the N₃ orbital always increases, while the occupations on the $\pi_{C2=N1}$ and $\pi_{C4=C5}$ orbitals vary with the positions of anion. In [Emim][BF₄](I) and [Emim][BF₄](II) ion pairs, the occupation on the $\pi_{C2=N1}$ orbital decreases, but on the $\pi_{C4=C5}$ the orbital increases. In [Emim][BF₄](III) ion-pair, the occupation of the $\pi_{C4=C5}$ orbital decreases, and the occupation on the $\pi_{C2=N1}$ orbital exhibits no significant change. Furthermore, the molecular orbitals provide an essential insight into the ion pairs. Figure 9 shows the orbitals and energies for both [Emim][BF₄](I) and [Emim][BF₄](III) ion-pairs. The HOMO of the isolated anion is degradation *p* orbitals (energy $E = -0.256$), and the LUMO of the cation is the anti- π (π^*) bond orbital (energy $E = -0.189$). However, in the ion pairs there are not the expected *p*- π orbital interactions, but the HOMO of the [Emim][BF₄](I) is the highest occupied *p* orbital of anion and the lowest empty $\pi^*_{(C2-H)}$ orbital of cation, and the LUMO of [Emim][BF₄](I) exhibits an anti- σ (σ^*) bond orbital (energy $E = -0.0522$). In the [Emim][BF₄](III) ion pair, the effective orbital overlap also occurs and the HOMO (energy $E = -0.304$) and the degradation HOMO-1 (energy $E = -0.302$) are the highest occupied *p* orbitals of anion and the lowest empty $\sigma^*_{(C5-H)}$ and $\sigma^*_{(C6-H)}$ orbitals of cation. The σ -type interaction rather than *p*- π overlap indicates a covalent bonding feature, but the formation requires a stronger intermolecular attraction. The electrostatic attraction drives anion to approach cation, and finally

Fig. 10 Measured FTIR spectrum of [Emim][BF₄] at room temperature conditions compared to the vibrational modes of the corresponding ion clusters ([Emim][BF₄])_n with n = 2, 3, 4, 5 calculated by DFT at B3LYP/6-31 + G** level (all of the calculated bands were corrected by the factor 0.964–0.967)



locates at the largest positive charge position of the cation. Although the repulsion of the electron between anion and cation increases the total energy, the orbital effective overlap and the partial electrons transfer result in an energetic reduction, and further stabilize the ion pairs.

Obviously from the two classes of ion-pairs with multiple atomic fluoro-anions, we find that more than one H-bonds can form between cation and anion, which is different from ionic liquids with a single atomic anion, like the dialkylimidazolium chloride ([Emim]Cl), and with only one H-bond between cation and anion [45–47].

3. The Structure of Ion Cluster

As reported [52–54], the ions clustering by ionic close contacts reflects the structural arrangement in the bulk phase of RTILs [55]. The clusters may become microscopic models to describe the structures of the bulk ionic liquids or their aqueous solutions. Figure 10 shows an experimental FTIR spectrum of [Emim][BF₄] IL and the calculated IR vibrational frequencies for the ([Emim][BF₄])_n ion clusters with different number, n = 2, 3, 4, 5 at B3LYP/6-31 + G** level. The strong agreement on major bands provided the possibility to explore the detailed structural information of [Emim][BF₄] IL, and these experimental vibrations can also be assigned rationally by the structures of these ion clusters.

The band at 3,000–3,500 cm⁻¹ is assigned to the symmetric stretches of three C–H bonds of the imidazolium ring. Two weaker peaks around 1,600 and 1,500 cm⁻¹ are assigned to the breadths of the rings and the scissors of the alkyl chains, respectively. The peaks around 1,208 cm⁻¹ are assigned to the interplanar wagging vibrations of the C–H bonds on rings. The strongest peak occurs around 1,136 cm⁻¹ and is assigned to the stretches of B–F bonds of [BF₄]⁻ anion, while these weak peaks around 750–880 cm⁻¹ are the out-of-planar wagging vibrations of the rings.

Structural investigation into the clusters has found that the ion arrangements are ordered and similar to the crystal structure shown by X-ray [40, 42]. The structures of clusters are shown in Fig. 11. It was found that these ions are connected by the H-bonds (dashed lines) together to form a three-dimensional network [47]. In the network, the ion packing is influenced very little by the intramolecular bonding

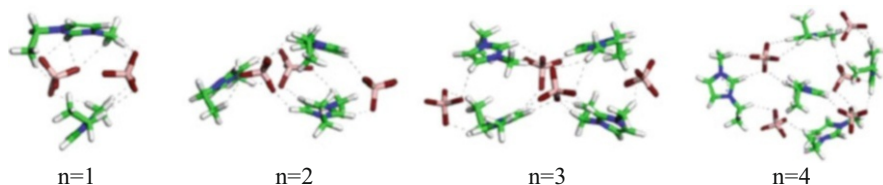


Fig. 11 The ion clusters of $([\text{Emim}][\text{BF}_4])_n$ with $n = 2, 3, 4, 5$ by tube fashion. The *dashed lines* denote the forming H-bonds

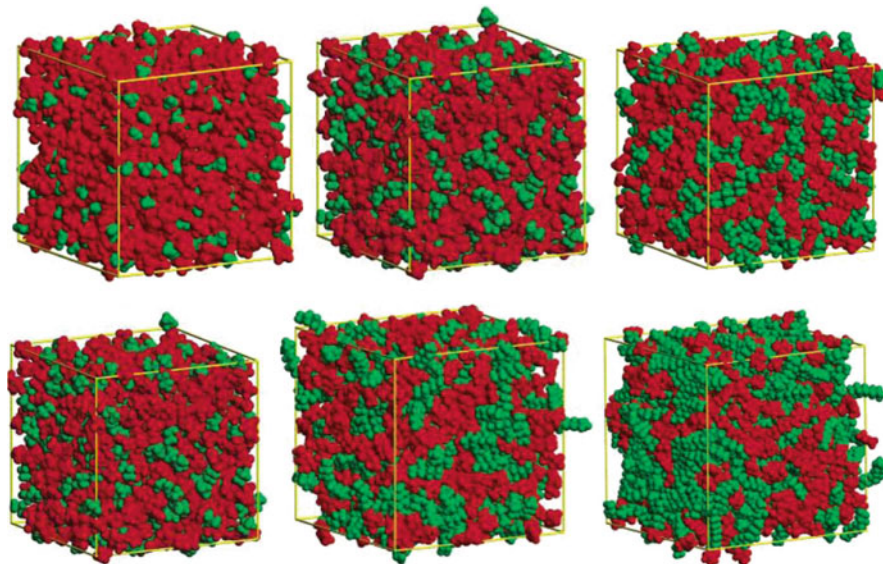


Fig. 12 The nano-clusters observed $[\text{C}_n\text{mim}][\text{PF}_6]$ ($n = 2, 4, 6, 8, 10, 12$) by molecular dynamic simulation [3]

structures, and the imidazolium cations are arranged in alternative layers and the $[\text{BF}_4]^-$ anions are sandwiched between two cations but do not locate above the rings and prefer to be near the C-H groups of rings in the clusters. The cation-cation distance is around 5.10 \AA between H(C_2) atom and the imidazolium ring center. No strong interaction between the ring proton and π -electron cloud of the imidazolium ring is observed and the ethyl groups stick out of the imidazolium ring planes ($\text{C}_2\text{-N}_1\text{-C}_6\text{-C}_7$ torsion angle around 74°). $[\text{BF}_4]^-$ anions form a pillar with a B...B distance of 5.7 \AA in two different anions. Neutron diffraction studies on some RTILs indicated that charge ordering endured in the liquid phase.

Larger nano-clusters have been observed in imidazolium-based ILs with alkyl chain length more than 4. Based small-wide-angle X-ray (SWAXS), Hardacre et al. have found low-Q peaks in $[\text{C}_n\text{mim}][\text{PF}_6]$ ($n = 4, 6, 8$) ILs, which are correlated with the heads (imidazolium rings) of cations and indicate the heads aggregate together [56, 57]. These observations have been supported by molecular dynamic simulation. Figure 12 shows the ion packings of $[\text{C}_n\text{mim}][\text{PF}_6]$ ($n = 2, 4, 6, 8, 10, 12$)

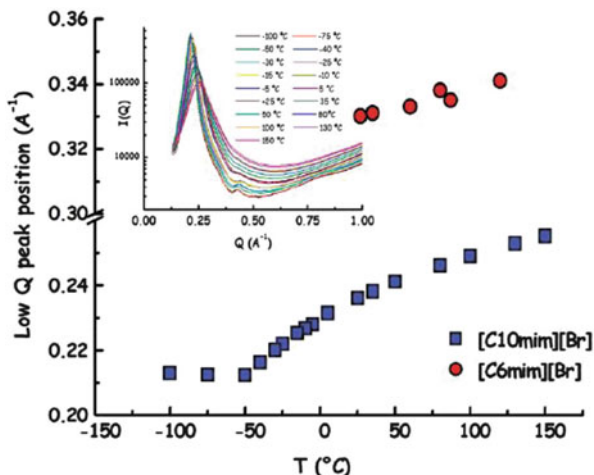


Fig. 13 The changes of low-Q peaks of $[C_6mim]Br$ and $[C_{10}mim]Br$ along with the increasing temperatures from $-100^\circ C$ to $150^\circ C$. The inserted shows the SWAXS Q values at different temperatures

ILs observed by molecular dynamic simulation [58]. It can be seen that the ions do not aggregate when connected with short chains ($n = 2$). When the lengths of the alkyl chains are increased ($n = 4, 6, 8$), the ions start to aggregate, and the polar domains (red color, the charged anions and imidazolium ring parts) and the non-polar domains (green color, the non-charged alkyl chains) are obvious. When the lengths of the alkyl chains were increased to $n = 12$, the aggregation is very obvious, and the larger clusters form. In the clusters, the anions and imidazolium rings aggregate together to form the polar domains by charged attraction, and the non-charged long alkyl chains “twist” together to form non-polar domains.

Except for the structural factors, the nano-clusters can be influenced by the temperature, pressure, and concentration in binary systems. Triolo et al. found that the low-Q peaks decrease with increasing temperatures in solid ILs, but the low-Q peaks increase with increasing temperatures in liquid ILs [59]. Figure 13 shows the low-Q peak curve of the $[C_6mim]Br$ and $[C_{10}mim]Br$ ILs with increasing temperatures [60]. It can be seen that the low-Q peaks of $[C_{10}mim]Br$ decrease with increasing temperatures in the $-100 \sim -50^\circ C$ range, but the low-Q peaks increase linearly with increasing temperature in the $-50 \sim 150^\circ C$ range. Nevertheless, over the complete temperature ranges the low-Q peaks are very low, indicating that the nano-clusters exist throughout, even at a temperature as high as $150^\circ C$, as shown by the Q values obtained at different temperatures. For $[C_6mim]Br$ the situation is not the same. The low-Q peaks increase linearly with temperature, increasing over the $0 \sim 150^\circ C$ range, but the change is not obvious.

In general, the ions in the bulk phase are not randomly packed and the electrostatic force, van der Waals, and H-bonds rationalize the preferable arrangement.

3 Non-covalent Interaction in ILs

3.1 Binding Energy of Ion Pair

S. Zahn et al. compared the binding energies of one [Mmim]Cl with the NaCl ion pair by the symmetry-adapted perturbation theory (SAPT) method, considering different contributions in analogy to a multipole expansion (Fig. 14) [61]. For the NaCl (red diamonds in Fig. 14a) the dispersion term is negligible, whereas this contribution is comparable in magnitude to the induction term for the two conformers of the ionic liquid pair [Mmim]Cl (blue and green diamonds). The total energy of NaCl consists of only electrostatic, exchange, and induction contributions (see Fig. 14b; the curve with red squares almost exactly matches the curve with diamonds). We can make another interesting observation concerning the minima. Whereas the NaCl features the minima for all curves exactly at the equilibrium distance (at zero, see black dotted vertical line), this is, surprisingly, not the case for the [Mmim]Cl pairs (see black arrows). This means that the equilibrium distance is not exclusively determined by the most important attractive force, namely, the electrostatic interaction.

This finding demonstrated that the ions interact in the repulsive region of electrostatic potential only if one considers that the hypothetical potential consists of electrostatic and exchange terms. This implies that ILs are not as ionic as one may naively imagine. Different contributions partly compensate each other, resulting in a very shallow potential energy curve. Consequently the system is highly flexible and liquid like, and is also able to adjust easily to different situations, which might also explain the good solvating properties of ILs.

Table 5 also lists the binding energies of [Emim]⁺-based complexes with different counter-anions. The binding energies follow the trend $[\text{CF}_3\text{CO}_2]^- > [\text{BF}_4]^- > [\text{CF}_3\text{SO}_3]^- > [\text{Tf}_2\text{N}]^- \sim [\text{PF}_6]^-$. However, the experimental properties (melting point, density, self-diffusion coefficient, and molar conductivity) have no defined correlation with these binding energies, which indicates that many properties of RTILs are not determined just by interaction energy.

Melting point is the basic property of ILs and reflects the molecular packing and interactions of cations and anions. A rough correlation of melting points (T_m , K) and binding energies (E , $\text{kJ} \cdot \text{mol}^{-1}$) for dialkylimidazolium chloride, bromide, dialkylimidazolium tetrafluoroborate, and dialkylimidazolium hexafluorophosphate ILs is shown in Fig. 17 [47]. A linear relationship was assumed for these ILs and their melting point decrease when the sizes of the *N*-alkyl side chains increase. Seven species of the Cl^- and Br^- series, except for [Pmim]Br, were correlated and the linear relationship is very pronounced. The melting points range from 300 to 400 K while the interaction energies lie between -375 and $-320 \text{ kJ} \cdot \text{mol}^{-1}$. A similar trend was observed for four species of the $[\text{PF}_6]^-$ series, but the linear relationship is very gross. For four species of $[\text{BF}_4]^-$, the linear relationship between melting points and interaction energies is also pronounced, but the difference between successive melting points is much greater than the difference between successive energies:

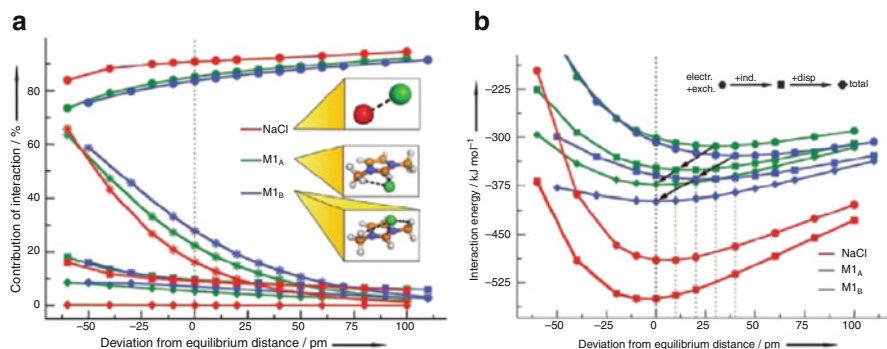


Fig. 14 (a) Contributions of different interactions to the total attractive (electrostatic + induction + dispersion) interaction energy. (b) Plot of the interaction energy versus distance [61]

Table 5 Binding energies and properties of ILs

	E^a	M_p^b	ρ^c	D^d	Λ_{imp}^e	Λ_{NMR}^f	$\Lambda_{imp}/\Lambda_{NMR}^g$
[Emim][CF ₃ CO ₂]	-89.8	-14	1.22	3.23	0.63	1.25	0.51
[Emim][BF ₄]	-85.2	11	1.20	2.72	0.69	1.04	0.66
[Emim][CF ₃ SO ₃]	-82.6	-9	1.30	3.02	0.64	1.10	0.58
[Emim][Tf ₂ N]	-78.8	-15	1.44	4.75	1.10	1.82	0.60
[Emim][PF ₆]	-78.4	62	1.37	1.21	0.31	0.46	0.68
[Py][BF ₄]	-82.8	26	1.44	3.91	0.94	1.44	0.66
[(C ₂ H ₅)(CH ₃) ₃ N][BF ₄]	-84.6	19	1.39	2.34	0.61	0.91	0.67

^aEnergies in kcal/mol

^bMelting points (°C)

^cDensity (g·cm⁻³)

^dSelf-diffusion coefficient (cation + anion) at 298 K (10⁻⁷ cm²·s⁻¹)

^eMolar conductivity obtained from impedance measurement (S·cm²·mol⁻¹) at 298 K

^fMolar conductivity obtained from ion diffusivity measurement by NMR (S·cm²·mol⁻¹) at 298 K

^gRatio of $\Lambda_{imp}/\Lambda_{NMR}$

the melting points are in a range 400–200 K while the interaction energies are between -350 and -340 kJ·mol⁻¹. Therefore, it is indicated that the more atoms the anions include, the more complicated are the interactions between cations and anions.

Molar conductivity is an important property of RTILs for their application as electrolytes for electrochemical devices. S. Tsuzuki et al. [18] reported the measurement of the molar conductivity of RTILs composed of [Bmim]⁺ cation. They found that the molar conductivity obtained from impedance measurement (Λ_{imp}) is smaller than that obtained from ion diffusivity measurement by NMR (Λ_{NMR}). They pointed out that the $\Lambda_{imp}/\Lambda_{NMR}$ value provides useful information on the ionic dissociation/association dynamics in the ionic liquid (Table 6). They reported that the $\Lambda_{imp}/\Lambda_{NMR}$ values of RTILs composed of [Bmim]⁺ follow the order [PF₆]⁻ > [BF₄]⁻ > [Tf₂N]⁻ > [CF₃SO₃]⁻ > [CF₃CO₂]⁻. A small $\Lambda_{imp}/\Lambda_{NMR}$ value shows that an ion prefers to move with a counterion. $\Lambda_{imp}/\Lambda_{NMR}$ is an important parameter

Table 6 Experimental spectroscopic studies on interactions and H-bonds in some typical ILs

Ionic liquid ^a	Spectra	H-Bond ^b	HBDA(α) ^c [65–67]	ΔE^d [18, 47]	Mp ^e	Td ^f
[Dim]Cl	X-Ray, IR[68],NMR [69],Neutron[70]	C–H···Cl(Br, I)	0.44 ^g	378.03	84	285
[Dim][BF ₄]	X-Ray, IR[71]	C–H···F	0.61	356.47	11	412
[Dim][PF ₆]	X-Ray[72], Neutron [70, 73],IR	C–H···F	0.64	319.00	10	375
[Dim] [OSO ₂ CF ₃]	X-Ray[74], NMR[13], IR[75]	C–H···O, C–H···F	0.60	345.60	–9	140
[Dim] [OCOFCF ₃]	X-Ray, NMR[13]	C–H···O, C–H···F	0.56	375.72	–14	150
[Dim][Tf ₂ N]	X-Ray[76], THz, IR [77], Neutron	C–H···N, C–H···F, C–H···O	0.66	313.60	–15	455
[Pyr][Tf ₂ N]	X-Ray, Raman[78]	–	0.48	–	26	–
[(C ₄ H ₉) (CH ₃) ₃ N] [Tf ₂ N]		–	0.47	–	19	–

^a[Dim]⁺ represents the 1,3-dialkylimidazolium cation, [Pyr]⁺ represents the pyridinium cation

^bPossible H-bonds between cation and anion in crystal and liquid phase

^cH-bonded donation abilities (only for [Bmim]⁺ cation)

^dAverage binding energies were calculated by the DFT and MP₂ methods (only for [Emim]⁺ cation)

^eMelting points (°C)

^fMeasured thermal decomposed temperature (°C) (for [Emim]⁺ cation)

^gMeasured in supercooled state

for designing highly conductive ionic liquids. The RTILs composed of round-shaped anions ([PF₆][–] and [BF₄][–]) have larger $\Lambda_{\text{imp}}/\Lambda_{\text{NMR}}$ values than those composed of the other rod-shaped anions. The round-shaped anions dissociate and associate with cations more easily in the RTILs. The interaction energy of the [Emim]⁺ complex with [PF₆][–] anion (–78.4 kcal · mol^{–1}) is smaller than that of the [BF₄][–] complex (–85.2 kcal · mol^{–1}). The [BF₄][–] binds with [Emim]⁺ more strongly than the [PF₆][–], which well explains the smaller $\Lambda_{\text{imp}}/\Lambda_{\text{NMR}}$ value for [Bmim][BF₄] than that for [Bmim][PF₆]. The interaction energy of complexes with [Tf₂N][–], [CF₃SO₃][–], and [CF₃CO₂][–] are –78.8, –82.6, and –89.8 kcal · mol^{–1}, respectively. The order of $\Lambda_{\text{imp}}/\Lambda_{\text{NMR}}$ of three RTILs composed of [Bmim]⁺ and the rod-shaped anions coincides with the reverse order of the magnitudes of the interaction energies of the [Emim]⁺ complexes.

Comparison of the calculated interaction energies of the ion pairs and experimental $\Lambda_{\text{imp}}/\Lambda_{\text{NMR}}$ values of RTILs suggests that three factors play important roles in determining the $\Lambda_{\text{imp}}/\Lambda_{\text{NMR}}$ value: (1) RTILs have large $\Lambda_{\text{imp}}/\Lambda_{\text{NMR}}$ values if the interaction between cation and anion is small; (2) RTILs that consist of round-shaped ions have large $\Lambda_{\text{imp}}/\Lambda_{\text{NMR}}$ values – probably the round shape of the ions enables a high mobility of the ions in RTILs; (3) RTILs have large $\Lambda_{\text{imp}}/\Lambda_{\text{NMR}}$ values if the orientation dependence of the interaction is small. A large anisotropy of the interaction would probably decrease the mobility of the ions.

3.2 Hydrogen Bonds

3.2.1 Structural Characteristic of H-Bonds

The particular resonance structure and high π electronic delocalization of the imidazolium cation result in large positive charges on the C₂-H, C₄-H and C₅-H groups that are the main interactive positions with anion [45, 62]. As discussed previously, H-bonds are explicit non-covalent interactions in ILs, but are not the same with different anions. For the anions with one atom, like the [Emim]Cl ion pair as shown in Fig. 15a, only one C-H...Cl H-bond forms between cation and anion. For anions with multiple atoms, like [Emim][BF₄] in Fig. 15b, more than one C-H...F H-bond forms between cation and anion [47].

The electronic structure investigation found that the HOMO of Cl⁻ can interact with the LUMO of the cation to form a σ -type orbital overlap such that the Cl⁻ anion can localize near to the C₂-H group as shown in the [Emim]Cl ion pair [47, 63]. A similar σ -type orbital overlap can also be found in the [Emim][BF₄] ion pair. Therefore the orbital overlap results in the significant energy reduction, further rationalizing the preferable location of the anion.

3.2.2 Evidence of H-Bonds in ILs

Many ILs have been studied by experimental spectroscopy (IR, Raman, NMR, neutron scattering, etc.) and results have indicated that the ions can array orderly over a larger range of temperatures [36]. The earliest X-ray studies found that there existed a discrete H-bond in halide-based ILs (anions = Cl⁻, Br⁻, and I⁻) [64]. The evidence from X-ray and IR spectra from [Emim]Cl IL have demonstrated unambiguously that the H-bond not only exists but the is also most explicit interaction between the ions (Table 6). The Cl⁻ anions are located with the cation by H-bonds rather than at random.

For the fluoro-anion-based ILs (e.g., anion = [BF₄]⁻, [PF₆]⁻, [(FH)_nF]⁻, [AsF₆]⁻, [OCOCF₃]⁻, [OSO₂CF₃]⁻, etc.), X-ray studies have indicated that F atoms of the anions can form C-H...F H-bonds with the imidazolium cation, in particular C-H₂, C-H₄ and C-H₅ groups on the ring as listed in Table 6 [36]. NMR studies have also provided structural depictions for [Mmim][PF₆] IL [72], in which the asymmetric unit contains one ion-pair, and the imidazolium cations form a weakly C-H... π hydrogen-bonded zigzag chain along the (0 0 1) direction. The [PF₆]⁻ anions are located between these chains and make closest contacts with the hydrogen atoms of the cation. The liquid phase of the [Dim][PF₆] shows a similar structure to the crystal state by neutron diffraction [79].

In crystal structures of dialkylimidazolium salts containing [OSO₂CF₃]⁻ or [OCOCF₃]⁻ anions, for example [Bmim][OSO₂CF₃] IL, the imidazolium ring and the -SO₃ group of the anion are connected by the C-H...O H-bonds to form a two-dimensional NaCl-like arrangement in each layer, and the butyl chain of the

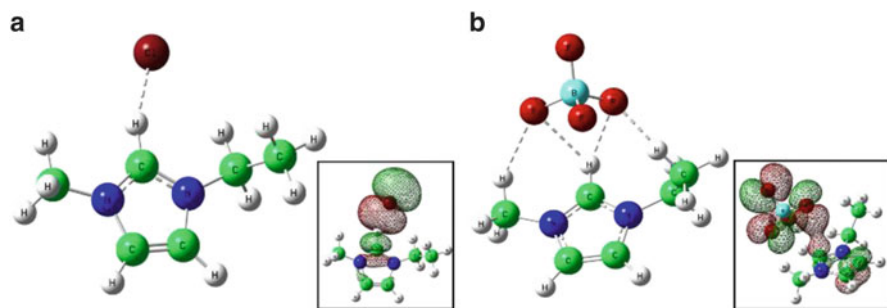


Fig. 15 The H-bond denoted by a *dashed line* in imidazolium-based ionic liquids. (a) The optimized geometry and molecular orbital of [Emim]Cl ion pair by DFT method. (b) The optimized geometry and molecular orbital of [Emim][BF₄] ion pair

cation and the -CF₃ group of the anion protrude out of the layer in the same direction. Therefore, this structure contains a layer of butyl and -CF₃ groups sandwiched between the two layers. In the liquid state this more ordered structure is not obvious, but except for the C-H...O H-bonds between the cation and the -SO₃ group of the anion, the -CF₃ group of the anion can connect with the other cation by C-H...F H-bonds [39]. For [Dim][Tf₂N] ILs, both crystallographically distinct [Tf₂N]⁻ anions adopt a *cis*-conformation [80]. The crystal lattice of [Dim][Tf₂N] consists of alternating two-dimensional sheets with an -AA-B-AA-pattern.

Neutron diffraction studies on some RTILs have indicated that charge ordering endures in the liquid phase. In the [Mmim]Cl and [Mmim][PF₆] salts, the molecular packing in the first two or three solvation shells are similar both in the crystal and in the liquid, although the atomic distances are altered in the liquid [70, 73]. In comparison, the [Mmim][Tf₂N] salt showed smaller charge ordering [79] because of the diffuse charge density and larger size of the [Tf₂N]⁻ anion. Moreover, its liquid structure is poorly correlated to its crystal structure [80]. This was attributed to the conformational flexibility of the [Tf₂N]⁻ anion [79, 80]. Nevertheless, it remains clear that ILs form “quasimolecular” structures through three-dimensional H-bonded networks. The network is maintained to a great extent even in solutions having low dielectric media, making the RTILs highly organized media.

Further evidences have demonstrated that by substituting a hydrogen atom for a -CH₃ group, which is incapable of H-bond formation, the bands associated with stretches or bends of H-bonds disappear completely. R. Ludwig et al. [48, 76, 77] had demonstrated that the bands that relate to H-bonds disappeared in [Emim][Tf₂N] IL when the proton atoms on the imidazolium-ring were replaced by -CH₃ groups. With the increased abilities and strengths of H-bonds, the [Tf₂N]⁻ anion was found in the *cis* conformation. Switching off these local interactions leads to the energetically favored *trans* conformation. These structural effects caused by H-bonds should have significant influence on IL properties, such as melting points and viscosities, as discussed later. Moreover, the vibrational frequencies of H-bonds themselves can be observed directly by far-IR spectrum even for the

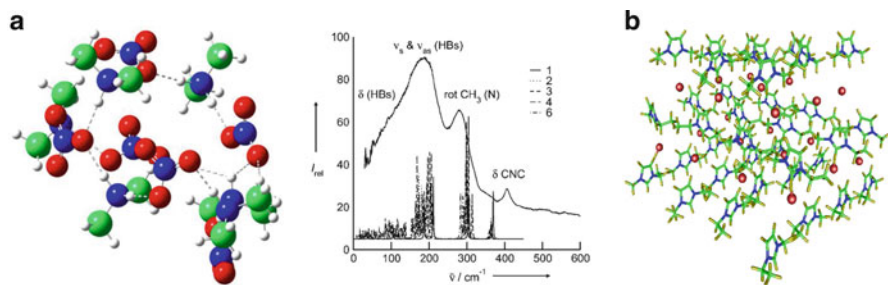


Fig. 16 The ion clusters and the local H-bonded network in ILs. (a) The ion cluster of dimethylammonium nitrate (DMAN) and the measured low-frequency vibrational FTIR spectrum of at 353 K compared to the vibrational modes of the corresponding PIL clusters $[(DMA)(NO_3)]_x$ with $x = 1, 2, 3, 4,$ and 6 calculated by DFT at the B3LYP/6-31 + G* level of theory [77]. (b) Schematic representation of H-bond network IN [Emim]Cl IL. All of the H-bonds were denoted by *dashed lines* [85]

complicated [Dmim][Tf₂N] IL as listed in Table 6. Wavenumbers above 150 cm^{-1} were assigned to intramolecular bending modes of cations and anions in the ILs, and the wavenumbers below 150 cm^{-1} were assigned to the bending and stretching vibrational modes of H-bonds [81].

The solvent properties of these ILs have also been investigated using chromatographic techniques [82, 83]. It is generally found that the ILs may be considered to be polar phases with the solvent properties being largely determined by the ability of the salt to act as an H-bond donor and/or acceptor. Table 1 lists the H-bonded donation abilities (HBDA, α) to denote qualitatively the acidity of ionic liquids. The α of the pyridinium-based and the quaternary amino ILs are obviously smaller than that of the imidazolium cation, which indicates that the interactions of H-bonds are not remarkable in these ILs.

3.2.3 Local H-Bonded Network

As previously described, involved in the interactions of many ions in bulk ILs, the forming H-bonds can be extended to form a three-dimensional network as in liquid water [84]. The network can even be observed on a smaller nanometer scale domain or in an ionic cluster in which non-homogeneity of local structure is found in ionic liquids. A network of ammonium nitrate IL (ANILs) is shown in Fig. 16, in which cations and anions are connected together by H-bonds (O atom as acceptor on anion and N–H as donor on cation) [48].

Crystallographic studies had also found that the H-bonded networks exist below melting points or at glass state temperatures in many ILs [35, 36, 86]. A remarkable three-dimensional H-bonded network of the [Emim]Cl [86] from X-ray and DFT calculations is shown in Fig. 16b, in which the asymmetric unit contains four $Emim^+ \dots Cl^-$ ion pairs. The $[Emim]^+$ ions cluster in four distinct layers

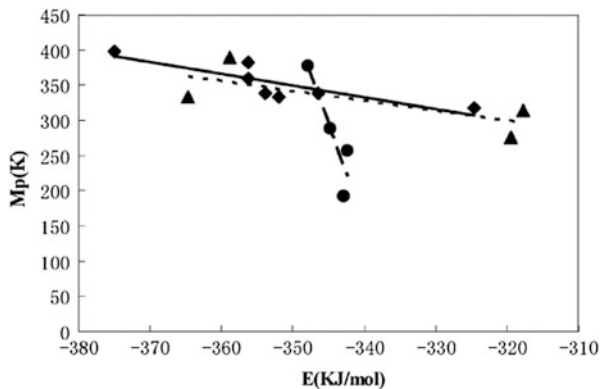


Fig. 17 The correlation of melting points and interaction energies for dialkylimidazolium ionic liquids: Cl and Br salts series (*filled triangles*); [BF₄] salts series (*filled circles*); and [PF₆] salts series (*filled diamonds*) [62]

perpendicular to the c axis. Similarly, the arrangement of Cl⁻ anions is a layered one. Each Cl⁻ interacts with three Emim⁺ cations and each [Emim]⁺ is associated with the three nearest Cl⁻ ions. The distance from Cl⁻ to a ring carbon atom averages 3.55 Å. The Cl⁻ anions are situated in H-bonded positions rather than randomly. In the [Bmim][PF₆] IL, the cations form an H-bonded zigzag chain motif via methyl hydrogen atoms and π -electrons, and [PF₆]⁻ anions are located between these chains with closest contacts with the methyl hydrogen atoms. Such connection results in the formation of an H-bonded network [72, 87].

Furthermore, molecular dynamical calculations have proved that ions clusters, when viewed over the course of a typical simulation (generally several nanoseconds), remain locked in a local place and the *cations* and *anions* cease to behave as discrete units but act rather as larger supermolecules, H-bonds being responsible for the spatial heterogeneity [52, 88, 89]. Experimental optical Kerr effect spectroscopy [90] also demonstrated the occurrence of heterogeneous domains in 1,3-dialkyl imidazolium salts. The translational and rotational motion of these larger units and their interactions with neighboring molecules explain the high experimental viscosities [91].

4 Effect of Structure on Application of ILs

4.1 Extraction and Separation

Some ILs have been used as solvents in separation processes due to their recovery and recycling properties. Rogers et al. [92] have reported the partition of substituted-benzene derivatives between water and the hydrophobic [Bmim][PF₆]. Their studies

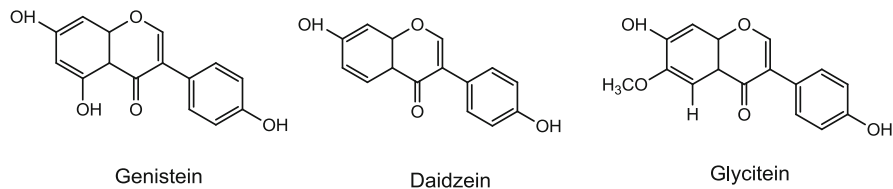


Fig. 18 Soybean isoflavone aglycone homologues

have included the removal of sulfides [93] and nitrides [94] from diesel and gasoline, the separation of aromatics from aliphatics [95], and the removal of pollutants (e.g., phenols, dyes, organic acids) from water, and they have demonstrated the abilities of ILs [94, 96, 97].

Some natural bioactive homologues with high structural similarity have been effectively separated by ILs. Cao et al. [97] have shown that ILs can be used to separate the soybean isoflavone aglycones, known as genistein, daidzein, and glycitein, as shown in Fig. 18. Furthermore, we investigated the interactive mechanism and found that ILs can form H-bonds with the homologues, but the magnitudes of interactions decrease in the order genistein > daidzein > glycitein, which was consistent with the distribution coefficients [98].

Another example is to separate the α -tocopherol from the four tocopherol homologues. The four homologues have different H-bonded acidities resulting from their structural differences in the number and position of methyl groups on the chromanol head. [Bmim]Cl, [Bmim][CF₃SO₃], and [Bmim][BF₄] ILs can extract α -tocopherol successfully from biphasic material in the order [Bmim][BF₄] < [Bmim][CF₃SO₃] < [Bmim]Cl under the same conditions [96]. This order is consistent with the that of these ILs' hydrogen-bond basicity strength [99]. This phenomenon further disclosed that the selectivity was based on the hydrogen-bonding interaction between ILs' anion and the -OH group on the tocopherols.

4.2 Dissolution of Cellulose

Biocompatible composites generated from renewable biomasses are regarded as promising materials that could replace traditional polymers and reduce global dependence on fossil fuels [100–102]. Rogers et al. applied ILs as green solvents to dissolving cellulose, which has opened up a new area for application of ILs in bio-energy [103]. The experiments have proved that many ILs, such as [Bmim]Cl, [Amim]Cl, [Emim]Cl, [BMPy]Cl, [Bmim][OAc], [Amim][OAc], [Emim][OAc], [Emim][XS], and [N₁₁₁C₂H₄OH][OAc], can effectively dissolve the biomass from wood, bagasse, wool, silk, chitin, etc. [100, 103–106]. Experiments and calculations have both proved that the formation of H-bonds between ILs and biomolecules play crucial roles in the dissolving process [107–109]. By means of ¹³C and ^{35/37}Cl NMR relaxation measurements, R. C. Remsing et al. demonstrated

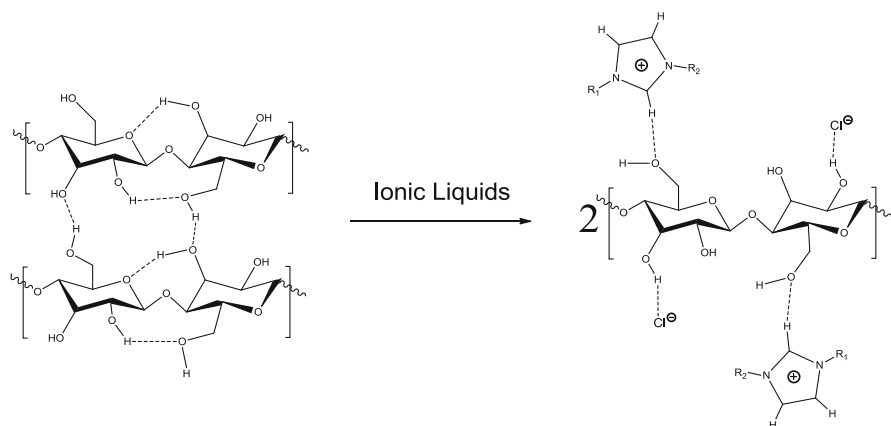


Fig. 19 A proposed mechanism of dissolution of cellulose in ionic liquids. *Dashed lines* show the hydrogen bonds

conclusively that the solvation of carbohydrates by $[\text{C}_4\text{mim}]\text{Cl}$ involves stoichiometric H-bonding between the hydroxyl protons of the cellulose and the chloride ions of the IL. There may be two steps for the dissolution; the first is to break the H-bonds between anions and cations, then the active chloride anions interact with the hydroxyl groups of cellulose by forming H-bonds. It is also thought that $[\text{C}_4\text{mim}]^+$ cations may possibly form H-bonds with cellulose and play a non-negligible role in the dissolution process.

Figure 19 showed the proposed dissolution mechanism of cellulose in ILs, and how the oxygen atoms and hydrogen atoms of the $-\text{OH}$ groups on cellulose form electron donor-acceptor complexes. The anion can combine with hydrogen atoms of cellulose by H-bonds, whilst the imidazolium cation interacts with the oxygen atoms by hydrogen bonding. Comparing with water, we found that the binding energies of the H-bonds between cellulose and ILs are three times stronger than that between cellulose and water, indicating that cellulose is more easily dissolved in $[\text{Emim}][\text{OAc}]$ [109]. The presence of water in the IL was shown to decrease significantly the solubility of cellulose, presumably through competitive hydrogen-bonding to the cellulose microfibrils which inhibits solubilization. This phenomenon can also corroborate that hydrogen bonding is a key interaction in the dissolving process of cellulose in ILs.

The increasing basicity of the anion resulting in the higher solubility of biomass is also in agreement with the H-bonding mechanism. C. S. Pereira recently reported that a class of biocompatible and biodegradable cholinium-based ILs, the cholinium alkanooates, showed a highly efficient and specific dissolution of the suberin domains from cork biopolymers. They found that the cholinium alkanooates of increasing alkyl chain length (ethanoate, butanoate, hexanoate) showed augmented dissolution efficiency since the basicity of the anion increases with chain length [110]. It indicates clearly that the H-bond basicity of the solvent system is essential for the dissolution of cellulose.

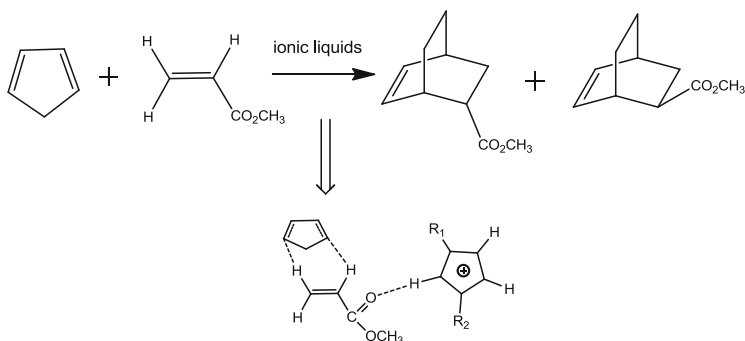


Fig. 20 Diels–Alder reaction by ILs catalysis and the H-bonds (Lewis acid) between imidazolium cation with the carbonyl oxygen of methyl acrylate

4.3 As Catalyst

Diels-Alder cycloaddition reactions have been explored using various ILs substituting for water. The reaction of cyclopentadiene with methyl acrylate and methyl vinyl ketone in IL is shown in Fig. 20 [111]. The studies have found that many ILs can influence the selectivity of the *endo/exo*. The theoretical investigation had demonstrated that the ability of the imidazolium cation to act as H-bond donor is responsible for the selectivity. The formation of H-bonds from the cation to dienophile is a Lewis acid–base interaction, as it is well known that Lewis acid catalysts can have a dramatic effect on both the rates and selectivities of Diels–Alder reactions [112].

4.4 Gas Absorption

Studies have shown that many environmental pollution gases, such as CO_2 , SO_2 , and NH_3 , can dissolve freely in ILs [25, 113–115]. The absorption of CO_2 in $[\text{Bmim}][\text{PF}_6]$ reaches a mole fraction of 0.6 at 25°C and 8.0 MPa [116], and $[\text{Bmim}][\text{BF}_4]$ and $[\text{TMG}][\text{BF}_4]$ ILs can absorb 1–2 mole SO_2 per mole of IL reversibly at the ambient pressure and temperature [117].

Figure 21 shows a physico-absorptive mechanics of CO_2 in $[\text{Bmim}][\text{PF}_6]$ IL. When CO_2 molecules enter the bulk phase of the IL, the O atoms of CO_2 form H-bonds with C–H groups of the imidazolium-ring, and C atoms (with positive charges) can be attracted by anions due to electrostatic interaction. The line-like nonpolar structure of CO_2 is thus changed to give a polar molecule (the angles of the $\angle\text{O–C–O}$ are distributed between $175 \sim 178^\circ$ according to ab initio molecular dynamic calculations, so the change of CO_2 structure results in easier absorption in ILs. The theoretical studies have also indicated that the “spontaneously forming cavities” by H-bonds are vital to accommodate CO_2 and

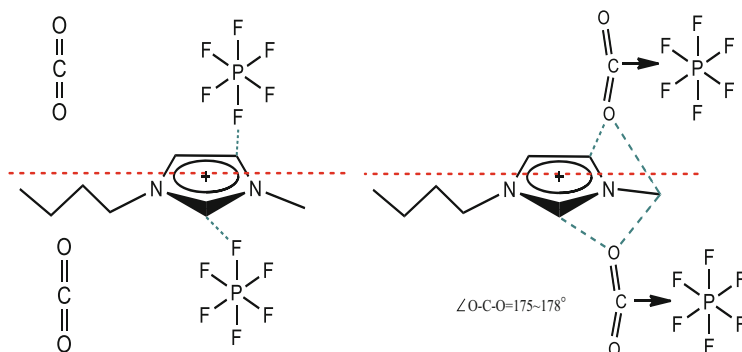


Fig. 21 Proposed mechanics of CO₂ absorption in ILs. The relative positions and the H-bonds change when CO₂ accommodates into the IL physically. Red dashed lines show the relative position and green dashed lines show the hydrogen bonds. Arrows show the electrostatic interactions

SO₂ molecules when they enter the bulk of ILs [118, 119]. However, particularly Ludwig et al. reveal that the experimentally observed “anomalous” temperature dependence of CO₂ in ILs is not due to cavity effects but is caused by attractive solute–solvent interactions. The contribution of the van der Waals interactions is found to dominate [120, 121].

5 Perspective

In the past two decades, explorations of ILs have experienced a fast development and the knowledge base of interdisciplinary data is rapidly being generated for ILs. This will fuel innovative ideas to take these liquids far beyond the realm of mere solvent. However, due to the complications and diversities in ILs’ family, it is very difficult to clarify all of the structural factors exerting effects on their properties.

The molecular interactions between ions depend on their geometry and charge distribution. Unlike in simple salts, the interactions are controlled by long-range Coulombic forces between the net charges of the ions. As for ILs with molecular ions, their bulky size and asymmetric charge distribution softens the Coulombic forces and generates highly directional interactions of shorter range. Therefore, almost all studies on the structures of ILs have involved the non-covalent interactions between cations and anions. In most ILs, in particular imidazolium-based ILs, the H-bonds present the structural characteristics and form the three-dimensional local network to connect the discrete ions. The melting points, viscosity, hydrophilic and hydrophobic properties, gas absorption, dissolution of cellulose, etc. are closely related to the interaction energy and H-bonds.

As for other chemistries, for example nano science and biotechnology, ILs give people the potential to deal with some unresolved problems and fulfill a task in

green chemical processes. Structural investigations can further provide a deep understanding of the unique properties of ILs and valuable hints for the design of new ILs. Based on this, we believe the following aspects are the most important for future research on ILs. First is to know the quantitative relationship between the structures and the properties of ILs, which will point us in the direction of how we may design efficient ionic liquids for a special application. Another aspect is to study how to scale up the systems with ILs for the chemical engineering processes. Additionally, with the development of materials science and engineering, ILs have found a new stage on which to play a role.

Acknowledgments This work was supported financially by the Projects of International Cooperation and Exchanges NSFC (No. 21210006, 21336002 and 21376242), Beijing Natural Science Foundation (No.2131005) and National High Technology Research and Development Program of China (863 Program) (No. 2012AA063001).

References

1. Walden P (1914) Molecular weights and electrical conductivity of several fused salts. *Bull Acad Imp Sci St Petersburg* 8:405–422
2. Li Chum H, Koch VR, Miller LL et al. (1975) Electrochemical scrutiny of organometallic iron complexes and hexamethylbenzene in a room temperature molten salt. *J Am Chem Soc* 97:3264–3265
3. Fuller J, Carlin RT, Long HCD et al. (1994) Structure of 1-ethyl-3-methylimidazolium hexafluorophosphate: model for room temperature molten salts. *J Chem Soc Chem Commun* 299–300
4. Wilkes JS, Zaworotko MJ (1992) Air and water stable 1-ethyl-3-methylimidazolium based ionic liquids. *J Chem Soc Chem Commun* 965–967
5. Hapiot P, Lagrost C (2008) Electrochemical reactivity in room-temperature ionic liquids. *Chem Rev* 108:2238–2264
6. Nockemann P, Thijs B, Driesen K et al. (2007) Choline saccharinate and choline acesulfamate: ionic liquids with low toxicities. *J Phys Chem B* 111:5254–5263
7. Pemak J, Syguda A, Mirska I et al. (2007) Choline-derivative-based ionic liquids. *Chem Eur J* 13:6817–6827
8. Fredlake CP, Crosthwaite JM, Hert DG et al. (2004) Thermophysical properties of imidazolium-based ionic liquids. *J Chem Eng Data* 49:945–964
9. Raabe G, Köhler J (2008) Thermodynamical and structural properties of imidazolium based ionic liquids from molecular simulation. *J Chem Phys* 128:154509
10. Weingartner H (2008) Understanding ionic liquids at the molecular level: facts, problems, and controversies. *Angew Chem Int Ed* 47:654–670
11. Zhang S, Sun N, He X et al. (2006) Physical properties of ionic liquids: database and evaluation. *J Phys Chem Ref Data* 35:1475–1517
12. Bonhôte P, Dias AP, Papageorgiou N et al. (1996) Hydrophobic, highly conductive ambient-temperature molten salts. *Inorg Chem* 35:1168–1178
13. Tokuda H, Hayamizu K, Ishii K et al. (2004) Physicochemical properties and structures of room temperature ionic liquids. 1. Variation of anionic species. *J Phys Chem B* 108:16593–16600
14. Mcewen AB, Ngo HL, Lecompte K et al. (1999) Electrochemical properties of imidazolium salt electrolytes for electrochemical capacitor applications. *J Electrochem Soc* 146:1687–1697

15. Hyun B, Dzyuba SV, Bartsch RA et al. (2002) Intermolecular dynamics of room-temperature ionic liquids: femtosecond optical Kerr effect measurements on 1-alkyl-3-methylimidazolium bis((trifluoromethyl)sulfonyl)imides. *J Phys Chem A* 106:7579–7585
16. Every HA, Bishop AG, Macfarlane D et al. (2004) Transport properties in a family of dialkylimidazolium ionic liquids. *Phys Chem Chem Phys* 6:1758–1765
17. Huddleston JG, Visser AE, Reichert WM et al. (2001) Characterization and comparison of hydrophilic and hydrophobic room temperature ionic liquids incorporating the imidazolium cation. *Green Chem* 3:156–164
18. Tsuzuki S, Tokuda H, Hayamizu K et al. (2005) Magnitude and directionality of interaction in ion pairs of ionic liquids: relationship with ionic conductivity. *J Phys Chem B* 109:16474–16481
19. Fitchett BD, Knepp TN, Conboy JC (2004) 1-Alkyl-3-methylimidazolium bis(perfluoroalkylsulfonyl)imide water-immiscible ionic liquids. *J Electrochem Soc* 151:E219–E225
20. Macfarlane D, Sun J, Golding JJ et al. (2000) High conductivity molten salts based on the imide ion. *Electrochim Acta* 45:1271–1278
21. Hyk W, Caban K, Donten M et al. (2001) Properties of microlayers of ionic liquids generated at microelectrode surface in undiluted redox liquids. Part II *J Phys Chem B* 105:6943–6949
22. Earle MJ, Esperanc JMSS, Gilea MA et al. (2006) The distillation and volatility of ionic liquids. *Nature* 439:831–834
23. Zaitsau DH, Kabo GJ, Strechan AA et al. (2006) Experimental vapor pressures of 1-alkyl-3-methylimidazolium bis(trifluoromethylsulfonyl)imides and a correlation scheme for estimation of vaporization enthalpies of ionic liquids. *J Phys Chem A* 110:7303–7306
24. Köddermann T, Paschek D, Ludwig R (2008) Ionic liquids: dissecting the heat of vaporization. *Chem Phys Chem* 9:549–555
25. Blanchard LA, Gu ZY, Brennecke JF (2001) High-pressure phase behavior of ionic liquid/CO₂ systems. *J Phys Chem B* 105:2437–2444
26. Cammarata L, Kazarian SG, Salterb PA et al. (2001) Molecular states of water in room temperature ionic liquids. *Phys Chem Chem Phys* 3:5192–5200
27. Devyatykh GG, Sennikov PG (1995) Spectroscopic determination and study of the molecular state of water in ultrapure volatile inorganic substances. *Russ Chem Rev* 64:817–830
28. Rivera-Rubero S, Baldelli S (2004) Influence of water on the surface of hydrophilic and hydrophobic room-temperature ionic liquids. *J Am Chem Soc* 126:11788–11789
29. Bhargava BL, Balasubramanian S (2006) Layering at an ionic liquid–vapor interface: a molecular dynamics simulation study of [bmim][PF₆]. *J Am Chem Soc* 128:10073–10078
30. Rogers RD (2007) Reflections on ionic liquids. *Nature* 447:917–918
31. Katritzky AR, Lomaka A, Petrukhin R et al. (2002) Correlation of the melting point for pyridinium bromides, potential ionic liquids. *J Chem Inf Comput Sci* 42:71–74
32. Elaiwi A, Hitchcock PB, Seddon KR et al. (1995) Hydrogen bonding in imidazolium salts and its implications for ambient-temperature halogenoaluminate(III) ionic liquids. *J Chem Soc Dalton Trans* 3467–3472
33. Dymek CJ, Grossie DA, Fratini AV et al. (1989) Evidence for the presence of hydrogen-bonded ion-ion interactions in the molten salt precursor, 1-methyl-3-ethylimidazolium chloride. *J Mol Struct* 213:25–34
34. Turner EA, Pye CC, Singer RD (2003) Use of ab initio calculations toward the rational design of room temperature ionic liquids. *J Phys Chem A* 107:2277–2288
35. Reichert WM, Holbrey JD, Swatloski RP et al. (2007) Solid-state analysis of low-melting 1,3-dialkylimidazolium hexafluorophosphate salts (ionic liquids) by combined X-ray crystallographic and computational analyses. *Cryst Growth Des* 7:1106–1114
36. Matsumoto K, Hagiwara R (2007) Structural characteristics of alkyylimidazolium-based salts containing fluoroanions. *J Fluorine Chem* 128:317–331
37. Xue H, Verma R, Shreeve JM (2006) Review of ionic liquids with fluorine-containing anions. *J Fluor Chem* 127:159–176

38. Swatloski RP, Holbrey JD, Rogers RD (2003) Ionic liquids are not always green: hydrolysis of 1-butyl-3-methylimidazolium hexafluorophosphate. *Green Chem* 5:361–363
39. Choudhury AR, Winterton N, Steiner A et al. (2005) In situ crystallization of low-melting ionic liquids. *J Am Chem Soc* 127:16792–16793
40. Hasan M, Kozhevnikov IV, Siddiqui MRH et al. (2001) N, N-Dialkylimidazolium chloroplatinate(II), chloroplatinate(IV), and chloroiridate(IV) salts and an N-heterocyclic carbene complex of platinum(II): synthesis in ionic liquids and crystal structures. *Inorg Chem* 40:795–800
41. Matsumoto K, Hagiwara R, Yoshida R et al. (2004) Syntheses, structures and properties of 1-ethyl-3-methylimidazolium salts of fluoro-complex anions. *Dalton Trans* 144–149
42. Matsumoto K, Hagiwara R, Mazej Z et al. (2006) Crystal structures of frozen room temperature ionic liquids, 1-ethyl-3-methylimidazolium tetrafluoroborate (EMImBF₄), hexafluoroantimonate (EMImSbF₆) and hexafluoroantimonate (EMImTaF₆), determined by low-temperature X-ray diffraction. *Solid State Sci* 8:1250–1257
43. Luo H, Baker GA, Dai S (2008) Isothermogravimetric determination of the enthalpies of vaporization of 1-alkyl-3-methylimidazolium ionic liquids. *J Phys Chem B* 112:10077–10081
44. Armstrong JP, Hurst C, Jones RG et al. (2007) Vapourisation of ionic liquids. *Phys Chem Chem Phys* 9:982–990
45. Hunt PA, Kirchner B, Welton T (2006) Characterising the electronic structure of ionic liquids: an examination of the 1-butyl-3-methylimidazolium chloride ion pair. *Chem Eur J* 12:6762–6775
46. Dong K, Song Y, Liu X et al. (2012) Understanding structures and hydrogen bonds of ionic liquids at the electronic level. *J Phys Chem B* 116:1007–1017
47. Dong K, Zhang S, Wang D et al. (2006) Hydrogen bonds in imidazolium ionic liquids. *J Phys Chem A* 110:9775–9782
48. Fumino K, Wulf A, Ludwig R (2009) Hydrogen bonding in protic ionic liquids: reminiscent of water. *Angew Chem Int Ed* 48:3184–3186
49. Zhao W, Leroy FD, Heggen B et al. (2009) Are there stable ion-pairs in room-temperature ionic liquids? Molecular dynamics simulations of 1-n-butyl-3-methylimidazolium hexafluorophosphate. *J Am Chem Soc* 131:15825–15833
50. Liu Z, Huang S, Wang W (2004) A refined force field for molecular simulation of imidazolium-based ionic liquids. *J Phys Chem B* 108:12978–12989
51. Talaty ER, Raja S, Storhaug VJ et al. (2004) Raman and infrared spectra and ab initio calculations of C₂₋₄MIM imidazolium hexafluorophosphate ionic liquids. *J Phys Chem B* 108:13177–13184
52. Wang Y, Voth GA (2005) Unique spatial heterogeneity in ionic liquids. *J Am Chem Soc* 127:12192–12193
53. Izvekov S, Violi A, Voth GA (2005) Systematic coarse-graining of nanoparticle interactions in molecular dynamics simulation. *J Phys Chem B Lett* 109:17019–17024
54. Liu X, Zhou G, Zhang S (2008) Molecular dynamics simulation of acyclic guanidinium-based ionic liquids. *Fluid Phase Equilib* 272:1–7
55. Mizuse K, Mikami N, Fujii A (2010) Infrared spectra and hydrogen-bonded network structures of large protonated water clusters H⁺(H₂O)_n (n = 20–200). *Angew Chem Int Ed* 49:10119–10122
56. Russina O, Triolo A, Gontrani L, Caminiti R (2012) Mesoscopic structural heterogeneities in room-temperature ionic liquids. *J Phys Chem Lett* 3:27–33
57. Hardacre C, McMath SEJ, Nieuwenhuyzen M, Bowron DT, Soper AK (2003) Liquid structure of 1,3-dimethylimidazolium salts. *J Phys Condens Matter* 15:S159–S166
58. Canongia Lopes JN, Padua AAH (2006) Nanostructural organization in ionic liquids. *J Phys Chem B* 110:3330–3335
59. Triolo A, Russina O, Bleif H-J, Di Cola E (2007) Nanoscale segregation in room temperature ionic liquids. *J Phys Chem B* 111:4641–4644

60. Auon B, Goldbatch A, Gonzalez M, Kohara S, Rice DL, Saboungi M-L (2011) Nanoscale heterogeneity in alkyl-methylimidazolium bromide ionic liquids. *J Chem Phys* 134:104509
61. Zahn S, Uhlig F, Thar J et al. (2008) Intermolecular forces in an ionic liquid ([Mmim]Cl) versus those in a typical salt (NaCl). *Angew Chem Int Ed* 47:3639–3641
62. Crowhurst L, Mawdsley PR, Perez-Arlandis JM et al. (2003) Solvent-solute interactions in ionic liquids. *Phys Chem Chem Phys* 5:2790–2794
63. Hunt PA, Gould IR (2006) Structural characterization of the 1-butyl-3-methylimidazolium chloride ion pair using ab initio methods. *J Phys Chem A* 110:2269–2282
64. Abdul-Sada AK, Greenway AM, Hitchcock PB et al. (1986) Upon the structure of room temperature halogenoaluminate ionic liquids. *J Chem Soc Chem Commun* 1753–1754
65. Khupse ND, Kumar A (2010) Contrasting thermosolvatochromic trends in pyridinium-, pyrrolidinium-, and phosphonium-based ionic liquids. *J Phys Chem B* 114:376–381
66. Tokuda H, Tsuzuki S, Susan MBH et al. (2006) How ionic are room-temperature ionic liquids? An indicator of the physicochemical properties. *J Phys Chem B* 110:19593–19600
67. Fukaya Y, Sugimoto A, Ohno H (2006) Superior solubility of polysaccharides in low viscosity, polar, and halogen-free 1,3-dialkylimidazolium formates. *Biomacromolecules* 7:3295–3297
68. Dieter KM, Dymek CJJ, Heimer NE et al. (1988) Ionic structure and interactions in 1-methyl-3-ethylimidazolium chloride-aluminum chloride molten salts. *J Am Chem Soc* 110:2722–2726
69. Remsing RC, Wildin JL, Rapp AL et al. (2007) Hydrogen bonds in ionic liquids revisited: ^{35/37}Cl NMR studies of deuterium isotope effects in 1-n-butyl-3-methylimidazolium chloride. *J Phys Chem B* 111:11619–11621
70. Hardacre C, Holbrey JD, Mcmath SEJ et al. (2003) Structure of molten 1,3-dimethylimidazolium chloride using neutron diffraction. *J Chem Phys* 118:273–279
71. Heimer NE, Sesto RED, Meng Z et al. (2006) Vibrational spectra of imidazolium tetrafluoroborate ionic liquids. *J Mol Liq* 124:84–95
72. Holbrey JD, Reichert WM, Nieuwenhuyzen M et al. (2003) Liquid clathrate formation in ionic liquid–aromatic mixtures. *Chem Commun* 476–477
73. Hardacre C, Mcmath SEJ, Nieuwenhuyzen M et al. (2003) Liquid structure of 1, 3-dimethylimidazolium salts. *J Phys Condens Matter* 15:S159–S166
74. Rijnberg E, Richter B, Thiele KH et al. (1998) A homologous series of homoleptic zinc bis (1,4-di-tert-butyl-1,4-diaza-1,3-butadiene) complexes: $K_x[Zn(t-BuNCHCHN-t-Bu)_2]$, $Zn(t-BuNCHCHN-t-Bu)_2$, and $[Zn(t-BuNCHCHN-t-Bu)_2](OTf)_x$ ($x = 1, 2$). *Inorg Chem* 37:56–63
75. Umebayashi Y, Fujimori T, Sukizaki T et al. (2005) Evidence of conformational equilibrium of 1-ethyl-3-methylimidazolium in its ionic liquid salts: Raman spectroscopic study and quantum chemical calculations. *J Phys Chem A* 109:8976–8982
76. Roth C, Poppel T, Fumino K et al. (2010) The importance of hydrogen bonds for the structure of ionic liquids: single-crystal X-ray diffraction and transmission and attenuated total reflection spectroscopy in the terahertz region. *Angew Chem Int Ed* 49:10221–10224
77. Fumino K, Wulf A, Ludwig R (2008) Strong, localized, and directional hydrogen bonds fluidize ionic liquids. *Angew Chem Int Ed* 47:8731–8734
78. Gjikaj M, Leye J-C, Xie T et al. (2010) Structural and spectroscopic elucidation of imidazolium and pyridinium based hexachloridophosphates and niobates. *CrystEngComm* 12:1474–1480
79. Deetlefs M, Hardacre C, Nieuwenhuyzen M et al. (2006) Liquid structure of the ionic liquid 1,3-dimethylimidazolium bis{(trifluoromethyl)sulfonyl}amide. *J Phys Chem B* 110:12055–12061
80. Holbrey JD, Reichert WM, Rogers RD (2004) Crystal structures of imidazolium bis(trifluoromethanesulfonyl)-imide ‘ionic liquid’ salts: the first organic salt with a cis-TFSI anion conformation. *Dalton Trans* 2267–2271

81. Wulf A, Fumino K, Ludwig R (2010) Spectroscopic evidence for an enhanced anion–cation interaction from hydrogen bonding in pure imidazolium ionic liquids. *Angew Chem Int Ed* 49:449–453
82. Shetty PH, Youngberg PJ, Kersten BR et al. (1987) Solvent properties of liquid organic salts used as mobile phases in microcolumn reversed-phase liquid chromatography. *J Chromatogr* 411:61–79
83. Ding J, Welton T, Armstrong DW (2004) Chiral ionic liquids as stationary phases in gas chromatography. *Anal Chem* 76:6819–6822
84. Geissler PL, Dellago C, Chandler D et al. (2001) Autoionization in liquid water. *Science* 291:2121–2124
85. Dong K, Zhang S (2012) Hydrogen bonds: a structural insight into ionic liquids. *Chem Eur J* 18:2748–2761
86. Downard A, Earle MJ, Hardacre C et al. (2004) Structural studies of crystalline 1-alkyl-3-methylimidazolium chloride salts. *Chem Mater* 16:43–48
87. Berg RW, Deetlefs M, Seddon KR et al. (2005) Raman and ab initio studies of simple and binary 1-alkyl-3-methylimidazolium ionic liquids. *J Phys Chem B* 109:19018–19025
88. Wang Y, Voth GA (2006) Tail aggregation and domain diffusion in ionic liquids. *J Phys Chem B* 110:18601–18608
89. Canongia Lopes JN, Padua AH (2006) Nanostructural organization in ionic liquids. *J Phys Chem B* 110:3330–3335
90. Xiao D, Rajian JR, Cady A et al. (2007) Nanostructural organization and anion effects on the temperature dependence of the optical Kerr effect spectra of ionic liquids. *J Phys Chem B* 111:4669–4677
91. Soutullo MD, Odom CI, Wicker BF et al. (2007) Reversible CO₂ capture by unexpected plastic-, resin-, and gel-like ionic soft materials discovered during the combi-click generation of a TSIL library. *Chem Mater* 19:3581–3583
92. Huddleston JG, Willauer HD, Swatloski RP et al. (1998) Room temperature ionic liquids as novel media for ‘clean’ liquid–liquid extraction. *Chem Commun* 1765–1766
93. Holbrey JD, Lopez-Martin I, Rothenberg G et al. (2008) Desulfurisation of oils using ionic liquids: selection of cationic and anionic components to enhance extraction efficiency. *Green Chem* 10:87–92
94. Xie LL, Favre-Reguillon A, Wang XX et al. (2008) Selective extraction of neutral nitrogen compounds found in diesel feed by 1-butyl-3-methyl-imidazolium chloride. *Green Chem* 10:524–531
95. Domanska U, Pobudkowska A, Krolkowski M (2007) Separation of aromatic hydrocarbons from alkanes using ammonium ionic liquid C₂NF₂ at $T = 298.15$ K. *Fluid Phase Equilib* 259:173–179
96. Zhang SG, Zhang QL, Zhang ZC (2004) Extractive desulfurization and denitrogenation of fuels using ionic liquids. *Ind Eng Chem Res* 43:614–622
97. Cao Y, Xing H, Yang Q et al. (2012) Separation of soybean isoflavone aglycone homologues by ionic liquid-based extraction. *J Agric Food Chem* 60:3432–3440
98. Dong K, Cao Y, Yang Q et al. (2012) Role of hydrogen bonds in ionic-liquid-mediated extraction of natural bioactive homologues. *Ind Eng Chem Res* 51:5299–5308
99. Anderson JL, Ding J, Welton T et al. (2002) Characterizing ionic liquids on the basis of multiple solvation interactions. *J Am Chem Soc* 124:14247–14254
100. Pinkert A, Marsh KN, Pang S et al. (2009) Ionic liquids and their interaction with cellulose. *Chem Rev* 109:6712–6728
101. Rinaldi R, Palkovits R, Schüth F (2008) Depolymerization of cellulose using solid catalysts in ionic liquids. *Angew Chem Int Ed* 47:8047–8050
102. Vispute TP, Zhang H, Sanna A et al. (2010) Renewable chemical commodity feedstocks from integrated catalytic processing of pyrolysis oils. *Science* 330:1222–1227
103. Swatloski RP, Spear SK, Holbrey JD et al. (2002) Dissolution of cellose with ionic liquids. *J Am Chem Soc* 124:4974–4975

104. Tan SSY, Macfarlane DR, Upfal J et al. (2009) Extraction of lignin from lignocellulose at atmospheric pressure using alkylbenzenesulfonate ionic liquid. *Green Chem* 11:339–345
105. Qin Y, Lu X, Sun N et al. (2010) Dissolution or extraction of crustacean shells using ionic liquids to obtain high molecular weight purified chitin and direct production of chitin films and fibers. *Green Chem* 12:968–971
106. Xie H, Li S, Zhang S (2005) Ionic liquids as novel solvents for the dissolution and blending of wool keratin fibers. *Green Chem* 7:606–608
107. Remsing RC, Swatloski RP, Rogers RD et al. (2006) Mechanism of cellulose dissolution in the ionic liquid 1-n-butyl-3-methylimidazolium chloride: a ^{13}C and $^{35/37}\text{Cl}$ NMR relaxation study on model systems. *Chem Commun* 28:1271–1273
108. Sun N, Rahman M, Qin Y et al. (2009) Complete dissolution and partial delignification of wood in the ionic liquid 1-ethyl-3-methylimidazolium acetate. *Green Chem* 11:646–655
109. Liu H, Sale KL, Holmes BM et al. (2010) Understanding the interactions of cellulose with ionic liquids: a molecular dynamics study. *J Phys Chem B* 114:4293–4301
110. Garcia H, Ferreira R, Petkovic M et al. (2010) Dissolution of cork biopolymers in biocompatible ionic liquids. *Green Chem* 12:367–369
111. Jaeger DA, Tucker CE (1989) Diels-Alder reactions in ethylammonium nitrate, a low-melting fused salt. *Tetrahedron Lett* 30:1785–1788
112. Aggarwal A, Lancaster NL, Sethi AR et al. (2002) The role of hydrogen bonding in controlling the selectivity of Diels–Alder reactions in room-temperature ionic liquids. *Green Chem* 4:517–520
113. Anthony JL, Maginn EJ, Brennecke JF (2002) Solubilities and thermodynamic properties of gases in the ionic liquid 1-n-butyl-3-methylimidazolium hexafluorophosphate. *J Phys Chem B* 106:7315–7320
114. Yuan X, Zhang S, Liu J et al. (2007) Solubilities of CO_2 in hydroxyl ammonium ionic liquids at elevated pressures. *Fluid Phase Equilib* 257:195–200
115. Zhang S, Chen Y, Ren RX-F et al. (2005) Solubility of CO_2 in sulfonate ionic liquids at high pressure. *J Chem Eng Data* 50:230–233
116. Blanchard LA, Hancu D, Beckman EJ et al. (1999) Green processing using ionic liquids and CO_2 . *Nature* 399:28–29
117. Huang J, Riisager A, Wasserscheid P et al. (2006) Reversible physical absorption of SO_2 by ionic liquids. *Chem Commun* 38:4027–4029
118. Huang X, Margulis CJ, Li Y et al. (2005) Why is the partial molar volume of CO_2 so small when dissolved in a room temperature ionic liquid? Structure and dynamics of CO_2 dissolved in $[\text{Bmim}]^+ [\text{PF}_6]^-$. *J Am Chem Soc* 127:17842–17851
119. Scovazzo P, Camper D, Kieft J et al. (2004) Regular solution theory and CO_2 gas solubility in room-temperature ionic liquids. *Ind Eng Chem Res* 43:6855–6860
120. Kerlé D, Ludwig R, Geiger A et al. (2009) Temperature dependence of the solubility of carbon dioxide in imidazolium-based ionic liquids. *J Phys Chem B* 113:12727–12735
121. Paschek D, Köddermann T, Ludwig R (2008) The solvophobic solvation and interaction of small apolar particales in imidazolium-based ionic liquids. *Phys Rev Lett* 100:115901–115904

Aggregation in Systems of Ionic Liquids

Jianji Wang and Huiyong Wang

Abstract Material preparation in ionic liquids and environmental pollution control by ionic liquids are often closely dependent on the aggregation behavior of ionic liquids in solution. Therefore, understanding the aggregation behavior of ionic liquids in solution is very important from both fundamental and applied aspects. In this chapter, our aim is to provide a summary of our current state of knowledge of the aggregation of ionic liquids in solutions modulated by alkyl chain length, cationic structure, and anionic type of ionic liquids, and by addition of inorganic salts, organic solvents, and surfactants. The possible mechanism for the effect of these factors on the aggregation behavior of ionic liquids has been analyzed, and the potential applications of ionic liquids aggregation in membrane separation of ionic liquids wastewater, controlled drug release, breakage of oil/water emulsions, and selective separation of protein (BSA) from aqueous saccharides has also been illustrated. In addition, the challenges in this field have been addressed and some suggestions are made for future work.

Keywords Ionic liquids • Aggregation in solution • Aggregate microstructure • Potential applications

1 Introduction

1.1 Ionic Liquids

Room temperature ionic liquids (ILs) are a special class of molten salts composed of organic cations and inorganic or organic anions, melting at temperatures below

J. Wang (✉) • H. Wang

School of Chemistry and Chemical Engineering, Key Laboratory of Green Chemical Media and Reactions, Ministry of Education, Henan Normal University, Xinxiang, Henan 453007, P. R. China

e-mail: jwang@henannu.edu.cn

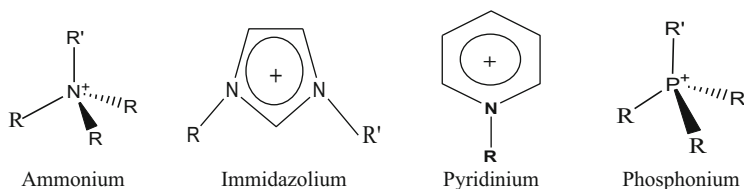


Fig. 1 Cationic structures of ILs commonly used

373 K. Usually, the most used cations include alkylimidazolium $[\text{RR}'\text{IM}]^+$, alkylpyridinium $[\text{RPy}]^+$, tetraalkylammonium $[\text{NR}_4]^+$, and tetraalkylphosphonium $[\text{PR}_4]^+$ (see Fig. 1). Anions consist of chloride Cl^- , bromide Br^- , iodide I^- , hexafluorophosphate $[\text{PF}_6]^-$, tetrafluoroborate $[\text{BF}_4]^-$, nitrate $[\text{NO}_3]^-$, methane sulfonate (mesylate) $[\text{CH}_3\text{SO}_3]^-$, trifluoromethane sulfonate (triflate) $[\text{CF}_3\text{SO}_3]^-$, bis-(trifluoromethanesulfonyl)amide $[\text{Tf}_2\text{N}]^-$, among others [1]. The number of potential ion combinations available reputedly equates to 10^{12} .

Compared with the traditional volatile organic compounds (VOCs), ILs have many unique physical and chemical properties. These properties can be summarized as follows [1]: (1) immeasurable vapor pressure and nonflammability under normal conditions; (2) thermal decomposition temperatures higher than 300°C , and a large liquid range from -200 to 300°C ; (3) excellent dissolution performance for organic, inorganic, and polymer materials; (4) wide electrochemical window of $2 \sim 5$ V; and (5) designable structures and properties for various practical applications.

Among these properties, negligible vapor pressure avoids atmospheric pollution and enhances their recycling, which are the main reason why ionic liquids are often called “green solvents.” However, recent studies have shown that some ionic liquids have a wide range of toxicity and, as a result, the use of the term “green solvents” has been questioned [2, 3].

Even so, the above properties have made ILs applicable to myriads of applications that include chemical synthesis [4], biocatalytic transformations [5, 6], electrochemistry [7, 8], and analytical and separation science [9, 10]. In addition, the opportunity of cation modification and anion selection as well as the enormous number of possible combinations allows us to fulfill technological demands, and provides novel task-specific media for the chemical and biochemical industries [11, 12].

In their applications, ILs exhibit many unique properties and much abnormal behavior. For example, ILs have the ability to dissolve inorganic compounds; at the same time, they can also dissolve organic and polymeric materials over a wide temperature range. It seems likely that the old rule of thumb that “like dissolves like” is not valid for ionic liquids. When CO_2 is added to ILs, the electric conductivity of the systems increases, although CO_2 is a nonpolar compound [13]. Ionic liquids dissolve very large amounts of CO_2 , while the solubility of neat ionic liquids in supercritical CO_2 is very low [14]. Ionic liquids can be used as stationary phases in gas-liquid chromatography, but they show “dual-nature” behavior: they are

capable of separating polar compounds as if they were polar stationary phases and can also separate nonpolar compounds as if they were nonpolar stationary phases [15]. These unique properties are ascribed not only to the nature of cations and anions but also to the interaction of ionic liquids with other components and the microstructure of ionic liquids in the systems. Therefore, aggregation of ionic liquids in solutions has been the focus of much research [16–19].

1.2 Significance of Ionic Liquids Aggregation

Many applications of ILs would be closely related to their aggregate formation. It may be expected from the amphiphilicity of ILs that interfacial phenomena play a major role in the behavior of such IL-containing systems. For example, the transfer of a compound through an interface is an important part of the extraction process which is controlled by molecules adsorbed at the interface. The presence of IL aggregates could reduce the efficiency of these processes because of partial extraction of the product into micelles. The formation of aggregation structure may also have consequences in a number of areas including synthesis and purification of bulk ILs, material preparation, environmental pollution control, formation of dispersed or phase-separated systems, distribution of ILs in the environment [12, 20], among others.

The transport and distribution of ILs through soil is also mainly dependent on their aggregation. The size and structure of an aggregate would affect the transport parameters of ILs. It was shown that ILs were adsorbed onto soils initially with electrostatic interaction with clay surface [21], and the aggregates of ILs can also be adsorbed onto mineral surfaces to form hemi-micelles on the surface. The aggregates have the ability to dissolve highly lipophilic substances and promote their distribution as part of a colloid-facilitated transport. This would influence the chemical fate of ILs and eventual possibilities of soils remediation.

Aggregation behavior is obviously very important for the future use and environmental fate analysis of ILs. Also, the knowledge of the aggregation behavior of ILs plays a vital part in understanding how these ionic compounds participate as components in a complex system. Therefore, in this chapter we will analyze and summarize the state-of-the-art on the studies of the formation, microstructure and possible applications of ILs aggregation in solutions in order to provide a better understanding of the progress in this field.

Table 1 Critical aggregation concentration (mM) of 1-alkyl-3-methyl-imidazolium chloride ($[C_n\text{mim}][\text{Cl}]$), 1-alkyl-3-methyl-imidazolium bromide ($[C_n\text{mim}][\text{Br}]$), *N*-alkyl-*N*-methylpyrrolidinium bromide ($C_n\text{MPB}$) and 1-alkylpyridiniumbromides ($C_n\text{PyrBr}$) as a function of alkyl chain length (n_c) determined by various methods at 298 K

n_c	$[C_n\text{mim}][\text{Cl}]$		$[C_n\text{mim}][\text{Br}]$		$C_n\text{PyrBr}$		$C_n\text{MPB}$		
	Surface conductivity tension	fluorescence other method	Surface conductivity tension	fluorescence other method	Surface conductivity tension	fluorescence other method	Surface conductivity tension	fluorescence other method	
2		$\text{N}[19]^a$	2,500[26]	1,900[26]		$\text{N}(\text{SANS})$ [26]			
4	$\text{N}[22]^a$	$\text{N}[19]^a$	800[26]	900[26]		$\text{N}(\text{SANS})$ [26] 2,579(NMR) [32] ^b			
6	$900[19]$ $\text{N}[27]^a$	$\text{N}[19]^a$	600[26] 470[28]	400[26] 770[31] ^b		600(SANS) [26] 800(volume) [31] ^b 797(NMR) [32] ^b			
8	$220[22]$ $100[16]$ $220[19]$	$234[22]$ $90[16]$ $200[36]$	150[26] 121[28] 170[38]	150[26] 160[31] ^b 169[38]		190[31] ^b 130[39] 141(NMR) [32] ^b 177(NMR) [38]	180[38]	184(NMR) [38]	
9			40[26]	30[26] 74[18]					
10	$59.9[22]$ $55[19]$ $10[23]$ $39.9[24]$	$53.8[22]$ $60[23]$ $40.47[24]$ $62[36]$	20[28] 29.3[29] 33[38]	40[27] 41[18] 32.9[29] 39[31] ^b 42[38]		46[31] ^b 25[39] 31(NMR) [32] ^b 39(NMR) [38]	30[38]	45(NMR) [38]	
12	$15[19]$ $13.17[24]$ $9.68[37]$	$20[23]$ $13.47[24]$ $14[36]$	13(NMR) [19] 13.8(ITC) [19]	4.3[28] 10.9[29] 9.68[37] 9.0[38]	9.8[18] 8.5[29] 9.5[30] 9[31] ^b 10[38]	12(volume) [31] ^b 11(NMR) [32] ^b 9.56(ITC) [37] 8.0(NMR) [38]	9.3[38]	10 [38] 9.3(NMR) [38]	
14	$3.4[22]$ $4[19]$ $2.98[24]$ $2.69[37]$	$3.15[22]$ $3.68[24]$ $3.8[36]$	4(NMR) [19] 3.3(ITC) [36]	2.69[37] 1.9[38]	2.5[18] 2.6[30] 2.5[38]	1.8[38] 2.52(ITC) [37] 1.4(NMR) [38]	2.2[38]	2.4[38] 1.5(NMR) [38]	
								13.5 [37] 13.5[37]	
									3.30[37] 3.30[37]

16	1.3[22]	1.14[22]	0.51[37]	0.8[28]	0.64(TTC) [37]	0.860[37]	0.856[37]
	0.88[25]	0.86[24]		0.61[18]			
	0.87[24]			0.65[30]			
	0.51[37]						
18	0.4[22]	0.45[22]					

^aNo critical micelle concentration was detected

^bmmol/kg

2 Aggregation of Ionic Liquids in Aqueous Solutions

2.1 Formation of Ionic Liquids Aggregates

Many research publications suggest that ILs form aggregates in aqueous solutions. It should be noted that different terminologies have been used in the literature for the aggregate/micelle formation of ionic liquids. The reason may lie in the fact that, sometimes, aggregates of ionic liquids could be formed, but the attractive interaction between the alkyl chains was not strong enough to form micelles, especially for ILs with shorter alkyl chains. Therefore, the terms “aggregate” and “critical aggregation concentration (CAC)” have been frequently used in this book.

A significant amount of research has been published on the determination of CAC of ILs in aqueous solution. The data available in the literature [16–39] are collected in Tables 1 and 2. It can be seen that the results from different laboratories are not always consistent. The main reason is that a large variety of experimental techniques, including conductivity, surface tension, molar volume, fluorescence quenching, small angle neutron scattering, isothermal titration calorimetry (ITC), nuclear magnetic resonance (NMR), sound speed, turbidity, etc., has been used to determine the CAC values. However, not all methodologies have been carried out with the same care and rigor, and therefore some uncertainties exist in the results of a number of ILs.

Aggregation behavior of 1-butyl-3-methylimidazolium tetrafluoroborate ($[C_4mim][BF_4]$) and 1-methyl-3-octylimidazoliumchloride and iodide ($[C_8mim]Cl$ and $[C_8mim]I$) in aqueous solution has been investigated by Bowers et al. with surface tension, conductivity, and small angle neutron scattering (SANS) measurements [16]. The results showed that these ILs act as short chain cationic surfactants in aqueous solution and form aggregates above their CAC values. The conductivity data for $[C_8mim]Cl$ and $[C_8mim]I$ indicated the possible presence of aggregates at concentrations below the CACs. From analysis of the SANS data, the $[C_4mim][BF_4]$ system was found to be best modeled as a dispersion of polydisperse spherical aggregates, whereas $[C_8mim]I$ can be modeled as a system of regularly sized near-spherical charged micelles at concentrations above their critical aggregation concentration. A solution of $[C_8mim]Cl$ displays weak long-range ordering of possibly disklike particles, culminating in the formation of structures with distinct long-range order at higher concentrations.

Miskolczy et al. [17] investigated the aggregation of 1-butyl-3-methylimidazolium octyl-sulfate ($[C_4mim][OctSO_4]$) and $[C_8mim]Cl$ in aqueous solutions by conductivity, turbidity, and 2-hydroxy-substituted Nile Red solvatochromic probe measurements. $[C_4mim][OctSO_4]$ was found to form micelles above 0.031 M which were within one's expectation, because a long-chained anion such as the octyl-sulfate has previously been shown to form micelles in its own right. On the other hand, $[C_8mim]Cl$ produced inhomogeneous solution of larger aggregates. As a continuation of research, these authors investigated the association of 1-alkyl-3-methyl-imidazolium bromide ($[C_nmim]Br$) ionic liquids in aqueous solution at

Table 2 Comparison of critical aggregate concentration (mM) of ionic liquids determined by various methods at 298 K

IL	Surface tension	Conductivity	Fluorescence	Other method
[C ₄ mim][BF ₄]	800[16]	820[16] 729[39]	960[31] ^a	800 (SANS) [16] 710 (volume) [31] ^a 705 (speed of sound) [39]
[C ₄ mim][OctSO ₄]	40.5[16]	31[17]	31[17]	
[C ₈ mim]I	100[16]	150[16]		
[C ₈ mim][BF ₄]		28[39]		25 (speed of sound) [39]
[C ₁₀ mim][NTf ₂]	N[19]	N[22]		
[C ₁₀ mim][PF ₆]	N[19]			
[C ₁₂ mim][BF ₄]	9.2[29]	7.6[29]		
[C ₁₆ mim][BF ₄]	1.37[25] ^b			

^ammol/kg^bAt 313 K

298 K by conductivity measurements [18]. A similar study was conducted by Sirieix-Plénet and coworkers [27]. They examined the properties of mixtures of 1-decyl-3-methylimidazolium bromide ([C₁₀mim]Br) with water by conductimetry and electromotive forces (EMF) measurements with bromide- or cationic surfactant-selective electrodes. It was shown that, at low concentrations, this ionic liquid behaves like a classical cationic amphiphile. As the concentration of [C₁₀mim]Br increased above the CAC, the association between the cationic aggregate and its counterion was enhanced.

Interfacial tension, fluorescence, and ¹H NMR measurements were used by Blesic et al. [19] to monitor the aggregation behavior of ionic liquids with 1-alkyl-3-methyl-imidazolium cations [C_{*n*}mim]⁺ (*n* = 2–14) and different counterions, Cl[−], [PF₆][−] and bis(trifluoromethylsulfonyl)imide anion ([NTf₂][−]) in aqueous solutions. It was found that [C₆mim]Cl showed no noticeable aggregation in water, and aggregates formation was detected for the ILs possessing at least eight carbon atoms in an imidazolium cation with Cl anion. When the Cl[−] anion in [C₁₀mim]Cl was replaced by [NTf₂][−] or [PF₆][−], no micelle formation was observed, because the low solubility of these ILs induced phase separation before their bulk aggregation.

Goodchild et al. [26] used conductivity, surface tension, and SANS to investigate the surface, phase, and aggregation behavior of 1-alkyl-3-methyl-imidazolium bromides in water. Aggregation for the ILs with alkyl chain length greater than six carbon atoms was observed, and their CACs were reported.

An investigation on the aggregation of [C₄mim][PF₆], [C₁₀mim]Cl, [C₁₂mim]Cl and 1-butyl-3-methylimidazolium methylsulfate; [C₄mim][CH₃SO₄] in aqueous solutions was completed by Modaressi et al. [23]. The methods used were electrical conductivity, density, and surface tension. The authors found that the ILs with a butyl chain do not favor an aggregate self-assembly.

Inoue et al. [30] used conductivity technology to study the aggregation behavior of long-chain imidazolium ionic liquids of 1-alkyl-3-methylimidazolium bromides

Table 3 Aggregation numbers (N_{agg}) of $[C_n\text{mim}]\text{Br}$ in aqueous solutions at 298 K

n_c	N_{agg}	Method	$C_n\text{TAB}$
8	22[26]	SANS	
	53[31]	Fluorescence quenching	
	22[31]	Molecular geometry	
	25[32]	NMR	
9	45[18]	Fluorescence quenching	
10	40[26]	SANS	
	42[18]	Fluorescence quenching	
	40[24]	Fluorescence quenching	
	48[24]	Molecular geometry	
	35[31]	Fluorescence quenching	
	33[31]	Molecular geometry	
	27[32]	NMR	
12	44[18]	Fluorescence quenching	55[33]
	43[30]	Electrical conductivity	
	58[24]	Fluorescence quenching	
	67[24]	Molecular geometry	
	44[31]	Fluorescence quenching	
	49[31]	Molecular geometry	
14	46[32]	NMR	
	59[18]	Fluorescence quenching	70[33]
	61[30]	Electrical conductivity	
	79[24]	Fluorescence quenching	
16	89[24]	Molecular geometry	
	66[18]	Fluorescence quenching	89[33]
	76[30]	Electrical conductivity	
	99[24]	Fluorescence quenching	
	114[24]	Molecular geometry	

Table 4 Aggregation numbers (N_{agg}) of $[C_n\text{mim}]\text{Cl}$ in aqueous solutions at 298 K

n_c	N_{agg}	Method	$C_n\text{TAB}$
8			
9			
10	23[36]	Electrical conductivity	
12	37[36]	Electrical conductivity	55[33]
14	46[36]	Electrical conductivity	70[33]
16			89[33]

with C_{12} – C_{16} alkyl chains in water. Based on the mixed electrolyte model of micellar solution, the aggregation number and the degree of counterion binding, β , were estimated. The results clearly demonstrate that the general behavior of aggregation of long-chain imidazolium ILs is analogous to the case of traditional surfactants. However, the CAC values of these ILs are lower by about 30 % compared to those of the typical cationic surfactants $C_n\text{TAB}$ with the same hydrocarbon chain, and their aggregation number (Tables 3 and 4) is 10–15 times smaller

than those of the C_n TAB surfactants. This may be attributed to the difference in the head group size.

Jungnickel et al. [22] reported a study on the aggregates formation of a homologous series of 1-alkyl-3-methylimidazolium derivatives with alkyl chain lengths $n = 4-18$. The CACs of these ILs were reproducibly determined by conductivity and surface tension. From these data, the degree of ionization and the standard Gibbs energy of aggregation were calculated as a function of alkyl chain length of the imidazolium cations. A significant correlation between retention times in reversed phase gradient high performance liquid chromatography (HPLC) and the CACs of the ILs was observed. It was also shown that the CACs were directly related to the lipophilicity of cations of the ionic liquids.

Wang et al. [31, 32] studied the aggregation behavior of $[C_n\text{mim}]\text{Br}$ ($n = 4, 6, 8, 10, 12$) and $[C_4\text{mim}][\text{BF}_4]$ in aqueous solutions by conductivity, volume, fluorescence probe, and NMR technologies. The critical aggregation concentrations of the ionic liquids, the ionization degree of the aggregates, and the standard Gibbs energy of aggregation were obtained. It was shown that no aggregation occurs for $[C_4\text{mim}]\text{Br}$ in aqueous solutions, $[C_6\text{mim}]\text{Br}$ and $[C_4\text{mim}][\text{BF}_4]$ form weak aggregates above the critical aggregation concentration, while the aggregation of $[C_8\text{mim}]\text{Br}$, $[C_{10}\text{mim}]\text{Br}$, and $[C_{12}\text{mim}]\text{Br}$ is strong enough to form micelles above their CACs. The alkyl chain length of a cation can then be tailored to switch the aggregation behavior of ILs in aqueous solutions.

The adsorption and aggregation behavior of a chiral long-chain ionic liquid, *S*-3-hexadecyl-1-(1-hydroxy-propan-2-yl)-imidazolium bromide ($[C_{16}\text{hpim}]\text{Br}$) in aqueous solution were described by Li et al. [34]. The CAC value obtained for this IL is similar to 1-cetyl-3-methylimidazolium bromide ($[C_{16}\text{mim}]\text{Br}$), but lower than the conventional ionic surfactants, demonstrating that long-chain imidazolium ILs have superior capability for the formation of aggregates. The maximum surface excess concentration of $[C_{16}\text{hpim}]\text{Br}$ is lower than $[C_{16}\text{mim}]\text{Br}$ due to the larger head group size of $[C_{16}\text{hpim}]\text{Br}$. This relatively large headgroup size of $[C_{16}\text{hpim}]\text{Br}$ and higher electrostatic repulsion between these headgroups also result in a looser packing of the resulting aggregates. Thus, a higher micropolarity and smaller aggregation number are observed compared with the conventional cationic surfactants with the same length of hydrophobic chain.

Zhang et al. [35] reported the results on the aggregation of 1-alkyl-3-methylimidazolium-based ionic liquids ($[C_n\text{mim}]\text{Br}$, $n = 8, 10, 12,$ and 16) in aqueous solutions using UV spectrum, electrical conductivity, and resonance light scattering. This investigation reveals the aggregation differences between the surface active $[C_n\text{mim}]\text{Br}$ and the traditional surfactants. Hydrogen bonds were suggested to play a dominant role in the aggregation of ILs in addition to coulombic and hydrophobic interactions. Compared with the traditional cationic surfactants, these ILs display a stronger aggregation due to the formation of the hydrogen bonded network. Such hydrogen bonded network also results in the loose arrangements of imidazolium rings in the subaggregates of $[C_n\text{mim}]\text{Br}$ ($n < 10$).

Eighteen mono- and di-cationic imidazolium bromide ILs were investigated by Baltazar et al. [28]. Surface tension measurements were used to determine the CAC

values of these ILs, and a correlation between the substituted alkyl chain length and the CAC values was reported. A comparison of the mono-cationic and di-cationic imidazolium ILs indicates that the mono-cationic imidazolium ILs generally have higher CACs than the di-cationic imidazolium ILs. The CAC values for different classes of di-cationic ionic liquids were found to decrease with increasing length of the linkage chain connecting the two imidazolium rings, and also to depend on the nature of the free alkyl side chain.

3 Thermodynamics of Aggregates Formation

Thermodynamic analysis on the aggregation behavior of ILs by using Gibbs energy, enthalpy and entropy of aggregate formation, is important for a deeper understanding of the driving forces and some molecular details involved in the aggregation processes [36]. The effect of the structure of ILs, in particular the alkyl chain length of the cations, can be reflected by thermodynamic parameters. Often these thermodynamic properties can be derived from measurements of the variation of the critical aggregation concentration of ILs with temperature by applying the mixed electrolyte model and phase separation model reported in the literatures [30, 40].

Using electrical conductivity methods [30, 40], CAC values of imidazolium ILs with alkyl chains length $n = C_{12}-C_{16}$ in aqueous solutions were determined at different temperatures. It is known that, for aqueous solutions of conventional ionic surfactant, the critical micelle concentration first decreases to a certain point and then increases with increasing temperature, which creates a U-shape dependence with a minimum temperature (T_{\min}) close to room temperature [41–44]. It can be seen from Fig. 2 that the curves of CACs vs temperature for ionic liquids have a similar shape. The effect of temperature on the CACs of surfactants in aqueous solution is usually a result of two opposing factors. It may be assumed that similar behavior could be observed in the case of aqueous IL solutions. First, when the temperature increases, the degree of hydration of the ionic imidazolium head domain decreases, leading to the increase of hydrophobicity of cations of the ionic liquids. This favors the aggregation process, and aggregation can take place at a lower concentration. On the other hand, with the increase of temperature, the structured water around the hydrophobic domain would be partially broken. This is unfavorable to the aggregation, as the low entropy of the structured water is a key driving force for the self-association process [45, 46]. Thus it is possible for us to assume that at lower temperatures the first effect is predominant, and after passing T_{\min} the second effect becomes evident. Values of T_{\min} depend on the hydrophobicity of the alkyl chain and the counterions. More hydrophobic amphiphiles have lower T_{\min} values [47].

The mixed electrolyte model [30] and phase separation model [40] have been used to estimate the thermodynamic parameters for the formation of ILs aggregates.

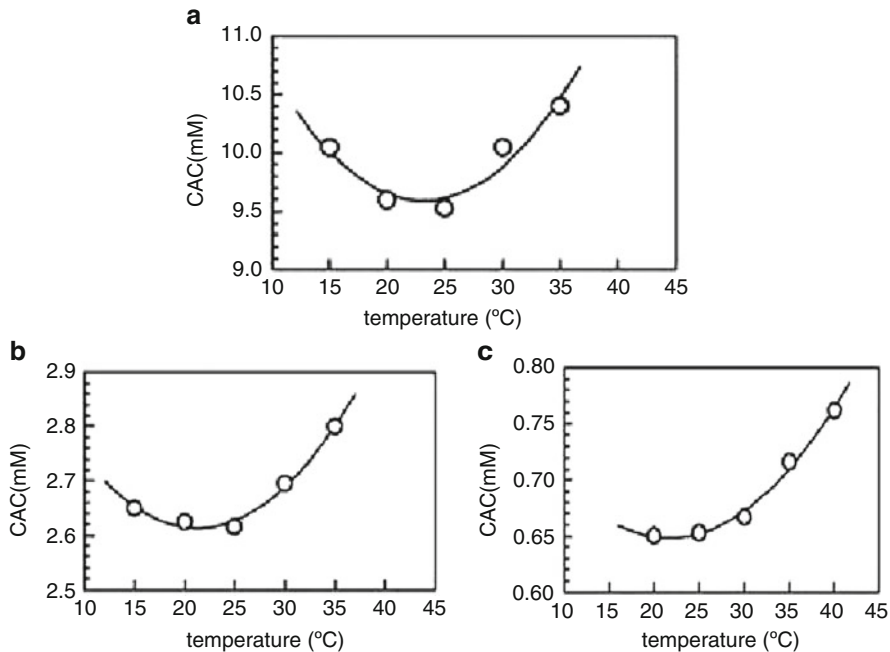


Fig. 2 Plots of CAC against temperature for the ILs: (a) [C₁₂mim]Br; (b) [C₁₄mim]Br; (c) [C₁₆mim]Br (Reprinted from [30])

The standard Gibbs energy of aggregation (ΔG_m^0) can be calculated from the following equation:

$$\Delta G_m^0 = (2 - \alpha)RT \ln \chi_{CAC} \quad (1)$$

where χ_{CAC} is the critical aggregation concentration expressed in mole fraction scale and α is the ionization degree of the aggregates. The standard enthalpy of aggregation (ΔH_m^0) can be derived from the ΔG_m^0 values as a function of temperature by applying the Gibbs–Helmholtz equation:

$$\Delta H_m^0 = \left[\frac{\partial(\Delta G_m^0/T)}{\partial(1/T)} \right] \quad (2)$$

and the standard entropy of aggregation ΔS_m^0 can be obtained from

$$\Delta S_m^0 = \frac{\Delta H_m^0 - \Delta G_m^0}{T} \quad (3)$$

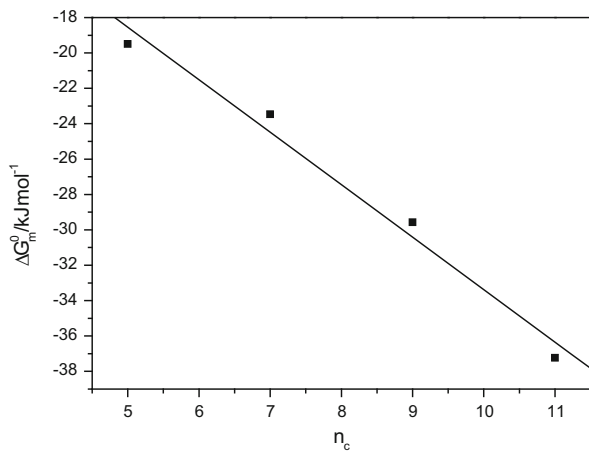


Fig. 3 Linear plot between ΔG_m^0 of $[\text{C}_n\text{mim}]\text{Br}$ at 298.15 K and the number of carbons in the alkyl chains (Reprinted from [31])

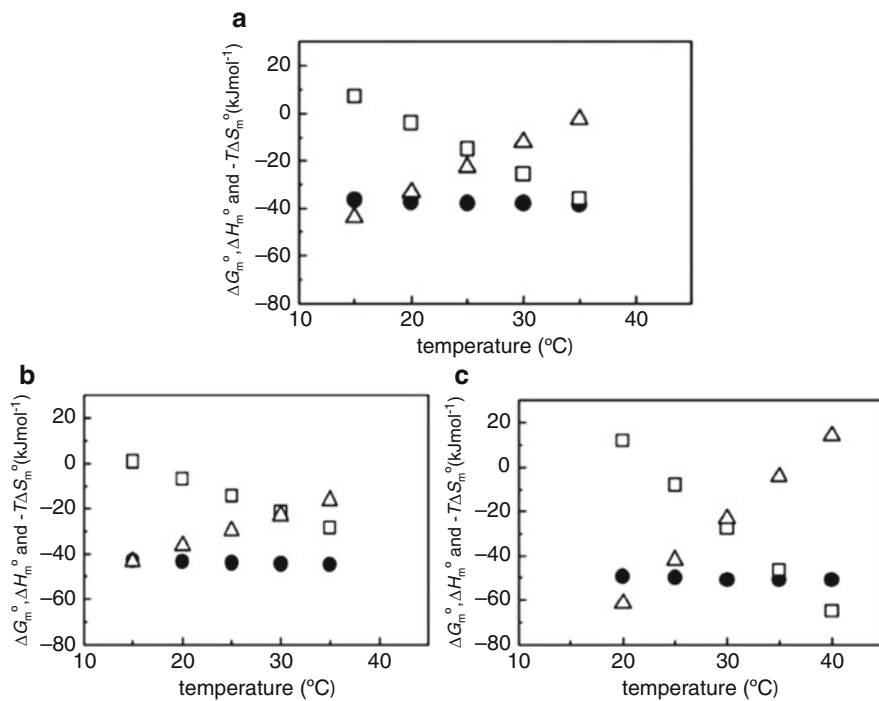


Fig. 4 Variation of the thermodynamic parameters for the micelle formation of ILs with temperature: (a) $[\text{C}_{12}\text{mim}]\text{Br}$; (b) $[\text{C}_{14}\text{mim}]\text{Br}$; (c) $[\text{C}_{16}\text{mim}]\text{Br}$. Symbols: circles ΔG_m^0 , squares ΔH_m^0 , triangles $T\Delta S_m^0$ (Reprinted from [30])

Figure 3 shows the standard Gibbs energy of aggregation of imidazolium ILs at 298.15 K as a function of the alkyl chain length of cations. This figure provides the following information: (1) the Gibbs energy change was found to be negative, implying as expected that aggregation of ionic liquids occurs spontaneously once the CAC is reached; (2) the longer the alkyl chain of ILs, the more negative the standard Gibbs energy of aggregation, indicating that the aggregation comes more easily with the increase of the alkyl chain length of ILs; (3) the aggregation is driven by alkyl chain-ion inductive and hydrocarbon-hydrocarbon interactions [31].

Figure 4 shows the thermodynamic parameters thus obtained for aggregate formation of long-chain imidazolium ILs as a function of temperature. As can be seen, first, ΔH_m^0 decreases with the increase in temperature, and then it changes its sign from positive to negative at 20–25°C. This means that the aggregate formation process is endothermic at lower temperature and exothermic at higher temperature, and this is the origin of the appearance of a minimum in CAC at 20–25°C. Second, $-T\Delta S_m^0$ increases with the increase in temperature, and intersects with ΔH_m^0 at 25–30°C. This indicates that the entropy term ($-T\Delta S_m^0$) plays a dominant role in negative ΔG_m^0 below the crossing temperature, while the contribution from an enthalpy term becomes dominant above this temperature. In other words, the process for aggregate formation of long-chain imidazolium ILs is driven by entropy at lower temperature, while driven by enthalpy at higher temperature.

Zhao et al. [48] also investigated the aggregation behavior of the ionic liquid *N*-alkyl-*N*-methylpyrrolidinium bromide (C_n MPB, $n = 12, 14$ and 16) in aqueous solutions by surface tension, electrical conductivity, and static luminescence quenching measurements. The critical aggregation concentrations at different temperatures and a series of thermodynamic parameters (ΔG_m^0 , ΔH_m^0 , and ΔS_m^0) for the ILs aggregation were evaluated from electrical conductivity measurements in the temperature range 25–45°C. Their thermodynamic parameters also show that the aggregate formation is an entropy-driven process at low temperature and an enthalpy-driven process at high temperature.

Because the enthalpy and entropy parameters have been derived indirectly from measurements of the variation of the critical aggregation concentration with temperature, these parameters have an intrinsic large uncertainty. Nowadays, more and more studies show that calorimetry is the most sensitive technique for the direct and precise measurements of the thermodynamic properties involving ILs aggregation [36, 37].

The thermodynamic parameters for the aggregation of $[C_n\text{mim}]\text{Cl}$ ($n = 8, 10, 12,$ and 14) in aqueous solution have been reported by Bai et al. [36] using isothermal titration calorimetry and conductivity. It was shown that the increase in alkyl chain length of the ILs causes a decrease in all thermodynamic parameters, ΔG_m^0 , ΔH_m^0 , and $T\Delta S_m^0$. The large negative values of the Gibbs energy are primarily due to an entropic contribution, an effect common in aggregation processes driven by hydrophobicity. Nevertheless, the percentage of the Gibbs energy change that is due to the enthalpic term increases with increasing alkyl chain length. Further it was

found that the aggregation process was mainly driven by entropy, as is common in aggregation processes induced by hydrophobicity.

Geng et al. [37] also used isothermal titration microcalorimetry and surface tension measurements to study the aggregation of three long-chain imidazolium ionic liquids, [C₁₂mim]Br, [C₁₄mim]Br, and [C₁₆mim]Br, in aqueous solutions. It was found that the process of aggregation is also driven by entropy. An enthalpy–entropy compensation study reveals the effect of alkyl chain length on the aggregation: the longer the alkyl chain, the easier it is to form aggregates. Their results showed that [C₁₄mim]Br and [C₁₆mim]Br act as ideal surfactants in the aggregation process because there are no aggregate–aggregate interactions, whereas [C₁₂mim]Br does not behave ideally because of aggregate–aggregate interactions in the high concentration solutions.

3.1 Effect of Cationic Structure on the Aggregation of Ionic Liquids

With the possibility of fine-tuning hydrophobicity of ILs by changing the alkyl chain length, the type of headgroup, and the nature of the anions, one can modulate the structure of these aggregates. This leads to the modification of some major characteristics such as the critical aggregate concentration, the average aggregation number (N_{agg}), and the physicochemical properties in the aggregation processes of ionic liquids. Therefore, a number of research projects have been focused on the effect of cationic structure on the self-aggregation of ILs in aqueous solutions.

For a homologous series of linear single-chain amphiphiles, the CACs follow the empirical Stauff-Klevens rule [49], which suggests a logarithmic relationship between CAC and the number of carbon atoms in the alkyl chain as shown in the following equation:

$$\log(\text{CAC}) = A - Bn_c \quad (4)$$

where A and B are constants for a given homologous series at a given temperature, and n_c is the number of carbon atoms in the alkyl chain. The constant A changes with the nature of the hydrophilic groups, while B is a constant which measures the effect of each additional methylene group on the CAC. It can be seen from Table 5 that the B value is approximately 0.5, 0.28–0.30, and 0.25 for nonionic amphiphiles, paraffin chain salts with a single ionic head group, and divalent ionic surfactants, respectively [50]. For different homologues, the A values are considerably variable, whereas B is close to $\log 2$, which indicates that addition of each $-\text{CH}_2$ group to a hydrocarbon chain reduces the CAC of these compounds by about a factor of 2. Based on this rule, the CAC values can be estimated for surfactants with various chain lengths [51].

Table 5 Values of *A* and *B* from Stauff-Klevens equation for various surfactants and ILs

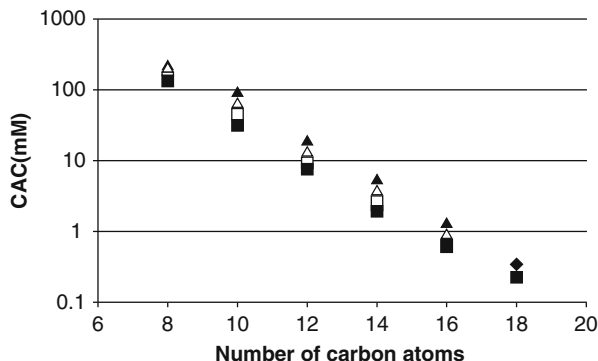
Compound	T/K	<i>A</i>	<i>B</i>
Typical surfactant [49]			
Na carboxylates	293	2.41	0.341
K carboxylates	298	1.92	0.290
K carboxylates	318	2.03	0.292
Alkane sulfonates	313	1.59	0.294
Alkane sulfonates	323	1.63	0.294
Alkyl sulfates	318	1.42	0.295
Alkylammonium chlorides	298	1.25	0.265
Alkylammonium chlorides	318	1.79	0.296
Alkyltrioxyethylene glycol monoether	298	2.32	0.554
Alkydimethylamine oxide	300	3.3	0.5
Alkyltrimethylammonium bromides	333	1.77	0.292
Ionic liquid			
Alkyl-methyl-imidazolium bromides [28]	298	0.29	4.29
Alkyl-methyl-imidazolium bromides [18]	298	0.30	4.6
Alkyl-methyl-imidazolium bromides [31]	298	0.325	1.845
Alkyl-methyl-imidazolium bromides [46]	298	0.32	1.78
Alkyl-methyl-imidazolium chlorides [19]	298	0.29	4.7
Alkyl-methyl-imidazolium chlorides [22]	298	0.28	4.51
Alkyl-butyl-imidazolium bromides[28]	298	0.34	4.41
Alkyl-bis-butyl-imidazolium bromides [28]	298	0.16	3.77
<i>N</i> -alkyl- <i>N</i> -Methylpyrrolidinium bromides [28]	298	0.30	4.72
1-alkylpyridinium bromides [46]	298	0.31	1.71

It is known that CAC values of single alkyl chain amphiphiles decrease with addition of $-\text{CH}_2$ groups to the alkyl chain, resulting from elongation of the hydrophobic part of the surfactant molecules, which favors aggregate formation. The CAC is also dependent on the relative sizes of their hydrophilic and hydrophobic domains. A larger hydrophobic domain would result in a lower CAC, and a more hydrophilic domain area would result in a higher CAC [50].

As far as ILs are concerned, the results indicate that elongation of the alkyl chain decreases the CAC values of ILs as shown in Table 1. This implies that an increase of hydrophobic alkyl chain of the cations favors the formation of ionic liquid aggregates as has been shown above for surfactants. For homologous series of ILs, the linear relationship described by Eq. 4 has been proved to be valid. The *B* value is comparable to that established for ionic surfactants, such as alkylpyridinium bromides, alkyltrimethylammonium chlorides, alkylpyridinium chlorides, and alkyltrimethylammonium bromides.

The introduction of the second alkyl substituent on the imidazolium cations may also play a dominant role in CAC values of ionic liquids. For example, the lower CAC values have been observed for the ILs with butyl substituents instead of methyl in the imidazolium ring [28].

Fig. 5 CAC dependence on the number of carbon atoms in alkyl chains of some ILs and cationic surfactants at 298 K: (filled diamonds) $[C_n\text{mim}]\text{Cl}$; (open squares) $[C_n\text{mim}]\text{Br}$; (filled triangles) $C_n\text{TAC}$; (Δ) $C_n\text{TAB}$ and (filled squares) SAS (Reprinted from [52])



In order to compare the critical aggregation properties of ILs with some typical cationic surfactants, the CAC values of trimethylammonium chloride ($C_n\text{TACl}$), bromide ($C_n\text{TAB}$), and sodium alkyl sulfate (SAS) were collected. It is shown that the CAC values of $[C_n\text{mim}]\text{Br}$ ionic liquids lay between those of $C_n\text{TAB}$ and SAS containing the same number of carbon atoms in the alkyl moiety. An analogical relationship was found for $[C_n\text{mim}]\text{Cl}$, $C_n\text{TACl}$ and SAS, as shown in Fig. 5. This might be ascribed to the special structure of the imidazolium head group which allows the possible formation of a hydrogen bond with water, but the same is not true for the head group of $C_n\text{TAB}$. This may also be the result of interactions between anion and aromatic ring in imidazolium derivatives which did not occur in the case of typical surfactants.

The influence of the type of ring in the cations on the aggregation behavior was also investigated. The underlying reason for this effect is very complex because head groups have two opposing effects: (1) repulsive interaction related with electrostatic repulsion, hydration and steric hindrance and (2) attraction interaction arising from a need to minimize hydrocarbon-water contacts. The stronger hydrophobicity of the cations favors the aggregation of the ILs in aqueous solutions, and the stronger binding strength of the cation with a given anion can decrease the repulsive interaction between the head groups and then the CAC values. In contrast, the bigger steric hindrance of the cations causes an increase in the CAC values of the ILs. For example, Wang et al. [53] reported that the CAC values of 1-octyl-methylimidazolium bromide ($[C_8\text{mim}]\text{Br}$), 1-octyl-4-methylpyridinium bromide (4 m- $[C_8\text{pyr}]\text{Br}$), and 1-methyl-1-octylpyrrolidinium ($[C_8\text{mpyr}]\text{Br}$) increase in the order 4 m- $[C_8\text{pyr}]\text{Br} < [C_8\text{mim}]\text{Br} < [C_8\text{mpyr}]\text{Br}$. This indicates that the ability of the cations to form aggregates follows the order $[C_8\text{mpyr}]^+ < [C_8\text{mim}]^+ < 4\text{ m-}[C_8\text{pyr}]^+$. It was reported that there was an increase in hydrophobic tendency for the cations in the order $[C_n\text{mim}]^+ < [C_n\text{mpyr}]^+ < [C_n\text{mpyr}]^+$ [54]. On the basis of this observation, the CAC values of the investigated ILs should increase in the order $[C_8\text{mpyr}]\text{Br} < 4\text{ m-}[C_8\text{pyr}]\text{Br} < [C_8\text{mim}]\text{Br}$. Obviously, the experimental result is not the case. However, the order of van der Waals volumes of the cations was found to be $[C_4\text{mpyr}]^+ (167 \text{ \AA}^3) > [C_4\text{mim}]^+ (150 \text{ \AA}^3) > [C_4\text{pyr}]^+ (144 \text{ \AA}^3)$ [55], and the qualitative order of $[C_4\text{mim}]^+ > [C_4\text{pyr}]^+ > [C_4\text{mpyr}]^+$ has

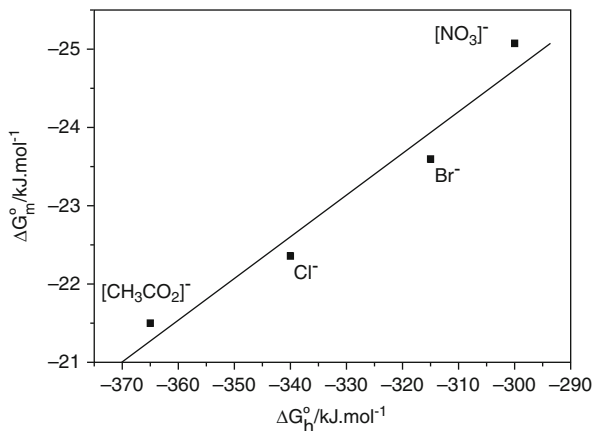
been observed for the intrinsic binding strength of the cations with Br^- [56]. From this information it seems likely that the aggregation is controlled mainly by the balance among the factors of hydrophobicity of the cations, binding strength of the cations with a given anion, and the steric repulsion between the cations. The aggregates of $[\text{C}_8\text{mpyr}]\text{Br}$ were formed unfavorably due to probably its biggest van der Waals volume, that is, the biggest steric hindrance and the weakest interaction with Br^- . On the other hand, it is clear that the difference in steric hindrance between $[\text{C}_8\text{mim}]^+$ and 4 m- $[\text{C}_8\text{pyr}]^+$ is small. Therefore, compared with $[\text{C}_8\text{mim}]^+$, the stronger aggregation of 4 m- $[\text{C}_8\text{pyr}]^+$ is driven by its stronger hydrophobicity.

Blesic et al. [57] found that 1-dodecyl-3-methylpyridinium bromide ($[\text{C}_{12}\text{mpy}]\text{Br}$) and 1-methyl-1-dodecylpiperidinium bromide ($[\text{C}_{12}\text{mpip}]\text{Br}$) have almost the same CAC values in water. Probably, in the case of $[\text{C}_{12}\text{mpip}]\text{Br}$, the two effects compensate each other. On the one hand, the higher hydrophobicity of the $[\text{C}_{12}\text{mpip}]^+$ cation and stronger bound anion, Br^- , in comparison with the $[\text{C}_{12}\text{mpy}]^+$ cation, where the positive charge is delocalized, would give a lower CAC. On the other hand, because these two cations have a different geometry and volume, we can expect that, compared with the boat and/or chair structures of a cyclic six-membered ring of a planar aromatic molecule, the more space-demanding $[\text{C}_{12}\text{mpip}]^+$ cation has a higher CAC because of the steric hindrance effect.

In the case of gemini ILs, the CAC values depend on the length of the alkyl linkage chain connecting the two cations, and on the length of the free alkyl substituents on three positions of the imidazolium head group. Increasing the lengths of the linking chains results in a linear decrease of the CACs. Analogically elongation of the free alkyl chain causes the same effect [28]. The partitioning behavior of such gemini IL aggregates in water is comparable to mono cationic aggregates, and it has been found that the size of the alkyl chain influences the partitioning of nonpolar solvents inside the aggregates. However, gemini ILs were found to have a lower partitioning to nonpolar solvents. It was theorized that the gemini IL aggregates, even though they have a lower CAC, form less well defined aggregates [58].

The degree of ionization (α) is also an important characteristic parameter for ILs aggregation in water. The degree of ionization is the fraction of charges of amphiphile ions in the aggregates neutralized by aggregate-bound counterions. Monomer amphiphiles are entirely dissociated in solution, but in their aggregates they are partially associated with the counterions. The degree of ionization of the aggregate was calculated from the ratio of the slopes of the two linear fragments of the experimental conductivity curves [59]. A lower α value indicates a better packed aggregate. Usually, slightly decreased α values are observed for conventional ionic surfactants with elongation of the alkyl chain. A similar trend is also found for ILs [28].

Fig. 6 Linear plot of the standard Gibbs energy of aggregation of the ILs (ΔG_m^0) vs the Gibbs energy of hydration of the anions (ΔG_h^0) (Reprinted from [53])



3.2 Effect of Anionic Type on the Aggregation of Ionic Liquids

For the ionic liquids of imidazolium salts, the nature of their anions determines the water solubility of ionic liquids and cation–anion interactions. Consequently, the aggregation of ILs in water is also affected by the nature of ILs anions. The role of anions in the aggregation of imidazolium ILs in water has been systemically studied by us [53]. It is found that, for a given $[\text{C}_8\text{mim}]^+$ cation, there is a pronounced effect of the anions on the values of CAC and α of the ILs. These values increase in the sequence: $[\text{CF}_3\text{COO}]^- < [\text{NO}_3]^- < \text{Br}^- < \text{Cl}^- < [\text{CH}_3\text{COO}]^-$. In other words, the ability of these anions to promote aggregation of the ILs follows the order $[\text{CF}_3\text{COO}]^- > [\text{NO}_3]^- > \text{Br}^- > \text{Cl}^- > [\text{CH}_3\text{COO}]^-$. This anionic effect correlates well with the Hofmeister series of the anions for cationic surfactants [60]. In general, the formation of IL aggregates in water is dictated by a balance between the repulsive headgroup interactions and the attractive forces arising from a need to minimize the exposure of the hydrophobic core to water. The anions act by altering both of these forces. Adsorption of the anions onto the surface of aggregates can reduce the repulsive headgroup interactions, thereby lowering the CAC values of the ILs. So the position of an anion in this series is considered to depend on its hydrated radius/polarizability, hydrophobicity, and bulkiness of the anions. A decreased hydration radius of the anions is usually accompanied by an increased polarizability. A high polarizability should enhance the binding of the anions at the aggregates surface and decrease the electrostatic repulsion between the head groups of the ILs, thus increasing the tendency towards aggregation and lowering both values of α and CAC. However, no formation of the aggregates was detected for the ILs with $[\text{CF}_3\text{SO}_3]^-$ and $[\text{ClO}_4]^-$ as anions, because the systems broken down into two phases before any bulk aggregation occurred. This ascribed to the much weaker hydration of the anions and then low solubility of the ILs in aqueous solutions. Rebelo et al. [19] also found that, when the Cl^- anion in

[C₁₀mim]Cl was replaced by [NTf₂]⁻ or [PF₆]⁻ anion, no micelle formation was detected because the low water solubility of these ILs induced phase separation before their bulk aggregation.

The anions also markedly affect the standard Gibbs energy of aggregation of ILs, and the effect follows the Hofmeister series. The ILs with the larger anions show the stronger effect, while those with smaller hydrophilic anions, which have higher values of hydration Gibbs energy, are only weakly incorporated in the aggregation phases. It can be seen from Fig. 6 that the ΔG_m^0 values correlate reasonably well with Gibbs energies of hydration of the anions [61], indicating that the Hofmeister series is strongly related to the nature of the hydration shell of the anions. Interaction of anions with cationic moiety of the headgroup of these ILs is stronger for readily dehydrated ions than for those with tight hydration shells. The decreased values of ΔG_m^0 indicate that the aggregation becomes much easier with increasing hydrophobicities of the anions. One possible explanation is that the increased hydrophobicity enhanced anionic penetration of the interface and the electrostatic interactions with the ILs headgroup accordingly decreased the repulsive headgroup interactions. These results are similar to those reported by Bunton et al. [62] for the interactions between cetyltrialkylammonium bromides and methyl naphthalene 2-sulfonate.

Aggregation number is a major parameter for the structure of IL aggregates. It was found that the average aggregation number generally increases with increasing hydrophobicity of the anions, indicating that the growth of aggregates is favored by the increased hydrophobicity. This result was similar to the counterionic effect of some typical surfactants [63]. Thus, it is appropriate to conclude that the anions with stronger hydrophobicity can bind the cations more strongly and reduce the repulsive interaction between head groups, and thus enhance the growth of the aggregates.

3.3 Effect of Added Salts on the Aggregation of Ionic Liquids

Aggregation behavior of ILs could be easily modulated by the addition of inorganic salts. It is well known that for typical ionic surfactants, the addition of an electrolyte reduces the repulsion between charged groups at the surface of the micelle by the screening effect. This phenomenon can be observed in the case of the CAC lowering. For ionic compounds this effect is more significant than for nonionic ones because the interaction is stronger in the case of the former. Presence of salts usually influences water structure and then hydration of the head groups, leading to salting-in and salting-out effects. When the monomers are salted-out by an electrolyte, the CAC would be reduced, and if the monomers are salted-in, the reverse takes place [60, 64]. For nonionic surfactants, the influence of salts is weaker but nevertheless significant.

The effect of salts on the formation of IL aggregates depends on the nature of anions and cations of the salts and the ionic liquids. For example, the addition of

NaCl, Na₂SO₄, and tetrabutylammonium bromide to aqueous IL solutions was investigated by Blesic et al. [19]. All these electrolytes diminish the CACs of the ILs; moreover, addition of the short chain IL of [C₂mim]Cl into aqueous solution of the long-chain IL of [C₁₀mim]Cl also causes the same effect. In this case, the short chain IL behaves as a simple electrolyte throughout the interaction with Stern layer of the micelle, and screens the ionic charge of that surface [19]. Zheng et al. [29, 65] studied the effect of sodium halides (NaCl, NaBr, and NaI) on the aggregation behavior of [C_{*n*}mim]Br (*n* = 10, 12, 16) in water. It was found that the addition of salts significantly decreases the CACs of the ILs, and the anion dependence of the salt effect is analogous to the case of conventional ionic surfactants: Cl⁻ < Br⁻ < I⁻. It is known that the hydration of these anions decreases in the order Cl⁻ > Br⁻ > I⁻, suggesting that the anion being less hydrated is more effective in neutralizing the charges on the micelle surface. The influence of NaCl and Na₂SO₄ on the surface chemical and aggregation characteristics of ionic liquids [C₈mim]Cl, [C₈mim]Br, and [C₈mim]I in water was monitored through surface tension and small angle neutron scattering measurements [66]. It was shown that the addition of salts also drastically decreased the CAC values and increased the area per adsorbed IL molecule. The co-ions of salts modify the surface of ILs and prefer to form aggregates through various interactions such as charge neutralization, specific interactions, and dehydration.

In recent work we systematically investigated the influence of 15 kinds of salts on the aggregation behavior of [C₁₀mim]Br in aqueous solutions by conductivity, fluorescence, and dynamic light scattering [67]. It was shown that NaCl, NaBr, NaI, CH₃CO₂Na, NaSCN, NaNO₃, NaBrO₃, NaClO₃, C₆H₅COONa, Na₂CO₃, Na₂SO₄, Na₂C₄H₄O₆, and Na₃CH₅O₇ have salting-out effects on the aggregation of [C₁₀mim]Br and, at a given salt concentration, the effect of anions of the added salts on the CAC value of the IL increases in the sequence SCN⁻ < I⁻ < C₆H₅COO⁻ < ClO₃⁻ < NO₃⁻, C₄H₄O₆²⁻ < C₆H₅O₇³⁻ < Br⁻ < SO₄²⁻ < CO₃²⁻ < Cl⁻ < BrO₃⁻ < CH₃COO⁻. This specific effect correlates well with the Hofmeister series of the anions, and can be explained by the hydrophobicity of these anions. For a given salt, the logarithm of CAC values of the IL decreases linearly with increasing concentration of the salt, which can be described by the empirical equation of salt effect for the conventional surfactants:

$$\log(CAC/CAC_0) = a - km_s \quad (5)$$

where *CAC* and *CAC*₀ are the critical aggregation concentrations with and without salt, *m_s* is molality of the added salt, and *a* and *k* are adjusted parameters.

The effect of the added salts on the degree of anions binding at the aggregates surface, the standard Gibbs energy of aggregation, and the aggregation number of [C₁₀mim]Br also basically follow the Hofmeister series of the anions. Values in the degree of anion binding and aggregation number of the IL increase with increasing salt concentrations to a different extent for a given salt. It was also found that the size of aggregates increases with increasing hydrophobicity of anions of the salts.

The results suggest that hydrophobicity of the anions plays an important role in the salt effect on the aggregation of $[\text{C}_{10}\text{mim}]\text{Br}$ in aqueous solutions. The possible reason is that the stronger hydrophobicity of anions enhances their binding on the aggregate surface and decreases the electrostatic repulsion between the ionic head groups of the IL, thus promoting the IL aggregation, increasing the aggregation number, and lowering the CAC value of the ionic liquid.

However, FeBr_3 and AlBr_3 were found to have salting-in effects on the aggregation of $[\text{C}_{10}\text{mim}]\text{Br}$ in aqueous solutions. The possible reason is that tetrahedral complex FeBr_4^- (or AlBr_4^-) was formed from Br^- and FeBr_3 (or AlBr_3) in aqueous solutions. FeBr_4^- and AlBr_4^- anions have larger radius and less charge density compared with Br^- . They cannot decrease effectively the electrostatic repulsion between the ionic head groups of the IL, but can interact with the hydrophobic moiety of the cation of the IL, thus decreasing the tendency of the IL aggregation and then increasing its CAC.

Based on the binding mechanisms of anions on the aggregates surface of cetyltrimethylammonium bromide (CTAB) [68] and cetyltrimethylammonium chloride (CTAC) [69], SCN^- , I^- , ClO_3^- , NO_3^- , $\text{C}_4\text{H}_4\text{O}_6^{2-}$, $\text{C}_6\text{H}_5\text{O}_7^{3-}$, Br^- , SO_4^{2-} , CO_3^{2-} , Cl^- , BrO_3^- , and CH_3COO^- can be considered to be adsorbed on the surface of the aggregates due to their weak or moderate association with the IL cation, whereas the aromatic anions, like $\text{C}_6\text{H}_5\text{COO}^-$, penetrate inside the aggregates with their hydrophilic groups staying in the IL head group region and the hydrophobic groups partially embedded into the hydrophobic core of the aggregates.

3.4 *Effect of Organic Additives on the Aggregation of Ionic Liquids*

Studies on the influence of organic solvents on the aggregation behavior of ILs are of great importance, not only in the field of colloid and interface science but also in the development of potential chromatographic applications of IL aggregates. Micellar liquid chromatography (MLC) is a chromatographic technique using surfactants in the mobile phase at concentrations above the CAC [70–72]. Most applications of MLC require the utilization of hybrid micellar mobile phases which contain surfactants at concentrations above the CAC and form ternary systems upon addition of organic solvents [71, 73, 74]. Few traditional surfactant systems have successfully been used in MLC [72, 75]. In this sense, it is important to understand the effect of organic solvents in aqueous solutions on the ILs aggregates when intending to expand the applicability of MLC with these designer surfactants.

It was reported that a few organic compounds can influence the CACs and other properties of micellar solutions. The presence of a small amount of surface active organic impurities may create a characteristic minimum in the area of CAC in the curves of surface tension against concentration. These impurities are usually

present in commercial materials and originate from the synthesis of surfactants. Such minima were also observed in the commercial ILs. The impurities may be adsorbed onto the interface at concentrations below CAC and then solubilized in the aggregates at concentrations above the CAC. Generally, CAC values may be affected by the compounds which can be incorporated in the outer region of the aggregates.

The addition of methanol, 1-propanol, 1-butanol, 1-pentanol, and acetonitrile to the aqueous solutions of ILs 1-hexadecyl-3-butylimidazolium bromide and 1,3-didodecylimidazolium bromide was investigated by Pino et al. [76]. Similar to the traditional ionic surfactants, increases in the CAC values have been observed for both ILs when concentration of the organic solvents increases in aqueous solutions, with the largest increase achieved with 1-pentanol, and being more significant for 1,3-didodecylimidazolium bromide. The authors suggest that when organic solvent content increases in water, the dielectric constant of the mixtures is lowered, producing an increase in the electrostatic forces of the ionic head groups in the ILs micelle. At the same time, the interactions between the hydrophobic groups of the ILs are gradually reduced. Both effects justify the higher CAC values observed as the content of organic solvent increases.

Recently we carried out a systematic study [77] on the influence of ethylene glycol, dimethylsulfoxide, diethylene glycol, triethylene glycol, formamide, acetonitrile, methanol, ethanol, 1-propanol, and acetone on the aggregation behavior of [C₁₂mim]Br in water. It was found that the critical aggregation concentration, the ionization degree of the aggregates, and the standard Gibbs energy of aggregation of the ionic liquid increase, while its aggregation number and aggregates size decrease with increasing concentration of organic additives in water. These observations were explained through the solvophobic effect of alkyl chain of the ionic liquid for the water-organic solvents. In a simple physical picture, aqueous organic solvents can better dissolve the alkyl chain of the IL than water, resulting in the decrease of aggregation ability of the IL, thus increasing the CAC values and decreasing the aggregation number and the aggregate size of the ionic liquid. Interestingly, a linear relationship between the logarithm of CAC of the IL and the solvophobic parameter (S_p) of hydrocarbon in the studied water-organic mixed solvents is found, and this linear relationship can be described by the equation

$$\log(\text{CAC}) = m + n S_p \quad (6)$$

Therefore, we can modulate the aggregation behavior of ILs by choosing the right S_p value for a particular application.

3.5 *Effect of Surfactant on the Aggregation of Ionic Liquids*

Modification of the surfactant CACs may also be completed by the addition of the second surfactant in the way of synergism, which may result in the desired properties and performance. For example, mixtures of ionic and nonionic surfactants are commonly used in many practical applications because the solution behavior of these surfactants can be complementary. Mixed micelles formed are considered to be more versatile than the micelles formed by single surfactant. Examples of such applications are detergency and enhanced oil recovery. As far as more complex systems are concerned, mixtures of ionic and nonionic surfactants and mixtures of surfactants with different alkyl chain lengths or different head group structures have been examined in some detail [78].

To date only the influence of SDS on the aggregation behavior of imidazolium ILs with variable alkyl chain lengths has been evaluated in aqueous solutions [17, 79]. It was shown that with the increase of SDS concentrations, [C₈mim]Cl can be dissolved in water. This phenomenon can be linked to the formation of mixed micelles. The results obtained indicate the possibility of using ionic liquids to modify the properties of conventional micelles in a controlled way, which is important in many applications. Ionic liquid cosurfactants may play important roles if micelles themselves cannot provide the desired properties, such as surface tension, viscosity, and dispersion stability [17]. It was also observed that short chain ILs increase the CAC values of SDS probably as a result of hindering ion pair formation, whereas in the case of long-chain ILs, synergism was observed as a decreased CAC [19].

4 Self-Aggregation of Ionic Liquids in Nonaqueous Solutions

It is well known that, unlike in aqueous solution, the aggregation behavior of traditional surfactants is very complex in nonaqueous solutions. Surfactants also forms micelles in polar organic solvents and invert micelles in nonpolar organic solvents. Sometimes, dimer, triplet, and micelles simultaneously exist in surfactant solutions. Therefore, studies on the aggregation of surfactant in nonaqueous solutions are limited, and the related aggregation behavior is poorly understood. It was reported that polarity, dielectric constant, and other physicochemical properties of the solvents affect the extent and the nature of self-assembly of surfactants in nonaqueous solutions. However, can the ionic liquids form aggregates in nonaqueous solution, and how do the solvent properties affect their aggregation behavior in nonaqueous solvents? Answers to these fundamental questions are not very clear at present.

Dorbritz et al. [80] studied the aggregation behavior of [C₄mim][BF₄] ionic liquid in methanol, 2-propanol, and ethyl acetate by electrospay ionization mass

spectrometry. They observed the formation of aggregates $[\text{C}_4\text{mim}]_n[\text{BF}_4]_{n-1}$ and $[\text{C}_4\text{mim}]_n[\text{BF}_4]_{n+1}$, and found that with increasing polarity of the solvent and decreasing concentration of the IL, the size of the formed aggregates decreased. Han and his coworkers [81] investigated the aggregation behavior of $[\text{C}_4\text{mim}][\text{BF}_4]$ and $[\text{C}_4\text{mim}][\text{PF}_6]$ in some organic solvents by UV-vis spectroscopy and conductivity measurements. It was demonstrated that the aggregation of these ILs depended strongly on the dielectric constant of the solvents. Dupont and coworkers [82] suggested that the ILs with 1,3-dialkylimidazolium as cation and tetrafluoroborate, hexafluorophosphate and tetraphenylborate as anions could form supramolecular aggregates in CHCl_3 . In our recent work, aggregation behavior of $[\text{C}_{12}\text{mim}]\text{Br}$ in acetonitrile, ethylene glycol, *N,N*-dimethylformamide, formamide, and dimethylsulfoxide solvents was investigated by conductivity and volume measurements [83]. Solvophobic parameters have been introduced to account for the interaction between alkyl chains of the IL and the solvents. It is shown that solvophobic effects and the hydrogen-bonding interaction between the IL anion and the solvents are the main factors affecting the aggregation of ILs in nonaqueous solvents.

5 Microscopic Structure of Ionic Liquids Aggregates

The unique properties and abnormal behavior exhibited in chemical synthesis and material preparation in ionic liquids are closely dependent on the microstructure of ILs in solutions. Thus study of the microstructure of IL aggregates has received increasing attention, and many methods such as small angle neutron scattering (SANS), transmission electron microscopy (TEM), nuclear magnetic resonance (NMR), and molecular dynamics simulations (MD) have been used in this field. In this context, Bowers and coworkers [16] investigated microstructure of the aggregates of $[\text{C}_8\text{mim}]\text{Cl}$, $[\text{C}_8\text{mim}]\text{I}$, and $[\text{C}_4\text{mim}][\text{BF}_4]$ in aqueous solutions by SANS. It was found that the $[\text{C}_4\text{mim}][\text{BF}_4]$ formed polydisperse spherical aggregates above its CAC, $[\text{C}_8\text{mim}]\text{I}$ behaved as regularly sized near-spherical charged micelles, while $[\text{C}_8\text{mim}]\text{Cl}$ displayed weak long-range ordering of possibly disklike particles. In addition, Goodchild et al. [26] also used SANS to study aggregate structure of $[\text{C}_n\text{mim}]\text{X}$ ($n = 2, 4, 6, 8, 10$; $\text{X} = \text{Cl}, \text{Br}$) in water. It was reported that at the concentration just above the CAC, $[\text{C}_8\text{mim}]^+$ - and $[\text{C}_{10}\text{mim}]^+$ -based ILs formed small near-spherical aggregates, which, after initial growth, possess core radii of $10.5 \pm 0.5 \text{ \AA}$ and $13.2 \pm 0.5 \text{ \AA}$, respectively, at the intermediate concentrations. Towards higher concentrations, the aggregates appear to grow, with the aggregates in the $[\text{C}_{10}\text{mim}]\text{Br}$ system becoming increasingly elongated (prolate) with increasing concentration. No evident aggregates are formed in the systems with $[\text{C}_2\text{mim}]^+$ and $[\text{C}_4\text{mim}]^+$. In the $[\text{C}_6\text{mim}]^+$ system, it appears that oblate aggregates with radius $\sim 9 \text{ \AA}$ are formed at the CAC and that the radius increases with increasing concentration of the ionic liquid.

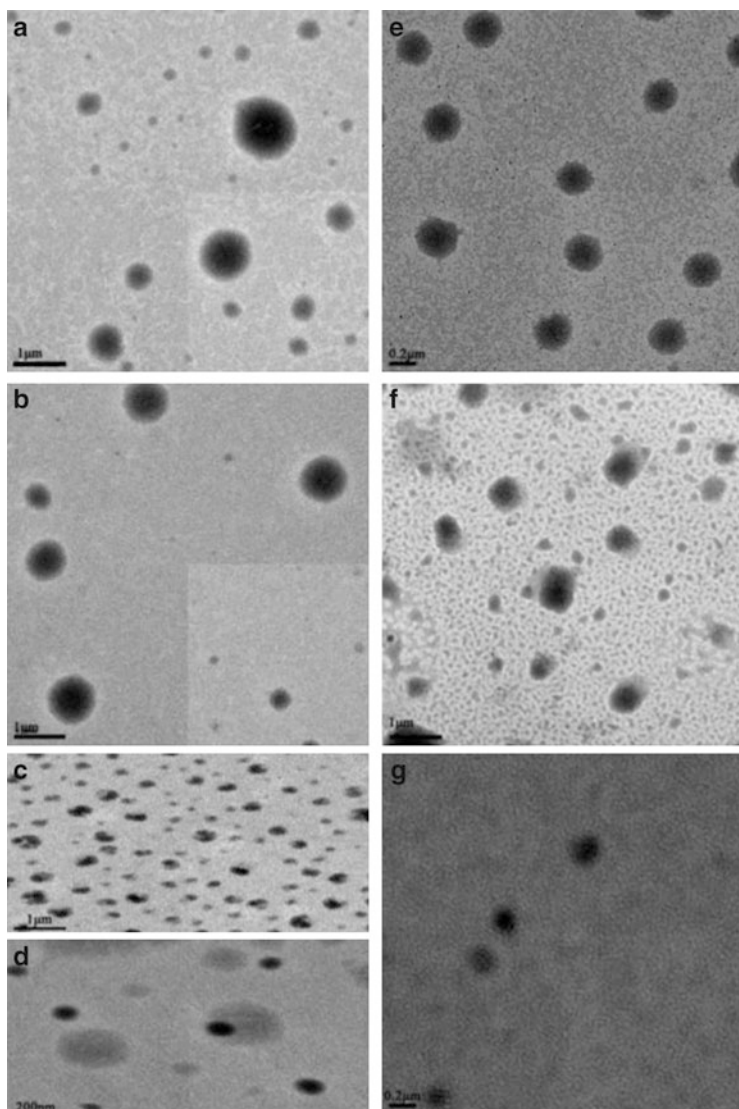
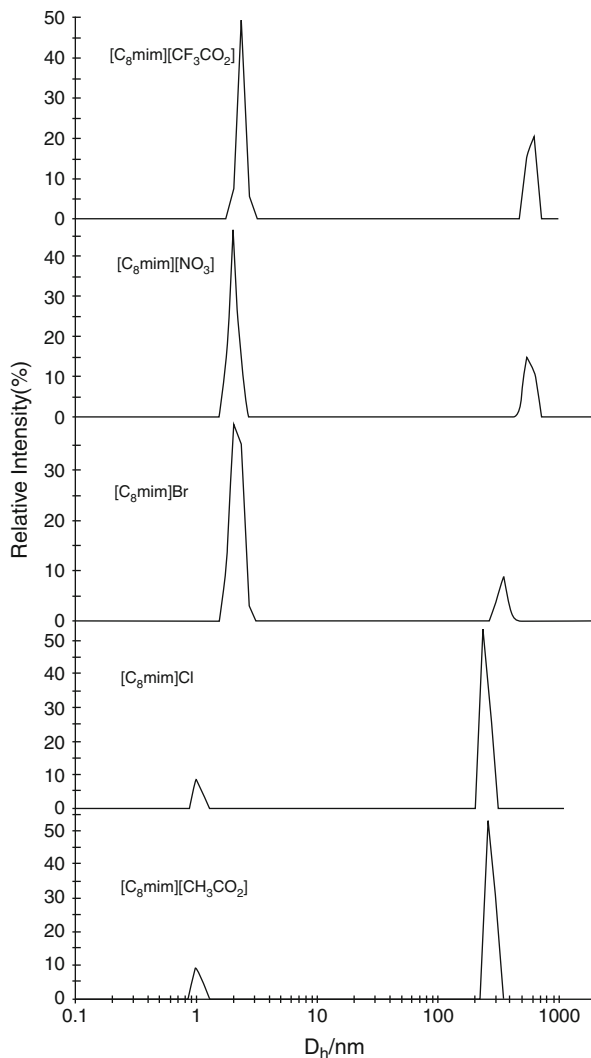


Fig. 7 TEM images of the aggregates of ILs: (a) $[\text{C}_8\text{mim}][\text{CF}_3\text{COO}]$; (b) $[\text{C}_8\text{mim}][\text{NO}_3]$; (c) $[\text{C}_8\text{mim}][\text{CH}_3\text{COO}]$; (d) $[\text{C}_8\text{mim}]\text{Br}$; (e) $[\text{C}_8\text{mim}]\text{Cl}$; (f) $[\text{C}_8\text{mpyr}]\text{Br}$; (g) $4\text{m}-[\text{C}_8\text{pyr}]\text{Br}$ at the ILs concentration of 0.45 mol/L (Reprinted from [53])

The morphologies and sizes of $[\text{C}_8\text{mim}]\text{X}$ ($\text{X} = \text{Cl}, \text{Br}, \text{NO}_3, \text{CH}_3\text{COO}$ and CF_3COO), $[\text{C}_8\text{mpyr}]\text{Br}$, and $4\text{m}-[\text{C}_8\text{pyr}]\text{Br}$ aggregates in water were examined by TEM and dynamic light scattering [53]. The investigated ILs were found to form spherical aggregates (Fig. 7). Structures of the anions and cations have a very weak

Fig. 8 Size distribution for the aggregates of the ILs from DLS measurements at 0.45 mol/L of $[C_8mim]X$ ($X = Cl, Br, NO_3, CH_3COO, CF_3COO$) at 298.15 K (Reprinted from [53])



effect on the morphology, but they do affect the aggregate sizes. The size of the spherical aggregates of the ILs with different anions increased with increasing hydrophobicity of the anions (Fig. 8).

Based on the chemical shift of various protons of $[C_4mim]Cl$, $[C_4mim][BF_4]$, $[C_8mim]Cl$, and $[C_4mpy]Cl$ in water as a function of IL concentrations, the schematic models of aggregates of these ILs were proposed by Singh et al. [84] as shown in Fig. 9. It can be seen that the imidazolium and pyridinium rings of $[C_4mim][BF_4]$ and $[C_4mpy]Cl$ are positioned at the aggregate surface in a configuration favorable for ring stacking through Π - Π interactions as evidenced by the

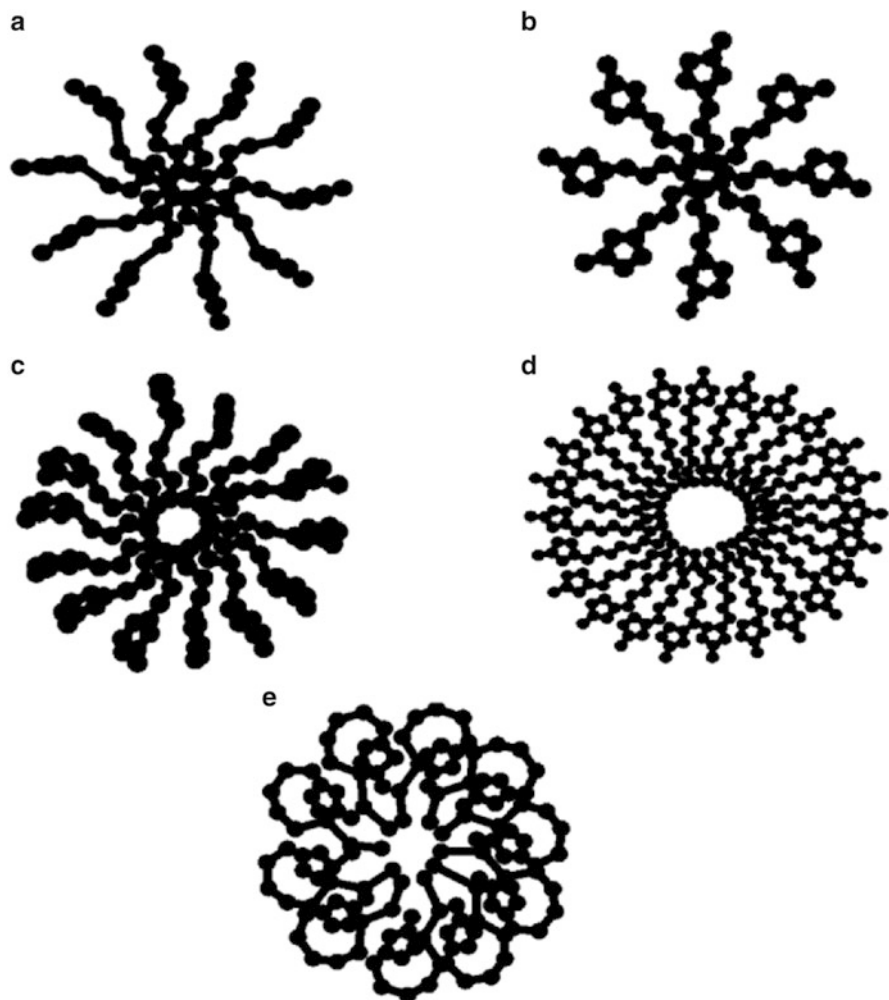


Fig. 9 Schematic models of the aggregates of different ILs: (a) $[\text{C}_4\text{mim}][\text{BF}_4]$; (b) $[\text{C}_4\text{mim}]\text{Cl}$; (c) $[\text{C}_4\text{mpy}]\text{Cl}$; (d) $[\text{C}_8\text{mim}]\text{Cl}$ (with $N_{\text{agg}} = 23$); (e) $[\text{C}_8\text{mim}]\text{Cl}$ (with $N_{\text{agg}} = 10$) (Reprinted from [84])

NMR measurements, whereas the imidazolium ring of $[\text{C}_4\text{mim}]\text{Cl}$ and $[\text{C}_8\text{mim}]\text{Cl}$ is shown in a configuration not favorable for ring stacking.

The microenvironment of different protons of cations of $[\text{C}_n\text{mim}]\text{Br}$ ($n = 4, 6, 8, 10, 12$) in the aggregated state was probed by the spin lattice relaxation rate for protons of the ILs [32]. It is suggested that the imidazolium rings of the cation in the aggregates were exposed to water and that the molecular motion of the aggregates is more restricted than that of the monomer of the ILs. The methyl group attached to the imidazolium ring stuck out from the surface of the aggregate into the water.

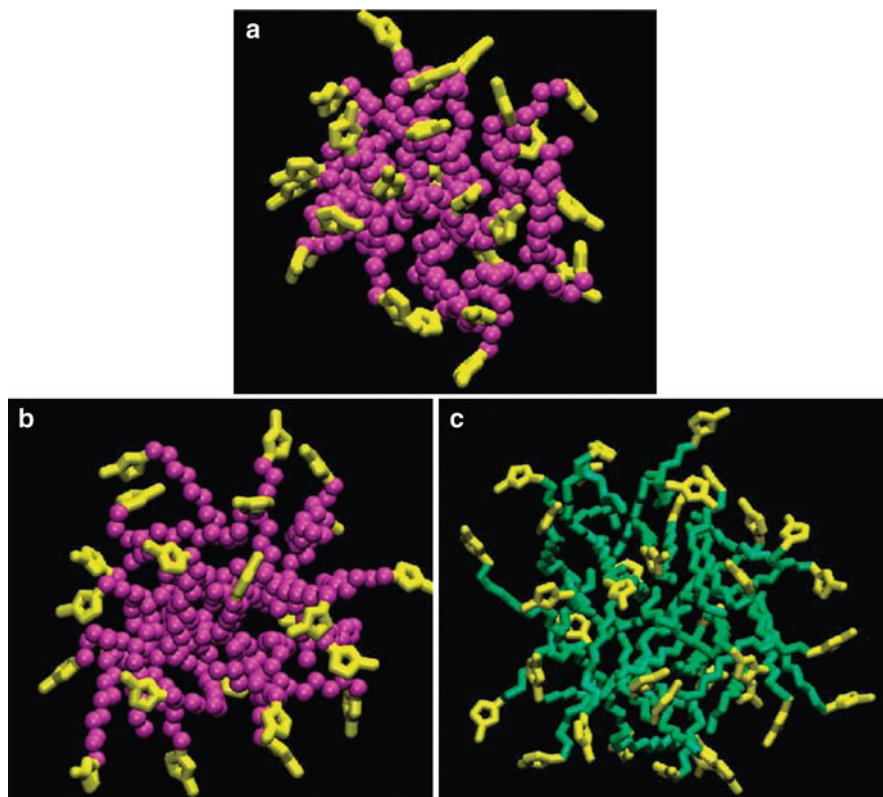


Fig. 10 Snapshot of aggregates from various aqueous solutions studied: (a) $[C_{10}\text{mim}]\text{Br}$; (b) $[C_{12}\text{mim}]\text{Br}$; (c) $[C_{14}\text{mim}]\text{Br}$. In parts (a) and (b) atoms belonging to the alkyl tail are represented as *magenta* spheres and those belonging to headgroup are shown in *yellow*. In part (c) tail group atoms are shown in *green* and headgroup atoms in *yellow*. Hydrogen atoms of the cations are not shown. Water molecules, anions, and cations not belonging to the shown aggregate are removed for ease of visualization (Reprinted from [86])

The aggregate structures of $[C_n\text{mim}]\text{Br}$ ($n = 10, 12, 14, 16$) in water were conducted by molecular dynamics simulations [85, 86]. It was found that in all the systems, quasi-spherical polydisperse aggregates were formed by the spontaneous self-assembly of the amphiphilic cations. As shown in Figs. 10 and 11, the alkyl tails of the cations are buried deep inside the aggregates with the polar imidazolium group exposed to exploit the favorable interactions with water. The aggregation numbers steadily increase with the chain length. The hexadecyl aggregates have the most ordered internal structure of the systems studied, and the alkyl chains in these cations show the least number of gauche defects. Anions and water are not found at the core of the aggregates, though water molecules are found to penetrate to some degree. The anions are found to be isotropically distributed throughout the system.

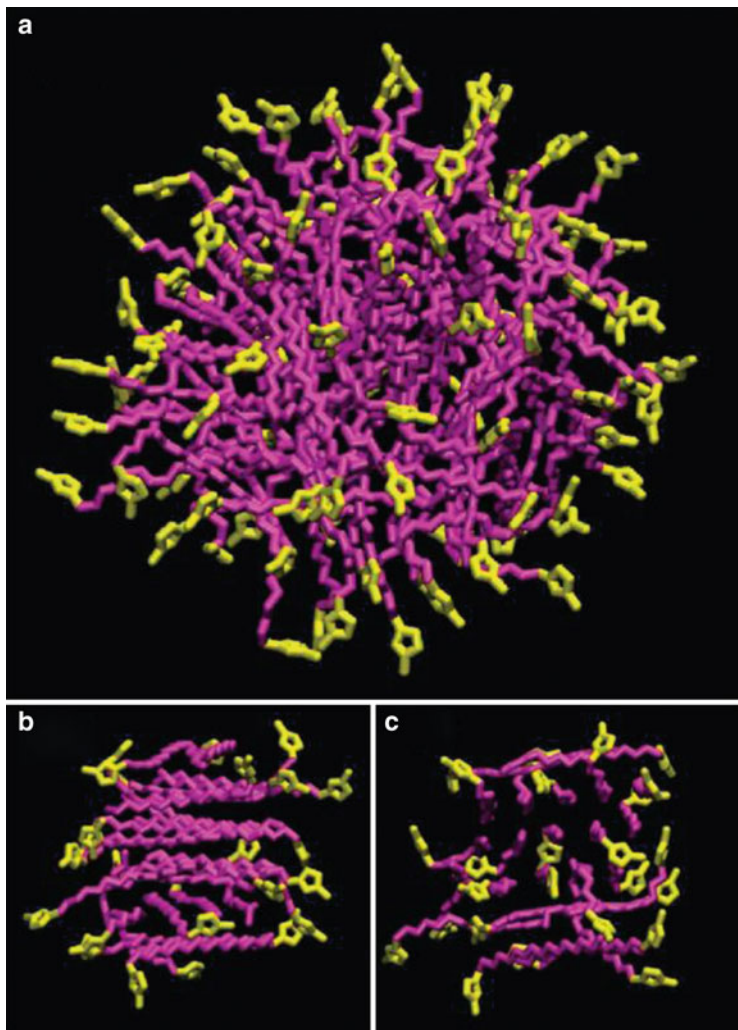


Fig. 11 Snapshot of aggregates from aqueous $[C_{16}mim]Br$ solutions: (a) largest aggregate observed; (b, c) another aggregate from different viewing angles. Tail group atoms are shown in *magenta* and headgroup atoms in *yellow*. Hydrogen atoms of the cations are not shown. Water molecules, anions, and cations not belonging to the shown aggregate are removed for ease of visualization (Reprinted from [86])

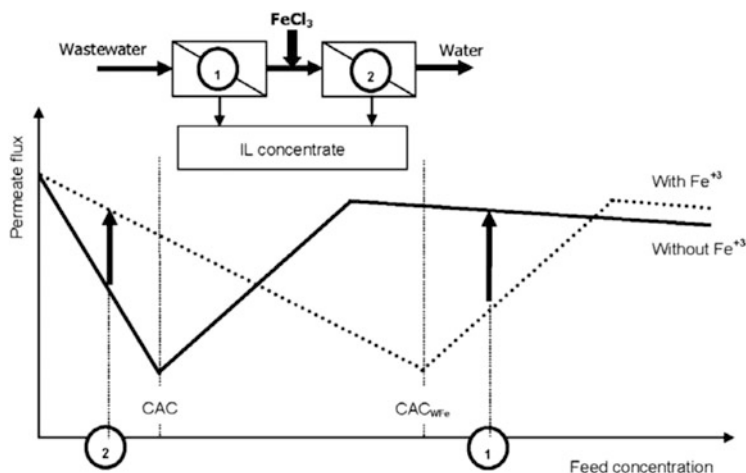


Fig. 12 Permeate flux obtained in a two-stage membrane filtration scheme (Reprinted from [87])

6 Application of Ionic Liquids Aggregation

The aggregation behavior of ILs in solutions plays an important role in the application of ILs in material synthesis, biochemicals separation, disposal of ILs wastewater, and others. Herein the role played by ILs can be understood through the following four examples.

Recycling of ILs from water/solutions is an important issue that addresses the economics of ionic liquid use, and also reduces concerns about disposal, biodegradation and toxicity of ionic liquids. Based on the fact that ionic liquids show a similar behavior to that of surfactants in membrane filtration and the aggregation behavior of ILs in water can be controlled and regulated by the addition of inorganic salt, Fernández et al. [87] analyzed the potential of aggregation control to improve the performance of downstream membrane separations by using the system of [C₈mim]Cl plus iron(III) chloride (FeCl₃). The addition of FeCl₃ has a significant salt-in effect on the aggregation of [C₈mim]Cl, and an increase in CAC value of the IL has consequences regarding the design of the corresponding membrane filtration system. A two-stage membrane filtration scheme was proposed and shown in Fig. 12. It can be seen that wastewater with higher ionic liquid concentration is fed to the first stage and at this moment, the IL aggregates are formed due to its lower CAC value, and then high permeate flux is obtained. The retentate stream with low ionic liquid concentration is fed to the second stage after adding FeCl₃. In this case, the permeate flux is located at the point indicated by arrow ② in Fig. 12. Obviously, permeate flux after the addition of FeCl₃ is higher than the original situation without FeCl₃ in the second stage.

Systems affording controllable formation and breakage of amphiphilic aggregates may be of significant value in the areas such as controlled release,

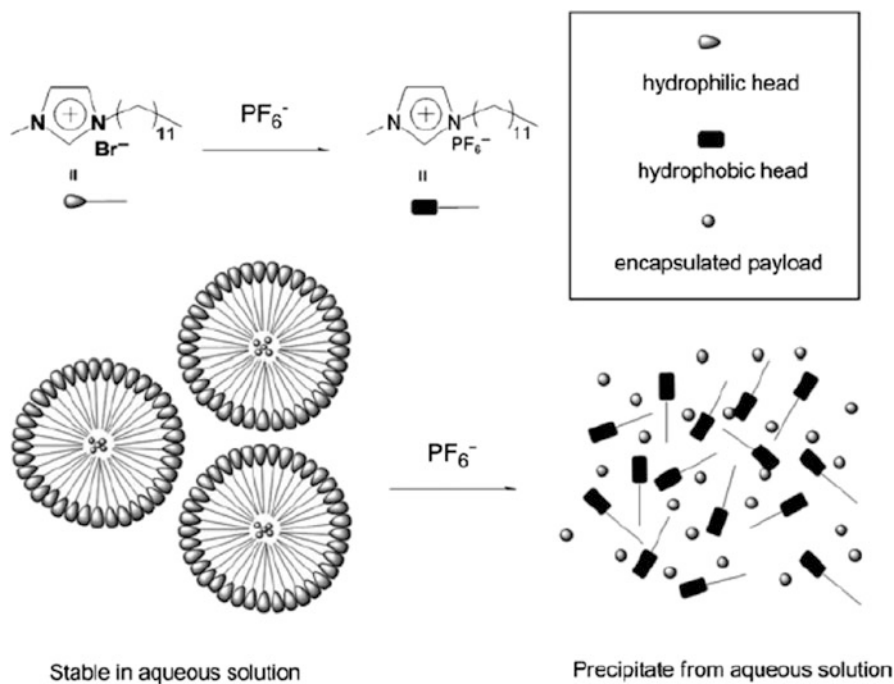


Fig. 13 Anion exchange to $[\text{PF}_6]^-$ and resulting micelle collapse (Reprinted from [88])

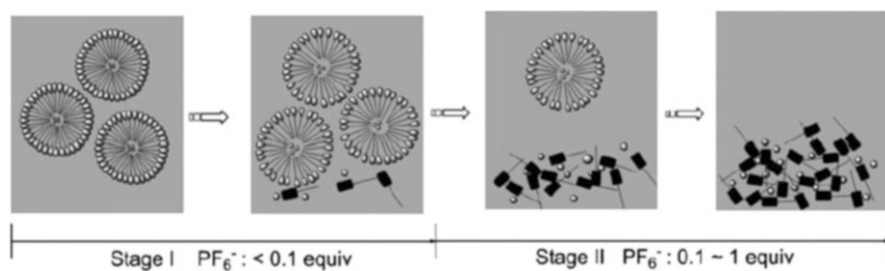


Fig. 14 Illustration of the dissociation of micelles and the release of encapsulated payload by adding $[\text{PF}_6]^-$ (Reprinted from [88])

drug delivery, nanosynthesis, cleaning, and petroleum recovery in oil fields. Niu et al. [88] succeeded in proposing a simple but efficient, rapid, and quantitative ion-responsive micelle system based on counter-anion change of an ionic liquid with $[\text{C}_{12}\text{mim}]^+$ as cation. As shown in Fig. 13, upon exchange of Br^- to $[\text{PF}_6]^-$, micelles that $[\text{C}_{12}\text{mim}]\text{Br}$ formed in aqueous system exhibited progressive, and ultimately complete disaggregation because $[\text{C}_{12}\text{mim}][\text{PF}_6]$ is insoluble in water. To explore the potential application of this system for controlled release of micellar payloads, different amounts of $[\text{PF}_6]^-$ were added to Nile-Red-loaded $[\text{C}_{12}\text{mim}]\text{Br}$

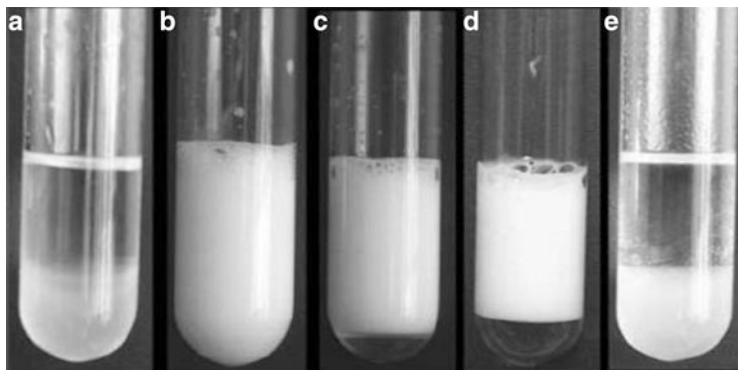


Fig. 15 The photographs of the oil–water emulsions: (a) 2:1 (v/v) cyclohexane/water mixture; (b) with $[C_{12}mim]Br$, shaken 3 min; (c) $[C_{12}mim]Br$ -induced emulsion after 1 h; (d) $[C_{12}mim]Br$ -induced emulsion after 50 h; (e) approximately 2 min after adding 1 equiv $NaPF_6$ to (b) (Reprinted from [88])

micellar solution. It is interesting to note that the controlled release of the hydrophobic dye (Nile-Red) was successfully achieved. Figure 14 shows the procedure of the dissociation of the micelles and the release of the encapsulated payload by adding $[PF_6]^-$. It can be seen that when ~ 0.1 equiv of $[PF_6]^-$ was added, conversion of $[C_{12}mim]Br$ to $[C_{12}mim][PF_6]$ (with subsequent extraction from the micelles and desolubilization) caused little overall micelle disruption. In this case (Stage I), the micelles remained metastable and minimal Nile Red was transferred to the aqueous phase from the micelle. However, as the concentration of added $[PF_6]^-$ was in the range 0.1 to 1 equiv (Stage II), micelle disassociation increased significantly with corresponding release of the encapsulated Nile Red. In this process, $[C_{12}mim][PF_6]$ was formed and then precipitated.

The applicability of $[C_{12}mim]Br$ for stabilizing – and $[C_{12}mim][PF_6]$ for subsequently breaking – oil–water emulsions was also investigated by Niu and coworkers [88]. Towards this end, 95 mg of $[C_{12}mim]Br$ was added to a vial containing 6 mL of 2:1 (v/v) cyclohexane/water. The mixture was shaken thoroughly and a milk-white emulsion (Fig. 15b) was observed. The resulting emulsion showed little evidence of separation until after ~ 1 h, at which point a clear lower liquid phase began to appear (Fig. 15c). However, after 50 h, the emulsion still occupied $\sim 80\%$ of the liquid volume (Fig. 15d). In contrast, adding 1 equiv of $Na[PF_6]$ to a freshly shaken emulsion resulted in complete separation into two liquid layers within 2 min, with $[C_{12}mim][PF_6]$ precipitating (Fig. 15e). These observations indicate that the ion-exchange/desolubilization mechanism discussed here might have promise for practical industrial emulsion forming/separating applications, including oil transport.

The IL-based aqueous two-phase systems are novel aqueous two-phase systems. 1-Butyl-3-methylimidazolium dicyanamide ($[C_4mim][N(CN)_2]$) + K_2HPO_4

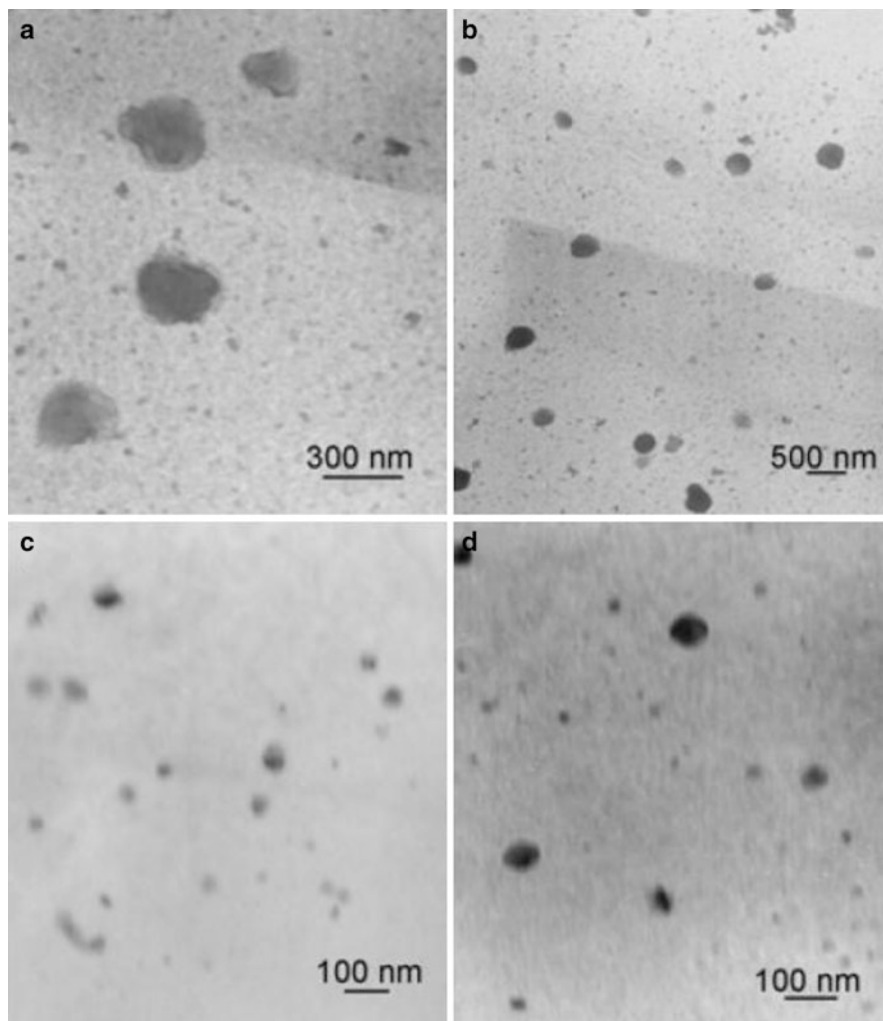


Fig. 16 TEM images of the aggregates of $[C_4mim][N(CN)_2]$ ($2.5 \text{ mol}\cdot\text{L}^{-1}$) with and without BSA ($1.23 \text{ g}\cdot\text{L}^{-1}$): (a, b) without BSA; (c, d) with BSA (Reprinted from [89])

aqueous two-phase system has been used by Wang et al. [89] to separate selectively bovine serum albumin (BSA) from aqueous saccharides. It was shown that 82.7–100 % BSA could be enriched into the top IL-rich phase and almost quantitative saccharides (arabinose, glucose, sucrose, raffinose or dextran) were preferentially extracted into the bottom phosphate-rich phase in a single-step extraction. Conductivity, DLS, and TEM studies indicated that the IL aggregates and IL aggregate-protein complexes were formed in the IL-rich phase (Fig. 16). It was suggested that the formation of the IL aggregate-protein complexes is the driving force for the selective separation.

7 Summary and Outlook

The above discussion has demonstrated that aggregation of ionic liquids takes place in both aqueous and nonaqueous solutions. Alkyl chain length, cationic structure, and anionic nature of ionic liquids, and addition of inorganic salts, organic solvents, and surfactants were found to have a vital effect on the critical aggregation concentration, the ionization degree of the aggregates, the standard Gibbs energy of aggregation, the aggregation number, and aggregate size. Therefore, the aggregation behaviors of ILs in solutions can be controlled and regulated by altering these factors. At the same time, the possible mechanism for the effect of these factors on the aggregation behavior of ILs in solutions has been analyzed, and the potential application of IL aggregation in the membrane separation of IL wastewater, controlled drug release, breakage of oil/water emulsions, and the selective separation of BSA from aqueous saccharides has been illustrated as well.

In summary, great progress has been made in fundamental and applied aspects on the aggregation behavior of ILs in solutions over the past decade. It can be expected that IL aggregation will find more and more applications in the future. However, research in this field is still in its infancy, and there are a number of issues which require further investigation. In future work, the following studies are suggested:

1. A deeper study should be carried out on the microstructure of IL aggregates. This is a very difficult task, and various experimental methods including macroscopic and microcosmic techniques and molecular simulation are needed. The structural information obtained would be used to establish the relationship between the structure of ionic liquids and their specific performance, which is valuable for the design and application of novel ionic liquids.
2. At present, the aggregation behavior of ionic liquids in nonaqueous and water-organic solutions is poorly understood. In this context, a better understanding of the interactions of alkyl chains of ionic liquids with various classes of organic molecules is essential although solvation of cations and anions of ionic liquids in nonaqueous media is also important.
3. The effect of light, heat, and solution pH on the aggregation behavior of ionic liquids in solutions should be investigated. Based on this knowledge, we can use light, heat, and solution pH to modulate the aggregation behavior of ionic liquids. This is a more advanced concept for the application of ionic liquids. For this purpose, design and synthesis of these functional ionic liquids are necessary.
4. Development of more technically relevant ILs is highly desired, and degradation, toxicity and environmental distribution of ILs aggregates ought to be examined as well.

References

1. Welton T (1996) Room-temperature ionic liquids. Solvents for synthesis and catalysis. *Chem Rev* 99:2071–2084
2. Swatloski RP, Holbrey JD, Rogers RD (2003) Ionic liquids are not always green: hydrolysis of 1-butyl-3-methylimidazolium hexafluorophosphate. *Green Chem* 5:361–363
3. Docherty KM, Kulpa J, Charles F (2005) Toxicity and antimicrobial activity of imidazolium and pyridinium ionic liquids. *Green Chem* 7:185–189
4. Wasserschein P, Welton T (2003) Ionic liquids in syntheses. VCH-Wiley, Weinheim
5. Rantwijk F, Lau RM, Sheldon RA (2003) Biocatalytic transformations in ionic liquids. *Trends Biotechnol* 21:131–138
6. Jain N, Kumar A, Chauhan S, Chauhan SMS (2005) Chemical and biochemical transformations in ionic liquids. *Tetrahedron* 61:1015–1060
7. Buzzeo MC, Evans RG, Compton RG (2004) Non-haloaluminate room-temperature ionic liquids in electrochemistry – a review. *Chemphyschem* 5:1106–1120
8. Endres F, Abedin SZE (2006) Air and water stable ionic liquids in physical chemistry. *Phys Chem Chem Phys* 8:2101–2116
9. Liu J, Jonsson JA, Jing G (2005) Application of ionic liquids in analytical chemistry. *Trends Anal Chem* 24:20–27
10. Zhao H, Xia S, Ma P (2005) Use of ionic liquids as ‘green’ solvents for extractions. *J Chem Technol Biotechnol* 80:1089–1096
11. Seddon KR (2003) Ionic liquids: a taste of the future. *Nat Mater* 2:363–365
12. Visser A, Swaltowski RP, Reichert RM, Mayton R, Sheff S, Wierzbicki A, Davis JH, Rogers RD (2002) Task-specific ionic liquids incorporating novel cations for the coordination and extraction of Hg^{2+} and Cd^{2+} : synthesis, characterization, and extraction studies. *Environ Sci Technol* 36:2523–2529
13. Zhang J, Yang C, Hou Z (2003) Effect of dissolved CO_2 on the conductivity of the ionic liquid [bmim][PF₆]. *New J Chem* 27:333–336
14. Ianchard LA, Gu Z, Brennecke JF (2001) High-pressure phase behavior of ionic liquid/ CO_2 systems. *J Phys Chem B* 105:2437–2444
15. Armstrong W, Anderson JL (2003) High-stability ionic liquids: a new class of stationary phases for gas chromatography. *Anal Chem* 75:4851–4858
16. Bowers JP, Butts CJ, Martin PC, Vergara-Gutierrez M (2004) Aggregation behaviour of aqueous solutions in ionic liquids. *Langmuir* 20:2191–2198
17. Miskolczy Z, Sebok-Nagy K, Biczok L, Gokturk S (2004) Aggregation and micelle formation of ionic liquids in aqueous solution. *Chem Phys Lett* 400:296–300
18. Vanyur R, Biczok L, Miskolczy Z (2007) Micelle formation of 1-alkyl-3-methylimidazolium bromide ionic liquids in aqueous solution. *Colloids Surf A Physicochem Eng Aspects* 299:256–261
19. Blesic M, Marques MH, Plechkova NV, Seddon KR, Rebelo LPN, Lopes A (2007) Self-aggregation of ionic liquids: micelle formation in aqueous solution. *Green Chem* 9:481–490
20. Huddleston JG, Visser AE, Reichert MW, Willauer HD, Broker GA, Rogers RD (2001) Characterization and comparison of hydrophilic and hydrophobic room temperature ionic liquids incorporating the imidazolium cation. *Green Chem* 3:156–164
21. Stepnowski P, Mrozik W, Nienhauser J (2007) Adsorption of alkylimidazolium and alkylpyridinium ionic liquids onto natural soils. *Environ Sci Technol* 41:511–516
22. Jungnickel C, Łuczak J, Ranke J, Fernández JF, Müller A, Thöing J (2008) Micelle formation of imidazolium ionic liquids in aqueous solution. *Colloids Surf A Physicochem Eng Aspects* 316:278–284
23. Modaressi A, Sifaoui H, Mięlczarz M, Domanska U, Rogalski M (2007) Influence of the molecular structure on the aggregation of imidazolium ionic liquids in aqueous solutions. *Colloids Surf A Physicochem Eng Aspects* 302:181–185

24. El Seoud OA, Pires PAR, Abdel-Moghny T, Bastos EL (2007) Synthesis and micellar properties of surface-active ionic liquids: 1-alkyl-3-methylimidazolium chlorides. *J Colloid Interface Sci* 313:296–304
25. Thomaier S, Werner K (2007) Aggregates in mixtures of ionic liquids. *J Mol Liq* 130:104–107
26. Goodchild I, Collier L, Millar SL, Prokš I, Lord JCD, Butts CPB, Bowers J, Webster JRP, Heenan RK (2007) Structural studies of the phase, aggregation and surface behaviour of 1-alkyl-3-methylimidazolium halide + water mixtures. *J Colloid Interface Sci* 307:455–468
27. Sirieix-Plénet J, Gaillon L, Letellier P (2004) Behaviour of a binary solvent mixture constituted by an amphiphilic ionic liquid, 1-decyl-3-methylimidazolium bromide and water: potentiometric and conductimetric studies. *Talanta* 63:979–986
28. Baltazar QQ, Chandawalla J, Sawyer K, Anderson JL (2007) Interfacial and micellar properties of imidazolium-based monocationic and dicationic ionic liquids. *Colloids Surf A Physicochem Eng Aspects* 302:150–156
29. Dong B, Li N, Zheng L, Yu L, Inoue T (2007) Surface adsorption and micelle formation of surface active ionic liquids in aqueous solution. *Langmuir* 23:4178–4182
30. Inoue T, Ebina H, Dong B, Zheng L (2007) Electrical conductivity study on micelle formation of long-chain imidazolium ionic liquids in aqueous solution. *J Colloid Interface Sci* 314:236–241
31. Wang J, Wang H, Zhang S, Zhang H, Zhao Y (2007) Conductivities, volumes, fluorescence, and aggregation behavior of ionic liquids $[C_n\text{mim}][\text{BF}_4]$ and $[C_n\text{mim}]\text{Br}$ ($n = 4, 6, 8, 10, 12$) in aqueous solutions. *J Phys Chem B* 111:6181–6188
32. Zhao Y, Gao S, Wang J, Tang J (2008) Aggregation of ionic liquids $[C_n\text{mim}]\text{Br}$ ($n = 4, 6, 8, 10, 12$) in D_2O : a NMR study. *J Phys Chem B* 112:2031–2039
33. Lianos P, Zana R (1981) Fluorescence probe studies of the effect of concentration on the state of aggregation of surfactants in aqueous solution. *J Colloid Interface Sci* 84:100–107
34. Li XW, Gao YA, Liu J, Zheng LQ, Chen B, Wu LZ, Tung CH (2010) Aggregation behavior of a chiral long-chain ionic liquid in aqueous solution. *J Colloid Interface Sci* 343:94–101
35. Zhang H, Li K, Liang H, Wang J (2008) Spectroscopic studies of the aggregation of imidazolium-based ionic liquids. *Colloids Surf A Physicochem Eng Aspects* 329:75–81
36. Bai G, Lopes A, Bastos M (2008) Thermodynamics of micellization of alkylimidazolium surfactants in aqueous solution. *J Chem Thermodyn* 40:1509–1516
37. Geng F, Liu J, Zheng L, Yu L, Li Z, Li G, Tung C (2010) Micelle formation of long-chain imidazolium ionic liquids in aqueous solution measured by isothermal titration microcalorimetry. *J Chem Eng Data* 55:147–151
38. Cornellas A, Perez L, Comelles F, Ribosa I, Manresa A, Garcia MT (2011) Self-aggregation and antimicrobial activity of imidazolium and pyridinium based ionic liquids in aqueous solution. *J Colloid Interface Sci* 355:164–171
39. Singh T, Kumar A (2008) Self-aggregation of ionic liquids in aqueous media: a thermodynamic study. *Colloids Surf A Physicochem Eng Aspects* 318:263–268
40. Łuczak J, Hupka J, Thoeming J, Jungnickel C (2007) In: Wilk KA (ed) International scientific conference, surfactants and dispersed systems in theory and practice. PALMA Press, Wrocław/Ksiaz Castle
41. Rodriguez JR, Gonzalez-Perez A, Del Castillo JL, Czapkiewicz J (2005) Thermodynamics of micellization of alkyl dimethylbenzylammonium chlorides in aqueous solutions. *J Colloid Interface Sci* 250:438–443
42. Chen L, Shi-Yow L, Chung-Chang H, En-Ming C (1998) Temperature dependence of critical micelle concentration of polyoxyethylenated non-ionic surfactants. *Colloids Surf A Physicochem Eng Aspects* 135:175–181
43. Mehta SK, Bhasin KK, Chauhan R, Dham S (2005) Effect of temperature on critical micelle concentration and thermodynamic behavior of dodecyl dimethylammonium bromide and dodecyl trimethylammonium chloride in aqueous media. *Colloids Surf A Physicochem Eng Aspects* 255:153–157

44. Muller N (1993) Temperature dependence of critical micelle concentrations and heat capacities of micellization for ionic surfactants. *Langmuir* 9:96–100
45. Richard CR, Wildin JL, Rapp AL, Moyna GM (2007) Hydrogen bonds in ionic liquids revisited: (35/37)Cl NMR studies of deuterium isotope effects in 1-n-butyl-3-methylimidazolium chloride. *J Phys Chem B* 111:11619–11621
46. Stepnowski P, Nichthauser J, Mrozik W, Buszewski B (2006) Usefulness of $\pi \dots \pi$ aromatic interactions in the selective separation and analysis of imidazolium and pyridinium ionic liquid cations. *Anal Bioanal Chem* 385:1483–1491
47. Gonzalez-Perez A, Ruso JM, Prieto G, Sarmiento F (2004) Self-assembly of sodium heptafluorobutylate in aqueous solution. *Colloids Surf A Physicochem Eng Aspects* 249:41–44
48. Zhao M, Zheng L (2011) Micelle formation by N-alkyl-N-methylpyrrolidinium bromide in aqueous solution. *Phys Chem Chem Phys* 13:1332–1337
49. Klevens HB (1953) Structure and aggregation in dilute solution of surface active agents. *J Am Oil Chem Soc* 30:74–80
50. Huibers PDT, Lobanov VS, Katritzky AR, Shah DO, Karelson M (1997) Prediction of critical micelle concentration using a quantitative structure–property relationship approach. *J Colloid Interface Sci* 187:113–120
51. Baker GA, Pandey S, Pandey S, Baker SN (2004) A new class of cationic surfactants inspired by N-alkyl-N-methyl pyrrolidinium ionic liquids. *Analyst* 12:890–892
52. Łuczaka J, Hupkaa J, Thöing J, Jungnickel C (2008) Self-organization of imidazolium ionic liquids in aqueous solution. *Colloids Surf A Physicochem Eng Aspects* 329:125–133
53. Wang H, Wang J, Zhang S, Xuan X (2008) Structural effects of anions and cations on the aggregation behavior of ionic liquids in aqueous solutions. *J Phys Chem B* 112:16682–16689
54. Freire MG, Neves CMSS, Carvalho PJ, Gardas RL, Fernandes AM, Marrucho IM, Santos LMNBF, Coutinho JAP (2007) Mutual solubilities of water and hydrophobic ionic liquids. *J Phys Chem B* 111:13082–13089
55. Tokuda H, Ishii K, Suan MABH, Tauzaki S, Hayamizu K, Watanabe M (2006) Physicochemical properties and structures of room-temperature ionic liquids. 3. Variation of cationic structures. *J Phys Chem B* 110:2833–2839
56. Bini R, Bortolini O, Chiappe C, Pieraccini D, Siciiano T (2007) Development of cation/anion “interaction” scales for ionic liquids through ESI-MS measurements. *J Phys Chem B* 111:598–604
57. Blesic M, Lopes A, Melo E, Petrovski Z, Plechkova NV, Canongia Lopes JN, Seddon KR, Rebelo LPN (2008) On the self-aggregation and fluorescence quenching aptitude of surfactant ionic liquids. *J Phys Chem B* 112:8645–8650
58. Pino V, Baltazar QQ, Anderson JL (2007) Examination of analyte partitioning to monocationic and dicationic imidazolium-based ionic liquid aggregates using solid-phase microextraction-gas chromatography. *J Chromatogr A* 1148:92–99
59. Zana R (1996) Critical micellization concentration of surfactants in aqueous solution and free energy of micellization. *Langmuir* 12:1208–1211
60. Sepúlveda L, Cortés J (1985) Ionization degrees and critical micelle concentrations of hexadecyltrimethylammonium and tetradecyltrimethylammonium micelles with different counterions. *J Phys Chem* 89:5322–5324
61. Marcus Y (1991) Thermodynamics of solvation of ions. Part 5. – Gibbs free energy of hydration at 298.15 K. *J Chem Soc Faraday Trans* 87:2995–2999
62. Bunton CA, Cowell C (1988) The binding of phenols and phenoxide ions to cationic micelles. *J Colloid Interface Sci* 122:154–162
63. Abdel-Rahem R (2008) The influence of hydrophobic counterions on micellar growth of ionic surfactants. *Adv Colloid Interface Sci* 141:24–36
64. Shaw DJ (1992) Introduction to colloid and surface chemistry. Butterworth, Heinemann, Oxford

65. Dong B, Zhao X, Zheng L, Zhang J, Li N, Inoue T (2008) Aggregation behavior of long-chain imidazolium ionic liquids in aqueous solution: micellization and characterization of micelle microenvironment. *Colloids Surf A Physicochem Eng Aspects* 317:666–672
66. Vaghela NM, Sastry NV, Aswal VK (2011) Effect of additives on the surface active and morphological features of 1-octyl-3-methylimidazolium halide aggregates in aqueous media. *Colloids Surf A Physicochem Eng Aspects* 373:101
67. Wang H, Feng Q, Wang J, Zhang H (2010) Salt effect on the aggregation behavior of 1-decyl-3-methylimidazolium bromide in aqueous solutions. *J Phys Chem B* 114:1380–1387
68. Lin Z, Cai JJ, Scriven LE, Davis HT (1994) Spherical-to-wormlike micelle transition in CTAB solutions. *J Phys Chem* 98:5984–5993
69. Magid LJ, Han Z, Warr GG, Cassidy MA, Butler PD, Hamilton WA (1997) The effect of counterion competition for cetyltrimethylammonium micellar surfaces on micellar growth horizons: electrostatics and specific binding. *J Phys Chem B* 101:7919–7927
70. Armstrong DW, Henry SJ (1980) Use of an aqueous micellar mobile phase for separation of phenols and polynuclear aromatic hydrocarbons via HPLC. *J Liq Chromatogr* 3:657–662
71. Berthod A, García-álvarez-Coque C (2000) *Micellar liquid chromatography*. Marcel Dekker, New York
72. Esteve-Romero J, Carda-Broch S, Gil-Agustí M, Capella-Peiró ME, Bose D (2005) Micellar liquid chromatography for the determination of drug materials in pharmaceutical preparations and biological samples. *Trends Anal Chem* 24:75–91
73. Armstrong DW (1985) Micelles in separations: application and theory. *Sep Purif Methods* 14:213–304
74. Thomas DP, Foley JP (2007) Efficiency enhancements in micellar liquid chromatography through selection of stationary phase and alcohol modifier. *J Chromatogr A* 1149:282–293
75. Ruiz-ángel MJ, Torres-Lapasíó JR, García-álvarez-Coque MC (2008) Retention mechanisms for basic drugs in the submicellar and micellar reversed-phase liquid chromatographic modes. *Anal Chem* 80:9705–9713
76. Pino V, Yao C, Anderson JL (2009) Micellization and interfacial behavior of imidazolium-based ionic liquids in organic solvent–water mixtures. *J Colloid Interface Sci* 333:548–556
77. Wang J, Zhang L, Wang H, Wu C (2012) Aggregation behavior modulation of 1-dodecyl-3-methylimidazolium bromide by organic solvents in aqueous solution. *J Phys Chem B* 115:4955–4962
78. Sugihara S, Era Y, Funatsu M, Kunitake T, Lee S, Sasaki Y (1997) Micelle formation of dodecylammonium surfactant with mixed counterions: perfluorocarboxylate and alkanesulfonate ions. *J Colloid Interface Sci* 187:435–442
79. Beyaz A, Oh WS, Reddy VP (2004) Ionic liquids as modulators of the critical micelle concentration of sodium dodecyl sulfate. *Colloids Surf B Biointerfaces* 35:119
80. Dorbritz S, Ruth W, Kragl U (2005) Investigation on aggregate formation of ionic liquids. *Adv Synth Catal* 347:1273–1279
81. Li W, Zhang Z, Zhang J, Han B, Wang B, Hou M, Xie Y (2006) Micropolarity and aggregation behavior in ionic liquid + organic solvent solutions. *Fluid Phase Equilibria* 248:211–216
82. Consorti CS, Suarez PAZ, de Souza RF, Burrow RA, Farrar DH, Lough AJ, Loh W, da Silva HML, Dupont J (2005) Identification of 1,3-dialkylimidazolium salt supramolecular aggregates in solution. *J Phys Chem B* 109:4341–4349
83. Feng Q, Wang H, Zhang S, Wang J (2010) Aggregation behavior of 1-dodecyl-3-methylimidazolium bromide ionic liquid in non-aqueous solvents. *Colloids Surf A Physicochem Eng Aspects* 367:7–11
84. Singh T, Kumar A (2007) Aggregation behavior of ionic liquids in aqueous solutions: effect of alkyl chain length, cations, and anions. *J Phys Chem B* 111:7843–7851
85. Bhargava BL, Klein ML (2009) Molecular dynamics studies of cation aggregation in the room temperature ionic liquid [C₁₀mim][Br] in aqueous solution. *J Phys Chem A* 113:1898–1904
86. Bhargava BL, Klein ML (2009) Initial stages of aggregation in aqueous solutions of ionic liquids: molecular dynamics studies. *J Phys Chem B* 113:9499–94505

87. Fernández JF, Waterkamp D, Thöming J (2008) Recovery of ionic liquids from wastewater: aggregation control for intensified membrane filtration. *Desalination* 224:52–56
88. Shen Y, Zhang Y, Kuehner D, Yang G, Yuan F, Niu L (2008) Ion-responsive behavior of ionic-liquid surfactant aggregates with applications in controlled release and emulsification. *Chemphyschem* 9:2198–2202
89. Pei YC, Li ZY, Liu L, Wang JJ, Wang HY (2010) Selective separation of protein and saccharides by ionic liquids aqueous two-phase systems. *Sci China Chem* 53:1554–1560

Dissolution of Biomass Using Ionic Liquids

Hui Wang, Gabriela Gurau, and Robin D. Rogers

Abstract Ionic liquids (ILs) have been shown to be effective in dissolving cellulose and other biopolymers that are structurally quite different from each other. It would be quite interesting to figure out the common points of the dissolution of structurally different biopolymers in various kinds of ILs. In this chapter, the IL dissolution of pure biopolymers such as cellulose, lignin, hemicellulose, chitin, silk, wool, etc., is reviewed. By analyzing the structures of the biopolymers and those of the ILs, it is concluded that the dissolution of most of these biopolymers (except lignin) in ILs is mainly due to the disruption of the intra- and intermolecular hydrogen bonding in the polymers by the ILs. Both the cations and anions of the ILs influence the dissolution process, although current work suggests the anions have a larger effect.

Keywords Ionic liquids • Biopolymers • Dissolution • Hydrogen Bonding

1 Introduction

Biomass can be considered to be any organic matter that can be used as an energy source, which includes aquatic or terrestrial vegetation, as well as residues from forestry or agriculture, animal waste, and municipal waste [1]. Due to a worldwide emphasis on sustainable development and a sharp increase in the demand for fuels and chemicals, biomass as a renewable energy source is now considered to be increasingly important [2]. Many countries have put or are putting great emphasis on the exploration and utilization of various types of biomass [3] and several technologies (e.g., combustion, gasification, pyrolysis, etc.) are being

H. Wang • G. Gurau • R.D. Rogers (✉)
Center for Green Manufacturing and Department of Chemistry, The University of Alabama,
3006D Shelby Hall, 250 Hackberry Lane, Box 870336, Tuscaloosa, AL 35487, USA
e-mail: rdrogers@as.ua.edu

scaled-up [4]. At the same time, the debate about using food crops continues to fuel discussion about which biomass crops are appropriate for conversion to chemicals and energy.

The main components of natural biomass are quite different, depending on the biomass type. For instance, lignocellulosic biomass mainly contains cellulose, hemicellulose, and lignin [5], while shrimp shells are composed of chitin, protein, mineral salts, carotenoids, and lipids [6]. The structures of the most common natural biopolymers, including cellulose, hemicellulose, lignin, chitin, silk fibroin, wool keratin, starch, pectin, agarose, and dextrin are shown in Fig. 1.

Conversion of such diverse types of biomass or extraction of the biopolymers, especially of or from lignocellulosic biomass, is often an energy- and chemical-intensive process, using large quantities of energy, volatile organic solvents, or other undesirable chemical solvents [7]. At the same time, the molecular weights of the biopolymers are significantly reduced during the processing. Thus, there is an increasing need for new technologies which have lower energy demands and which can produce the pure natural biopolymers with high molecular weights. Here we will discuss one such new processing strategy, using ionic liquids (ILs) to extract and process biomass.

Generally speaking, ILs refers to a specific class of molten salts which are liquids at temperatures of 100 °C or below [8]. Many ILs have unique physico-chemical properties such as negligible vapor pressure, high thermal stability, and wide liquid range [9, 10] which have led to numerous potential applications in a variety of fields. Furthermore, ILs can be easily modified by changing the structure of the cations or anions [11], which has broadened their fields of application to such areas as extraction [12], catalysis [13], electrochemistry [14], and organic synthesis [15, 16], among others. Here we will discuss the rapidly expanding use of ILs in the dissolution and processing of biomass and focus on the ability of certain ILs to dissolve a diverse range of biopolymers.

The first application of ILs in processing biomass was the dissolution of pure cellulose using imidazolium ILs [17]. Since then, studies on the application of ILs in biomass chemistry have made great progress and now many ILs have been found to be able to dissolve cellulose [18–27], to serve as the reaction medium to functionalize cellulose [22, 28–30], to allow ready formation of cellulose fibers and films [25, 31, 32], and, importantly, to dissolve many other kinds of biopolymers, such as lignin [33, 34], hemicellulose [35], chitin [36–38], silk fibroin [39], wool keratin [40], etc. In addition, the dissolution of raw biomass, including lignocellulosic biomass [41–44], shrimp shells [38], etc., has also been reported.

ILs have been shown to be efficient solvents for dissolution and processing of biomass, with no emission of volatile organic solvents and no significant degradation of the regenerated biopolymers [18, 38]. Importantly from an economic point of view, ILs can be recycled and reused [45, 46]. Thus, ILs may provide a new and versatile platform for the wide utilization of biomass resources and preparation of novel biomass-based materials [35].

Scientifically, it is interesting to note that a given type of IL might dissolve quite different biopolymers. As an example, 1-butyl-3-methylimidazolium chloride

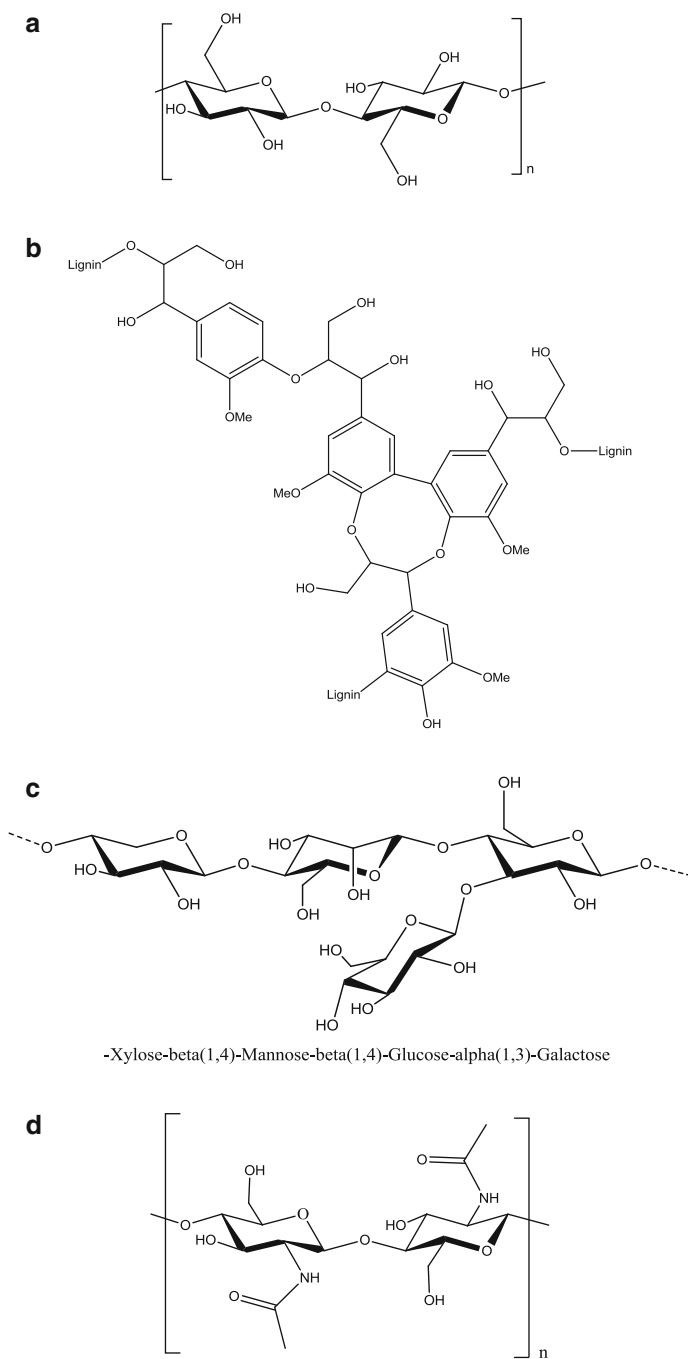


Fig. 1 (continued)

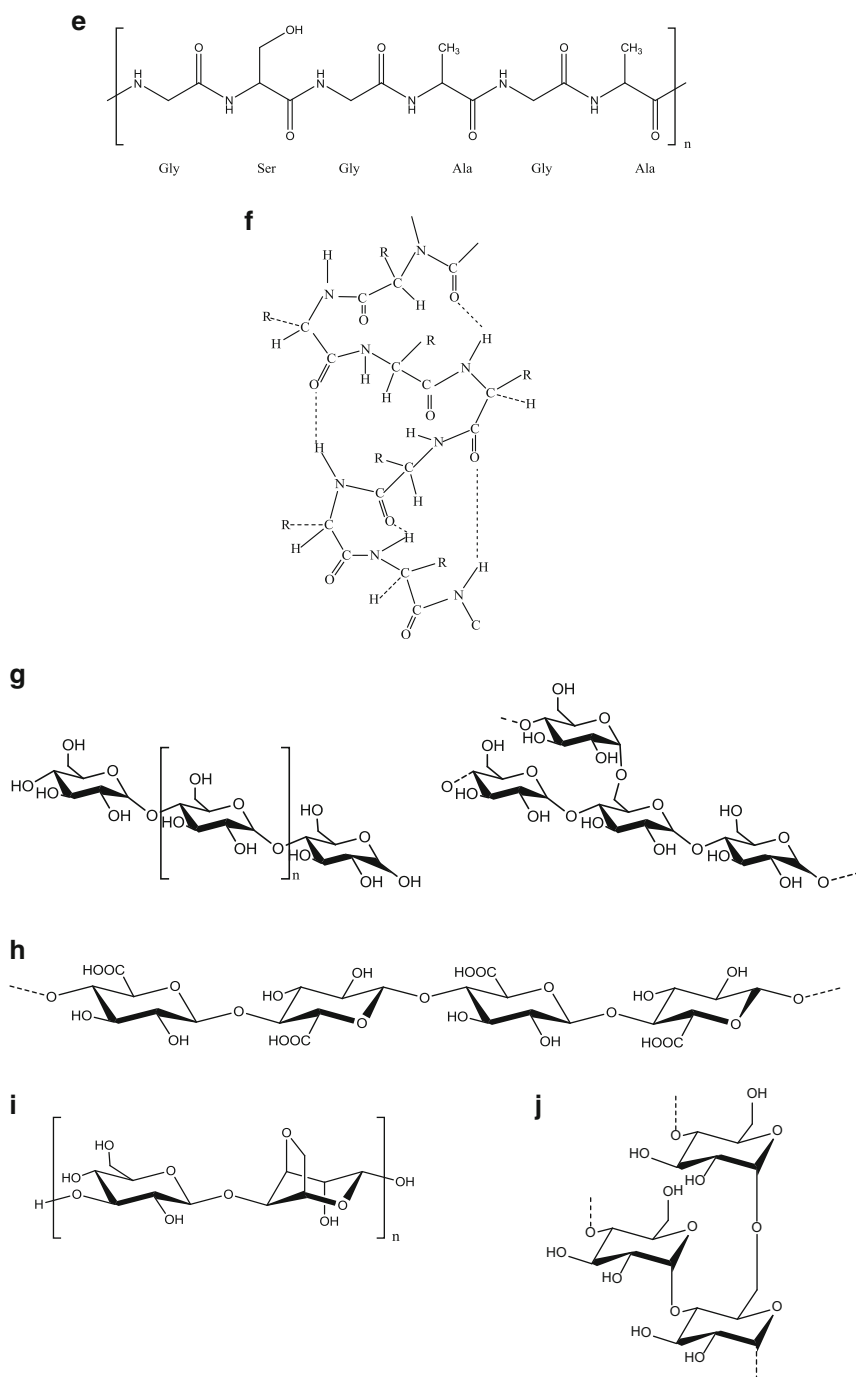


Fig. 1 Structures of cellulose (a), lignin (b), hemicellulose (c), chitin (d), silk fibroin (e), wool keratin (f), starch (amylose-left; amylopectin-right) (g), pectin (h), agarose (i), and dextrin (j)

([C₄mim]Cl) can dissolve cellulose [17], hemicellulose [47], lignin [33], chitin (to some degree) [38], silk [39], and wool [40]. From the structures of the biopolymers shown in Fig. 1, it is clear that these biopolymers have quite different structures. One question to be resolved is what are the key structural features of each ion or the combination on the ions which are responsible for the dissolution of such diverse natural polymers? In this chapter, we will review the dissolution of different biopolymers using various ILs and then analyze the chemical structures of both the ILs and the polymers to try and find the common features.

2 Dissolution of Pure Biopolymers Using Ionic Liquids

The study of the applications of ILs in the biomass field started with the pure biopolymer, cellulose, and in this section we will discuss the dissolution of pure biopolymers in ILs. Table 1 summarizes the different kinds of ILs that have been used to dissolve cellulose, lignin, hemicellulose, chitin, silk, wool, starch, pectin, agarose, and dextrin.

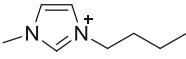
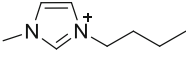
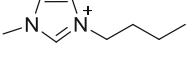
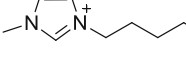
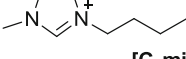
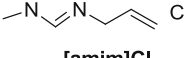
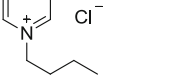
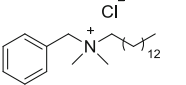
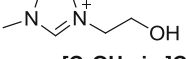
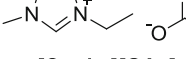
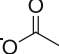
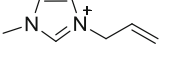
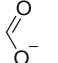
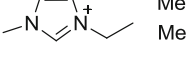
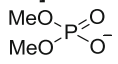
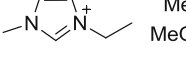
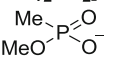
2.1 Dissolution of Cellulose

Cellulose is the major carbohydrate produced by plant photosynthesis, and is therefore the most abundant organic polymer produced on Earth. Cellulose can be used as a “green” polymer for producing new and attractive materials, by chemical modification or mixing with other components [27]. Its derivatized products have many important applications in the fiber, paper, membrane, polymer, and paint industries [48].

Cellulose consists of β -(1 \rightarrow 4)-linked glucose repeating units. Because of the stiff molecules and close chain packing via numerous intermolecular and intramolecular hydrogen bonds, it is extremely difficult to dissolve cellulose in water and common organic solvents. Solvent systems including *N*-methylmorpholine oxide (NMMO), *N,N*-dimethylacetamide/lithium chloride (DMAc/LiCl), *N,N*-dimethylformamide/nitrous tetroxide (DMF/N₂O₄), dimethylsulfoxide (DMSO), tetrabutylammonium fluoride (TBAF), and LiSCN · 2H₂O [49–53] have been reported to dissolve cellulose, but these solvent systems have drawbacks such as toxicity, high cost, difficulty in solvent recovery, or harsh processing conditions [21].

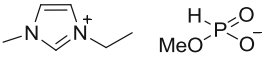
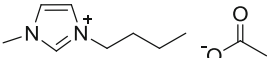
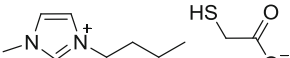
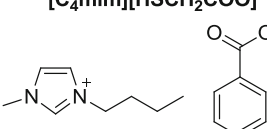
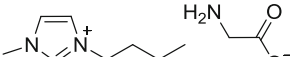
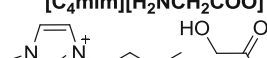
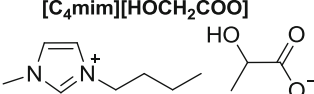
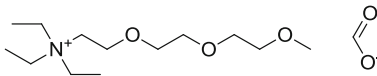
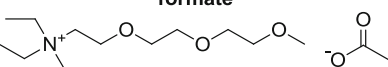
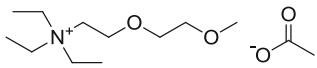
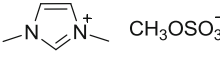
In 2002 we reported that cellulose could be dissolved without derivatization in high concentrations using ILs such as [C₄mim]Cl as the solvent [17], which opened up the development of a class of new cellulose solvent systems. The effects of ILs with varying structures of cations and anions on the dissolution properties of cellulose were studied and these initial results showed that, among the dialkylimidazolium chloride ILs, the longer-chain substituted ILs [C₆mim]Cl and [C₈mim]Cl were less efficient at dissolving cellulose. With gentle heating to 100–110°C,

Table 1 Dissolution of pure biopolymers in different ILs^a

Biopolymer	ILs	References
Cellulose	 Cl ⁻ [C₄mim]Cl	[17, 18]
	 Br ⁻ [C₄mim]Br	[17]
	 SCN ⁻ [C₄mim][SCN]	[17]
	 Cl ⁻ [C₆mim]Cl	[17]
	 Cl ⁻ [C₈mim]Cl	[17]
	 Cl ⁻ [amim]Cl	[19, 20, 26]
	 Cl ⁻ [C₄mpy]Cl	[18]
	 Cl ⁻ BDTAC	[18]
	 Cl ⁻ [C₂OHmim]Cl	[54]
	  [C₂mim][OAc]	[25]
	  [amim][HCOO]	[26]
	  [C₂mim][[(MeO)₂PO₂]	[27]
	  [C₂mim][[(MeO)MePO₂]	[27]

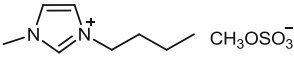
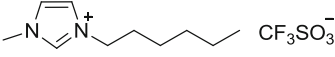
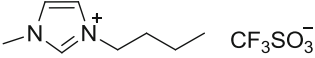
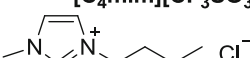
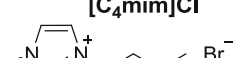
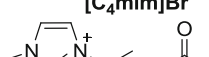
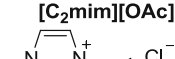
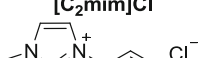
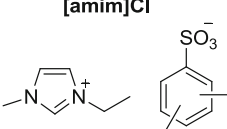
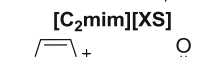
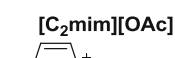


(continued)

Table 1 (continued)

Biopolymer	ILs	References
	 [C₂mim][(MeO)HPO₂]	[27]
	 [C₄mim][OAc]	[21]
	 [C₄mim][HSCH₂COO]	[21]
	 [C₄mim][C₆H₅COO]	[21]
	 [C₄mim][H₂NCH₂COO]	[21]
	 [C₄mim][HOCH₂COO]	[21]
	 [C₄mim][CH₃CHOHCH₂COO]	[21]
	 N,N,N-triethyl-3,6,9-trioxadecylammonium formate	[57]
	 N,N,N-triethyl-3,6,9-trioxadecylammonium acetate	[56]
	 N,N,N-triethyl-3,6-dioxaheptylammonium acetate	[56]
Lignin	 [C₁mim][MeSO₄]	[33, 34]

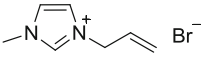
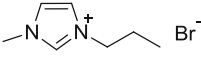
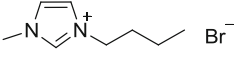
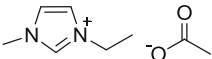
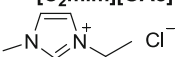
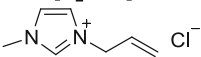
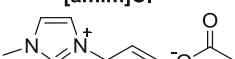
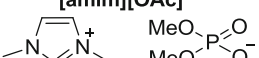
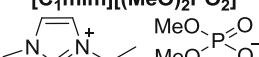
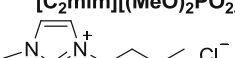
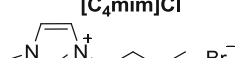
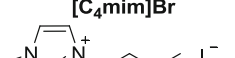
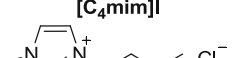
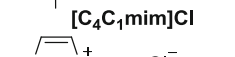
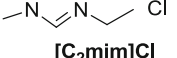
(continued)

Table 1 (continued)

Biopolymer	ILs	References
	 [C₄mim][MeSO₄]	[33]
	 [C₆mim][CF₃SO₃]	[33]
	 [C₄mim][CF₃SO₃]	[34]
	 [C₄mim]Cl	[33, 34, 69]
	 [C₄mim]Br	[33]
	 [C₂mim][OAc]	[34, 69]
	 [C₂mim]Cl	[69]
	 [amim]Cl	[34]
	 [C₂mim][XS]	[68]
Hemicellulose	 [C₂mim][OAc]	[35, 69]
	 [C₂mim]Cl	[69]
	 [C₄mim]Cl	[47, 69]
Chitin	 [C₄mim]Cl	[36, 38]

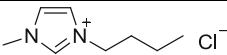
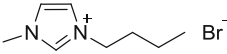
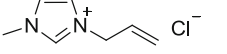
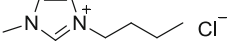
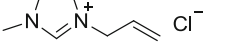
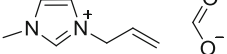
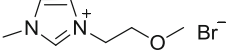
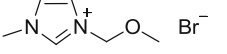
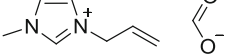
(continued)

Table 1 (continued)

Biopolymer	ILs	References
	 [amim]Br	[37]
	 [C ₃ mim]Br	[37]
	 [C ₄ mim]Br	[37]
	 [C ₂ mim][OAc]	[38]
	 [C ₂ mim]Cl	[38]
	 [amim]Cl	[87]
	 [amim][OAc]	[87]
	 [C ₁ mim][(MeO) ₂ PO ₂]	[87]
	 [C ₂ mim][(MeO) ₂ PO ₂]	[87]
Silk	 [C ₄ mim]Cl	[39]
	 [C ₄ mim]Cl	[39]
	 [C ₄ mim]Br	[39]
	 [C ₄ mim]I	[39]
	 [C ₄ C ₁ mim]Cl	[39, 94]
	 [C ₂ mim]Cl	[39, 94]

(continued)

Table 1 (continued)

Biopolymer	ILs	References
Wool	 Cl ⁻	[40, 96, 97]
	[C₄mim]Cl	
	 Br ⁻	[40]
	[C₄mim]Br	
	 Cl ⁻	[40]
	[amim]Cl	
Starch	 Cl ⁻	[99]
	[C₄mim]Cl	
	 Cl ⁻	[98]
	[amim]Cl	
Pectin		[26]
	[amim][HCOO]	
Agarose	 Br ⁻	[100]
	[moemim]Br	
	 Br ⁻	[100]
	[mommim]Br	
Dextrin		[26]
	[amim][HCOO]	

^aC₄mim: 1-butyl-3-methylimidazolium, C₆mim: 1-hexyl-3-methylimidazolium, C₈mim: 1-octyl-3-methylimidazolium, C₄mpy: 3-methyl-1-butyl-*N*-pyridinium, amim: 1-allyl-3-methylimidazolium, BDTAC: benzyl dimethyl(tetradecyl) ammonium chloride, C₂OHmim: 1-(2-hydroxyethyl)-3-methylimidazolium, C₂mim: 1-ethyl-3-methylimidazolium, [(MeO)₂PO₂]: dimethylphosphonate, [(MeO)MePO₂]: methyl methylphosphonate CF₃SO₃: trifluoromethanesulfonate, MeSO₄: methylsulfate, XS: xylenesulfonate, C₄C₁mim: 1-butyl-2,3-dimethylimidazolium, [moemim]: 1-methoxyethyl-3-methylimidazolium, [momim]: 1-methoxymethyl-3-methylimidazolium

cellulose could be dissolved in ILs containing Cl⁻, Br⁻, and [SCN]⁻ anions. However, cellulose could not be dissolved in ILs containing non-coordinating anions, such as [BF₄]⁻ or [PF₆]⁻. It was also demonstrated that microwave heating could significantly increase the solubility of cellulose in ILs, for example, the solubility of cellulose in [C₄mim]Cl increased to 25 wt% with microwave heating, compared to only 10 wt% with general heating.

Zhang et al. [19, 20] found that the IL [amim]Cl is a powerful and nonderivatizing solvent to dissolve cellulose. Untreated or alkali activated cellulose

Table 2 Solubility and DP of cellulose samples in ILs: [C₄mim]Cl, [C₄mpy]Cl, and BDTAC [18]

Cellulose		Solubility in ILs					
		[C ₄ mim]Cl		[C ₄ mpy]Cl		BDTAC	
Type	DP	%	DP ^a	%	DP ^a	%	DP ^a
Avicel	286	18	307	39	172	5	327
Spruce sulfite pulp	593	13	544	37	412	2	527
Cotton linter	1,198	10	812	12	368	1	966

^aAfter regeneration

could be dissolved rapidly in this IL. For example, 5 wt% cellulose with a degree of polymerization (DP) of 650 could be dissolved in [amim]Cl in only 30 min at 80 °C. A solution containing up to 14.5 wt% cellulose with a DP as high as 650 in [amim]Cl could also be readily prepared.

Heinze et al. used three kinds of ILs – [C₄mim]Cl, [C₄mpy]Cl, and BDTAC – as solvents and discussed the change in the degree of polymerization of cellulose in the dissolution process (Table 2, [18]). It was found that the solubility of cellulose decreased with increasing degree of polymerization. It was also shown that, in the case of [C₄mim]Cl and BDTAC, no depolymerization of the polysaccharide occurred for the microcrystalline cellulose Avicel, while spruce sulfite pulp and cotton linters were slightly degraded. In contrast, the dissolution of cellulose in [C₄mpy]Cl led to a remarkable degradation. Side reactions forming cellulose derivatives did not occur in the process of dissolution, and thus all three ILs were direct solvents for cellulose.

Hydroxyl groups were introduced to the imidazolium cation and the hydroxyl-containing cation ILs, such as 1-(2-hydroxyethyl)-3-methylimidazolium chloride ([C₂OHmim]Cl), were synthesized [54]. These ILs have also been reported to dissolve cellulose, and the solubility is 6.8 % at 70°C. The hydroxyl group in the cation side chain could also probably form hydrogen bonds with cellulose hydroxyl groups, leading to the dissolution of the biopolymer.

The dissolution of cellulose can also be achieved by introducing the acetate anion to the IL. The IL, 1-ethyl-3-methylimidazolium acetate ([C₂mim][OAc]), has a very low melting point (−20°C) and viscosity (~140 cP at 25°C) [24], and it showed a much higher capability to dissolve cellulose. Recent studies showed that the cellulose concentration in [C₂mim][OAc] could be as high as 20 wt% [25]. Moreover, [C₂mim][OAc] was considered to be less toxic and corrosive than comparable chlorides [55]. These features make [C₂mim][OAc] a promising solvent for the processing and homogeneous derivatization of cellulose and indeed lignocellulosic biomass [35, 43, 44].

Fukaya et al. found that a series of 1,3-dialkylimidazolium formate ILs exhibited superior solubility for a wide range of polysaccharides including cellulose [26]. These ILs had significantly lower viscosity than previously reported halogenated imidazolium ILs, for example, [amim][HCOO] has a viscosity of 66 cP at 25°C. Because having a stronger hydrogen bond basicity than chloride salts, [amim][HCOO] could dissolve cellulose at lower temperatures. To solubilize 10 wt% cellulose, [amim]Cl had to be heated to 100°C, whereas [amim][HCOO] had to be heated only to 60°C.

Several alkyylimidazolium ILs containing $[\text{MeSO}_3]^-$, $[\text{MeOSO}_3]^-$, $[\text{EtOSO}_3]^-$, and $[(\text{MeO})_2\text{PO}_2]^-$ were synthesized by a facile, one-pot procedure [27]. These ILs also have the potential to solubilize cellulose under mild conditions. The IL $[\text{C}_2\text{mim}][(\text{MeO})_2\text{PO}_2]$ was used to prepare a 10 wt% cellulose solution by keeping it at 45°C for 30 min with stirring. It was also found that 2 wt% cellulose could be completely dissolved in these ILs at room temperature (25°C) within 3 h, and 4 wt% within 5 h.

Xu et al. [21] synthesized a series of ILs by pairing the $[\text{C}_4\text{mim}]^+$ cation with the Brønsted basic anions $[\text{OAc}]^-$, $[\text{HSCH}_2\text{COO}]^-$, $[\text{HCOO}]^-$, $[(\text{C}_6\text{H}_5)\text{COO}]^-$, $[\text{H}_2\text{NCH}_2\text{COO}]^-$, $[\text{HOCH}_2\text{COO}]^-$, $[\text{CH}_3\text{CHOHCOO}]^-$, and $[\text{N}(\text{CN})_2]^-$, and the solubilities of microcrystalline cellulose (MCC) in these ILs were determined. The structure of the anions significantly affects the solubility of the cellulose. Among the investigated ILs, $[\text{C}_4\text{mim}][\text{OAc}]$ was the most efficient IL for the dissolution of cellulose. In contrast, cellulose was insoluble in $[\text{C}_4\text{mim}][\text{N}(\text{CN})_2]$.

The hydrogen bond accepting ability of the anions of the ILs are closely linked to the solubility of cellulose and the solubility of cellulose increases almost linearly with increasing hydrogen bond accepting ability of anions in the ILs. The solubility of cellulose in these ILs decreases in the order $[\text{C}_4\text{mim}][\text{OAc}] > [\text{C}_4\text{mim}][\text{HSCH}_2\text{COO}] > [\text{C}_4\text{mim}][\text{HCOO}] > [\text{C}_4\text{mim}][(\text{C}_6\text{H}_5)\text{COO}] > [\text{C}_4\text{mim}][\text{H}_2\text{NCH}_2\text{COO}] > [\text{C}_4\text{mim}][\text{HOCH}_2\text{COO}] > [\text{C}_4\text{mim}][\text{CH}_3\text{CHOHCOO}] > [\text{C}_4\text{mim}][\text{N}(\text{CN})_2]$.

It has also been reported that cellulose can be dissolved in a series of ammonium ILs such as *N,N,N*-triethyl-3,6,9-trioxadecylammonium formate, *N,N,N*-triethyl-3,6,9-trioxadecylammonium acetate, and *N,N,N*-triethyl-3,6-dioxaheptylammonium acetate [56, 57]. The solubility of cellulose in these ILs could reach 10 wt% at 110°C. Unlike other ILs, these ammonium ILs are reported not to denature enzymes, allowing further enzymatic modification of dissolved carbohydrates in ILs [56].

In order to understand further the dissolution process of cellulose in different solvents, the mechanisms of dissolving cellulose in traditional solvents and ILs were compared. The solvent system DMAc/LiCl, a good solvent for cellulose, was chosen as an example of the traditional solvents. It is assumed that the Li^+ ions interact with the oxygens of the carbonyl groups of the DMAc, and the $[\text{Li}(\text{DMAc})_n]^+$ complex cation interacts with both the hydroxyl and the ring oxygens in cellulose [58], while the chloride ions are left unencumbered. In this model, the Cl^- would be highly active as a nucleophilic base and could play a major role in breaking up the inter- and intramolecular hydrogen bonds [59]. However, the only alkali metal salt which led to cellulose dissolution was LiCl; other chloride salts, such as sodium, potassium, barium, and calcium, were found to be ineffective [19]. Thus, both the cation and anion structures of the solvent affect the dissolution process.

In the case of ILs used as solvents for cellulose, it is assumed that the anions such as Cl^- , OAc^- , $[\text{HCOO}]^-$, etc., interact with the hydrogen atoms in the hydroxyl groups [17, 19]. As the basicity of the acetate anion or formate anion is higher than Cl^- , the acetate- or formate-containing ILs are more efficient in disrupting the inter- and intramolecular hydrogen bonding in this biopolymer [25, 26]. Meanwhile, it has also been suggested that the hydrogens in the cations of the ILs can interact

with the oxygens in cellulose [19], although this conclusion seems contrary to other published results [60, 61]. It is nonetheless quite clear that the chemical structure of the cations of ILs will affect the cellulose dissolution and the reasons for this need further delineation.

We found that the solubility of cellulose decreased with increasing size of the cations, such as lengthy alkyl groups substituted on the imidazolium ring [17]. The ILs containing [amim]⁺, a smaller size cation due to the nature of the allyl substituent, has higher cellulose dissolution ability compared with the corresponding [C₄mim]⁺-containing ILs [19]. Thus, in both traditional and IL solvent systems, it is generally recognized that, in order to dissolve cellulose, disrupting its great number of intra- and intermolecular hydrogen bonds is required, but other factors do come into play.

2.2 Dissolution of Lignin

Lignin is one of the three major components of lignocellulosic biomass [62]. It is a three-dimensional amorphous polymer consisting of methoxylated phenylpropane structures [63]. The biggest structural difference between lignin and cellulose is that lignin contains aromatics (Fig. 1). Lignin can be regarded as the major aromatic resource of the bio-based economy [63].

In plant cell walls, lignin fills the spaces between cellulose and hemicellulose, with a covalent bond between lignin and hemicellulose, and lignin acts like a resin that holds the lignocellulose matrix together [64]. The growing interest in developing new lignin-based products is driven by the fact that lignin is a renewable, low-cost bioresource with unique functionalities, and is an environmentally benign material [33]. However, many of the technologies currently used in lignin isolation or processing employ high temperature, pressure, harsh alkaline or acidic conditions, and organic solvents [65–67]. These processes are far from favorable and generally not considered green. This has prompted the study of ILs to dissolve lignin and develop new chemistries for lignin.

The dissolution of lignin has been investigated in several imidazolium ILs containing methyl-, ethyl-, butyl-, hexyl-, and benzyl groups in the imidazolium ring with a number of common anions, such as Cl⁻, Br⁻, [CF₃SO₃]⁻, [MeSO₄]⁻, [BF₄]⁻, and [PF₆]⁻ ([33]; Table 3). Lignin obtained from softwood was observed to dissolve in [C₁mim][MeSO₄] (74 g/L) and [C₄mim][MeSO₄] (62 g/L) at room temperature, but not in [C₆mim][CF₃SO₃] under ambient conditions. Upon heating, lignin was rapidly dissolved in [C₁mim][MeSO₄], [C₆mim][CF₃SO₃], and [C₄mim][MeSO₄] to yield viscous mixtures. The greatest lignin solubility was obtained using [C₁mim][MeSO₄] and [C₄mim][MeSO₄] at slightly elevated temperatures (50°C). For the [C₄mim]⁺-containing ILs, the order of lignin solubility for varying anions was [MeSO₄]⁻ > Cl⁻ ~ Br⁻ » [PF₆]⁻, indicating that the solubility of lignin was principally influenced by the nature of the anions. The ILs

Table 3 Solubility of residual softwood Kraft pulp lignin in ILs [33]

ILs	Temperature (°C)	Solubility (g/L)
[C ₁ mim][MeSO ₄]	50	344
	25	74.2
[C ₆ mim][CF ₃ SO ₃]	70	275
	50	<10
[C ₄ mim][MeSO ₄]	50	312
	25	61.8
[C ₄ mim]Cl	75	13.9
[C ₄ mim]Br	75	17.5
[C ₄ mim][PF ₆]	70–120	Insoluble
[C ₄ C ₁ mim][BF ₄] ^a	70–100	14.5
[C ₄ mpy][PF ₆]	70–120	Insoluble

^a[C₄C₁mim][BF₄]: 1-butyl-2,3-dimethylimidazolium tetrafluoroborate

containing large, non-coordinating anions such as [BF₄]⁻ and [PF₆]⁻ exhibited no or very limited ability to dissolve lignin.

The solubility of Kraft lignin (Indulin AT), as well as wood flour in the ILs [C₁mim][MeSO₄], [C₄mim][CF₃SO₃], [C₂mim][OAc], [amim]Cl, [C₄mim]Cl, and 1-benzyl-3-methylimidazolium chloride ([bz₃mim]Cl) was reported by Lee et al. [34]. The highest lignin solubility was obtained using [C₁mim][MeSO₄] and [C₄mim][CF₃SO₃]. Chloride anions enabled relatively high wood flour solubility (10–30 g/kg) with lignin solubilities higher than 100 g/kg. Again, [C₄mim][BF₄] and [C₄mim][PF₆] were ineffective at dissolving either lignin or wood flour.

Another recent interesting trial was reported by Tan et al., in which [C₂mim]⁺ salts with a mixture of alkylbenzene sulfonate (ABS) anions (predominantly xylene sulfonate (XS)) were used to extract lignin from sugarcane plant waste (bagasse) at atmospheric pressure and elevated temperatures (170–190°C) [68]. An extraction yield of over 93 % was reported, and the lignin obtained was of relatively uniform molecular weight.

Our study shows that Indulin AT could be readily dissolved in [C₄mim]Cl, [C₂mim]Cl, and [C₂mim][OAc] at 90°C ([69]; Table 4). We have also dissolved physical mixtures of cellulose, xylan (the major component of hemicellulose), and Indulin AT (weight percentage of each component is 33.33 %) in [C₂mim][OAc] at 90°C [35]. It was found that all three components can be dissolved in this IL to form a viscous liquid. The viscous solution was cast as a film on a glass plate and immersed in water at room temperature. The IL is miscible with water, xylan is also water soluble; thus [C₂mim][OAc] and xylan were the two compounds expected to be extracted from the film. Lignin was soluble in the mixture of acetone and water (1:1, v/v), while cellulose is insoluble in this mixture. After washing out the IL and xylan, the film was immersed in a mixture of acetone and water to separate cellulose and lignin. By evaporating the acetone in the lignin/acetone-water solution, lignin could be precipitated and recovered.

Reviewing the available data suggests that the two most powerful solvents for lignin are [C₄mim][CF₃SO₃] and [C₁mim][MeSO₄] [34], followed by several nearly equally good solvents, such as [C₄mim][MeSO₄], [C₂mim][OAc], and

Table 4 Solubility (wt%) of standard biopolymers in ILs at 90 °C [69]

ILs	MCC	Xylan	Indulin AT
[C ₄ mim]Cl	~ 28	~ 8	~ 14
[C ₂ mim]Cl	~ 35	~ 10	~ 20
[C ₂ mim][OAc]	~ 30	~ 10	~ 25

[amim]Cl [33]. However, direct comparison of the dissolution power is difficult in some cases, since the dissolution temperatures, the lignin raw materials, and IL parameters (e.g., viscosity) were all different. Nonetheless, [C₁mim][MeSO₄] was efficient in lignin dissolution at 50 °C.

The ILs [bzmim]Cl and [C₄mim]Cl are reported to be relatively poor solvents for lignin [34]. The former has a benzyl group similar to the aromatic rings in lignin, linked to the imidazolium ring, which one might presume would help improve the interactions with lignin, but any such effect was minor. [C₄mim]Cl is a good solvent for cellulose, but appears to be less so for lignin.

In a study by Lee et al. [34], the lignin solubility in ILs was rationalized by examining their Hildebrand solubility parameters (δ_H), widely used for predicting the solubilities of various polymers in solvents. Maximum solubility is observed when the δ_H values of the polymer and solvent are identical, since the solubility of two materials is facilitated when their intermolecular attractive forces are similar [70]. Thus, the high solubility of lignin in [C₄mim][CF₃SO₃] is not surprising given the very close similarity of the δ_H values for both the IL and lignin (24.9 and 24.6, respectively). Conversely, the δ_H values for [C₄mim][PF₆] and [C₄mim][BF₄] are 30.2 and 31.6, respectively [71, 72], which are sufficiently distinct from that of lignin, and hence do not favor high lignin solubility.

2.3 Dissolution of Hemicellulose

Hemicellulose is another abundant natural polysaccharide. Unlike cellulose, which is a unique molecule differing only in degree of polymerization and crystallinity, hemicellulose contains many different sugar monomers. For instance, sugar monomers in hemicellulose contain glucose, xylose, mannose, galactose, etc. [73]. Hemicellulose can be used in polymeric form for industrial applications such as in hydrogels, or, once hydrolyzed, it can serve as a source of sugars for fermentation to fuels [74, 75].

ILs are known to be capable of dissolving complex macromolecules and polymeric materials with high efficiency [17, 76, 77] and the dissolution or functionalization of hemicellulose can also be carried out in ILs. We have also shown that [C₄mim]Cl, [C₂mim]Cl, and [C₂mim][OAc] could dissolve xylan with desirable solubilities ([69]; Table 4). As mentioned above, physical mixtures of cellulose, xylan, and Indulin AT can also be co-dissolved in [C₂mim][OAc] at 90 °C [35]. All three components can be dissolved in this IL to form a viscous liquid. As [C₂mim][OAc] and xylan are water soluble, the IL and xylan could be

separated from the other two components by adding water. Any xylan remaining in the regenerated cellulose could be removed by adding alkali and the resulting xylan in the alkali solution could be precipitated by adding ethanol.

It was found that hemicellulose from wheat straw is completely soluble in $[C_4mim]Cl$ on heating to $90^\circ C$ for 1.5 h, up to a concentration of 2.6 wt% [47]. It was also demonstrated that ILs could be used as a solvent for the chemical modification of hemicellulose, such as acetylation with acetic anhydride in $[C_4mim]Cl$ [47]. Since the acetylation of hemicellulose could be carried out in a homogeneous system, high acetylation yields and degrees of substitution (DS) were possible. This method has other obvious advantages in that the reaction could be carried out under mild conditions, is more rapid, and is complete.

The structure of hemicellulose (Fig. 1c) is similar to that of cellulose, and there also exist multiple hydrogen bonds. The dissolution of hemicellulose in ILs to a first approximation can also be attributed to the disruption of the intra- and intermolecular hydrogen bonds in hemicellulose. As with cellulose and most polymers, however, further studies are needed to clarify the role of each ion. The dissolution of hemicellulose in ILs has not been widely studied, and there are no reports on the corresponding dissolution mechanism.

2.4 Dissolution of Chitin

Chitin is a linear polysaccharide and is the second most abundant polysaccharide [78] after cellulose. Chitin is structurally similar to cellulose, but it is an amino polysaccharide having acetamide groups at the C-2 positions in place of hydroxyl groups in cellulose (Fig. 1d) [79]. Due to its low toxicity, biocompatibility, and biodegradability, chitin and its derivatives have had many applications in the fields of water purification, food, pharmaceutical and cosmetic formulations, and in the biomedical fields of drug/gene delivery systems, tissue engineering, as well as in intelligent biosensors, to name but a few [80].

Chitin exists in three polymorphic forms: α , β , and γ [81]. The most abundant naturally occurring polymorph is α -chitin. α -Chitin, from crab and shrimp shells, is known to be sparingly soluble and to have poor reactivity due to its rigid crystalline structure [82]. β -Chitin, usually from squid bone, forms slurries easily when it is ground with water due to its loose crystalline structure [82], while γ -chitin is reported to be a variant of the α family [83]. Also, the softness and hydrophilicity of β -chitin is superior to α -chitin, which can be explained by the crystalline structural differences between them.

In industrial processing, chitin is extracted (e.g., from crustaceans) by acid treatment to dissolve calcium carbonate followed by alkaline extraction to solubilize proteins. In addition, a decolorization step is often added to remove leftover pigments and obtain a colorless product [84].

Despite its huge annual production and easy accessibility, chitin still remains an underutilized biomass resource, primarily because of its intractable bulk

structure [85]. Although considerable efforts are still being made to extend novel applications of chitin, lack of solubility of this polysaccharide in water and common organic solvents causes difficulties in improving the processability and functionality. The solubility problem is caused by the stiff molecules and close chain packing via the numerous intra- and intermolecular hydrogen bonds caused by hydroxyl groups as well as the acetamide groups [37]. Until the use of ILs, only a limited number of solvent systems for chitin have been found, such as DMAc/LiCl, concentrated acid, alkaline-ice mixtures, $\text{CaCl}_2 \cdot 2\text{H}_2\text{O}$ -saturated methanol, etc. [86, 87]. Besides other disadvantages of these solvents, such as corrosivity, toxicity, volatility, and difficulty in recycling, the use of these solvents also tends to reduce the molecular weight of the chitin, especially in strong acid [88].

Since the structure of chitin is similar to that of cellulose, and cellulose could be readily dissolved in ILs, ILs should be a potential solvent for chitin. Xie et al. reported the dissolution of chitin in $[\text{C}_4\text{mim}]\text{Cl}$ [36] where they indicated the preparation of clear, viscous 10 wt% chitin/IL solutions in 5 h by heating at 110°C . (As discussed below, the nature of the chitin is quite important and it is believed that Xie et al. used 'pure chitin'.) In order to prove further the degree of dissolution of chitin in $[\text{C}_4\text{mim}]\text{Cl}$, the chitin/IL solution was studied by wide-angle X-ray diffraction (WAXD), and the lack of a diffraction pattern indicated that the crystalline domains of chitin were completely disrupted. The chitin could be regenerated in the same manner as cellulose, by coagulation with an antisolvent such as methanol or water [36].

In other work, the ILs $[\text{amim}]\text{Br}$, $[\text{C}_3\text{mim}]\text{Br}$, and $[\text{C}_4\text{mim}]\text{Br}$ were also used to dissolve (presumably pure) chitin [37]. When $[\text{amim}]\text{Br}$ was used for the dissolution, clear liquids were formed with the concentration of chitin up to 5 wt%, whereas the other ILs, $[\text{C}_3\text{mim}]\text{Br}$ and $[\text{C}_4\text{mim}]\text{Br}$, did not show an ability to form clear solutions even at low 1 wt% concentrations of chitin. The X-ray diffraction (XRD), thermogravimetric analysis (TGA), and infrared spectra (IR) results of the regenerated chitin, as well as the analysis of derivatives, confirmed that degradation of chitin did not occur frequently during the experimental process.

In the work of Wang et al. [87], the dissolving behavior of chitin with different degrees of deacetylation (DA) and molecular weight were studied in a series of ILs, $[\text{amim}]\text{Cl}$, $[\text{C}_4\text{mim}]\text{Cl}$, $[\text{C}_2\text{OHmim}]\text{Cl}$, $[\text{C}_1\text{mim}][\text{Me}_2\text{PO}_4]$, $[\text{C}_2\text{mim}][\text{Me}_2\text{PO}_4]$, and $[\text{amim}][\text{OAc}]$ (Table 5). Untreated chitin could be dissolved in $[\text{amim}]\text{OAc}$ to 5 wt% at 110°C and could also be dissolved in $[\text{amim}]\text{Cl}$, $[\text{C}_1\text{mim}][\text{Me}_2\text{PO}_4]$, and $[\text{C}_2\text{mim}][\text{Me}_2\text{PO}_4]$ below 60°C . This study indicated a lack of solubility in $[\text{C}_4\text{mim}]\text{Cl}$ or $[\text{C}_2\text{OHmim}]\text{Cl}$ from 10°C to 180°C .

In our own attempts to dissolve chitin and explain results contrary to those reported by Xie et al., we discovered that the degree of processing used to obtain the chitin is critical to the ability to dissolve it in certain ILs. Pure chitin has been doubly processed and has the highest purity but lowest molecular weight. Practical grade chitin (PG-chitin) has not been subjected to a final methanesulfonic acid purification and thus is less pure but of higher molecular weight.

Table 5 Dissolution of untreated pure chitin in different ILs^a [87]

ILs	Solubility (wt%)	Notes
[C ₄ mim]Cl	Insoluble	Insoluble
[amim]Cl	0.5	Below 45°C
[C ₂ OHmim]Cl	Insoluble	Insoluble
[C ₁ mim][Me ₂ PO ₄]	1.5	Below 60°C
[C ₂ mim][Me ₂ PO ₄]	1.5	Below 60°C
[amim][OAc]	5	At 110°C

^aUntreated chitin: $MW = 1.23 \times 10^5$, 200 mesh

We tested the ability of [C₂mim][OAc], [C₄mim]Cl, and [C₂mim]Cl to dissolve a given mass of pure chitin vs PG-chitin [38] and found that much more of the pure chitin sample (80.0 %) could be dissolved in [C₂mim][OAc] than either [C₄mim]Cl (24.4 %) or [C₂mim]Cl (13.9 %). Even at a lower loading of PG-chitin (1 g PG-chitin to 10 g IL vs 0.5 g pure chitin to 2 g IL), much less (15.2 %) could be dissolved than pure chitin in [C₂mim][OAc], presumably because of the higher mineral content of the PG-chitin. Nonetheless, [C₂mim][OAc] could dissolve much more of the PG-chitin samples than either [C₂mim]Cl (4.2 %) or [C₄mim]Cl (6.8 %). It was even demonstrated that [C₂mim][OAc] can directly extract high molecular weight pure chitin from raw shrimp shells which can subsequently be spun into chitin fibers [38].

It is thus quite important to state the nature and source of the chitin being used in any dissolution studies. Various kinds of chitin have quite different crystalline structures, purities, molecular weights, etc., all of which influence the solubility of chitin in various ILs.

These results suggest that ILs with strong hydrogen bond acceptor abilities, such as acetate, could dissolve chitin effectively [38, 87]. This also strengthens the premise that the anion must be able to break the hydrogen bonds between the chitin chains. The basic acetate anion was strong enough to cleave the hydrogen bond network of chitin, while the chloride and dimethylphosphate anions were less efficient and could only dissolve chitin to a limited degree.

2.5 Dissolution of Silk

Silk is a well-known natural fiber produced by the silk worm, *Bombyx mori*, which has been used traditionally in the form of threads. It is composed of two kinds of protein: fibrous fibroin and glue-like sericin. The fibroin forms the thread core, while the sericin surrounds the fibroin fibers to cement them together [89]. The fibroin protein consists of layers of antiparallel β -sheets. Its primary structure mainly consists of the recurrent amino acid sequence (Gly-Ser-Gly-Ala-Gly-Ala)_n [89; Fig. 1e].

Traditionally, silk fibers have been widely used in biomedical applications as a suture material for repairing wound injuries. Recently, the ability to fabricate silk-based materials, such as films, sponges, and fibers, from purified silk fibroin

solution has resulted in the reemergence of silk as a biomaterial [90]. Silk is an attractive tissue engineering scaffold because of its slow degradation, excellent mechanical properties, and biocompatibility [91].

Unfortunately, due to its stabilized secondary protein structure, silk fibroin has limited solubility characteristics, which results in significant limitations regarding the fabrication of tissue engineering scaffolds. To date, it is reported that silk fibroin is soluble in certain high ionic-strength aqueous salt solutions, such as DMAc/LiCl, aqueous LiSCN, LiBr, NaSCN, Ca(SCN)₂, CaCl₂, etc. [92, 93]. It is possible to dissolve silk and produce regenerated silk fibers from such spinning solutions; however, these solvents are harsh, very difficult to recycle, and will cause environmental problems.

The ability of ILs, such as [C₄mim]Cl, to disrupt hydrogen bonds also makes them an attractive solvent for silk in which unusual arrangements of hydrogen bonds play an important role in defining its strength [39]. In the study of Mantz et al. [39], the suitability of ILs for dissolving and regenerating silkworm (*Bombyx mori*) silk was tested. The ILs [C₄mim]Cl, [C₄mim]Br, [C₄mim]I, [C₄mim][BF₄], [C₄C₁mim]Cl, [C₂mim]Cl, [C₂mim][BF₄], and [C₄mim][AlCl₄] were evaluated to determine their ability to dissolve silk (Table 6). For most of the experiments, sericin was extracted from silk prior to solubilizing in the ILs; however, for the [C₄mim]Br, [C₄mim]I, and [C₄mim][BF₄] experiments, the sericin remained in the fibers, which were dried under vacuum. When [C₄mim]Br, [C₄mim]I, and [C₄mim][BF₄] were used to dissolve both silk and sericin, sericin was soluble in [C₄mim]Br and [C₄mim]I but insoluble in [C₄mim][BF₄]. Silk dissolved in the ILs could also be regenerated by adding antisolvents such as methanol or acetonitrile. Regenerated silk fibroin from *Bombyx mori* silk worms could also be extruded into fibers from the [C₂mim]Cl solvent system [94].

The dissolution of the silk fibroin in [C₄mim]Cl was examined with wide-angle X-ray scattering (WAXS) [39]. The data from a 12.24 wt% silk solution shows a broad amorphous halo centered near 20° 2θ, indicating that the silk is amorphous, which is contrasted with the diffractogram of crystalline cocoon silk which shows several peaks that can be indexed to an antiparallel β-sheet structure. As with cellulose and chitin, the available evidence suggests true dissolution of these biopolymers with the disruption of the interchain hydrogen bonding, a requirement for this to occur.

2.6 Dissolution of Wool

Natural wool is another abundant natural material. Wool contains amino acids linked together in ladder-like polypeptide chains [95]. The insulating and moisture absorbing properties of wool make it a desirable fiber for textiles. Every year large amounts of wool are wasted during wool shearing and weaving, but it is economically and environmentally quite challenging to develop a simple, inexpensive process to use and reuse wool resources.

Table 6 Solubility of silk in ILs [39]

Cation	Anion				
	Cl ⁻	Br ⁻	I ⁻	[BF ₄] ⁻	[AlCl ₄] ⁻
[C ₄ mim] ⁺	13.2%	0.7% ^a	0.2% ^a	0.0% ^a	— ^c
[C ₄ C ₁ mim] ⁺	8.3%	— ^c	— ^c	— ^c	— ^c
[C ₂ mim] ⁺	23.3%	— ^c	— ^c	0.0%	0.0% ^b

^aBoth sericin and fibroin were added to the solvent; only the sericin was soluble

^bSolvent was the [C₂mim]Cl/[C₂mim][AlCl₄] mixture with a 1.0:0.7 molar ratio

^cSystem not tested

Wool has a stable three-dimensional conformation maintained by a range of noncovalent and covalent interactions [40]. Thus, it is also difficult to process wool by directly dissolving it into common solvents, although some solvent systems such as urea/H₂O₂/H₂O and urea/2-mercaptoethanol have been used for the processing of wool [96]. The volatility and flammability of these solvents with the associated human health and environmental problems has led to increasing pressure for minimizing their use.

A study of ILs to dissolve wool keratin fibers, which occupy about 50 wt% of the cortical cells in wool, was reported by Xie et al. [40]. In this study, [C₄mim]Cl, [C₄mim]Br, [C₄mim][BF₄], [C₄mim][PF₆], and [amim]Cl were used (Table 7) to investigate the relationship between the solubility of wool keratin and the structure of the ILs. It is clear from the results that ILs containing the chloride anion are better solvents for wool keratin fibers than those with Br⁻ or non-coordinating anions such as [BF₄]⁻ and [PF₆]⁻.

Regenerated keratin fibers could be obtained by adding methanol, ethanol, or water into the wool/IL solution. The regenerated wool keratin exhibited a β -sheet structure with the disappearance of the original α -helix structure. It was reported that the thermal stability of the regenerated wool keratin was slightly superior to that of the natural wool keratin fibers.

Blends of wool and cellulose were prepared in [C₄mim]Cl by co-dissolution followed by coagulation [40, 96]. One study showed that the wool/cellulose blend films show significant improvement in thermal stability compared with the coagulated wool or cellulose. FT-IR analysis of the blends revealed the hydrogen bonding interactions between the hydroxyl groups of the wool and the cellulose [96]. Moreover, the blend films exhibited increasing tensile strength with increasing cellulose content. This work suggested the use of ILs for the development of wool-based materials with improved mechanical properties.

The dyeing behavior of [C₄mim]Cl treated wool was also reported [97]. Characterization of the IL-treated wool indicated that eroded marks were observed on treated wool fiber surfaces, and the tensile strength of treated wool fibers was slightly decreased compared with that of untreated wool fibers. Dyeing kinetics experiments revealed that the IL treatments greatly increased the initial dyeing rate and shortened half-dyeing time and time to reach dyeing equilibrium. The final exhaustion and color depth of IL-treated wool were also increased, accompanied by slightly decreased color fastness.

Table 7 Solubility of wool keratin fibers in ILs [40]

ILs	Temperature (°C)	Time (h)	Solubility (wt%)
[C ₄ mim]Cl	100	10	4
	130	10	11
[C ₄ mim]Br	130	10	2
[amim]Cl	130	10	8
[C ₄ mim][BF ₄]	130	24	Insoluble
[C ₄ mim][PF ₆]	130	24	Insoluble

It is clear from the structure of wool keratin (Fig. 1f) that there are multiple hydrogen bonds in wool. The dissolution of wool in ILs might also be attributed to the disruption of the intra- and intermolecular hydrogen bonds. However, there is no report on this mechanism, and further study on the mechanism of the dissolution of wool in ILs should be carried out.

2.7 Dissolution of Other Biopolymers

In addition to the above-mentioned six biopolymers, other polysaccharides, such as starch [98, 99], pectin [26], agarose [100], and dextrin [26], have also been dissolved in a variety of ILs (Table 1). (For example, starch can be dissolved in [C₄mim]Cl up to 15 wt% at 80°C [99].) From the structures of these polysaccharides (Fig. 1g–j), it is clear that these biopolymers contain multiple hydrogen bonds in common with the biopolymers already discussed above. It is perhaps no longer surprising that ILs with strong hydrogen bond acceptor anions have been identified as solvents for these biomacromolecules [26].

The dissolution temperature of pectin is higher than that of dextrin or amylose, which might be attributed to the difference in hydrophilicity of these polysaccharides [26]. Thus, it is reasonable to assume that the dissolution of these polysaccharides in ILs is also caused by the disruption of the hydrogen bonding by the ions in ILs.

3 Conclusions

The ability of ILs to dissolve directly biological macromolecules, such as cellulose, lignin, chitin, etc., has generated intense worldwide academic and industrial interest in a relatively short period of time. Dissolution of these biological macromolecules using ILs can now be carried out under mild conditions, with no volatilization of organic substances, and the ILs can be easily recycled and reused. Moreover, there is no significant decrease in the degree of polymerization of the regenerated macromolecules and chemical modifications of the macromolecules can easily be conducted in the IL solutions. All these advantages make the dissolution of

macromolecules with ILs a desirable and promising process, and we fully expect great progress in the use of ILs to untap the tremendous technological potential of natural biopolymers.

These natural, abundant biopolymers have a key role to play in any sustainable future. The ready dissolution of these biopolymers using ILs provides new platforms for their utilization, but perhaps from a different perspective than the current view that such biopolymers should be chopped up into platform chemicals. True dissolution without sacrificing molecular weight offers other processing options, allowing the modification of the architecture (e.g., fibers, membranes, beads, etc. [31]), rheology (e.g., with additives or blending with other polymers [96]), and indeed modifying their functions by covalently or noncovalently adding functional groups for further chemical processing [32].

However, the search for more and better IL solvents for these polymers needs further insight into the factors which govern solubility. The current published results seem to indicate a major role for the anion in breaking the many intermolecular hydrogen bonds. It is clear that there is also a role for the cation, since not every cation for a given anion will work, but it does seem that the effect is lessened. Some researchers continue to suggest that cations such as dialkylimidazolium are hydrogen bonding to the biopolymers, while other work suggests they are not. This point also needs clarification.

In summary, ILs are promising solvents for biomass processing, providing a new and powerful platform for the biomass industry. Although the technologies related to IL biomass processing are only at the laboratory stages, they may offer better pathways, less energy intensive processes, and significantly improved environmental benefits when compared with traditional processes. Current work is underway worldwide to demonstrate whether ILs can truly unlock the carbohydrate economy.

4 Prospects

The rapid increase in the number of publications on the use of ILs in the dissolution, treatment, and functionalization of biomass is a good indicator of the promising future of ILs in this area. With the significant progress in fundamental research, it is time to focus more attention on their potential industrial applications. However, progress in several key aspects is needed in order to industrialize any of the potential IL processes.

There is a current perception that the cost of ILs is too high to develop an economic process. This concern needs to be addressed in part by education and in part by the development of new manufacturing methods, efficient scale-up technologies, and by developing better ILs. It is hoped that the goals of sustainability will guide this process rather than just the expense of an ultimate IL or process. For example, better sources of raw materials, or new and effective synthetic routes (e.g., atom efficient methods), could be developed. Better and more complete data on physicochemical properties, toxicity, corrosivity, and

biodegradability would help inform better choices for process solvents. Even better data on such operating constraints as stability of the ILs at relatively high temperatures over extended periods of time and under shearing conditions would help promote their adoption.

Finally, from the point of view of environmental protection, as well as economics of the process, it is essential that effective and energy-saving IL recycling methods should be developed for each intended process. The current method to recycle ILs in biomass processing mainly centers on evaporation of the antisolvent, which would consume a lot of energy, especially in the case of IL/water solutions. Thus, further efforts to develop effective methods and facilities for IL recycling are needed.

Yes, the particular ability of some ILs, accompanied by a series of advantages, does enable the development of improved processing strategies and use for a plethora of biomass processing. However, this field is still new and it requires a better fundamental understanding of the mechanisms of dissolution and a wider exploration of the classes of ILs that can be used for a specific biopolymer. Much of this work is now underway around the world and we look forward to the fascinating results which will continue to appear.

Footnote: In our recent review (H. Wang, G. Gurau, R. D. Rogers, *Chem. Soc. Rev.*, 2012, **41**, 1519–1537), we pointed out that the use of more chemical units of solubility, such as “g cellulose per mole of IL” or “mol hydroxyl in cellulose per mole of IL” could provide more consistency in data reporting and more insight into the dissolution mechanism. However, in this chapter, the solubilities of the various biopolymers, often of unknown structure (e.g., lignin), are provided in terms of “wt%” as reported in the original literature. We would caution that even the term wt% can be somewhat confusing based on differing bases for determination of this number; some using true weight percent (percent of total mass) and some using mass fraction percent (percent of IL only).

References

1. Biomass (2004) The Need Project, PO BOX, 10101, Manassas
2. Kim JS, Park SC, Kim JW et al (2010) Production of bioethanol from lignocellulose: status and perspectives in Korea. *Bioresour Technol* 101:4801–4805
3. Wu YQ, Wu SY, Li Y et al (2009) Physico-chemical characteristics and mineral transformation behavior of ashes from crop straw. *Energy Fuel* 23:5144–5150
4. Cao Y, Wang Y, Riley JT et al (2006) A novel biomass air gasification process for producing tar-free higher heating value fuel gas. *Fuel Process Technol* 87:343–353
5. Knauf M, Moniruzzaman M (2004) Lignocellulosic biomass processing: a perspective. *Int Sugar J* 106:147–150
6. Bi W, Tian M, Zhou J et al (2010) Task-specific ionic liquid-assisted extraction and separation of astaxanthin from shrimp waste. *J Chromatogr B Anal Technol Biomed Life Sci* 878:2243–2248
7. Hecht SE, Niehoff RL, Narasimhan K et al (2006) Extracting biopolymers from a biomass using ionic liquids. *PCT Int. Appl. WO/2006/116126*

8. Leitner W (2004) Recent advances in catalyst immobilization using supercritical carbon dioxide. *Pure Appl Chem* 76:635–644
9. Dupont J, de Souza RF, Suarez PAZ (2002) Ionic liquid (molten salt) phase organometallic catalysis. *Chem Rev* 102:3667–3691
10. Kosmulski M, Gustafsson J, Rosenholm JB (2004) Thermal stability of low temperature ionic liquids revisited. *Thermochim Acta* 412:47–53
11. Matsumoto H, Yanagida M, Tanimoto K et al (2000) Highly conductive room temperature molten salts based on small trimethylalkylammonium cations and bis(trifluoromethylsulfonyl)imide. *Chem Lett* 6:922–923
12. Bosmann A, Datsevich L, Jess A et al (2001) Deep desulfurization of diesel fuel by extraction with ionic liquids. *Chem Commun* 2494–2495
13. Hagiwara H, Sugawara Y, Isobe K et al (2004) Immobilization of Pd(OAc)₂ in ionic liquid on silica: application to sustainable Mizoroki-Heck reaction. *Org Lett* 6:2325–2328
14. Galinski M, Lewandowski A, Stepniak I (2006) Ionic liquids as electrolytes. *Electrochim Acta* 51:5567–5580
15. Adams CJ, Earle MJ, Roberts G et al (1998) Friedel-Crafts reactions in room temperature ionic liquids. *Chem Commun* 2097–2098
16. Fischer T, Sethi A, Welton T et al (1999) Diels-Alder reactions in room-temperature ionic liquids. *Tetrahedron Lett* 40:793–796
17. Swatloski RP, Spear SK, Holbrey JD et al (2002) Dissolution of cellulose with ionic liquids. *J Am Chem Soc* 124:4974–4975
18. Heinze T, Schwikal K, Barthel S (2005) Ionic liquids as reaction medium in cellulose functionalization. *Macromol Biosci* 5:520–525
19. Zhang H, Wu J, Zhang J et al (2005) 1-Allyl-3-methylimidazolium chloride room temperature ionic liquid: a new and powerful nonderivatizing solvent for cellulose. *Macromolecules* 38:8272–8277
20. Ren Q, Wu J, Zhang J et al (2003) Synthesis of 1-allyl-3-methylimidazolium-based room temperature ionic liquid and preliminary study of its dissolving cellulose. *Acta Polymer Sinica* 3:448–451
21. Xu AR, Wang JJ, Wang HY (2010) Effects of anionic structure and lithium salts addition on the dissolution of cellulose in 1-butyl-3-methylimidazolium-based ionic liquid solvent systems. *Green Chem* 12:268–275
22. Feng L, Chen ZL (2008) Research progress on dissolution and functional modification of cellulose in ionic liquids. *J Mol Liq* 142:1–5
23. Ohno H, Fukaya Y (2009) Task specific ionic liquids for cellulose technology. *Chem Lett* 38:2–7
24. Welton T (1999) Room-temperature ionic liquids. Solvents for synthesis and catalysis. *Chem Rev* 99:2071–2083
25. Kosan B, Michels C, Meister F (2008) Dissolution and forming of cellulose with ionic liquids. *Cellulose* 15:59–66
26. Fukaya Y, Sugimoto A, Ohno H (2006) Superior solubility of polysaccharides in low viscosity, polar, and halogen-free 1,3-dialkylimidazolium formates. *Biomacromolecules* 7:3295–3297
27. Fukaya Y, Hayashi K, Wada M et al (2008) Cellulose dissolution with polar ionic liquids under mild conditions: required factors for anions. *Green Chem* 10:44–46
28. Barthel S, Heinze T (2006) Acylation and carbanilation of cellulose in ionic liquids. *Green Chem* 8:301–306
29. Wu J, Zhang J, Zhang H et al (2004) Homogeneous acetylation of cellulose in a new ionic liquid. *Biomacromolecules* 5:266–268
30. Bose S, Armstrong DW, Petrich JW (2010) Enzyme-catalyzed hydrolysis of cellulose in ionic liquids: a green approach toward the production of biofuels. *J Phys Chem B* 114:8221–8227

31. Bagheri M, Rodríguez H, Swatloski RP et al (2008) Ionic liquid-based preparation of cellulose-dendrimer films as solid supports for enzyme immobilization. *Biomacromolecules* 9:381–387
32. Sun N, Swatloski RP, Maxim ML et al (2008) Magnetite-embedded cellulose fibers prepared from ionic liquid. *J Mater Chem* 18:283–290
33. Pu YQ, Jiang N, Ragauskas AJ (2007) Ionic liquid as a green solvent for lignin. *J Wood Chem Technol* 27:23–33
34. Lee SH, Doherty TV, Linhardt RJ et al (2009) Ionic liquid-mediated selective extraction of lignin from wood leading to enhanced enzymatic cellulose hydrolysis. *Biotechnol Bioeng* 102:1368–1376
35. Sun N, Rodríguez H, Rahman M et al (2011) Where are ionic liquid strategies most suited in the pursuit of chemicals and energy from lignocellulosic biomass? *Chem Commun* 47:1405–1421
36. Xie HB, Zhang SB, Li SH (2006) Chitin and chitosan dissolved in ionic liquids as reversible sorbents of CO₂. *Green Chem* 8:630–633
37. Prasad K, Murakami M, Kaneko Y et al (2009) Weak gel of chitin with ionic liquid, 1-allyl-3-methylimidazolium bromide. *Int J Biol Macromol* 45:221–225
38. Qin Y, Lu XM, Sun N et al (2010) Dissolution or extraction of crustacean shells using ionic liquids to obtain high molecular weight purified chitin and direct production of chitin films and fibers. *Green Chem* 12:968–971
39. Phillips DM, Drummy LF, Conrady DG et al (2004) Dissolution and regeneration of *bombyx mori* silk fibroin using ionic liquids. *J Am Chem Soc* 126:14350–14351
40. Xie HB, Li SH, Zhang SB (2005) Ionic liquids as novel solvents for the dissolution and blending of wool keratin fibers. *Green Chem* 7:606–608
41. Kilpeläinen I, Xie H, King A et al (2007) Dissolution of wood in ionic liquids. *J Agric Food Chem* 55:9142–9148
42. Fort DA, Remsing RC, Swatloski RP et al (2007) Can ionic liquids dissolve wood? Processing and analysis of lignocellulosic materials with 1-n-butyl-3-methylimidazolium chloride. *Green Chem* 9:63–69
43. Sun N, Rahman M, Qin Y et al (2009) Complete dissolution and partial delignification of wood in the ionic liquid 1-ethyl-3-methylimidazolium acetate. *Green Chem* 11:646–655
44. Sun N, Jiang XY, Maxim ML et al (2011) Use of polyoxometalate catalysts in ionic liquids to enhance the dissolution and delignification of woody biomass. *ChemSusChem* 4:65–73
45. Li B, Asikkala J, Filpponen I et al (2010) Factors affecting wood dissolution and regeneration of ionic liquids. *Ind Eng Chem Res* 49:2477–2484
46. Cao Y, Wu J, Zhang J et al (2009) Room temperature ionic liquids (RTILs): a new and versatile platform for cellulose processing and derivatization. *Chem Eng J* 147:13–21
47. Ren JL, Sun RC, Liu CF et al (2007) Acetylation of wheat straw hemicelluloses in ionic liquid using iodine as a catalyst. *Carbohydr Polym* 70:406–414
48. Edgar KJ, Buchanan CM, Debenham JS et al (2001) Advances in cellulose ester performance and application. *Prog Polym Sci* 26:1605–1688
49. Fink HP, Weigel P, Purz HJ et al (2001) Structure formation of regenerated cellulose materials from NMMO-solutions. *Prog Polym Sci* 26:1473–1524
50. McCormick CL, Dawsey TR (1990) Preparation of cellulose derivatives via ring-opening reactions with cyclic reagents in lithium chloride/N,N-dimethylacetamide. *Macromolecules* 23:3606–3610
51. Fischer S, Voigt W, Fischer K (1999) The behaviour of cellulose in hydrated melts of the composition LiX·nH₂O (X = I⁻, NO₃⁻, CH₃COO⁻, ClO₄⁻). *Cellulose* 6:213–219
52. Heinze T, Liebert T (2001) Unconventional methods in cellulose functionalization. *Prog Polym Sci* 26:1689–1762
53. Wang ZG, Yokoyama T, Chang HM et al (2009) Dissolution of beech and spruce milled woods in LiCl/DMSO. *J Agr Food Chem* 57:6167–6170

54. Luo HM, Li YQ, Zhou CR (2005) Study on the dissolubility of the cellulose in the functionalized ionic liquid. *Polym Mater Sci Eng* 21:233–235 (in Chinese)
55. Handy ST (2003) Greener solvents: room temperature ionic liquids from biorenewable sources. *Chem-A Eur J* 9:2938–2944
56. Zhao H, Baker GA, Song ZY et al (2008) Designing enzyme-compatible ionic liquids that can dissolve carbohydrates. *Green Chem* 10:696–705
57. Zhao H, Jones CL, Cowins JV (2009) Lipase dissolution and stabilization in ether-functionalized ionic liquids. *Green Chem* 11:1128–1138
58. Striegel AM (2003) Advances in the understanding of the dissolution mechanism of cellulose in DMAc/LiCl. *J Chil Chem Soc* 48:73–77
59. Dupont AL (2003) Cellulose in lithium chloride/N, N-dimethylacetamide, optimisation of a dissolution method using paper substrates and stability of the solutions. *Polymer* 44:4117–4126
60. Remsing RC, Swatloski RP, Rogers RD et al (2006) Mechanism of cellulose dissolution in the ionic liquid 1-n-butyl-3-methylimidazolium chloride: A ¹³C and ^{35/37}Cl NMR relaxation study on model systems. *Chem Commun* 12:1271–1273
61. Remsing RC, Hernandez G, Swatloski RP et al (2008) Solvation of carbohydrates in N, N'-dialkylimidazolium ionic liquids: a multinuclear NMR spectroscopy study. *J Phys Chem B* 112:11071–11078
62. Ragauskas AJ, Williams CK, Davison BH et al (2006) The path forward for biofuels and biomaterials. *Science* 311:484–489
63. Zakzeski J, Bruijninx PCA, Jongerijs AL et al (2010) The catalytic valorization of lignin for the production of renewable chemicals. *Chem Rev* 110:3552–3599
64. Metzger JO, Bicke C, Faix O et al (1992) Matrix-assisted laser desorption mass-spectrometry of lignins. *Angew Chem-Int Ed Eng* 31:762–764
65. Brauns FE (1939) Native lignin. I. Its isolation and methylation. *J Am Chem Soc* 61:2120–2127
66. Lu FC, Ralph J (2003) Non-degradative dissolution and acetylation of ball-milled plant cell walls: high-resolution solution-state NMR. *Plant J* 35:535–544
67. Ikeda T, Holtman K, Kadla JF et al (2002) Studies on the effect of ball milling on lignin structure using a modified DFRC method. *J Agric Food Chem* 50:129–135
68. Tan SSY, MacFarlane DR, Upfal J et al (2009) Extraction of lignin from lignocellulose at atmospheric pressure using alkylbenzenesulfonate ionic liquid. *Green Chem* 11:339–345
69. Rahman M, Sun N, Qin Y, et al (2010) Ionic liquid systems for the processing of biomass, their components and/or derivatives, and mixtures thereof. *PCT Int. Appl. WO* 2010056790 A1, 5/20/2010
70. Lee SH, Lee SB (2005) The Hildebrand solubility parameters, cohesive energy densities and internal energies of 1-alkyl-3-methylimidazolium-based room temperature ionic liquids. *Chem Commun* 5:3469–3471
71. Swiderski K, McLean A, Gordon CM et al (2004) Estimates of internal energies of vaporisation of some room temperature ionic liquids. *Chem Commun* 4:2178–2179
72. Thielemans W, Wool RP (2005) Lignin esters for use in unsaturated thermosets: Lignin modification and solubility modeling. *Biomacromolecules* 6:1895–1905
73. Sun RC, Tomkinson J, Ma PL et al (2000) Comparative study of hemicelluloses from rice straw by alkali and hydrogen peroxide treatments. *Carbohydr Polym* 42:111–122
74. Ebringerova A, Hromadkova Z, Kacurakova M et al (1994) Quaternized xylans-synthesis and structural characterization. *Carbohydr Polym* 24:301–308
75. Niu W, Molefe MN, Frost JW (2003) Microbial synthesis of the energetic material precursor 1,2,4-butanetriol. *J Am Chem Soc* 125:12998–12999
76. Armstrong DW, He LF, Liu YS (1999) Examination of ionic liquids and their interaction with molecules, when used as stationary phases in gas chromatography. *Anal Chem* 71:3873–3876
77. Liu QB, Janssen MHA, van Rantwijk F et al (2005) Room-temperature ionic liquids that dissolve carbohydrates in high concentrations. *Green Chem* 7:39–42

78. Poirier M, Charlet G (2002) Chitin fractionation and characterization in N, N-dimethylacetamide/lithium chloride solvent system. *Carbohydr Polym* 50:363–370
79. Jayakumar R, Egawa T, Furuike T et al (2009) Synthesis, characterization, and thermal properties of phosphorylated chitin for biomedical applications. *Polym Eng Sci* 49:844–849
80. Chen LY, Du YM, Wu HQ et al (2002) Relationship between molecular structure and moisture-retention ability of carboxymethyl chitin and chitosan. *J Appl Polym Sci* 83:1233–1241
81. Daraghme N, Rashid I, Al Omari MMH et al (2010) Preparation and characterization of a novel co-processed excipient of chitin and crystalline mannitol. *AAPS Pharm Sci Tech* 11:1558–1571
82. Suzuki D, Takahashi M, Abe M et al (2008) Comparison of various mixtures of β -chitin and chitosan as a scaffold for three-dimensional culture of rabbit chondrocytes. *J Mater Sci Mater Med* 19:1307–1315
83. Atkins EDT (1985) Conformations in polysaccharides and complex carbohydrates. *J Biosci* 8:375–387
84. Rinaudo M (2006) Chitin and chitosan: properties and applications. *Prog Polym Sci* 31:603–632
85. Mine S, Izawa H, Kaneko Y et al (2009) Acetylation of α -chitin in ionic liquids. *Carbohydr Res* 344:2263–2265
86. Einbu A, Naess SN, Elgsaeter A et al (2004) Solution properties of chitin in alkali. *Biomacromolecules* 5:2048–2054
87. Wang WT, Zhu J, Wang XL et al (2010) Dissolution behavior of chitin in ionic liquids. *J Macromol Sci Part B Phys* 49:528–541
88. Agboh OC, Qin Y (1997) Chitin and chitosan fibers. *Polym Adv Technol* 8:355–365
89. Yamada H, Nakao H, Takasu Y et al (2001) Preparation of undegraded native molecular fibroin solution from silkworm cocoons. *Mater Sci Eng C* 14:41–46
90. Gupta MK, Khokhar SK, Phillips DM et al (2007) Patterned silk films cast from ionic liquid solubilized fibroin as scaffolds for cell growth. *Langmuir* 23:1315–1319
91. Servoli E, Maniglio D, Motta A et al (2005) Surface properties of silk fibroin films and their interaction with fibroblasts. *Macromol Biosci* 5:1175–1183
92. Xu Y, Zhang YP, Shao HL et al (2005) Solubility and rheological behavior of silk fibroin (*Bombyx mori*) in N-methyl morpholine N-oxide. *Int J Biol Macromol* 35:155–161
93. Aoki N, Furuhashi KI, Sakamoto M (1994) Cationic graft-copolymerization of tetrahydrofuran onto bromodeoxycellulose. *J Appl Polym Sci* 51:721–730
94. Phillips DM, Drummy LF, Naik RR et al (2005) Regenerated silk fiber wet spinning from an ionic liquid solution. *J Mater Chem* 15:4206–4208
95. Hameed N, Guo QP (2009) Natural wool/cellulose acetate blends regenerated from the ionic liquid 1-butyl-3-methylimidazolium chloride. *Carbohydr Polym* 78:999–1004
96. Hameed N, Guo QP (2010) Blend films of natural wool and cellulose prepared from an ionic liquid. *Cellulose* 17:803–813
97. Yuan JG, Wang Q, Fan XR (2010) Dyeing behaviors of ionic liquid treated wool. *J Appl Polym Sci* 117:2278–2283
98. Xu Q, Kennedy JF, Liu L (2008) An ionic liquid as reaction media in the ring opening graft polymerization of ϵ -caprolactone onto starch granules. *Carbohydr Polym* 72:113–121
99. Biswas A, Shogren RL, Stevenson DG et al (2006) Ionic liquids as solvents for biopolymers: acylation of starch and zein protein. *Carbohydr Polym* 66:546–550
100. Kimizuka N, Nakashima T (2001) Spontaneous self-assembly of glycolipid bilayer membranes in sugar-philic ionic liquids and formation of ionogels. *Langmuir* 17:6759–6761

Structures and Thermodynamic Properties of Ionic Liquids

Tiancheng Mu and Buxing Han

Abstract This chapter gives a brief review on the structures and thermodynamic properties of ionic liquids. It is organized as follows. The introduction gives the definition and application fields of ionic liquids. Following that is the main part where we present a review on the density, phase behavior, enthalpy of vaporization, and heat capacity of ionic liquids. The properties of both pure ionic liquids and mixtures with ionic liquids are discussed. Some experimental pieces of apparatus for working with these properties are introduced briefly. We then review the correlations with the experimental data and prediction methods based on MD or ab initio methods. In the discussion of phase behavior, the vapor–liquid equilibria, liquid–liquid equilibria, and the activity coefficients at infinite dilution are presented separately. In the last part, a summary and outlook on this topic are given.

Keywords Ionic liquids • Density • PVT behavior • Heat capacity • Enthalpy of vaporization

Abbreviations

1-Alkyl-3-methylimidazolium [C_nMIM] or [AMIM] with A = M, E, P, B, Pe, H, O, D, as alkyl = methyl, ethyl, propyl, pentyl, hexyl, octyl, decyl

T. Mu (✉)

Department of Chemistry, Renmin University of China, Beijing 100872, China

e-mail: tcmu@chem.ruc.edu.cn

B. Han

Beijing National Laboratory for Molecular Sciences, Institute of Chemistry, Chinese Academy of Sciences, Beijing 100080, China

e-mail: hanbx@iccas.ac.cn

1-Alkyl-2,3-dimethylimidazolium	[C _n MMIM] with A = M, E, P, B, Pe, H, O, D, as alkyl = methyl, ethyl, propyl, pentyl, hexyl, octyl, decyl
[Ace]	Acesulfamate
[BETI]	Bis(perfluoroethanesulfonyl) imide
[BF ₄]	Tetrafluoroborate
[C(CN) ₃]	Tricyanomethane
[CH ₃ (OCH ₂) ₂ OSO ₃]	Diethyleneglycol monomethylethersulfate
[CH ₃ (OCH ₂ CH ₂) ₂ OSO ₃]	Diethyleneglycol monomethylether sulfate
[DCA]	Dicyanamide
[EtOSO ₃]	Ethylsulfate
ILs	Ionic liquids
[Lac]	Lactate
[Methide]	Tris(trifluoromethylsulfonyl) methide
[MeSO ₃]	Methanesulfonate
[MeOSO ₃]	Methylsulfate
[MeOHPO ₂]	Methylphosphonate
[N _{R1R2R3R4}]	Quaternary ammonium
[OcOSO ₃]	Octylsulfate
[OTf]	Trifluoromethanesulfonate or triflate
PEG	Polyethylene glycol
[PF ₆]	Hexafluorophosphate
[PF ₃ (CF ₂ CF ₃) ₃]	Tris(pentafluoroethyl) trifluorophosphate
[Py]	Pyridinium
[Pyr]	Pyrrolidinium
[P _{R1R2R3R4}]	Tetraalkylphosphonium
[SCN]	Thiocyanate
[TMG]	1,1,3,3-Tetramethylguanidine
[TFA]	Trifluoroacetate
[Tf ₂ N]	Bis(trifluoromethanesulfonyl) imide or triflimide

1 Introduction

Ionic liquids (ILs) have many unusual properties, such as low melting point, wide liquid range, excellent thermal stability, wide electrochemical window, and low volatilities [1]. They are regarded as green solvents and alternatives for volatile organic compounds. Furthermore, ILs are referred to as designer solvents because their properties can be easily tuned by choosing cationic or anionic constituents which expands their potential applications. The specifically designed properties include both physical properties such as density, viscosity, electrical and thermal conductivity, optical activity, and surface tension, and chemical properties such as electrophilicity, nucleophilicity, acidity, and basicity. Exponential growth is occurring in the research and applications of ILs. Plechkova and Seddon [2] reviewed the

Table 1 The application fields and examples of ILs

Property	Application field	Examples
Electric conductivity	Energy conversion and metallurgy	Electrolytes in battery and solar cells [4], electrodeposition of reactive metals, electropolishing
High heat capacity [5]	Heat storage	Medium for storing heat [6], heat transfer liquids [7], heat carriers for solar installations [8]
Good solvent power, low vapor pressure	Solvents for chemical processes	Extraction and separation [9], medium for various chemical reactions, stationary phases for gas chromatography [10]
Biocompatibility	Biotechnology	Medium for biocatalysis, biomass conversion, dissolution and regeneration of cellulose [11]
Other properties	Other applications	Inorganic materials [12, 13], microemulsion, surfactants

applications of ILs in the chemical industry. Short commented that “ILs are starting to leave academic labs and find their way into a variety of industrial applications” [3]. Some research and industrial applications of ILs are shown in Table 1 [14, 15].

The unique properties of ILs depend on their special structures. Besides the non-volatility and good solvent power, ILs are not very corrosive, which makes them good solvents for many organic and inorganic compounds. With the rapid development of ILs, large amounts of experimental investigations on the physico-chemical properties of ILs have been carried out. However, compared to the large number of possible ILs, the available data are still scarce, which greatly hinders the applications of ILs. In this chapter we intend to review the structures and thermodynamic properties of IL systems. We focus on the most commonly used ILs and the latest results. We would like to emphasize that huge number of excellent results have been reported, and this short chapter merely includes some of these.

2 Density

The density and its temperature and pressure dependence are important thermophysical properties and are necessary for analyzing isothermal compressibility, thermal expansion, and excess properties, the construction of equations of state, and so on. They are useful for designing industrial processes such as storage vessel sizing. The densities of ILs can be tuned by adjusting the structure of anions or cations. Luckily, the temperature and purity dependency of density is not very significant. At ambient pressure and temperature, the densities of most ILs are in the range of $0.9 \sim 1.7 \text{ g}\cdot\text{cm}^{-3}$. The densities of ILs are affected by their structure, such as anions, cations, and substituents on the cations. Usually the densities of imidazolium-based ILs are larger than 1, while tert-phosphonium-based ILs have a density less than 1, so in the imidazolium-based ionic liquid and water binary systems, the water-rich phase is usually the top phase. Many experimental pieces of work have been carried out on the measurement of density and its pressure and

temperature dependence [16, 17] for both pure ILs and solutions [18, 19]. However, the studies are focused on the commonly used type ILs, such as the imidazolium and tert-phosphonium-based ILs. The experimental density data of ILs are often discrepant and poorly consistent with each other. The main reasons are that the purities of the ILs synthesized by different laboratories vary considerably, and maybe the determination methods affect the data. So systematic works are still needed for both theoretical models development and industrial applications.

The experimental data in Table 2 indicate that phosphonium-based ILs have lower density than imidazolium-based ILs at the same temperature. The densities of the ILs containing phosphonium cations range from 0.88 to 1.05 g·cm⁻³, while those containing ammonium cations range from 1.08 to 1.37 g·cm⁻³ [21]. Systematic experiments were carried out by Tokuda et al. to study the effect of anion [28], cation [29], alkyl chain length of the [C_nMIM] cation [30], and temperature on the physicochemical properties of ILs.

The densities of the ILs formed from [BMIM] with a variety of fluorinated anions follow the order [BMIM][BETI] > [BMIM][Tf₂N] > [BMIM][PF₆] > [BMIM][OTf] > [BMIM][TFA] > [BMIM][BF₄] at the same temperature. The order of density of [BMIM]-based ILs approximately follows the decreasing of molecular weight of the anions [28]. The densities of cationic structures, [BMIM], [BPy], [BMPyrr], and [(*n*-C₄H₉)(CH₃)₃N] with anion [Tf₂N], were measured to investigate the cationic effect on the densities of the ILs. The results showed that the aromatic cation-based ILs have higher density than those the aliphatic cations-based ILs. The densities follow the order [BPy] > [BMIM] > [BMPyrr] > [(*n*-C₄H₉)(CH₃)₃N] [29]. The densities of [C_nMIM][Tf₂N], indicate that for the methyl-imidazolium-based ILs with a fixed anion, the density follows a linear decrease with the increasing of the alkyl chain length on the imidazolium cation [30]. In all cases, density decreases linearly with increasing temperature Eq. 1, but at a rate less than that for molecular organic compounds (Table 3):

$$\rho = b - aT \quad (1)$$

The effects of alkyl chain length on the densities are verified by the investigation of densities of quaternary ammonium RTILs ([N₄₁₁₁][Tf₂N], [N₄₁₁₃][Tf₂N], [N₆₁₁₁][Tf₂N], [N₆₁₁₃][Tf₂N], [N₆₂₂₂][Tf₂N], [N_{10,111}][Tf₂N], [N_{10,113}][Tf₂N], and [N₁₈₈₈][Tf₂N]) and quaternary phosphonium RTILs ([P_{14,666}][Tf₂N], [P₂₄₄₄][DEP], [N_{14,444}][DBS], [N_{14,666}][DCA], and [N_{14,666}Cl]) [21]. The experimental density data of the ILs consisting of [BMIM] with various perfluorinated anions and the [Tf₂N] anion with pyrrolidinium-, ammonium-, and hydroxyl-containing cations [31] give similar results with Tokuda's conclusion [28, 29]. Tariq et al. reported the densities of the following ILs: [C_nMIM][Tf₂N] with *n* = 2, 4, 6, 8, 10, 12, 14, and [C_nMIM][PF₆] with *n* = 4, 6, 8; [P_{14,666}], combined with the anions [Tf₂N], [OAc], and [OTf], and [BMIM] combined with the anions [OAc], [OTf], [MeOSO₃], and [BF₄] at four different temperatures ranging from 293 to 333 K [32]. The results show that the density of [C_nMIM][Tf₂N]-based ILs decrease with the increase of the alkyl chain length. The density of [P_{14,666}]-based ILs decreases with the order of

Table 2 Experimental densities of ILs

ILs	T (K)	Value/g·cm ⁻³	Ref
[EMIM][Tf ₂ N]	278.15–328.15	1.5391–1.4887	[20]
[BMIM][Tf ₂ N]	278.15–328.15	1.4561–1.4079	[20]
[N ₄₁₁₁][Tf ₂ N]	278.15–328.15	1.4123–1.3673	[20]
[N ₈₈₈₁][Tf ₂ N]	278.15–328.15	1.1198–1.0821	[20]
[EMIM][EtOSO ₃]	278.15–328.15	1.2551–1.2206	[20]
[BMIM][OcOSO ₃]	278.15–328.15	1.0773–1.0443	[20]
[P _{14,666}]Cl	298.15–333.15	0.8826–0.8644	[21]
[P _{14,666}][DCA]	298.15–333.15	0.9209–0.9024	[21]
[P _{14,666}][Tf ₂ N]	298.15–333.15	1.0501–1.0296	[21]
[P ₂₄₄₄][DEP]	298.15–333.15	0.9978–0.9758	[21]
[P _{14,444}][DBS]	298.15–333.15	0.9384–0.9201	[21]
[N ₄₁₁₃][Tf ₂ N]	298.15–333.15	1.3483–1.3215	[21]
[N ₆₁₁₃][Tf ₂ N]	298.15–333.15	1.2846–1.2585	[21]
[N _{10,113}][Tf ₂ N]	298.15–333.15	1.2007–1.1760	[21]
[N ₄₁₁₁][Tf ₂ N]	298.15–333.15	1.3747–1.3439	[21]
[N ₆₁₁₁][Tf ₂ N]	298.15–333.15	1.3106–1.2839	[21]
[N _{10,111}][Tf ₂ N]	298.15–333.15	1.2263–1.2003	[21]
[N ₆₂₂₂][Tf ₂ N]	298.15–333.15	1.2793–1.2530	[21]
[N ₁₈₈₈][Tf ₂ N]	298.15–333.15	1.0823–1.0611	[21]
[EMIM][OTF]	268.45–355.90	1.4115–1.3392	[22]
[BMIM][OTF] (Merke KGaA)	293.37–355.85	1.3027–1.240	[22]
[BMIM][OTF] (Solvionic SA)	292.94–342.95	1.3022–1.2611	[22]
[HMIM][OTF]	293.96–355.40	1.2423–1.1962	[22]
[HMIM][BF ₄]	268.65–356.07	1.1666–1.1066	[22]
[EMIM][PF ₃ (CF ₂ CF ₃)]	283.15–338.15	1.72705–1.66221	[23]
[MIM][BF ₄]	293.15–363.15	1.38797–1.33156	[24]
[BMIM][BF ₄]	283.15–363.15	1.21309–1.15630	[24]
[OMIM][BF ₄]	283.15–363.15	1.11411–1.06071	[24]
[BMPy][BF ₄]	293.15–363.15	1.19298–1.14565	[24]
[BMIM][DCA]	293.15–363.15	1.06205–1.01849	[24]
[BMPy][DCA]	293.15–363.15	1.05171–1.01026	[24]
[BMPyr][DCA]	293.15–363.15	1.11870–1.07702	[24]
[BMPyr][TFA]	293.15–363.15	1.17574–1.12772	[24]
[BMIM][SCN]	293.15–363.15	1.07282–1.03225	[24]
[BMPy][SCN]	293.15–363.15	1.06436–1.02522	[24]
[BMPyr][SCN]	293.15–363.15	1.03287–0.99643	[24]
[BMIM][MeOSO ₃]	293.15–363.15	1.21018–1.16470	[24]
[BMPyr][MeOSO ₃]	293.15–363.15	1.21605–1.17024	[24]
[EMIM][EtOSO ₃]	278.15–348.15	1.25112–1.20401	[25]
[EMIM][OTF]	278.15–348.15	1.40052–1.34230	[26]
[EMIM][TFA]	278.15–348.15	1.30689–1.25163	[26]
[N ₄₄₄₁][Ser]	293.15–363.15	1.019–0.976	[27]
[N ₄₄₄₁][Tau]	293.15–363.15	1.054–1.012	[27]
[N ₄₄₄₁][Lys]	293.15–363.15	0.983–0.941	[27]
[N ₄₄₄₁][Thr]	293.15–363.15	1.003–0.960	[27]
[P ₄₄₄₄][Ser]	293.15–363.15	0.996–0.953	[27]

(continued)

Table 2 (continued)

ILs	T (K)	Value/g·cm ⁻³	Ref
[P ₄₄₄₄][Tau]	293.15–363.15	1.030–0.987	[27]
[P ₄₄₄₄][Lys]	293.15–363.15	0.971–0.929	[27]
[P ₄₄₄₄][Thr]	293.15–363.15	0.983–0.941	[27]
[P ₄₄₄₄][Pro]	293.15–363.15	0.996–0.953	[27]
[P ₄₄₄₄][Val]	313.15–363.15	0.932–0.902	[27]
[P ₄₄₄₄][Cys]	293.15–363.15	1.037–0.993	[27]

Table 3 Molecular weight, density equation parameters, and molar concentration at 303.15 K of [BMIM]-based, [C_nMIM][Tf₂N], and [Tf₂N]-based ILs [28–30]

ILs	MW	a/10 ⁻⁴ g·cm ⁻³ ·K ⁻¹	b/g·cm ⁻³	M ₃₀ /10 ⁻³ mol·cm ⁻³
[BMIM][BETI]	519.4	10.3	1.81	2.91
[BMIM][Tf ₂ N]	419.4	9.40	1.72	3.42
[BMIM][OTf]	288.2	8.00	1.54	4.49
[BMIM][PF ₆]	284.2	8.69	1.63	4.80
[BMIM][TFA]	252.2	7.54	1.44	4.81
[BMIM][BF ₄]	226.0	7.26	1.42	5.30
[MMIM][Tf ₂ N]	377.3	10.6	1.87	4.15
[EMIM][Tf ₂ N]	391.3	10.0	1.82	3.87
[HMIM][Tf ₂ N]	447.4	10.20	1.67	3.05
[OMIM][Tf ₂ N]	475.5	10.00	1.62	2.77
[BPy][Tf ₂ N]	416.4	9.26	1.73	3.47
[BMPPro][Tf ₂ N]	422.4	9.09	1.67	3.29
[(n-C ₄ H ₉)(CH ₃) ₃ N][Tf ₂ N]	396.4	9.09	1.66	3.50

[OAc] < [OTf] < [Tf₂N], while the density of [C_nMIM][X]-based ILs increases in the order [OAc] < [BF₄] ≈ [MeOSO₃] < [OTf] < [PF₆] < [Tf₂N] [32].

Similar results have been obtained by the investigation of the effects of cation's alkyl chain lengths on the densities of [PMIM][Tf₂N] and [PeMIM][Tf₂N] in the temperature range from 298 to 333 K at pressures up to 60 MPa using a vibrating-tube densimeter [33]. Klomfar et al. measured the densities of [C_nMIM]-based ILs at atmospheric pressure in the temperature range of 268–356 K [22, 34]. The estimated total standard uncertainty of density average values are less than ± 0.4 kg m⁻³. The results verify that longer alkyl chains are associated with lower densities of the corresponding ILs. The densities of the *n*-alkylsubstituted guanidinium ILs, containing Cl, [BF₄], [Ace], saccharinate, and tosylate as anions, are reported and considered as a function of the length of the *n*-alkyl substituent R and the nature of the anions [35]. Densities of the RTILs decrease slightly with temperature.

Alkyl-phosphonium amino acid ILs have low densities, ranges from 0.886 to 0.945 g·cm⁻³ at 25°C [36]. The densities of the amino acid ILs depend mainly on the number of carbon atoms in the cations, while are almost independent of the symmetry of the cations.

The influences of pressure and the anion on properties of phosphonium-based ILs $[(C_6H_{13})_3P(C_{14}H_{29})]Cl$, $[(C_6H_{13})_3P(C_{14}H_{29})][Tf_2N]$, and $[(C_6H_{13})_3P(C_{14}H_{29})][Ac]$ have been studied up to 65 MPa in the temperature range 298–333 K. A simple ideal-volume model was employed for the prediction of the molar volumes of the phosphonia at ambient condition [37]. The measurements of expansivities and isothermal compressibilities of [BMIM][PF₆], [OMIM][PF₆], [OMIM][BF₄], and [BPy][BF₄] at pressures up to 206.9 MPa reveal that ILs are less compressible than organic solvents, and are similar to that of water [38].

Most of the densities of ILs reported are determined by vibrating-tube densimeter based on a simple physical model of the undamped spring-mass system. The cost of the vibrating-tube densimeter is relatively low, and the measurement range is large. However, the viscosity of sample must be considered because most ILs are highly viscous. Sanmamed [39] et al. investigated viscosity-induced errors in the density determination of ILs using vibrating tube densitometry. Equation 2 quantified viscosity-induced or damping errors with $\eta_0 = 30$ being a reference viscosity value and a , b , and c being the fitting coefficients:

$$\Delta\rho(\eta) = \frac{(\eta - \eta_0)^2}{a + b(\eta - \eta_0) + c(\eta - \eta_0)^2} \quad (2)$$

Iglesias-Otero et al. [40] designed a densimeter that automatically corrected the data for the viscosity effect on the vibrating-tube densimeters measurement. A high-pressure densimeter [41] was used to determine the expansivities and isothermal compressibilities of [BMIM][PF₆], [OMIM][PF₆], [OMIM][BF₄], and [BPy][BF₄] at pressures to 206.9 MPa [38].

Sometimes it is difficult to obtain a large number of samples, and small-scale characterization processes are necessary. The product of viscosity-density of [BMIM][OTf] + water and [BMIM][Tf₂N] + methanol obtained using impedance analysis of a quartz crystal microbalance are consistent with those obtained using a viscometer and density meter, but only requires a sample volume two orders of magnitude smaller. The pure ILs have the largest difference to about 10 % [42, 43]. A dual Quartz Crystal Microbalance setup with one smooth, and one patterned surface using chemically compatible materials was used to separate viscosity and density measurements of ILs. The measurement results are consistent with standard measurement techniques [44].

A large number of models to correlate and predict the density of liquids have been proposed [45, 46]. Some of the expressions are based on adjustable parameters for each fluid (correlations), while other expressions are based on group contribution methods (semiemperical and predictive), or on molecular mechanical or quantum chemical principles (predictive) [47, 48].

Ye et al. [49] proposed a group contribution model to estimate the density of ionic liquid. The model was checked by predicting 59 common imidazolium-, pyridinium-, pyrrolidinium-, tetraalkylammonium-, and phosphonium-based RTILs. The mean absolute deviation (MAD) of the densities is $0.007 \text{ g}\cdot\text{cm}^{-3}$,

while for 35 imidazolium-based ILs, the MAD is $0.020 \text{ g}\cdot\text{cm}^{-3}$. A further modified version [50], Eq. 3, enables the estimation of the densities of ILs in wide ranges of temperature and pressure using the previously proposed parameter table [49]:

$$\rho = \frac{W}{NV_0(a + bT + cP)} \quad (3)$$

where ρ is the density, W is the molar mass, N is the Avogadro constant, V is the molecular volume, T is the temperature in K, and P is the pressure in MPa. The coefficients a , b , and c are estimated by fitting the equation to experimental data. The new density correlation data are in good agreement with experimental literature data in a temperature range 273.15–393.15 K and pressure range 0.1–100 MPa. The mean percent deviation (MPD) for imidazolium-, phosphonium-, pyridinium-, and pyrrolidinium-based ILs is 0.45 %, 1.49 %, 0.41 %, and 1.57 %, separately. For imidazolium-based ILs [EMIM][MeOSO₃], [EMIM][EtOSO₃], [EMIM][Tf₂N], and [DMIM][Tf₂N] in pressure ($0.10 < P/\text{MPa} < 35.00$) and temperature ($293.15 < T/\text{K} < 393.15$) domains, the experimental densities are in good agreement with the predicted densities obtained by Eq. 2 and the correlation using the Tait equation and Sanchez-Lacombe equation of state [51]. Based on the experimental density of four [BMIM]-based ILs [52] and five [EMIM]-based ILs [53], (3) was modified to Eq. 4 to calculate the temperature dependence of density:

$$\rho = \frac{W}{NV_0(a_1 + a_2T + (b_1P + b_2P^2))} \quad (4)$$

A generalized correlation (Eqs. 5 and 6) with five parameters (a , b , c , d and δ) and four properties (critical temperature, the critical volume, the normal boiling temperature and the molecular mass) [54, 55]) to predict the density of ionic liquid at temperatures (270–360 K) was proposed [56]:

$$\rho = \left(\frac{A}{B}\right) + \left(\frac{2}{7}\right) \left\{ \frac{A \cdot \ln B}{B} \right\} \frac{(T - T_B)}{T_C - T_B} \quad (5)$$

$$A = a + b \cdot \frac{M}{V_C}, \quad B = \left(\frac{c}{V_C} + \frac{d}{M}\right) \cdot V_C^\delta \quad (6)$$

The parameters $a = 0.3411$, $b = 2.0443$, $c = 0.5386$, $d = 0.0393$, and $\delta = 1.0476$ were obtained from fitting the experimental data. The results show that the new simple correlation gives low deviations and can be used with confidence in thermodynamic and engineering calculations.

Experimental density data and correlation results with the Tait equation for the ILs [EMIM][OTF], [PMPy][Tf₂N], [PMPyrr][Tf₂N], [BMPyrr][Tf₂N], and [PMpip][Tf₂N] were provided by Gardas et al. over a wide range of pressure and temperature to help understand the influence of cations on the physicochemical

properties of the ILs [57]. The AARD is smaller than 0.02%. Gardas [58] et al. further provided the density of ILs ([BMIM][BF₄], [OMIM][BF₄], [HMIM][PF₆], [OMIM][PF₆], [BMMIM][PF₆], and [BMIM][OTf]) at pressures up to 10 MPa and temperature range from 293.15 to 393.15 K to investigate the influence of the cation alkyl chain length, the number of cation substitutions, and the anion on the properties. They proposed a simple ideal-volume model for the prediction of the imidazolium molar volumes, which agree well with the experimental results. Guan et al. [59] presented a group contribution method to predict the molecular volume, the standard molar entropy, the parachor, the surface tension, and the molar enthalpy of vaporization, of amino acid ionic liquid [C_nMIM][Glu] (n = 1, 2, 3, 4, 5, 6), in good agreement with the experimental thermal expansion coefficient for [PMIM][Glu].

Wang et al. [60] developed a group contribution equation of state based on electrolyte perturbation theory to predict the densities of ILs at different temperatures and pressures. An ionic liquid is divided into cation, anion, and alkyl substituents. A total number of 202 data points of density for 12 ILs and 2 molecular liquids (i.e., 1-methylimidazole and 1-ethylimidazole) were used to fit the group parameters. The performance of the model was examined by describing the densities of 29 imidazolium-based ILs at varying temperatures and pressures. The overall mean relative deviations for correlation is 0.41% and for prediction is 0.63%, which demonstrates the applicability of the model.

Lazzus et al. combined an artificial neural network and a simple group contribution method to predict liquid densities of imidazolium-based ILs [61]. The train set includes 1,736 data points of density at several temperatures and pressures, corresponding to 131 ILs. The prediction results compared to experimental data from the literature are within acceptable accuracy (AARD = 0.44; R² = 0.9934), for a wide range of temperatures and pressures. A similar method was developed to correlate and predict the densities of ILs with the training set having a total of 399 points and the prediction set 83 points [62]. The average relative percent deviations and maximum deviations between predicted and experimental densities are -0.01 % and 2.41 %, respectively. The authors provided the program codes and the necessary input files to calculate the density for other ILs.

Hu et al. [63] extended the simple equations [64] for predictions of the density, viscosity, and conductivity of mixed electrolyte solutions to predict the related properties of mixed ionic liquid solutions.

The above group contribution models are based on parameters derived from experimental data, so they are not pure predictive methods. Molecular modeling simulation based on the force field is a powerful tool to predict solvent properties, which are very useful in case the required parameters are not available. Molecular dynamics simulation has been used to estimate the densities of ILs. The simulation results of [C_nMIM]I (n = 4, 6, 8) are quite consistent with the experimental data, with a maximum deviation of 3.0 % due to [OMIM]I at 358 K [65]. Derecskei et al. [66] investigated the density and two-component solubility parameter of a variety of ILs using atomistic level molecular modeling and the Materials Studio software package. It was found that the density of ILs comprised of all possible

combinations of ethyl, butyl, and hexyl imidazolium cations and anions (Cl, [DCA], [TFA], and [Tf₂N]) can be calculated with satisfactory accuracy with the exception of systems containing the Cl.

The COSMO-RS [67] method based on quantum chemistry calculations was used to predict the specific density and molar liquid volume of 40 imidazolium-based ILs [68]. The pure ionic liquid compounds were simulated by the combination of cation and anion. The cations include [MMIM], [EMIM], [BMIM], [HMIM], and [OMIM] with the anions Cl, [BF₄], [FeCl₄], [PF₆], [Tf₂N], [MeOSO₃], [EtOSO₃], and [OTF]. The calculated and experimental density values of ILs were fitted by linear regressions with correlation coefficient $R > 0.99$. Molar liquid volumes predicted by COSMO-RS are very accurate [68].

Mokhtarani et al. [69] proposed a model with only one adjustable parameter which was determined by fitting of the experimental data to calculate densities, viscosities, and refractive indices of RTIL + organic solvent mixtures from pure component physical properties and their mole fractions. The model has reasonable accuracy for the physical properties of binary systems. Iglesias-Otero et al. [70] proposed a model to correlation density of ionic liquid mixtures. More work is still being done on the model development for density prediction.

3 Phase Behavior

Numerous works have been carried out on the phase equilibria of mixtures with ILs. We would like to review vapor–liquid equilibria (VLE) and liquid–liquid equilibria (LLE) separately. With regard to VLE, we put emphasis on the ILs + carbon dioxide systems [71]. In addition, the phase equilibria of sulfur dioxide-IL systems are discussed [72]. Regarding LLE, we focus on the phase behavior of ILs plus commonly used organic solvents and water.

3.1 Vapor–Liquid Equilibria

ILs have potential as solvents to separate gases according to physical or chemical interactions. In these cases, the phase behaviors of the ILs plus gases are prerequisite.

The solubilities and the related properties such as Henry's constants and enthalpies and entropies of dissolution for CO₂, ethylene, ethane, methane, argon, oxygen, carbon monoxide, hydrogen, and nitrogen in [BMIM][PF₆] up to a gas pressure of 1.3 MPa at 283.15, 298.15, and 323.15 K have been studied [73]. Results showed that CO₂ had the highest solubility in [BMIM][PF₆], followed by ethylene and ethane. Argon and oxygen have very low solubility while the solubility of carbon monoxide, hydrogen, and nitrogen are below the detection limit. The limitation of solubilities of hydrogen, oxygen, and carbon monoxide indicates

that [BMIM][PF₆] is not a very good industrial solvent for reactions involving these gases, because these reactions would be limited by interphase mass transfer. The mole fraction-pressure curves of CO₂ at fixed temperature exhibit a nonlinear trend and tend to flatten out, indicating pressure-independent capacity for CO₂ [73]. The solubilities of all other gases studied in the IL at a fixed temperature are linear with pressure. Therefore it is sufficient to use Henry's constants to describe these behaviors. The enthalpy and entropy of dissolution give information about the strength of interaction and the level of ordering in the IL/gas mixture, respectively. CO₂ exhibits significantly stronger molecular interactions and a higher degree of ordering than the other gases. The enthalpy and entropy values for ethylene and ethane indicate that their interactions with the ionic liquid are similar to those with both polar and nonpolar solvents. Methane shows no interaction or ordering in the ionic liquid. Argon and oxygen exhibit positive enthalpy and entropy of dissolution, indicating that the dissolution is entropy driven [73]. The entropy driven process is not unusual for gases with low solubilities in liquids [74, 75]. The positive enthalpy and entropy changes for gases in the ionic liquid are much greater than in other solvents. This may be due to the high Coulombic attraction between the ions. The study also showed that ILs have good potential to use as gas-separation media [73].

Many research groups have investigated the phase equilibria of the binary or ternary mixtures containing ILs and supercritical CO₂ [76]. Brennecke and coworkers reported that CO₂ dissolved in ionic liquid, while ionic liquid did not dissolve in CO₂ [77]. Therefore, supercritical CO₂ is a candidate solvent to extract organic compounds from ILs without cross contamination. For this purpose, an understanding of the phase behavior of supercritical CO₂ with ILs is necessary to design the processes. The high-pressure phase behaviors of CO₂ with six ILs – [BMIM][PF₆], [OMIM][PF₆], [OMIM][BF₄], [BMIM][NO₃], [EMIM][EtSO₄], and [BPy][BF₄] – show that a large quantity of CO₂ dissolves in the ionic liquid phase, but no appreciable amount of ionic liquid is solubilized in the CO₂ phase. The liquid phase volume expansion with the introduction of CO₂ is negligible, in contrast to the large volume expansion observed for neutral organic liquids [78]. The solubilities of CO₂ in different ILs increase with increasing pressure and decrease with increasing temperature. They are strongly dependent on the properties of the anions. In particular, CO₂ solubility is greater in ILs with anions containing fluoroalkyl groups. An increase in the alkyl chain length on the cation increases the CO₂ solubility marginally [79, 80].

Zhang et al. [81] determined the solubilities of CO₂ in [BMIM][PF₆] and 1,1,3,3-tetramethylguanidine lactate ([TMG][Lac]) [82] at temperatures ranging from 297 to 328 K and pressures up to 11 MPa. There is a basic functional group guanidinium in [TMG][Lac]. Therefore [TMG][Lac] is a potential solvent for CO₂ capture. Experimental results show that the solubility of CO₂ in [TMG][Lac] is slightly higher than that in [BMIM][PF₆]. Compared with aqueous amine, the solvency of [TMG][Lac] is limited and cannot be used to capture CO₂ efficiently in industry. Bates et al. reported CO₂ capture with the amino-functionalized ionic liquid, and the absorption capacity reaches 0.5 mol CO₂ per mole of the ionic liquid [83]. For the dual amino-functionalized phosphonium ILs [84, 85] and imidazolium

ionic liquid [86], the absorption capacities reach about 1 mol CO₂ per mole of ionic liquids. The interactions between these amino-functionalized ILs and CO₂ are mainly chemical interactions [87, 88].

Liu et al. constructed an apparatus to determine the VLE of CO₂/ionic liquid/organic solvent multisystems and the viscosity of the liquid phase at elevated pressure [89]. The solubility of CO₂ in [BMIM][PF₆] and the viscosity of CO₂-saturated [BMIM][PF₆] were determined at three different temperatures and at pressures up to 12.5 MPa. The viscosity of the systems at 313.15 K decreases dramatically from 92 to 51 cp as the pressure of CO₂ changes from 0 to 0.93 MPa, and under this condition the mole fraction of CO₂ in the liquid phase just reaches to 0.12 [89]. This demonstrates that compressed CO₂ may be used as viscosity reducing reagent of ILs in applications. The phase behavior of CO₂/[BMIM][PF₆]/methanol ternary mixture and the viscosity of the liquid phases were determined at 313.15 K and at 7.15 and 10.00 MPa. The partition coefficients and the fugacity coefficients of the components in the ternary system were calculated [89]. The mole fraction of methanol in the CO₂-rich phase is much lower than that in the IL-rich phase, indicating that the IL-methanol interaction is stronger than that of CO₂-methanol. The fugacity coefficient of CO₂ in an IL-rich phase is larger than that of methanol, which demonstrates that IL-methanol interaction is also stronger than the IL-CO₂ interaction [89].

Blanchard reported that the solubility of ionic liquid in pure CO₂ is negligible [77]. It is well known that organic cosolvents can enhance the solubility of compounds in supercritical CO₂ [74, 75]. Wu et al. investigated the cosolvent effect (ethanol, acetone, *n*-hexane, methanol, and acetonitrile) on the solubility of ILs in supercritical CO₂ [90, 91]. The results show that solubilities of ILs with cosolvents increase slowly at a cosolvent concentration lower than 10 mol%. However, the solubilities increase dramatically with polar cosolvents as the concentration of the cosolvents in supercritical CO₂ exceeds 10 mol%, while the effect of a nonpolar cosolvent on the solubility is very limited even when its concentration reaches 30 mol% [90, 91]. The effect of a cosolvent on the solubility of the ILs in CO₂ depends mainly on its polarity [91]. The phase behavior of the CO₂-water-[BMIM][BF₄] system was studied at different conditions in the temperature range from 278.15 to 298.15 K and pressures up to 16 MPa [92]. At a fixed temperature or pressure there can exist four phases. At a fixed temperature, the concentration difference of the ionic liquid in IL-rich phases and water-rich phases becomes larger with increasing pressure. At a fixed pressure of 5.0 MPa, IL concentration in the IL-rich phase decreases as temperature rises, while in the water-rich phase it increases with increasing temperature. The distribution coefficients of [BMIM][BF₄] between IL-rich phase and water-rich phase indicate that separation of ionic liquid and water is possible [92].

The mixture of choline chloride with urea shows a large eutectic effect. Its melting point is 285 K at the mole ratio of choline chloride to urea 1:2, much lower than those of pure choline chloride and urea [93]. The solubility of CO₂ in choline chloride + urea eutectic mixtures was determined at three different temperatures and three different mole ratios of choline chloride to urea around 1:2 under

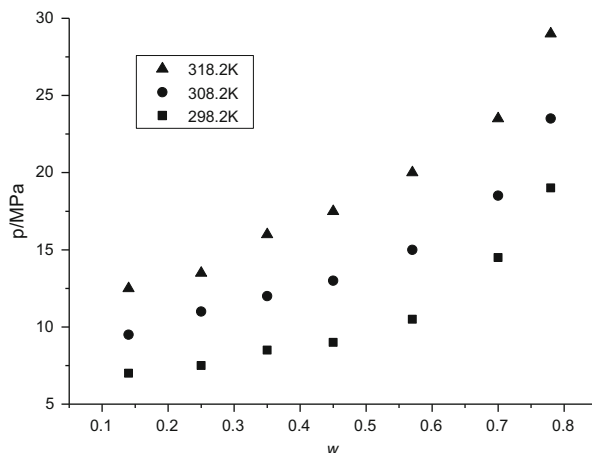
pressures up to 13 MPa [94]. The solubility of CO₂ in the mixtures increases with increasing pressure and decreases with increasing temperature at all the pressures. The enthalpy of solution calculated based on the solubility data is negative under all conditions [94]. Polyethylene glycol (PEG) is a well-known green solvent. The mixture of the PEG200 with green ionic liquid [Choline][Pro], of which both cation and anion came from renewable materials, was used to absorb the greenhouse gas CO₂ [95]. The IL/PEG200 mixture can absorb/desorb CO₂ effectively. PEG200 enhances the rates of absorption and desorption of CO₂ significantly. The solubility of CO₂ in [Choline][Pro]/PEG200 at different pressures from 0 to 0.11 MPa was measured, and the enthalpy and entropy of solution of CO₂ were large negative values, indicating that the absorption process is exothermic [95].

As discussed above, both ILs and supercritical CO₂ are green solvents. We have already discussed the extraction of organics from ILs by CO₂. There is another route to combine them together for a special purpose, the creation of reverse micelles in supercritical CO₂ with ionic liquid domains. Although the solubility of ILs in CO₂ is negligible, they can be dispersed in supercritical CO₂, and the systems may combine some advantages of the two fluids, and may have some new features. Liu et al. reported the formation of reverse micelles in supercritical CO₂ with [TMG][Ac], [TMG][Lac], and [TMG][TFA] domains. Figure 1 indicates the effect of temperature and the ionic liquid-to-surfactant molar ratio, *w*, on cloud-point pressure for the CO₂/N-EtFOSA/[TMG]acetate system [96]. Detailed study showed that ionic liquid-in-carbon dioxide (IL-in-CO₂) microemulsions could form at suitable conditions.

Chandran et al. elucidated the formation of IL-in-CO₂ microemulsions via a computer simulation technique that demonstrated the entire process of self-aggregation at the atomic level. The results of simulation match very well with the data of small-angle neutron scattering. The study reveals that the stability of the microemulsions mainly pertains to the ionic liquid anion-head group interactions. Understanding all of this is useful in designing new surfactants for improving the uptake of ionic liquid in CO₂ [97].

Besides the abundant works carried out on mixtures of ILs + CO₂, the capture of another important acidic gas SO₂ by ILs is another interesting topic. Wu et al. [98] investigated the absorption of SO₂ by [TMG][Lac], and the results indicated that the IL could adsorb SO₂ from gases effectively. Yu et al. [99] performed ab initio calculation of the structure and interionic interaction of the [TMG][Lac] ion pair to deepen the understanding of cation-anion interaction in the ILs. The intermolecular -NH₂- associated hydrogen bonds can substantially increase the cation-anion interaction. Wang et al. [100] developed an all-atom force field by using a combination of density functional theory calculation and force field parameter values for [TMG][Lac], and then molecular dynamic simulations were conducted to investigate the solubility of the SO₂ and CO₂ in [TMG][Lac]. The results of simulation showed that the organization of SO₂ around [TMG] and [Lac], especially [Lac], were relatively stronger than that of CO₂, which could explain the selectivity of the [TMG][Lac] toward the SO₂ and CO₂ [100]. Later, they performed quantum chemical calculations to investigate the interaction between SO₂ or CO₂ molecules

Fig. 1 The effect of temperature and w on cloud-point pressure for the $\text{CO}_2/\text{N-EtFOSA}/[\text{TMG}]$ acetate system. $[\text{N-EtFOSA}] = 0.064 \text{ g}\cdot\text{mL}^{-1}$ [96]



and ions of $[\text{TMG}][\text{Lac}]$ ionic liquid. The SO_2 and CO_2 molecules can interact with the $[\text{TMG}]$ cations forming an $\text{N-H}\cdots\text{O}$ interaction; however, the interaction with CO_2 is weaker than that with SO_2 . The theoretical results indicate that the oxygen atoms of the $[\text{Lac}]$ anion are the main active sites for the absorption of SO_2 [101]. Yu et al. [102] investigated the mechanism of capturing SO_2 by three guanidinium-based ILs – $[\text{TMG}][\text{Lac}]$, $[\text{TMG}][\text{Tf}_2\text{N}]$, and $[\text{TMG}][\text{BF}_4]$ – by using molecular dynamic simulation and ab initio calculation. The results of molecular dynamic simulation for the mixtures of SO_2 and these three ILs indicate that SO_2 favorably organizes around the anions through Lewis acid–base interaction. Gas phase ab initio calculations show that $[\text{TMG}][\text{Lac}]$ chemically interacts with SO_2 while the other two ILs do not. The S atom is bonded to the N atom on $-\text{NH}_2$ of $[\text{TMG}]$ and aminosulfate or aminosulfonic acid fragment may be formed [102].

Other investigations on the absorption of industrial wastes include hydrogen sulfide [103, 104], vinyl chloride [105, 106], dioxin [107], and so on. There are large numbers of reports on the phase behavior of ILs with gases.

3.2 Liquid–Liquid Equilibria

Experimental measurements and theoretical correlations or predictions on LLE of mixtures including ILs have been conducted. Most of the research is focused on conventional ILs such as imidazolium-based ILs with commonly used solvents including alcohols, ketones, acetonitrile, tetrahydrofuran (THF), dimethylsulfoxide (DMSO), and water, etc.

Water is another green solvent. The combination of ILs with water may form interesting systems. Since the water content sometimes greatly affects the properties of ILs, and many ILs are hygroscopic, the uptake of steam is an important

issue. The LLE of water/ionic liquid is important in the case of water acting as a solvent to extract solutes from ILs.

Many experimental [108, 109] and theoretical works [110] on the ILs + water mixtures have been carried out, such as [HMIM][Tf₂N] + water [111] and [EMIM][CH₃(OCH₂CH₂)₂OSO₃] + methanol + water [112]. Anthony et al. [113] carried out systematic research on the ILs + water mixtures. They investigated the phase behavior and associated thermodynamic properties of water with three ILs – [BMIM][PF₆], [OMIM][PF₆], and [OMIM][BF₄]. The Henry's law constants of the water in the mixtures range from 0.0033 to 0.045 MPa. The enthalpies and entropies of absorption indicate that the interactions between water and these ILs are similar to that between water and alcohols. Chloride impurities from 14 to 1,000 ppm do not have any measurable effect on the water vapor solubility and LLE of water + ILs. The increasing of the length of alkyl chain on the methylimidazolium ionic liquid induces the reduction of mutual solubility of water and ionic liquid; [OMIM][BF₄] has larger mutual solubility with water than [OMIM][PF₆] as over 10 wt% water dissolves in [OMIM][BF₄] [113]. Rebelo et al. presented liquid–liquid phase diagram of water + [BMIM][BF₄] and the pressure dependence [114].

Phase equilibria for the binary systems [BMIM][SCN] with an alcohol (1-octanol, 1-nonanol, 1-decanol, 1-undecanol, or 1-dodecanol) or water were determined at ambient pressure [115]. All these alcohols are completely miscible with [BMIM][SCN] in the liquid phase at room temperature, and this indicates that there are strong interaction between the IL and alcohols [115]. LLE for the binary systems of [BMIM][SCN] with an alkane (*n*-hexane, *n*-heptane, *n*-octane, *n*-nonane, or *n*-decane), benzene, an alkylbenzenes (toluene or ethylbenzene), THF, cycloalkanes (cyclohexane or cycloheptane), or ethers, di-*n*-propyl ether, di-*n*-butyl ether, di-*n*-pentyl ether, *n*-butylmethyl ether, *tert*-butylmethyl ether, or *tert*-butylethyl ether have been determined at ambient pressure. An upper critical solution temperature exists in the mixtures IL + alkane, cycloalkane, or ether, while a lower critical solution temperature exists in the systems of IL + benzene, alkylbenzene, or THF. In the case of *n*-alkane with alkyl chain length from C6 to C10, the solubility of *n*-alkane in the [BMIM][SCN] decreases with an increase of the alkyl chain length; the upper critical solution temperature shifts to the higher temperatures and to the higher ionic liquid mole fraction with the increase of the chain length of *n*-alkane. The experimental results show that the effect of anions on the solubility of *n*-hexane in the IL is larger than cations [115]. In the case of ILs with the same cation [BMIM], the solubility increases in the order [OcSO₄] > [CH₃SO₄] > [PF₆] > [MDEGSO₄] > [SCN]. The solubility of *n*-hexane in [BMIM][OcSO₄] is more than two times larger than that in [BMIM][SCN]. [BMIM][SCN] and *n*-alkanes are nearly completely immiscibility in the liquid phase. The solubilities of the IL in the above-mentioned solvents are very small, around 10⁻⁵ to 10⁻² in mole fractions. The mutual (liquid + liquid) solubility of different solvents with the [BMIM][SCN] increases in the order alcohols > water > ethers > aromatic hydrocarbons > cycloalkanes > *n*-alkanes [115]. The experimental data of LLE for ternary mixtures [OMIM]Cl + benzene + heptane,

dodecane, or hexadecane at 298.2 K can be well correlated by the nonrandom two liquid equation (NRTL). The effectiveness of the extraction of benzene from an alkane by [OMIM]Cl was evaluated by the ratio of solubilities in the two phases. The selectivity increases with increasing carbon number of the alkanes because heptane is the most soluble one in the IL-rich phase [116].

The unique properties of the mixtures of ILs + common solvents come from the structure of the mixtures. Ionic association is essential in the solutions of ILs and has an important influence on their applications. Many studies have been reported for the ionic association behavior of ILs in solution. Wang et al. [117] provided quantitative results based on the conductivities of the ILs $[C_n\text{MIM}]\text{Br}$ ($n = 4, 6, 8, 10, 12$), [BMIM][BF₄], and [BMIM][PF₆] in various molecular solvents (water, methanol, 1-propanol, 1-pentanol, acetonitrile, and acetone) at 298.15 K as a function of IL concentration. The Lee-Wheaton conductivity equation was applied to analyze the conductance data in terms of the ionic association constant and the limiting molar conductance. The alkyl chain length of the cations and types of anions affect the ionic association constants and limiting molar conductivities. In all the molecular solvents, the limiting molar conductance values decrease as the alkyl chain length of the cations increases for a given anion (Br^-), whereas the ionic association constant values of the ILs decrease in organic solvents but increase in water with increasing alkyl chain length of the cations [117]. Similar to the classical electrolytes, a linear relationship exists between ionic association constants of the ILs and the dielectric constants of the molecular solvents. It can be expected to modulate the IL conductance by the alkyl chain length of the cations, types of anions, and physical properties of the molecular solvents [117].

Other systems studied include [BMIM][SCN] + 1-alcohols [118], [EMIM][BETI] + methanol or + acetone [119], [BMIM][PF₆] + THF or DMSO [120], [BMIM][BF₄] + ethanol or + nitromethane [121], [BMIM][MeOSO₃] + ethanol or + nitromethane [121], [BMIM][PF₆] + benzyl alcohol or benzaldehyde [122], [BMIM][PF₆] or [BMIM][BF₄] + acetonitrile, or + benzene or + 1-propanol [122], [BMIM][BF₄] + benzaldehyde [123], [EMIM][CH₃(OCH₂)₂OSO₃] or [BMIM][CH₃(OCH₂)₂OSO₃] or [OMIM][CH₃(OCH₂)₂OSO₃] + methanol [124], [EMIM][CH₃(OCH₂CH₂)₂OSO₃] [124], [OMIM][BF₄] or [BMIM] perchlorate + ethanol [125], [BMIM][PF₆] + methyl methacrylate [126], [BMIM][BF₄] + (methanol, or 1,3-dichloropropane, or dimethyl carbonate) [40], and so on.

Domanska et al. [127] measured the LLE of [HMIM][SCN], with water, alcohols, *n*-alkanes (*n*-hexane, *n*-heptane, *n*-octane, *n*-nonane, or *n*-decane), aromatic hydrocarbons (benzene, toluene, or ethylbenzene), and cyclic hydrocarbons (cyclohexane or cycloheptane) at ambient pressure from 200 to 420 K and correlated the LLE using the NRTL equation. The average RMSD of the correlation and experimental data was 0.0021 [127]. They further reported solid liquid equilibria (SLE) and LLE for [BMIM] tosylate + water, or an alcohol (ethanol, or 1-butanol, or 1-hexanol, or 1-octanol, or 1-decanol), or *n*-hexane, or an aromatic hydrocarbons (benzene, or toluene, or ethylbenzene, or propylbenzene, or thiophene)). UNIQUAC, Wilson, and NRTL equations were used to correlate experimental data [128, 129]. Several other thermodynamic models such as

heterosegmented statistical associating fluid theory [130, 131] (SAFT) and heteronuclear square-well chain fluids [132], and the group-contribution nonrandom lattice fluid equation of state [133], represent the density and phase equilibria of the ionic liquid.

From the above information, we can conclude that, although the research on phase equilibria is abundant, most of the systems contain common ILs and commonly used solvents. More work need to be done on other ILs and solvents.

3.3 Activity Coefficients at Infinite Dilution

Activity coefficients at infinite dilution (γ^∞) are of great practical importance for the simulation of various industrial processes, environmental protection, etc. They usually represent the deviation from ideal behavior. γ^∞ can be determined by gas-liquid chromatography (GLC) [134, 135] or dilutor technology [136]. The GLC technique is the most common. Heintz et al. systemically determined γ^∞ of organic compounds in ILs using GLC, the systems investigated include: alkanes, alkenes, and alkylbenzenes in [MBPyr][BF₄] [135]; alkanes, alkenes, and alkylbenzenes as well as linear and branched C1-C6 alcohols, acetone, acetonitrile, ethyl acetate, alkyl ethers, and chloromethanes in the ILs [EMIM][Tf₂N] and [EMMIM][Tf₂N] [137]; and so on. Recently, more work has been done on the measurement of γ^∞ for organic compounds in ILs. Yan et al. determined γ^∞ by GLC of both polar and nonpolar solutes in the ILs [C_nPY][Tf₂N] (n = 2, 4, 5) [138], [EMIM][FAP] [139], [EMIM][TCB] [140], etc. Domanska afforded γ^∞ for water in ILs 1-butyl-1-methylpiperidinium thiocyanate [141], [C₈iQuin][Tf₂N] [142], [EMIM][(CN)₄] [143], and so on. The γ^∞ for water in [BMIM][PF₆], [OMIM][PF₆], and [OMIM][BF₄] ranging from slight deviations from Raoult's law to as high as 8.62 [113]. Marciniak [144] gave a review on the γ^∞ of ILs + other compounds. He analyzed the structure of the cation and anion of the ionic liquid and the effect of the temperature on the selectivity and capacity for aliphatics/aromatics and *n*-hexane/hex-1-ene separation problems based on γ^∞ [144]. In total, 9,374 experimental activity coefficients at infinite dilution data points were available for 74 ILs from the published literature at the end of September 2009 [144]. ILs based on imidazolium, pyridinium, pyrrolidinium, sulfonium, phosphonium, and ammonium cations were taken into consideration. It can be concluded that the majority of ILs may replace conventional entrainers applied for the separation processes of aliphatic/aromatic hydrocarbons [144].

Various methods such as modified UNIFAC(Do) [145] and COSMO-RS [67] have been developed to predict γ^∞ [146]. However, γ^∞ of systems including ILs are not abundant. Recently, modified UNIFAC(Do) [147] and COSMO-RS [148, 149] were extended to predict γ^∞ of the mixtures with ILs. Chen et al. [150] employed the nonrandom two-liquid segment activity coefficient (NRTL-SAC) model to correlate values of γ^∞ for organic compounds in ILs and then to predict the phase behavior of various mixtures involving these ILs. Four molecular descriptors are

designed to capture molecular surface interaction characteristics: hydrophobicity, hydrophilicity, polarity, and solvation strength. The results show that NRTL-SAC is a qualitative predictive model to predict γ^∞ for organic compounds in ILs. An artificial neural network with a multilayer feed-forward network with the Levenberg-Marquardt optimization algorithm was employed to predict γ^∞ for organic solutes in ILs too [151]. The unavailable input data concerning softness of organic compounds and dipole moment of ILs were calculated using GAMESS suites. The validation of the model was tested based on the investigation of up to 24 structurally different organic compounds (alkanes, alkenes, alkynes, cycloalkanes, aromatics, and alcohols) in 16 common imidazolium-based ILs at different temperatures within the range 298 to 363 K. The results show a satisfactory agreement between the predicted artificial neural network and experimental data where the root mean square error of the designed neural network is 0.103 for training data and 0.128 for testing data, respectively [151].

From the temperature dependence of the γ^∞ values, the partial molar excess enthalpies at infinite dilution of the solutes in the ILs can be calculated. Other thermodynamic properties such as the isothermal compressibility, the isobaric expansivity, and the thermal pressure coefficient can be derived from density and its pressure-temperature data. One should be cautious when using these data because the data are very sensitive to the functions used to describe the PVT relation [152]. The excess molar volumes of most of the above systems come from experimental density data, and are fitted by the Redlich-Kister equation. The results show that excess molar volumes decrease slightly when temperature increases, which is interpreted in terms of ion-dipole interactions and structural factors of the ILs and the organic molecular liquids [153].

4 Enthalpy of Vaporization

Some of the thermodynamic properties of ILs have been thoroughly investigated, while systematic studies on the vaporization of ILs have lagged behind the pace of other research. The vapor pressure, the enthalpy of vaporization ($\Delta_{\text{vap}}H$), and the boiling temperature T_b indicate the relative physical stability of ILs. In fact, the vapor pressure of ILs is too low to be detected at room temperature and ambient pressure. However, Earle et al. [154] presented experimental data to demonstrate that several ILs can be vaporized and recondensed at 200–300°C and low pressure without significant decomposition. It indicates that low pressure is the answer to the myth that ILs cannot be distilled, which has shaken the assumption of ILs' stability and has led to doubts about ILs restrictions and definitions (Fig. 2).

The vapor pressures and the $\Delta_{\text{vap}}H$ of any particular ionic liquid may not always be measured easily and accurately. Øye et al. [155] reported the first data concerning vapor pressure of ILs. Rooney et al. [156] have summarized well the various methods, including microcalorimetry, TGA, TPD, MD calculations, and surface tension, to obtain estimated values of enthalpies of vaporization (Table 4).

Fig. 2 The Kugelrohr oven and distillation apparatus at 200–300°C and 10 Pa [154]

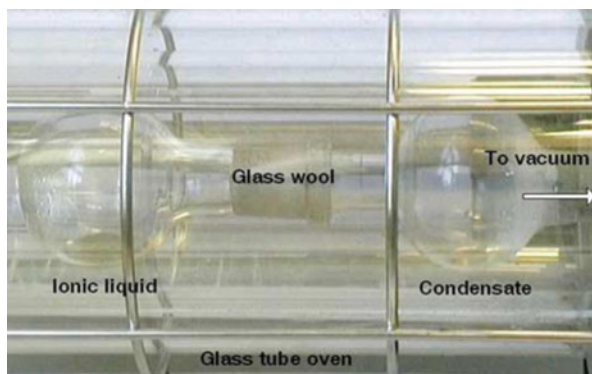


Table 4 Estimated values of enthalpies of vaporization ($\Delta_{\text{vap}}H_{298}$ in $\text{kJ}\cdot\text{mol}^{-1}$) for ILs obtained using various methods [156]

ILs	Surface tension [157]	TPD [158]	Microcalorimetry [159]	TGA [160]	MD calculations [161]
[EMIM] [Tf ₂ N]	136.1	134	132.9	120.6	159
[BMIM] [Tf ₂ N]	134.6	134	137.9	118.5	174
[HMIM] [Tf ₂ N]	141.6	139	142.9	124.1	184
[OMIM] [Tf ₂ N]	149.0	149	147.9	132.3	201
[DMIM] [Tf ₂ N]	155.5	–	–	134	–
[BMIM] [BF ₄]	122.0	162	160.4	–	–
[BMIM] [PF ₆]	144.3	169	168.9	–	–

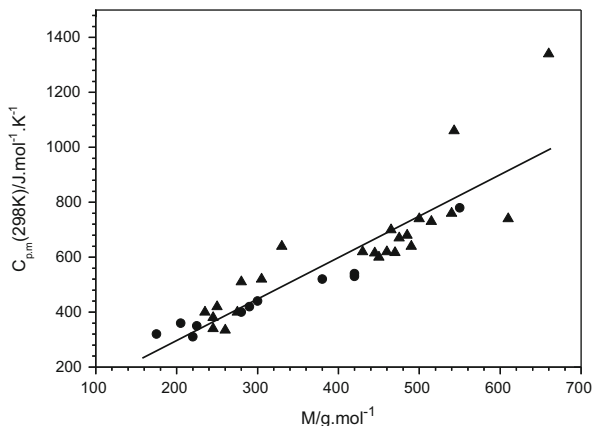
The boiling temperature is inaccessible experimentally, and therefore is usually avoided as the parameter of stability; thus calculation was introduced to assess stability with the boiling temperature as a minor standard [162].

In conclusion, the studies on vapor pressure and the boiling point of the ILs are still scarce. More work need to carry out on in this field.

5 Heat Capacity

The heat capacity of a compound is defined as the enthalpy dependency with temperature. It is one of the basic pure component properties for any materials. The knowledge of heat capacity is essential in determining the heat transfer properties of ILs and for the calculations of enthalpy in process simulation.

Fig. 3 Ionic liquid heat capacities as a function of the molar mass [166]



ILs are potential heat transfer fluids [6, 7] for heat exchange in chemical plants and solar thermal power generation. The heat capacity is an important criterion in determining the applicability of these liquids. At the same time, the investigations on heat capacity of ILs are relatively scarce [163]. Paulechka gave a critical review on the heat capacity of ILs [164].

Holbrey et al. [165] first reported the experimental heat capacity data of five imidazolium-based ILs. Figure 3 gives the molar mass dependence of heat capacity of some common ILs [166]. We can conclude that the heat capacity of ILs increases linearly with increasing molar mass. For the simple compounds that are comprised of a limited number of different atoms, it makes sense since heat capacity depends on the number of translational, vibrational, and rotational energy storage modes.

Adiabatic calorimetry was used to measure the low temperature heat capacity down to 5 K [167]. The heat capacity of $[C_n\text{MIM}][\text{Tf}_2\text{N}]$ ($n = 6, 8$) was measured by Tian-Calvet type differential calorimeter from 323 to 573 K at 10 MPa [168]. Yang et al. [169] compared the thermodynamic properties of [BMIM] bis(oxalato)borate and [HMIM] bis(oxalato)borate with those of other [BMIM]-based ILs, and concluded that, for a given cation (or anion) and at a certain temperature, the more atoms in the anion (or cation), the higher the heat capacity. Ge et al. [170] determined the impact of impurities (water and chloride content) in the ionic liquid on the heat capacity and found that water content was more influential than chloride. A critical analysis of the effect of impurities on the measured thermodynamic properties was performed [171]. Other work was carried out on the heat capacity measurement of pure ILs [172–179].

The mixtures' heat capacity [180, 181] of ILs with water [182–184], methanol [185], acetonitrile [186], ethanol, and 1-octanol [187], and so on were investigated too. We only take some important examples to review. In the case of the systems water + [EMIM][EtSO₄], water + [EMIM][OTf], and water + [EMIM][TFA], the molar heat capacities decrease with water concentration increases, with the molar heat capacities of the pure ILs being four to five times greater than that of water [182]. It is due to the molecular weights difference between ILs and water [181],

while the specific heat capacity of water is much higher than that of the pure ILs. The molar heat capacities temperature dependence can be well correlated with a two-parameter empirical equation; a straight line is adequate for the correlation of molar heat capacities with mole fraction. The excess enthalpies for the system of water + [EMIM][OTf] are positive values; however, for the systems of water + [EMIM][EtSO₄] and water + [EMIM][TFA] they are negative values [182].

The excess molar heat capacities of systems [HMIM][BF₄] + acetonitrile as well as [OMIM][BF₄] + acetonitrile calculated from experimental values of systems specific heat capacities are negative deviations from the additivity of the molar heat capacities. This indicates the differences in nonspecific interactions between the ILs and acetonitrile (negative contribution to the excess molar heat capacities) are larger than the heteromolecular association (positive contribution to the excess molar heat capacities) of relatively weak acetonitrile-ILs complexes [186]. In the case of systems [HMIM][BF₄] + methanol as well as [OMIM][BF₄] + methanol, the excess molar heat capacities show positive deviations from the additivity of molar heat capacities, which suggests that the main contribution to the excess molar heat capacities is the breaking of the hydrogen-bonded structure of methanol during mixing [185]. The excess heat capacity provides information on intermolecular interaction and they are dependent on the intermolecular interaction.

Although the heat capacity data for some commonly used ILs are available, we can find some problems while looking into these data. The data are far from abundant in that most of the measurements are focused on the most commonly used ILs. The mixture data are scarce. Moreover, the data are not consistent with each other. For example, the deviation of heat capacity of [BMIM][Tf₂N] reported by different authors [163, 165, 170, 171, 179] reaches more than 30 %.

Several works on the prediction of heat capacity of ILs have been carried out. Since the heat capacity of an ionic liquid is closely related to its mole mass [166] and its atom number [169], it is reasonable to predict heat capacity by group contribution methods. Gardas and Coutinho [188] proposed a second-order group additivity method [189] (Eq. 7) for the estimation of the heat capacity of ILs covering a wide range of temperature (196.36–663.10 K):

$$C_p = R \left[\sum_{i=1}^k n_i a_i + \sum_{i=1}^k n_i b_i \left(\frac{T}{100} \right) + \sum_{i=1}^k n_i d_i \left(\frac{T}{100} \right)^2 \right] \quad (7)$$

where R is the gas constant and T is the absolute temperature, n_i is the number of groups of type i , k is the total number of different types of groups, and a_i , b_i , and d_i are parameters estimated for ILs. The MPD is 0.36% for ca. 2,400 data points from 19 ILs. Soriano et al. [190] proposed a similar group additivity method for heat capacity estimation. The overall AAD for all the 3,149 data points of the 32 considered ILs is 0.69 %.

By the generation of contribution parameters for -SO₂-, B, and P groups, Ge et al. [170] extended the Joback method for predicting the heat capacities of ILs.

New parameters led to an overall RAD of 2.9 % for 961 data points from 53 kinds of ILs.

A correlation of heat capacities with molar volumes of the ILs was given by Paulechka et al. [191] for the estimation of heat capacity at 298.15 K (Eq. 8):

$$C_p(\text{J} \cdot \text{mol}^{-1} \cdot \text{K}^{-1}) = (1.937 \pm 0.0045)V/\text{cm}^3 \cdot \text{mol}^{-1} \quad (8)$$

To apply the above correlation method, the molar volumes of ILs are necessary, so they are not purely predictive models. Preiss et al. [192] proposed in silico method COSMO implemented to Turbomole [193] for the molecular volume calculation, to realize a reliable pure prediction of the heat capacity of ILs.

A correlation scheme (Eq. 9) for estimation of low temperature heat capacity of ILs in a range from 190 to 370 K was developed [194]:

$$C_p(\text{J} \cdot \text{mol}^{-1} \cdot \text{K}^{-1}) = [7.71 - 2.12 \cdot 10^{-2}T - 1.17 \cdot 10^{-2}M + 2.27 \cdot 10^{-5}T^2 + 1.11 \cdot 10^{-5}TM + 9.77 \cdot 10^{-6}M^2] \cdot C_{\text{vib}} \quad (9)$$

where C_{vib} is the intramolecular vibrational contribution to the heat capacity, which can be obtained from the quantum chemical calculations by the Gaussian 03 software package [195].

Based on the concept of mass connectivity index [196, 197], Valderrama et al. [198] proposed a predictive model heat capacity prediction:

$$C_p = a + bV + c\lambda + d\left(\frac{M^+}{M^-}\right) + \lambda \left[p(T - T_0) + q(T - T_0)^2 \right] \quad (10)$$

where a , b , c , d , p , and q are universal constants for any ILs, V is molar volume, λ is the mass connectivity index, T_0 is a reference temperature defined as 298.15 K, and T is the temperature in Kelvin, and M^+ and M^- are the mass of the cation and that of the anion, separately. The average absolute deviations are 2.3 % in correlation and 2.1 % in prediction.

As was stated, a number of works have been carried out on the correlation and prediction of the heat capacity of pure ionic liquid, while less work has been done on the correlation or prediction on the heat capacity of mixtures with ionic liquids. The molar heat capacities for aqueous solutions of two [EMIM]-based ILs were measured by DSC. An excess molar heat capacity expression derived using a Redlich-Kister type equation (Eqs. 11 and 12). The correlations gave an overall average deviation of 0.1% for molar heat capacity [184]:

$$C_p = C_p^E + \sum_i x_i C_{p,i} \quad (11)$$

$$C_p^E / (\text{J} \cdot \text{mol}^{-1} \cdot \text{K}^{-1}) = x_1 x_2 \sum_{i=1}^n (b_{i,0} + b_{i,1}(T/K))(x_1 - x_2)^{i-1} \quad (12)$$

6 Summary and Outlook

Increasing numbers of researchers have begun to be interested in ILs. Some of them have been attracted by the possibility of developing new technologies using the unique features of ILs, while others have been driven by inherent scientific interest. Investigation of the thermodynamic properties of IL systems is of great importance from both theoretical and practical points of view. Much research has been carried out on the synthesis of ILs with different structures and the measurement and correlation of the thermodynamic properties of IL systems. However, more work should be carried out on this interesting and important topic. For example, more accurate pieces of apparatus to determine the thermodynamic properties of IL systems need to be designed and constructed. The experimental data on the thermodynamic properties of multicomponent systems are scarce and more data are required. The accurate models to predict the thermodynamic properties of IL systems should be developed, especially for complex systems. The relationship between the thermodynamic properties and intermolecular interaction of IL systems needs to be established. Thermodynamic theories for prediction the association of the cations and anions in IL systems should be developed too.

Acknowledgments This work was supported by National Natural Science Foundation of China (21173267, 21073207, 21133009) and the Basic Research Funds in Renmin University of China from the Central Government (12XNLL05).

References

1. Wilkes JS (2002) A short history of ionic liquids – from molten salts to neoteric solvents. *Green Chem* 4(2):73–80
2. Plechkova NV, Seddon KR (2008) Applications of ionic liquids in the chemical industry. *Chem Soc Rev* 37(1):123–150
3. Short P (2006) Out of the ivory tower. *Chem Eng News* 84(14):15–21
4. Wang P, Zakeeruddin SM, Moser JE et al (2003) A new ionic liquid electrolyte enhances the conversion efficiency of dye-sensitized solar cells. *J Phys Chem B* 107(48):13280–13285
5. Holbrey JD (2007) Heat capacities of common ionic liquids – potential applications as thermal fluids? *Chim Oggi-Chem Today* 25(6):24–26
6. Franca JMP, de Castro CAN, Lopes MM et al (2009) Influence of thermophysical properties of ionic liquids in chemical process design. *J Chem Eng Data* 54(9):2569–2575
7. van Valkenburg ME, Vaughn RL, Williams M et al (2005) Thermochemistry of ionic liquid heat-transfer fluids. *Thermochim Acta* 425(1–2):181–188

8. Moens L, Blake DM, Rudnicki DL et al (2003) Advanced thermal storage fluids for solar parabolic trough systems. *J Sol Ener Eng Trans-ASME* 125(1):112–116
9. Visser AE, Swatloski RP, Reichert WM et al (2001) Task-specific ionic liquids for the extraction of metal ions from aqueous solutions. *Chem Commun* 1:135–136
10. Pandey S (2006) Analytical applications of room-temperature ionic liquids: a review of recent efforts. *Anal Chim Acta* 556(1):38–45
11. Swatloski RP, Spear SK, Holbrey JD et al (2002) Dissolution of cellulose with ionic liquids. *J Am Chem Soc* 124(18):4974–4975
12. Li ZH, Luan YX, Mu TC et al (2009) Unusual nanostructured ZnO particles from an ionic liquid precursor. *Chem Commun* 10:1258–1260
13. Li ZH, Jia Z, Luan YX et al (2009) Ionic liquids for synthesis of inorganic nanomaterials. *Curr Opin Solid State Mater Sci* 12(1):1–8
14. Karadas F, Atilhan M, Aparicio S (2010) Review on the use of ionic liquids (ILs) as alternative fluids for CO₂ capture and natural gas sweetening. *Energy Fuel* 24:5817–5828
15. http://www.kuleuven.be/ionic-liquids/ionic_liquid.php
16. Wang JF, Li CX, Shen C et al (2009) Towards understanding the effect of electrostatic interactions on the density of ionic liquids. *Fluid Phase Equilib* 279(2):87–91
17. Seddon KR, Stark A, Torres MJ (2002) Viscosity and density of 1-alkyl-3-methylimidazolium ionic liquids. In: Abraham MA, Moens L (eds) *Clean solvents – alternative media for chemical reactions and processing*. ACS symposium series, vol 819. American Chemical Society, Washington, DC, pp 34–49
18. Zhang ZF, Wu WZ, Han BX et al (2005) Phase separation of the reaction system induced by CO₂ and conversion enhancement for the esterification of acetic acid with ethanol in ionic liquid. *J Phys Chem B* 109(33):16176–16179
19. Zhang ZF, Wu WZ, Wang B et al (2007) High-pressure phase behavior of CO₂/acetone/ionic liquid system. *J Supercrit Fluids* 40(1):1–6
20. Wandschneider A, Lehmann JK, Heintz A (2008) Surface tension and density of pure ionic liquids and some binary mixtures with 1-propanol and 1-butanol. *J Chem Eng Data* 53(2):596–599
21. Kilaru P, Baker GA, Scovazzo P (2007) Density and surface tension measurements of imidazolium-, quaternary phosphonium-, and ammonium-based room-temperature ionic liquids: data and correlations. *J Chem Eng Data* 52(6):2306–2314
22. Klomfar J, Souckova M, Patek J (2010) Temperature dependence measurements of the density at 0.1 MPa for 1-alkyl-3-methylimidazolium-based ionic liquids with the trifluoromethanesulfonate and tetrafluoroborate anion. *J Chem Eng Data* 55(9):4054–4057
23. Liu QS, Tong J, Tan ZC et al (2010) Density and surface tension of ionic liquid C₂mim PF₃(CF₂CF₃)₃ and prediction of properties C_nmim PF₃(CF₂CF₃)₃ (n = 1, 3, 4, 5, 6). *J Chem Eng Data* 55(7):2586–2589
24. Sanchez LG, Espel JR, Onink F et al (2009) Density, viscosity, and surface tension of synthesis grade imidazolium, pyridinium, and pyrrolidinium based room temperature ionic liquids. *J Chem Eng Data* 54(10):2803–2812
25. Rodriguez H, Brennecke JF (2006) Temperature and composition dependence of the density and viscosity of binary mixtures of water plus ionic liquid. *J Chem Eng Data* 51(6):2145–2155
26. Pereiro AB, Santamarta F, Tojo E et al (2006) Temperature dependence of physical properties of ionic liquid 1,3-dimethylimidazolium methyl sulfate. *J Chem Eng Data* 51(3):952–954
27. Gardas RL, Ge R, Goodrich P et al (2010) Thermophysical properties of amino acid-based ionic liquids. *J Chem Eng Data* 55(4):1505–1515
28. Tokuda H, Hayamizu K, Ishii K et al (2004) Physicochemical properties and structures of room temperature ionic liquids. 1. Variation of anionic species. *J Phys Chem B* 108(42):16593–16600

29. Tokuda H, Ishii K, Susan MABH et al (2006) Physicochemical properties and structures of room-temperature ionic liquids. 3. Variation of cationic structures. *J Phys Chem B* 110 (6):2833–2839
30. Tokuda H, Hayamizu K, Ishii K et al (2005) Physicochemical properties and structures of room temperature ionic liquids. 2. Variation of alkyl chain length in imidazolium cation. *J Phys Chem B* 109(13):6103–6110
31. Jin H, O'Hare B, Dong J et al (2008) Physical properties of ionic liquids consisting of the 1-butyl-3-methylimidazolium cation with various anions and the bis(trifluoromethylsulfonyl) imide anion with various cations. *J Phys Chem B* 112(1):81–92
32. Tariq M, Forte PAS, Gomes MFC et al (2009) Densities and refractive indices of imidazolium- and phosphonium-based ionic liquids: effect of temperature, alkyl chain length, and anion. *J Chem Thermodyn* 41(6):790–798
33. Esperanca J, Visak ZP, Plechkova NV et al (2006) Density, speed of sound, and derived thermodynamic properties of ionic liquids over an extended pressure range. 4. C₃mim NTf₂ and C₅mim NTf₂. *J Chem Eng Data* 51(6):2009–2015
34. Klomfar J, Souckova M, Patek J (2009) Buoyancy density measurements for 1-alkyl-3-methylimidazolium based ionic liquids with tetrafluoroborate anion. *Fluid Phase Equilib* 282(1):31–37
35. Bogdanov MG, Petkova D, Hristeva S et al (2010) New guanidinium-based room-temperature ionic liquids. Substituent and anion effect on density and solubility in water. *Z Naturforsch B Chem Sci* 65(1):37–48
36. Kagimoto J, Taguchi S, Fukumoto K et al (2010) Hydrophobic and low-density amino acid ionic liquids. *J Mol Liq* 153(2–3):133–138
37. Esperanca J, Guedes HJR, Blesic M et al (2006) Densities and derived thermodynamic properties of ionic liquids. 3. Phosphonium-based ionic liquids over an extended pressure range. *J Chem Eng Data* 51(1):237–242
38. Gu ZY, Brennecke JF (2002) Volume expansivities and isothermal compressibilities of imidazolium and pyridinium-based ionic liquids. *J Chem Eng Data* 47(2):339–345
39. Sanmamed YA, Gonzalez-Salgado D, Troncoso J et al (2007) Viscosity-induced errors in the density determination of room temperature ionic liquids using vibrating tube densitometry. *Fluid Phase Equilib* 252(1–2):96–102
40. Iglesias-Otero MA, Troncoso J, Carballo E et al (2007) Density and refractive index for binary systems of the ionic liquid [BMIM][BF₄] with methanol, 1,3-dichloropropane, and dimethyl carbonate. *J Solut Chem* 36(10):1219–1230
41. Rossen WR, Kohn JP (1984) Behavior of microemulsions under compression. *SPEJ Soc Pet Eng J* 24(5):536–544
42. Doy N, McHale G, Newton MI et al (2010) Small volume laboratory on a chip measurements incorporating the quartz crystal microbalance to measure the viscosity-density product of room temperature ionic liquids. *Biomicrofluidics* 4(1):014107
43. McHale G, Hardacre C, Ge R et al (2008) Density-viscosity product of small-volume ionic liquid samples using quartz crystal impedance analysis. *Anal Chem* 80(15):5806–5811
44. Doy N, McHale G, Newton MI et al (2009) Density and viscosity measurements of room temperature ionic liquids using patterned quartz crystal microbalances. In: 2009 joint meeting of the European Frequency and Time Forum and the IEEE International Frequency Control Symposium, vols 1 and 2, pp 1043–1045
45. Jacquemin J, Nancarrow P, Rooney DW et al (2008) Prediction of ionic liquid properties. II. Volumetric properties as a function of temperature and pressure. *J Chem Eng Data* 53 (9):2133–2143
46. Xu XC, Peng CJ, Liu HL et al (2009) Modeling PVT properties and phase equilibria for systems containing ionic liquids using a new lattice-fluid equation of state. *Ind Eng Chem Res* 48(24):11189–11201
47. Yang JZ, Lu XM, Gui JS et al (2004) A new theory for ionic liquids – the interstice model part 1. The density and surface tension of ionic liquid EMISE. *Green Chem* 6(11):541–543

48. Yang L, Sandler SI, Peng CJ et al (2010) Prediction of the phase behavior of ionic liquid solutions. *Ind Eng Chem Res* 49(24):12596–12604
49. Ye CF, Shreeve JM (2007) Rapid and accurate estimation of densities of room-temperature ionic liquids and salts. *J Phys Chem A* 111(8):1456–1461
50. Gardas RL, Coutinho JAP (2008) Extension of the Ye and Shreeve group contribution method for density estimation of ionic liquids in a wide range of temperatures and pressures. *Fluid Phase Equilib* 263(1):26–32
51. Tome LIN, Carvalho PJ, Freire MG et al (2008) Measurements and correlation of high-pressure densities of imidazolium-based ionic liquids. *J Chem Eng Data* 53(8):1914–1921
52. Soriano AN, Doma BT, Li MH (2009) Measurements of the density and refractive index for 1-n-butyl-3-methylimidazolium-based ionic liquids. *J Chem Thermodyn* 41(3):301–307
53. Soriano AN, Doma BT, Li MH (2010) Density and refractive index measurements of 1-ethyl-3-methylimidazolium-based ionic liquids. *J Taiwan Inst Chem Eng* 41(1):115–121
54. Valderrama JO, Robles PA (2007) Critical properties, normal boiling temperatures, and acentric factors of fifty ionic liquids. *Ind Eng Chem Res* 46(4):1338–1344
55. Valderrama JO, Sanga WW, Lazzus JA (2008) Critical properties, normal boiling temperature, and acentric factor of another 200 ionic liquids. *Ind Eng Chem Res* 47(4):1318–1330
56. Valderrama JO, Zarricueta K (2009) A simple and generalized model for predicting the density of ionic liquids. *Fluid Phase Equilib* 275(2):145–151
57. Gardas RL, Costa HF, Freire MG et al (2008) Densities and derived thermodynamic properties of imidazolium-, pyridinium-, pyrrolidinium-, and piperidinium-based ionic liquids. *J Chem Eng Data* 53(3):805–811
58. Gardas RL, Freire MG, Carvalho PJ et al (2007) High-pressure densities and derived thermodynamic properties of imidazolium-based ionic liquids. *J Chem Eng Data* 52(1):80–88
59. Guan W, Tong J, Chen SP et al (2010) Density and surface tension of amino acid ionic liquid 1-alkyl-3-methylimidazolium glutamate. *J Chem Eng Data* 55(9):4075–4079
60. Wang JF, Li ZB, Li CX et al (2010) Density prediction of ionic liquids at different temperatures and pressures using a group contribution equation of state based on electrolyte perturbation theory. *Ind Eng Chem Res* 49(9):4420–4425
61. Lazzus JA (2009) Estimation of density as a function of temperature and pressure for imidazolium-based ionic liquids using a multilayer net with particle swarm optimization. *Int J Thermophys* 30(3):883–909
62. Valderrama JO, Reategui A, Rojas RE (2009) Density of ionic liquids using group contribution and artificial neural networks. *Ind Eng Chem Res* 48(6):3254–3259
63. Hu YF, Chu HD, Li JG et al (2011) Extension of the simple equations for prediction of the properties of mixed electrolyte solutions to the mixed ionic liquid solutions. *Ind Eng Chem Res* 50(7):4161–4165
64. Patwardhan VS, Kumar A (1986) A unified approach for prediction of thermodynamic properties of aqueous mixed-electrolyte solutions. Part II: volume, thermal, and other properties. *AIChE J* 32(9):1429–1438
65. Ghatee MH, Zare M, Moosavi F et al (2010) Temperature-dependent density and viscosity of the ionic liquids 1-alkyl-3-methylimidazolium iodides: experiment and molecular dynamics simulation. *J Chem Eng Data* 55(9):3084–3088
66. Derecskei B, Derecskei-Kovacs A (2008) Molecular modelling simulations to predict density and solubility parameters of ionic liquids. *Mol Simul* 34(10–15):1167–1175
67. Klamt A (1995) Conductor-like screening model for real solvents – a new approach to the quantitative calculation of solvation phenomena. *J Phys Chem* 99(7):2224–2235
68. Palomar J, Ferro VR, Torrecilla JS et al (2007) Density and molar volume predictions using COSMO-RS for ionic liquids. An approach to solvent design. *Ind Eng Chem Res* 46(18):6041–6048
69. Mokhtarani B, Mojtahedi MM, Mortaheb HR et al (2008) Densities, refractive indices, and viscosities of the ionic liquids 1-methyl-3-octylimidazolium tetrafluoroborate and 1-methyl-

- 3-butylimidazolium perchlorate and their binary mixtures with ethanol at several temperatures. *J Chem Eng Data* 53(3):677–682
70. Iglesias-Otero MA, Troncoso J, Carballo E et al (2008) Density and refractive index in mixtures of ionic liquids and organic solvents: correlations and predictions. *J Chem Thermodyn* 40(6):949–956
71. Sairi NA, Yusoff R, Alias Y et al (2011) Solubilities of CO₂ in aqueous N-methyldiethanolamine and guanidinium trifluoromethanesulfonate ionic liquid systems at elevated pressures. *Fluid Phase Equilib* 300(1–2):89–94
72. Hong SY, Im J, Palgunadi J et al (2011) Ether-functionalized ionic liquids as highly efficient SO₂ absorbents. *Energy Environ Sci* 4(5):1802–1806
73. Anthony JL, Maginn EJ, Brennecke JF (2002) Solubilities and thermodynamic properties of gases in the ionic liquid 1-n-butyl-3-methylimidazolium hexafluorophosphate. *J Phys Chem B* 106(29):7315–7320
74. Zhang XG, Han BX, Hou ZS et al (2002) Why do co-solvents enhance the solubility of solutes in supercritical fluids? New evidence and opinion. *Chem Eur J* 8(22):5107–5111
75. Mu TC, Zhang XG, Liu ZM et al (2004) Enthalpy of solution of 1,4-naphthoquinone in CO₂ plus n-pentane in the critical region of the binary mixture: mechanism of solubility enhancement. *Chem Eur J* 10(2):371–376
76. Gao L, Jiang T, Zhao GY et al (2004) Transesterification between isoamyl acetate and ethanol in supercritical CO₂, ionic liquid, and their mixture. *J Supercrit Fluids* 29(1–2):107–111
77. Blanchard LA, Hancu D, Beckman EJ et al (1999) Green processing using ionic liquids and CO₂. *Nature* 399(6731):28–29
78. Blanchard LA, Gu ZY, Brennecke JF (2001) High-pressure phase behavior of ionic liquid/CO₂ systems. *J Phys Chem B* 105(12):2437–2444
79. Aki S, Mellein BR, Saurer EM et al (2004) High-pressure phase behavior of carbon dioxide with imidazolium-based ionic liquids. *J Phys Chem B* 108(52):20355–20365
80. Keskin S, Kayrak-Talay D, Akman U et al (2007) A review of ionic liquids towards supercritical fluid applications. *J Supercrit Fluids* 43(1):150–180
81. Zhang SJ, Yuan XL, Chen YH et al (2005) Solubilities of CO₂ in 1-butyl-3-methylimidazolium hexafluorophosphate and 1,1,3,3-tetramethylguanidium lactate at elevated pressures. *J Chem Eng Data* 50(5):1582–1585
82. Gao HX, Han BX, Li JC et al (2004) Preparation of room-temperature ionic liquids by neutralization of 1,1,3,3-tetramethylguanidine with acids and their use as media for Mannich reaction. *Synth Commun* 34(17):3083–3089
83. Bates ED, Mayton RD, Ntai I et al (2002) CO₂ capture by a task-specific ionic liquid. *J Am Chem Soc* 124(6):926–927
84. Gurkan BE, de la Fuente JC, Mindrup EM et al (2010) Equimolar CO₂ absorption by anion-functionalized ionic liquids. *J Am Chem Soc* 132(7):2116–2117
85. Zhang YQ, Zhang SJ, Lu XM et al (2009) Dual amino-functionalised phosphonium ionic liquids for CO₂ capture. *Chem Eur J* 15(12):3003–3011
86. Xue ZM, Zhang ZF, Han J et al (2011) Carbon dioxide capture by a dual amino ionic liquid with amino-functionalized imidazolium cation and taurine anion. *Int J Greenhouse Gas Control* 5(4):628–633
87. Yu GR, Zhang SJ, Zhou GH et al (2007) Structure, interaction and property of amino-functionalized imidazolium ILs by molecular dynamics simulation and *ab initio* calculation. *AIChE J* 53(12):3210–3221
88. Zhang JM, Zhang SJ, Dong K et al (2006) Supported absorption of CO₂ by tetrabutylphosphonium amino acid ionic liquids. *Chem Eur J* 12(15):4021–4026
89. Liu ZM, Wu WZ, Han BX et al (2003) Study on the phase behaviors, viscosities, and thermodynamic properties of CO₂/C₄mimPF₆/methanol system at elevated pressures. *Chem Eur J* 9(16):3897–3903

90. Wu WZ, Zhang JM, Han BX et al (2003) Solubility of room-temperature ionic liquid in supercritical CO₂ with and without organic compounds. *Chem Commun* 12:1412–1413
91. Wu WZ, Li WJ, Han BX et al (2004) Effect of organic cosolvents on the solubility of ionic liquids in supercritical CO₂. *J Chem Eng Data* 49(6):1597–1601
92. Zhang ZF, Wu WZ, Gao HX et al (2004) Tri-phase behavior of ionic liquid-water-CO₂ system at elevated pressures. *Phys Chem Chem Phys* 6(21):5051–5055
93. Abbott AP, Capper G, Davies DL et al (2003) Novel solvent properties of choline chloride/urea mixtures. *Chem Commun* 1:70–71
94. Li XY, Hou MQ, Han BX et al (2008) Solubility of CO₂ in a choline chloride plus urea eutectic mixture. *J Chem Eng Data* 53(2):548–550
95. Li XY, Hou MQ, Zhang ZF et al (2008) Absorption of CO₂ by ionic liquid/polyethylene glycol mixture and the thermodynamic parameters. *Green Chem* 10(8):879–884
96. Liu JH, Cheng SQ, Zhang JL et al (2007) Reverse micelles in carbon dioxide with ionic-liquid domains. *Angew Chem Int Ed* 46(18):3313–3315
97. Chandran A, Prakash K, Senapati S (2010) Self-assembled inverted micelles stabilize ionic liquid domains in supercritical CO₂. *J Am Chem Soc* 132(35):12511–12516
98. Wu WZ, Han BX, Gao HX et al (2004) Desulfurization of flue gas: SO₂ absorption by an ionic liquid. *Angew Chem Int Ed* 43(18):2415–2417
99. Yu GG, Zhang SJ (2007) Insight into the cation-anion interaction in 1,1,3,3-tetramethylguanidinium lactate ionic liquid. *Fluid Phase Equilib* 255(1):86–92
100. Wang Y, Pan H, Li H et al (2007) Force field of the TMGL ionic liquid and the solubility of SO₂ and CO₂ in the TMGL from molecular dynamics simulation. *J Phys Chem B* 111(35):10461–10467
101. Wang Y, Wang CM, Zhang LQ et al (2008) Difference for SO₂ and CO₂ in TGML ionic liquids: a theoretical investigation. *Phys Chem Chem Phys* 10(39):5976–5982
102. Yu GR, Chen XC (2011) SO₂ capture by guanidinium-based ionic liquids: a theoretical study. *J Phys Chem B* 115(13):3466–3477
103. Koech PK, Rainbolt JE, Bearden MD et al (2011) Chemically selective gas sweetening without thermal-swing regeneration. *Energy Environ Sci* 4(4):1385–1390
104. Sakhaeinia H, Jalili AH, Taghikhani V et al (2010) Solubility of H₂S in ionic liquids 1-ethyl-3-methylimidazolium hexafluorophosphate ([emim][PF₆]) and 1-ethyl-3-methylimidazolium bis(trifluoromethyl)sulfonylimide ([emim][Tf₂N]). *J Chem Eng Data* 55(12):5839–5845
105. Cheng XP, Mu TC, Wang XL et al (2008) Low pressure solubilities of vinyl chloride in ionic liquids. *J Chem Eng Data* 53(12):2807–2809
106. Cheng XP, Yang GY, Mu TC et al (2009) Absorption of vinyl chloride by room temperature ionic liquids. *Clean-Soil Air Water* 37(3):245–248
107. Kulkarni PS, Branco LC, Crespo JG et al (2008) Capture of dioxins by ionic liquids. *Environ Sci Technol* 42(7):2570–2574
108. Wang JJ, Wang HY, Zhang SL et al (2007) Conductivities, volumes, fluorescence, and aggregation behavior of ionic liquids C₄mim BF₄ and C_nmim Br (n = 4, 6, 8, 10, 12) in aqueous solutions. *J Phys Chem B* 111(22):6181–6188
109. Wang JJ, Pei YC, Zhao Y et al (2005) Recovery of amino acids by imidazolium based ionic liquids from aqueous media. *Green Chem* 7(4):196–202
110. Gao Y, Zhang LQ, Wang Y et al (2010) Probing electron density of h-bonding between cation-anion of imidazolium-based ionic liquids with different anions by vibrational spectroscopy. *J Phys Chem B* 114(8):2828–2833
111. Widegren JA, Magee JW (2007) Density, viscosity, speed of sound, and electrolytic conductivity for the ionic liquid 1-hexyl-3-methylimidazolium bis(trifluoromethylsulfonyl)imide and its mixtures with water. *J Chem Eng Data* 52(6):2331–2338
112. Deenadayalu N, Kumar S, Bhuirajh P (2007) Liquid densities and excess molar volumes for (ionic liquids plus methanol plus water) ternary system at atmospheric pressure and at various temperatures. *J Chem Thermodyn* 39(9):1318–1324

113. Anthony JL, Maginn EJ, Brennecke JF (2001) Solution thermodynamics of imidazolium-based ionic liquids and water. *J Phys Chem B* 105(44):10942–10949
114. Rebelo LPN, Najdanovic-Visak V, Visak ZP et al (2004) A detailed thermodynamic analysis of $C_4\text{mim BF}_4$ plus water as a case study to model ionic liquid aqueous solutions. *Green Chem* 6(8):369–381
115. Domanska U, Laskowska M, Pobudkowska A (2009) Phase equilibria study of the binary systems (1-butyl-3-methylimidazolium thiocyanate ionic liquid plus organic solvent or water). *J Phys Chem B* 113(18):6397–6404
116. Letcher TM, Deenadayalu N (2003) Ternary liquid-liquid equilibria for mixtures of 1-methyl-3-octyl-imidazolium chloride plus benzene plus an alkane at $T=298.2$ K and 1 atm. *J Chem Thermodyn* 35(1):67–76
117. Wang HY, Wang JJ, Zhang SL et al (2009) Ionic association of the ionic liquids $C_4\text{mim BF}_4$, $C_4\text{mimPF}_6$, and $C_n\text{mimBr}$ in molecular solvents. *Chemphyschem* 10(14):2516–2523
118. Domanska U, Laskowska M (2009) Effect of temperature and composition on the density and viscosity of binary mixtures of ionic liquid with alcohols. *J Solut Chem* 38(6):779–799
119. Deenadayalu N, Bhujrajh P (2008) Density, speed of sound, and derived thermodynamic properties of ionic liquids $\text{EMIM}^+\text{BETI}^-$ or $\text{EMIM}^+\text{CH}_3(\text{OCH}_2\text{CH}_2)_2\text{OSO}_3^-$ plus methanol or plus acetone at $T = (298.15 \text{ or } 303.15 \text{ or } 313.15)$ K. *J Chem Eng Data* 53(5):1098–1102
120. Zafarani-Moattar MT, Majdan-Cegincara R (2007) Viscosity, density, speed of sound, and refractive index of binary mixtures of organic solvent plus ionic liquid, 1-butyl-3-methylimidazolium hexafluorophosphate at 298.15 K. *J Chem Eng Data* 52(6):2359–2364
121. Iglesias-Otero MA, Troncoso J, Carballo E et al (2008) Densities and excess enthalpies for ionic liquids plus ethanol or plus nitromethane. *J Chem Eng Data* 53(6):1298–1301
122. Huo Y, Xia SQ, Ma PS (2007) Densities of ionic liquids, 1-butyl-3-methylimidazolium hexafluorophosphate and 1-butyl-3-methylimidazolium tetrafluoroborate, with benzene, acetonitrile, and 1-propanol at $T = (293.15 \text{ to } 343.15)$ K. *J Chem Eng Data* 52(5):2077–2082
123. Gao HY, Qi F, Wang HJ (2009) Densities and volumetric properties of binary mixtures of the ionic liquid 1-butyl-3-methylimidazolium tetrafluoroborate with benzaldehyde at $T = (298.15 \text{ to } 313.15)$ K. *J Chem Thermodyn* 41(7):888–892
124. Bhujrajh P, Deenadayalu N (2007) Liquid densities and excess molar volumes for binary systems (ionic liquids plus methanol or water) at 298.15, 303.15 and 313.15 K, and at atmospheric pressure. *J Solut Chem* 36(5):631–642
125. Mokhtarani B, Sharifi A, Mortaheb HR et al (2009) Density and viscosity of pyridinium-based ionic liquids and their binary mixtures with water at several temperatures. *J Chem Thermodyn* 41(3):323–329
126. Fan W, Zhou Q, Sun J et al (2009) Density, excess molar volume, and viscosity for the methyl methacrylate + 1-butyl-3-methylimidazolium hexafluorophosphate ionic liquid binary system at atmospheric pressure. *J Chem Eng Data* 54(8):2307–2311
127. Domanska U, Krolikowska M, Arasimowicz M (2010) Phase equilibria of (1-hexyl-3-methylimidazolium thiocyanate plus water, alcohol, or hydrocarbon) binary systems. *J Chem Eng Data* 55(2):773–777
128. Domanska U, Krolkowski M (2010) Phase equilibria study of the binary systems (1-butyl-3-methylimidazolium tosylate ionic liquid plus water, or organic solvent). *J Chem Thermodyn* 42(3):355–362
129. Simoni LD, Lin Y, Brennecke JF et al (2008) Modeling liquid-liquid equilibrium of ionic liquid systems with NRTL, electrolyte-NRTL, and UNIQUAC. *Ind Eng Chem Res* 47(1):256–272
130. Ji XY, Adidharma H (2009) Thermodynamic modeling of ionic liquid density with heterosegmented statistical associating fluid theory. *Chem Eng Sci* 64(9):1985–1992
131. Karakatsani EK, Economou LG, Kroon MC et al (2007) TPC-PSAFT modeling of gas solubility in imidazolium-based ionic liquids. *J Phys Chem C* 111(43):15487–15492

132. Wang TF, Peng CJ, Liu HL et al (2007) Equation of state for the vapor–liquid equilibria of binary systems containing imidazolium-based ionic liquids. *Ind Eng Chem Res* 46 (12):4323–4329
133. Kim YS, Jang JH, Lim BD et al (2007) Solubility of mixed gases containing carbon dioxide in ionic liquids: measurements and predictions. *Fluid Phase Equilib* 256(1–2):70–74
134. Mollmann C, Gmehling J (1997) Measurement of activity coefficients at infinite dilution using gas–liquid chromatography. 5. Results for N-methylacetamide, N, N-dimethylacetamide, N, N-dibutylformamide, and sulfolane as stationary phases. *J Chem Eng Data* 42(1):35–40
135. Heintz A, Kulikov DV, Verevkin SP (2001) Thermodynamic properties of mixtures containing ionic liquids. 1. Activity coefficients at infinite dilution of alkanes, alkenes, and alkylbenzenes in 4-methyl-n-butylpyridinium tetrafluoroborate using gas–liquid chromatography. *J Chem Eng Data* 46(6):1526–1529
136. Krummen M, Wasserscheid P, Gmehling J (2002) Measurement of activity coefficients at infinite dilution in ionic liquids using the dilutor technique. *J Chem Eng Data* 47 (6):1411–1417
137. Heintz A, Kulikov DV, Verevkin SP (2002) Thermodynamic properties of mixtures containing ionic liquids. 2. Activity coefficients at infinite dilution of hydrocarbons and polar solutes in 1-methyl-3-ethyl-imidazolium bis(trifluoromethyl-sulfonyl) amide and in 1,2-dimethyl-3-ethyl-imidazolium bis(trifluoromethyl-sulfonyl) amide using gas–liquid chromatography. *J Chem Eng Data* 47(4):894–899
138. Yan PF, Liu QS, Yang M et al (2010) Activity coefficients at infinite dilution of organic solutes in N-alkylpyridinium bis(trifluoromethylsulfonyl)imide (C_nPYNTf₂, n = 2, 4, 5) using gas–liquid chromatography. *J Chem Thermodyn* 42(12):1415–1422
139. Yan PF, Yang M, Liu XM et al (2010) Activity coefficients at infinite dilution of organic solutes in 1-ethyl-3-methylimidazolium tris(pentafluoroethyl)trifluorophosphate EMIMFAP using gas–liquid chromatography. *J Chem Eng Data* 55(7):2444–2450
140. Yan PF, Yang M, Liu XM et al (2010) Activity coefficients at infinite dilution of organic solutes in the ionic liquid 1-ethyl-3-methylimidazolium tetracyanoborate EMINI TCB using gas–liquid chromatography. *J Chem Thermodyn* 42(6):817–822
141. Domanska U, Krolikowska M (2011) Measurements of activity coefficients at infinite dilution for organic solutes and water in the ionic liquid 1-butyl-1-methylpiperidinium thiocyanate. *J Chem Eng Data* 56(1):124–129
142. Domanska U, Zawadzki M, Krolikowska M et al (2011) Measurements of activity coefficients at infinite dilution of organic compounds and water in isoquinolinium-based ionic liquid C₈iQuin NTf₂ using GLC. *J Chem Thermodyn* 43(3):499–504
143. Domanska U, Krolikowska M, Acree WE et al (2011) Activity coefficients at infinite dilution measurements for organic solutes and water in the ionic liquid 1-ethyl-3-methylimidazolium tetracyanoborate. *J Chem Thermodyn* 43(7):1050–1057
144. Marciniak A (2010) Influence of cation and anion structure of the ionic liquid on extraction processes based on activity coefficients at infinite dilution. A review. *Fluid Phase Equilib* 294 (1–2):213–233
145. Gmehling J, Li JD, Schiller M (1993) A modified UNIFAC model. 2. Present parameter matrix and results for different thermodynamic properties. *Ind Eng Chem Res* 32(1):178–193
146. Mu TC, Rarey J, Gmehling J (2007) Performance of COSMO-RS with sigma profiles from different model chemistries. *Ind Eng Chem Res* 46(20):6612–6629
147. Nebig S, Bolts R, Gmehling J (2007) Measurement of vapor–liquid equilibria (VLE) and excess enthalpies (H-F) of binary systems with 1-alkyl-3-methylimidazolium bis(trifluoromethylsulfonyl)imide and prediction of these properties and gamma(infinity) using modified UNIFAC (Dortmund). *Fluid Phase Equilib* 258(2):168–178
148. Kato R, Gmehling J (2005) Systems with ionic liquids: Measurement of VLE and [gamma] [infinity] data and prediction of their thermodynamic behavior using original UNIFAC, mod. UNIFAC(Do) and COSMO-RS(OI). *J Chem Thermodyn* 37(6):603–619

149. Diedenhofen M, Eckert F, Klamt A (2003) Prediction of infinite dilution activity coefficients of organic compounds in ionic liquids using COSMO-RS. *J Chem Eng Data* 48(3):475–479
150. Chen CC, Simoni LD, Brennecke JF et al (2008) Correlation and prediction of phase behavior of organic compounds in ionic liquids using the nonrandom two-liquid segment activity coefficient model. *Ind Eng Chem Res* 47(18):7081–7093
151. Nami F, Deyhimi F (2011) Prediction of activity coefficients at infinite dilution for organic solutes in ionic liquids by artificial neural network. *J Chem Thermodyn* 43(1):22–27
152. Troncoso J, Cerdeirina CA, Navia P et al (2010) Unusual behavior of the thermodynamic response functions of ionic liquids. *J Phys Chem Lett* 1(1):211–214
153. Zhong YW, Wang HJ, Diao KS (2007) Densities and excess volumes of binary mixtures of the ionic liquid 1-butyl-3-methylimidazolium hexafluorophosphate with aromatic compound at T (298.15 to 313.15) K. *J Chem Thermodyn* 39(2):291–296
154. Earle MJ, Esperanca J, Gilea MA et al (2006) The distillation and volatility of ionic liquids. *Nature* 439(7078):831–834
155. Øye H, Jagtoyen M, Oksefjell T et al (1991) In: Vapour pressure and thermodynamics of the system 1-methyl-3-ethyl-imidazolium chloride-aluminium chloride. *Trans Tech Publ*, pp 183–190
156. Rooney D, Jacquemin J, Gardas R (2010) Thermophysical properties of ionic liquids. *Top Curr Chem* 290:185–212
157. Zaitsau DH, Kabo GJ, Strechan AA et al (2006) Experimental vapor pressures of 1-alkyl-3-methylimidazolium bis(trifluoromethylsulfonyl) imides and a correlation scheme for estimation of vaporization enthalpies of ionic liquids. *J Phys Chem A* 110(22):7303–7306
158. Armstrong JP, Hurst C, Jones RG et al (2007) Vaporisation of ionic liquids. *Phys Chem Chem Phys* 9(8):982–990
159. Verevkin SP (2008) Predicting enthalpy of vaporization of ionic liquids: a simple rule for a complex property. *Angew Chem Int Ed* 47(27):5071–5074
160. Luo HM, Baker GA, Dai S (2008) Isothermogravimetric determination of the enthalpies of vaporization of 1-alkyl-3-methylimidazolium ionic liquids. *J Phys Chem B* 112(33):10077–10081
161. Santos L, Lopes JNC, Coutinho JAP et al (2007) Ionic liquids: first direct determination of their cohesive energy. *J Am Chem Soc* 129(2):284–285
162. Esperanca J, Lopes JNC, Tariq M et al (2010) Volatility of aprotic ionic liquids – a review. *J Chem Eng Data* 55(1):3–12
163. Fredlake CP, Crosthwaite JM, Hert DG et al (2004) Thermophysical properties of imidazolium-based ionic liquids. *J Chem Eng Data* 49(4):954–964
164. Paulechka YU (2010) Heat capacity of room-temperature ionic liquids: a critical review. *J Phys Chem Ref Data* 39(3). doi: 10.1063/1.3463478
165. Holbrey JD, Reichert WM, Reddy RG et al (2003) Heat capacities of ionic liquids and their applications as thermal fluids. In: Rodgers RD, Seddon KR (eds) *Ionic liquids as green solvents: progress and prospects*. ACS symposium series, vol 856. American Chemical Society, Washington, DC, pp. 121–133
166. Crosthwaite JM, Muldoon MJ, Dixon JK et al (2005) Phase transition and decomposition temperatures, heat capacities and viscosities of pyridinium ionic liquids. *J Chem Thermodyn* 37(6):559–568
167. Shimizu Y, Ohte Y, Yamamura Y et al (2006) Low-temperature heat capacity of room-temperature ionic liquid, 1-hexyl-3-methylimidazolium bis(trifluoromethylsulfonyl)imide. *J Phys Chem B* 110(28):13970–13975
168. Bochmann S, Hefter G (2010) Isobaric heat capacities of the ionic liquids C_nmim Tf₂N (n = 6, 8) from (323 to 573) K at 10 MPa. *J Chem Eng Data* 55(5):1808–1813
169. Yang M, Zhao JN, Liu QS et al (2011) Low-temperature heat capacities of 1-alkyl-3-methylimidazolium bis(oxalato)borate ionic liquids and the influence of anion structural characteristics on thermodynamic properties. *Phys Chem Chem Phys* 13(1):199–206

170. Ge R, Hardacre C, Jacquemin J et al (2008) Heat capacities of ionic liquids as a function of temperature at 0.1 MPa. Measurement and prediction. *J Chem Eng Data* 53(9):2148–2153
171. Troncoso J, Cerdeirina CA, Sanmamed YA et al (2006) Thermodynamic properties of imidazolium-based ionic liquids: densities, heat capacities, and enthalpies of fusion of bmim PF₆ and bmim NTf₂. *J Chem Eng Data* 51(5):1856–1859
172. Yamamuro O, Minamimoto Y, Inamura Y et al (2006) Heat capacity and glass transition of an ionic liquid 1-butyl-3-methylimidazolium chloride. *Chem Phys Lett* 423(4–6):371–375
173. Zhang ZH, Cui T, Zhang JL et al (2010) Thermodynamic investigation of room temperature ionic liquid – the heat capacity and thermodynamic functions of BMIPF₆. *J Therm Anal Calorim* 101(3):1143–1148
174. Tong B, Liu QS, Tan ZC et al (2010) Thermochemistry of alkyl pyridinium bromide ionic liquids: calorimetric measurements and calculations. *J Phys Chem A* 114(11):3782–3787
175. Diedrichs A, Gmehling J (2006) Measurement of heat capacities of ionic liquids by differential scanning calorimetry. *Fluid Phase Equilib* 244(1):68–77
176. Zhang ZH, Tan ZC, Sun LX et al (2006) Thermodynamic investigation of room temperature ionic liquid: the heat capacity and standard enthalpy of formation of EMIES. *Thermochim Acta* 447(2):141–146
177. Yu YH, Soriano AN, Li MH (2009) Heat capacities and electrical conductivities of 1-ethyl-3-methylimidazolium-based ionic liquids. *J Chem Thermodyn* 41(1):103–108
178. Strechan AA, Kabo AG, Paulechka YU et al (2008) Thermochemical properties of 1-butyl-3-methylimidazolium nitrate. *Thermochim Acta* 474(1–2):25–31
179. de Castro CAN, Langa E, Morais AL et al (2010) Studies on the density, heat capacity, surface tension and infinite dilution diffusion with the ionic liquids C₄mim NTf₂, C₄mim dca, C₂mimEtOSO₃ and Aliquat dca. *Fluid Phase Equilib* 294(1–2):157–179
180. Mu TC, Zhang XG, Han BX et al (2003) Effect of phase behavior on the constant volume heat capacity of ethane plus ethanol and ethane plus acetone mixed fluids near the critical region and the intermolecular interaction. *Fluid Phase Equilib* 214(1):53–65
181. Mu TC, Liu ZM, Han BX et al (2003) Effect of phase behavior, density, and isothermal compressibility on the constant-volume heat capacity of ethane plus n-pentane mixed fluids in different phase regions. *J Chem Thermodyn* 35(12):2033–2044
182. Ficke LE, Rodriguez H, Brennecke JF (2008) Heat capacities and excess enthalpies of 1-ethyl-3-methylimidazolium-based ionic liquids and water. *J Chem Eng Data* 53(9):2112–2119
183. Anouti M, Caillon-Caravanier M, Dridi Y et al (2009) Liquid densities, heat capacities, refractive index and excess quantities for protic ionic liquids + water binary system. *J Chem Thermodyn* 41(6):799–808
184. Lin PY, Soriano AN, Leron RB et al (2010) Electrolytic conductivity and molar heat capacity of two aqueous solutions of ionic liquids at room-temperature: measurements and correlations. *J Chem Thermodyn* 42(8):994–998
185. Waliszewski D (2008) Heat capacities of the mixtures of ionic liquids with methanol at temperatures from 283.15 K to 323.15 K. *J Chem Thermodyn* 40(2):203–207
186. Waliszewski D, Piekarski H (2010) Heat capacities of the mixtures of ionic liquids with acetonitrile. *J Chem Thermodyn* 42(2):189–192
187. Anouti M, Jacquemin J, Lemordant D (2010) Volumetric properties, viscosities, and isobaric heat capacities of imidazolium octanoate protic ionic liquid in molecular solvents. *J Chem Eng Data* 55(12):5719–5728
188. Gardas RL, Coutinho JAP (2008) A group contribution method for heat capacity estimation of ionic liquids. *Ind Eng Chem Res* 47(15):5751–5757
189. Chickos JS, Hesse DG, Liebman JF (1993) A group additivity approach for the estimation of heat-capacities of organic liquids and solids at 298 K. *Struct Chem* 4(4):261–269
190. Soriano AN, Agapito AM, Lagumbay L et al (2010) A simple approach to predict molar heat capacity of ionic liquids using group-additivity method. *J Taiwan Inst Chem Eng* 41(3):307–314

191. Paulechka YU, Kabo AG, Blokhin AV et al (2010) Heat capacity of ionic liquids: experimental determination and correlations with molar volume. *J Chem Eng Data* 55 (8):2719–2724
192. Preiss U, Slattery JM, Krossing I (2009) In silico prediction of molecular volumes, heat capacities, and temperature-dependent densities of ionic liquids. *Ind Eng Chem Res* 48 (4):2290–2296
193. Schafer A, Klamt A, Sattel D et al (2000) COSMO implementation in TURBOMOLE: extension of an efficient quantum chemical code towards liquid systems. *Phys Chem Chem Phys* 2(10):2187–2193
194. Strechan AA, Paulechka YU, Blokhin AV et al (2008) Low-temperature heat capacity of hydrophilic ionic liquids BMIMCF₃COO and BMIMCH₃COO and a correlation scheme for estimation of heat capacity of ionic liquids. *J Chem Thermodyn* 40(4):632–639
195. Frisch MJ, Trucks GW, Schlegel HB et al (2004) Gaussian 03, revision C.02. Gaussian, Wallingford
196. Randic M (1975) Characterization of molecular branching. *J Am Chem Soc* 97 (23):6609–6615
197. Valderrama JO, Rojas RE (2010) Mass connectivity index, a new molecular parameter for the estimation of ionic liquid properties. *Fluid Phase Equilib* 297(1):107–112
198. Valderrama JO, Martinez G, Rojas RE (2011) Predictive model for the heat capacity of ionic liquids using the mass connectivity index. *Thermochim Acta* 513(1–2):83–87

Effect of the Structures of Ionic Liquids on Their Physical Chemical Properties

Yufeng Hu and Xiaoming Peng

Abstract ILs are referred to as “designer solvents” [1], and one of their most important advantages is that their properties can be tuned/controlled by tailoring their structures. To do this, however, it is crucial to assume that ILs are solvents of which the local structural (that is, electronic and steric) features may be correlated with their properties and then deal with the effect of their cation and anion structures in altering the related properties. This is exactly the subject of this chapter. The structural factors of the cations are focused on the status of alkylation of H atoms on the ring and tail groups (the polar/nonpolar character, the chain length and its flexibility, the cyclic and branched structures, and the functional tail group). The anion characters include the symmetry, the size, the charge delocalization either by large volume of the central atom or by the presence of the perfluoroalkyl chain, the chain length and its flexibility, and the functional group. The general patterns through which the examined properties vary on changing the cation and anion structures are explored and the reasons behind the trends are briefly discussed on the basis of the structural effect on the interactions between the counterpart ions.

Keywords Ionic liquid • Interaction • Structure • H-bonding • Nanostructure • Thermal property • Volume property • Transport property

Y. Hu (✉) • X. Peng

State Key Laboratory of Heavy Oil Processing and High-Pressure Fluid Phase Behavior & Property Research Laboratory, China University of Petroleum, Beijing 102249, China
e-mail: huyf3581@sina.com

1 Effect of Ionic Structures on Ion–Ion Interactions in Ionic Liquids

For pure IL (denoted by the subscript 1) the hypothetical ideal mixing (the completely random mixing) process is the process where all particles mix randomly while the charge neutrality is maintained. Such a process produces an “ideal” mixture with the following Gibbs energy:

$$G_1^{\text{Ideal}} = n_1 \mu_1^o + \nu_1 n_1 RT \ln m_1 (\nu_+^{\nu_+} \nu_-^{\nu_-})^{1/\nu_1} \quad (1)$$

with $\nu_1 = \nu_+ + \nu_-$ and $\mu_1^o = \nu_+ \mu_{X^{z+}}^o + \nu_- \mu_{Y^{z-}}^o$, where m and ν denote molality and salt stoichiometric coefficient, and $\mu_{X^{z+}}^o$ and $\mu_{Y^{z-}}^o$ are the chemical potentials of the cation $[X]^{z+}$ and anion $[Y]^{z-}$ in the hypothetical ideal solution. The real Gibbs energy of an IL is

$$G_1 = n_1 \mu_1^o + \nu_1 n_1 RT \left[\ln \gamma_1 + \ln m_1 (\nu_+^{\nu_+} \nu_-^{\nu_-})^{1/\nu_1} \right] \quad (2)$$

where γ is the activity coefficient. The excess Gibbs energy

$$G_1^E = G_1 - G_1^{\text{Ideal}} = \nu_1 n_1 RT \ln \gamma_1 \quad (3)$$

is the sum of two contributions, that is

$$G_1^E = G_{\text{entropic}}^E + G_{\text{enthalpic}}^E \quad (4)$$

where G_{entropic}^E is the entropic contribution arising from the differences in the sizes and shapes of the cation and anion, and $G_{\text{enthalpic}}^E$ is the enthalpic contribution primarily from intermolecular forces. The typical interactions between the cation and anion of an IL include Coulombic interactions, van der Waals interactions, and the specific interactions such as H-bondings and $\pi - \pi$ and $n - \pi$ interactions. Therefore, the $G_{\text{enthalpic}}^E$ of an IL can be expressed as

$$G_{\text{enthalpic}}^E = G_{\text{ion-ion}}^E + G_{\text{van}}^E + G_{\text{sc}}^E \quad (5)$$

where G_{van}^E and G_{sc}^E are the excess Gibbs energy resulted from the short-range (the van der Waals) interactions and the specific interactions. $G_{\text{ion-ion}}^E$ is that arising from the long-range ion–ion interactions. The ion-interaction model of Pitzer [2] has achieved wide acceptance. The model assumes that the solvent is a dielectric continuum (due to the lack of the adequate theory for water and other ionizing solvents) and that the excess Gibbs energy comprises two terms, i.e., a short-range term that accounts for the physical interactions between ions and a Debye–Hückel

term that has its origin in the pressure equation of statistical mechanics for the long-range ion-ion interactions. The equation has proved to be successful for ionic systems from dilute ionic solutions to fused salts. $G_{\text{ion-ion}}^E$ is given by

$$G_{\text{ion-ion}}^E = -A(4I/1.2) \ln\left(1 + 1.2I^{\frac{1}{2}}\right) \quad (6)$$

with $G_{\text{ion-ion}}^E \rightarrow 0$ as $I = m \rightarrow 0$ and

$$A = \frac{1}{3}(2\pi N_A \rho / M)^{\frac{1}{2}}(e^2 / DkT)^{\frac{3}{2}} \quad (7)$$

and

$$I = m = \frac{1000}{M} \quad (8)$$

where ρ , M , V , and D are the density, molar mass, molar volume, and dielectric constant of the IL, respectively. N_A and k are Avogadro's and Boltzmann's constants. e , I , and m are the electronic charge, ionic strength, and molality, respectively. It is found that the polarity of ILs does not change appreciably as the cation alkyl chain is elongated, and thus the dielectric constant of $[\text{C}_4\text{mim}][\text{PF}_6]$ [3] at 293.15 K along with the densities and molar masses of various typical ILs are substituted into Eqs. 6 and 7 to yield the $G_{\text{ion-ion}}^E$ for these ILs, including $[\text{C}_n\text{mim}][\text{PF}_6]$ and $[\text{C}_n\text{mim}][\text{Tf}_2\text{N}]$ with $0 \leq n \leq 10$ [4–12], $[\text{C}_4\text{mim}][\text{Cl}]$, $[\text{C}_4\text{mim}][\text{BF}_4]$, $[\text{C}_4\text{mim}][\text{PF}_6]$, $[\text{C}_4\text{mim}][\text{TA}]$, $[\text{C}_4\text{mim}][\text{HB}]$, $[\text{C}_4\text{mim}][\text{Tf}_2\text{N}]$, and $[\text{C}_4\text{mim}][\text{BETI}]$, $[\text{2-MeC}_4\text{mim}][\text{P}_{1,4}]$, $[\text{C}_4\text{Py}][\text{Tf}_2\text{N}]$, and $[\text{C}_4\text{Isoq}][\text{BETI}]$ [4–9, 13–20]. The results, represented in Fig. 1, show that the $|G_{\text{ion-ion}}^E|$ decreases progressively with increasing cation tail length and decreases noticeably in the order of $[\text{C}_4\text{Py}][\text{Tf}_2\text{N}] > [\text{C}_4\text{mim}][\text{Tf}_2\text{N}] > [\text{P}_{1,4}][\text{Tf}_2\text{N}] > [\text{C}_4\text{Isoq}][\text{BETI}]$, which is in line with the order observed for their melting points [3, 4, 21, 22].

Methylation at the C(2)-position of the imidazolium ring reduces the value of $|G_{\text{ion-ion}}^E|$, and the same is true for the better charge delocalization (see the results from $[\text{C}_4\text{Py}]^+$ to $[\text{C}_4\text{Isoq}]^+$). It can be seen from Fig. 1 that the order for the $|G_{\text{ion-ion}}^E|$, $[\text{C}_4\text{mim}][\text{Cl}] > [\text{C}_4\text{mim}][\text{PF}_6] > [\text{C}_4\text{mim}][\text{Tf}_2\text{N}] > [\text{P}_{1,4}][\text{Tf}_2\text{N}] > [\text{C}_4\text{Isoq}][\text{BETI}]$, which is obeyed by their melting points, indicates that the melting points of the ILs with the shorter alkyl chains are strongly related to, but not necessarily controlled by {as $[\text{C}_4\text{mim}][\text{BF}_4]$, $[\text{C}_4\text{mim}][\text{TA}]$, $[\text{C}_4\text{mim}][\text{HB}]$, and $[\text{C}_4\text{mim}][\text{BETI}]$ tend to form glasses} [4, 10, 16, 18, 21–23] the Coulombic interactions. The result for $[\text{2-MeC}_4\text{mim}][\text{Tf}_2\text{N}]$ is an exception because the additional alkyl- π interactions induced by methylation at the C(2)-position of the cation is omitted.

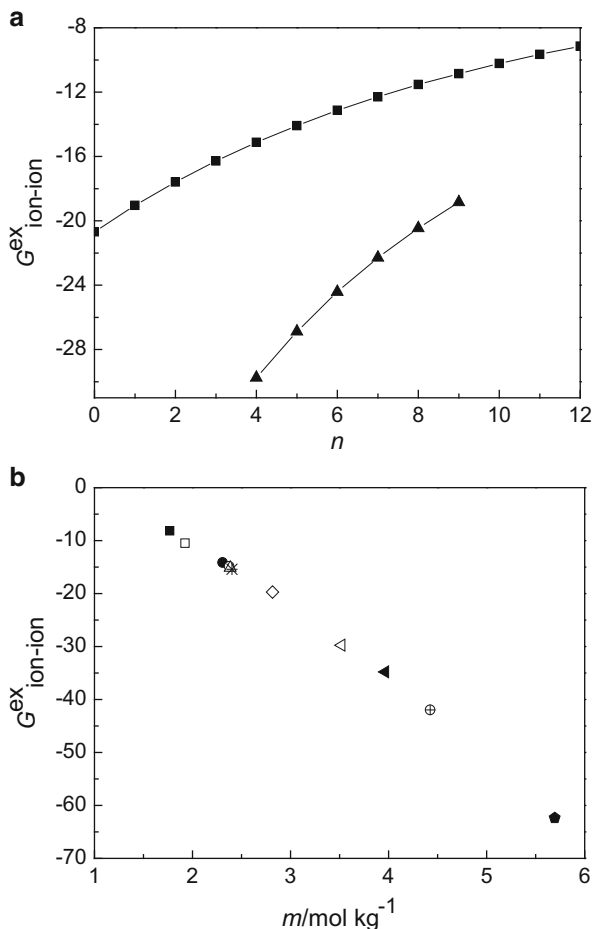


Fig. 1 (a) Plots of $G_{\text{ion-ion}}^{\text{E}}$ vs n for $[\text{C}_n\text{mim}][\text{Tf}_2\text{N}]$ (filled squares) and $[\text{C}_n\text{mim}][\text{PF}_6]$ (filled triangles) at 298.15 K. (b) Plots of $G_{\text{ion-ion}}^{\text{E}}$ vs m for $[\text{C}_4\text{isoq}][\text{BETI}]$ (filled squares), $[\text{C}_4\text{mim}][\text{BETI}]$ (open squares), $[2\text{-MeC}_4\text{mim}][\text{Tf}_2\text{N}]$ (filled circles), $[\text{P}_{1,4}][\text{Tf}_2\text{N}]$ (open circles), $[\text{C}_4\text{mim}][\text{Tf}_2\text{N}]$ (open triangles), $[\text{C}_4\text{Py}][\text{Tf}_2\text{N}]$ (asterisks), $[\text{C}_4\text{mim}][\text{HB}]$ (open diamonds), $[\text{C}_4\text{mim}][\text{PF}_6]$ (open left pointing triangles), $[\text{C}_4\text{mim}][\text{TA}]$ (filled left pointing triangles), $[\text{C}_4\text{mim}][\text{BF}_4]$ (circles with interior cross), and $[\text{C}_4\text{mim}][\text{Cl}]$ (filled pentagons) at 298.15 K. The $G_{\text{ion-ion}}^{\text{E}}$ values were calculated using Eqs. 6 and 7 along with the dielectric constant of $[\text{C}_4\text{mim}][\text{PF}_6]$ [3] at 293.15 K and the densities and molar masses of the examined ILs [4–9, 16, 17, 19, 22]

2 Effect of Ionic Structures on H-Bondings in Ionic Liquids

The H-bondings between the counterions are closely related to the properties of the ILs such as viscosity, conductivity, density, and crystalline packing [10]. Recently their effects on organic reactions, specifically the Diels–Alder reaction [24, 25], neutral allylic substitutions [26], and addition of $[\text{ICl}_2]^-$ to double and triple bonds [27], were reported. Therefore their effects have received growing attention [28–30].

2.1 *Effect of Cation Structures on H-Bondings Between the Counterions*

The C(2)-H of the imidazolium ring is bonded to a carbon locating between two electronegative nitrogen atoms and, thereby, would be acidic. Similarly, the C(4)- and C(5)-H would also be acidic but to a less extent. Therefore, the C(*n*)-H (*n* = 2, 4, and 5) could engage in H-bonding interactions with a range of anions. The existence of the H-bondings has been established [10, 29, 31–42] in the crystal structures of [C₂mim] (Cl, Br, I, and [NO₃]) and ([C₂mim]₂ and [2-MeC₂mim]₂)[MCl₄](M = Co and Ni). Both the NMR chemical shifts (CS) measurements and the ab initio calculations show that H-bondings exist in [C₄mim]([BF₄] and [PF₆]) and the H-bonding ability of C(2)-H is greater than those of C(4)- and C(5)-H [4–9, 42–56]. It is found that the strong H-bonds can be formed via the H atom on a carbon attached to a quaternary nitrogen such as R₃N⁺-C-H [57], suggesting that a similarly located H atom on the CH₃ of [P_{1,*n*]⁺ would also be expected to exhibit the H-bonding ability. Note that the CH...[Y][−] H-bondings were reported to exist between the iminium ions and the halides (Cl[−], Br[−], and I[−]) [58].}

2.2 *Effect of Anion Structures on H-Bondings Between the Counterions*

The anions that could form the H-bondings with the C(*n*)-H on the imidazolium ring are halide anion, [AlCl₄][−], and [AcO][−] [24, 28, 29, 34, 35]. It was shown [50–52, 59] that the anion's H-bond basicity follows the order Cl[−] > [SbF₆][−] > [TfO][−] > [BF₄][−] > [Tf₂N][−] > [PF₆][−], which correlates neither with the volume of the central atom, [Tf₂N][−] > [TfO][−] > [AsF₆][−] > [PF₆][−] > [BF₄][−] [13–15, 20, 60], nor with the volume of the anion. [Tf₂N][−] is more strongly coordinating than [TA][−] [13–15, 20] due to its larger effective charge density [28, 61]. For halide ions, Cl[−] is the hardest, most charge dense, and most coordinating. However, while the central atom of [SbF₆][−] is larger than that of [PF₆][−], an inverse trend is observed for their H-bond basicities (the IR spectrum of [C₄mim][PF₆] [62] indicates no H-bonding bands in the region 3,000–3,100 cm^{−1} where C–H...Cl[−] interactions on imidazolium chloride were observed [32]). This means that, for example, [AsF₆][−] would be more weakly coordinating than [PF₆][−] because of its larger size. The H-bonds between the imidazolium cations and [BPh₄][−] have also been reported [50]; however, [BPh₄][−] and [Barf][−] were later shown to offer no ability for the H-bonding interactions [23, 51, 53, 54]. The weak abilities of [PF₆][−] and [BPh₄][−] may be a result of their symmetrical shapes and their low charge densities. Recently, the relative H-bond strengths of several ILs have been estimated in the gas phase by ESI-MS [52]. The conclusion thus obtained is that the anion's H-bonding ability strongly depends on its effective charge density and its symmetry.

3 Effect of Ionic Structures on Nanostructures of Ionic Liquids

In recent years there has been considerable interest in self-organized nanostructures of ILs, which can be used either as oriented solvents to prepare anisotropic materials [63, 64] and to induce catalytic selectivity (or micelle catalysis) by orienting reactants [65–67] or as templates for the synthesis of mesoporous, nanostructured, and zeolitic materials and in the formation of ordered thin films [68–72]. The recognition of the nano-segregation in ILs is also crucial for systematic interpretations and predictions of the properties of ILs [73, 74].

Therefore the existence of nanostructures in ILs has received more and more attention and has been identified by various methods, including Raman spectroscopy [75], X-ray diffraction [76], SWAXS (small-wide angle X-ray scattering), OHD-RIKES (femtosecond optical heterodyne-detected Raman-induced Kerr effect spectroscopy) [77], NSE (Neutron spin echo) [78], and so on. The most direct picture of the nanostructures to date was obtained from MD simulations [79–82] and FF-TEM (freeze-fracture transmission electron microscopy) [73].

The FF-TEM images [73] and the MD simulations [83, 84] on $[C_n\text{mim}](\text{Cl}, [\text{BF}_4], [\text{PF}_6], [\text{Tf}_2\text{N}])$ showed that the cation tail groups protrude outwards from the surface of the nanodomains while the cation rings lie beneath. The size of nanodomains of the tested ILs is smaller than the wavelength of visible light (< 100 nm), consistent with the fact that these ILs are all transparent. The CARS (coherent anti-Stokes Raman scattering) signals also imply that the size of nanodomains formed in $[C_n\text{mim}][\text{PF}_6]$ is most likely to be several tens of nanometers [75, 85]. The characteristic size of the structural heterogeneities in $[C_n\text{mim}](\text{Cl}, [\text{BF}_4], [\text{PF}_6], [\text{Tf}_2\text{N}])$ increases either with increasing cation chain length or with decreasing anion size [76, 77, 86, 87]. The FF-TEM images [73] and the MD simulations [88] on $[C_n\text{mim}](\text{Cl}, [\text{BF}_4], [\text{NO}_3])$ [79] showed that the nanodomains of the $[C_n\text{mim}]^+$ -based ILs have significant aggregation of the C_4 – C_8 tail groups, but the $n = 3$ compound is close to the transition. The FF-TEM images [73], the MD simulations [88], and the NSE measurements [78] showed that, at 298 K, extensive nanostructures are formed in $[C_6\text{mim}][\text{Tf}_2\text{N}]$, whereas $[C_4\text{mim}][\text{Tf}_2\text{N}]$ is the onset of the transition. The SWAXS and the OHD-RIKES measurements showed that the nanoscale structural heterogeneities occurred in $[C_n\text{mim}][\text{Tf}_2\text{N}]$ with $n \geq 3$ [77, 86]. The FF-TEM images [73], the low-frequency Raman spectrum [75, 85], and the spatial distribution pattern of the CARS signals of $[C_n\text{mim}][\text{PF}_6]$ [75, 85] showed that the variation of the nanostructures are more remarkable on going from $n = 4$ to $n = 6$ than on going from $n = 6$ to $n = 8$.

The ILs composed of $[C_n\text{mim}]^+$ ($n = 3 - 10$) and inorganic anions tend to undergo nanoscale segregation of polar and nonpolar domains in the liquid [16, 74–78, 80–86, 88–106], while the $n > 10$ ILs possess liquid crystalline phases [107–111]. However, the size of the self-organized nanostructures suffers from disagreement [75, 82, 85, 94, 104]. Furthermore, it appears from theoretical, computational, and experimental studies that the formation of nanodomains fundamentally changes the character of the ILs [63, 74, 75, 81, 85, 90–92, 102].

4 Effect of Ionic Structures on Thermal Property

4.1 Melting Point

4.1.1 Effect of Cation Head Groups

Methylation at the C(*n*)-positions or ethylation at the C(2)-position of the imidazolium cation considerably promotes the melting points of [(C₂)₂im][(Tf₂N)] and [TfO]), [NC(CH₂)₃mim]Cl, [C₂im][BETI], and [C_{*n*}mim]([Sac], [BETI], [BF₄], Br, Cl, [CB₁₁H₁₂], [CB₁₁H₆Cl₆], [Tf₂N], [TfO], [TA] and [PF₆]) with *n* = 2, 3, and 4 [4, 5, 10–12, 16–18, 20, 23, 33, 34, 36, 54, 62, 110, 112–136]. As expected, the results for [2-EtC₂mim]([Tf₂N] and [TfO]) and [2-MeC₂mim]([Tf₂N] and [TfO]) imply that ethylation at the C(2)-position augments the melting points to a higher extent than methylation [4, 18, 128].

4.1.2 Effect of Cation Tail Groups

The Gibbs free energy of the melting is zero if the system is at thermodynamic equilibrium, that is

$$\Delta G_m = \Delta H_m - T_m \Delta S_m = 0 \quad (9)$$

where ΔG_m , ΔH_m , and ΔS_m are the Gibbs free energy, enthalpy, and entropy of melting. Therefore, the melting temperature, T_m , depends on ΔH_m and ΔS_m , i.e.,

$$T_m = \Delta H_m / \Delta S_m \quad (10)$$

The enthalpy of melting depends on the interactions between the molecules/ions. The dominant force in inorganic salts, Coulombic attractions between ions, is extremely strong so that these compounds have very high melting points. The intermolecular forces governing the melting points of organic compounds are the van der Waals interactions and/or intermolecular H-bondings and other specific interactions such as $\pi - \pi$ and $n - \pi$ interactions. For ILs, the ΔH_m primarily depends on the Coulombic interactions ($\Delta H_m^{\text{ion-ion}}$), van der Waals interactions (ΔH_m^{van}), and H-bondings and other specific interactions (ΔH_m^{sc}). That is

$$\Delta H_m = \Delta H_m^{\text{ion-ion}} + \Delta H_m^{\text{van}} + \Delta H_m^{\text{sc}} \quad (11)$$

The ΔS_m is a measure of the changes in molecular translational, rotational, and conformational freedoms that accompany melting [44]:

$$\Delta S_m = \Delta S_m^{\text{tr}} + \Delta S_m^{\text{rot}} + \Delta S_m^{\text{conf}} \quad (12)$$

with

$$\Delta S_m^{\text{rot}} = C_{\Delta S_m} - R \ln \psi \quad (13)$$

and

$$\Delta S_m^{\text{conf}} = R \ln \varphi \quad (14)$$

where $C_{\Delta S_m}$ is the entropy of melting constant and ψ is the external rotational symmetry number of the molecule, which is a measure of the probability of the molecule being in the proper orientation for incorporation into the crystal. φ is a function of chain length and is defined by [45, 46]

$$\varphi = 2.85^\tau \quad (15)$$

where τ is the number of torsional angles and the value of 2.85 is based on an equation developed by Temperley with the assumption that the *trans* conformation is more stable than the *gauche* conformation by 2.26 kJ mol⁻¹ [45, 46]. The number of the torsional angles for any compound is calculated by [45, 46]

$$\tau = n_{\text{SP}^3} + 0.5n_{\text{SP}^2} + 0.5n_{\text{Ring}} - 1 \quad (16)$$

where n_{SP^3} and n_{SP^2} are the number of the sp³ and sp² chain atoms, and n_{Ring} is the number of fused-ring systems. For organic compounds, ΔS_m is assumed to be primarily determined by the changes in the rotational and conformational freedoms (due to the slight increase in the volume accompany the melting process), i.e.,

$$\Delta S_m = C_{\Delta S_m} - R \ln \psi + R \ln \varphi \quad (17)$$

Equations 12, 13, 14, 15, 16, and 17 are the simple semiempirical equations that estimate the entropy of melting by using the simple molecular geometric parameters. Comparisons with the experimental results for more than 930 different compounds show that their estimate accuracy is within the range of experimental errors [45]. These equations, combined with the approach utilizing the molecular group contributions to calculate the enthalpy of melting, have proved capable of providing accurate predictions for the melting points of 1,040 organic compounds containing various functionalities directly from the molecular structures [46].

Increasing the alkyl chain length enhances the molar volume and chain flexibility of the cation, and thus gives rise to the positive contributions to ΔS_m^{conf} and ΔH_m^{van} and the positive deviations from the ideal mixing entropy. At the same time, the $|G_{\text{ion-ion}}^E|$ and thereby the $|\Delta H_m^{\text{ion-ion}}|$ decreases with increase in chain length. Therefore, the variation in melting point of an IL is a result of the competition of the above effects: its melting point decreases if the value of $\Delta H_m/\Delta S_m$ decreases; otherwise, it increases with increasing chain length. That is

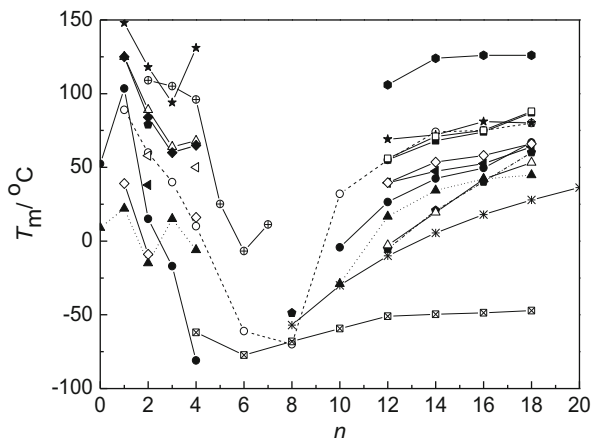


Fig. 2 U-shape plots of melting point vs chain length (T_m vs n) for $[C_n\text{Py}]\text{Cl}$ (filled stars), $[C_n\text{Py}][\text{PF}_6]$ (filled hexagons), $[C_{n-3}\text{MePy}][\text{PF}_6]$ (filled squares), $[C_{n-4}\text{MePy}][\text{PF}_6]$ (open squares), $[C_n\text{mim}][\text{BF}_4]$ (filled circles), $[C_n\text{mim}][\text{PF}_6]$ (open circles), $[C_n\text{mim}][\text{NO}_3]$ (filled left pointing triangles), $[C_n\text{mim}][\text{AuCl}_4]$ (open left pointing triangles), $[C_n\text{mim}][\text{TfO}]$ (open diamonds), $[C_n\text{mim}][\text{AlCl}_4]$ (filled diamonds), $[C_n\text{mim}]\text{Br}$ (filled pentagons), $[C_n\text{mim}]\text{Cl}$ (open triangles), $[C_n\text{mim}][\text{Tf}_2\text{N}]$ (filled triangles), $[C_n\text{Isoq}][\text{BETI}]$ (squares with interior cross), $[N_{n,n,n,n}][\text{Tf}_2\text{N}]$ (circles with interior cross), and n -alkane (asterisks) [4, 5, 10–13, 16–18, 20, 22–25, 33, 34, 36, 52, 54, 62, 107, 108, 110–114, 116, 119–154]

to say, the competition of these factors may yield the u-shape plots as shown in Fig. 2, in which the plots of T_m vs n are illustrated for the ILs involving $[C_n\text{Py}]^+$, $[C_n\text{mim}]^+$, $[C_n\text{Isoq}]^+$, and $[N_{n,n,n,n}]^+$.

The typical examples are that the melting points of $[C_n\text{mim}](\text{BF}_4)$, Br, Cl, $[\text{NO}_3]$, $[\text{PF}_6]$, $[\text{Tf}_2\text{N}]$, and $[\text{TfO}]$ in general decrease rapidly when $n = 2-5$, but remain nearly constant when $n = 6$ and 7 , and then gradually increase with further increasing of the chain length from $n = 8$ to $n = 18$. Another feature of these ILs is that the change in their melting points with increasing chain length is much less pronounced and sometimes (see, for example, the melting points of $[C_n\text{mim}][\text{BF}_4]$ and $[C_n(\text{C}_2\text{im})_2][\text{PF}_6]_2$) it follows an odd–even alternating pattern due to the deviation of the even length chains from the linear structure of the favored all-*trans* configuration found for the odd chain lengths [110].

For the ILs with shorter cation alkyl chains and rigid anions, the dominant forces for the melting points are electrostatic forces, which are inversely related to the molar volumes and molar masses of the ILs. Therefore, for the ILs based on the same cation/anion, the anion/cation with smaller molar volume and smaller molar mass yields a higher melting point. Indeed, the melting points of the ILs having a given cation are found to increase from $[\text{AsF}_6]^-$ to $[\text{PF}_6]^-$, from I^- to Br^- to Cl^- , and from $[\text{AuCl}_4]^-$ to $[\text{NiCl}_4]^-$ to $[\text{CoCl}_4]^-$. However, the melting points of the ILs with rigid anions and with longer cation alkyl chains are dominated by the short-range van der Waals interactions. This means that their melting points should correlate with the density of the arrangement of their alkyl chains. Because the

layer separations decrease with increasing the anion size/decreasing the anion basicity [106], their enthalpies of melting and thereby their melting points should increase with increasing anion size. The supporting examples are that the melting points of the ILs based on $[C_n\text{mim}]^+$ ($n \geq 8$) increase from Cl^- to $[\text{BF}_4]^-$ to $[\text{PF}_6]^-$. It is noticeable that the same anion order is followed by the densities of the $[C_n\text{mim}]^+$ -based ILs with $n \leq 8$ (no density data for the case with $n > 10$ are available for comparison). This implies that elongating the chain length reverses the anion order observed for the melting points of the ILs with the short chains. Indeed, as can be seen from Fig. 2, the melting points of the ILs with $[C_n\text{-mim}]^+$ ($n \leq 4$) increase through the anion series of $[\text{TfO}]^-$, $[\text{NO}_3]^-$, Br^- , and Cl^- , but the inverse trend appears when $n \geq 8$. It should be emphasized that the melting points are affected not only by the enthalpy of melting but also by the entropy of melting; the above statements primarily concern the enthalpic contributions and thus in general should be limited to the cations or anions with the simple or similar structures. For instance, the melting points of $[C_n\text{mim}][\text{Tf}_2\text{N}]$ are less than those of $[C_n\text{mim}][\text{TfO}]$, $[\text{BF}_4]$, $[\text{NO}_3]$, and $[\text{PF}_6]$ progressively from $n = 0$ to $n = 3$ and from $n = 10$ to $n = 18$. This does not necessarily mean the breakdown of the above statements, because the enthalpies of melting of $[C_n\text{mim}][\text{Tf}_2\text{N}]$ [107] are still higher than those [107, 110, 140] of the rest of the ILs. The reason for this is attributed to the chain flexibility of $[\text{Tf}_2\text{N}]^-$, which introduces additional entropy (ΔS_m^{conf}). The effect of the anion chain flexibility on reducing the melting points of the ILs can also be seen from the results for the ILs based on $[C_n\text{BF}_3]^-$.

It is well known that $[C_1\text{mim}][\text{Tf}_2\text{N}]$ and $[\text{BF}_4]$ present higher melting points than $[\text{mim}][\text{Tf}_2\text{N}]$ and $[\text{BF}_4]$, which is usually explained by assuming that the van der Waals interactions dominate over the H-bonding influences. However, the increased cation symmetry from $[\text{mim}]^+$ to $[C_1\text{mim}]^+$ (the ψ increases from 1 to 2), which apparently decreases the ΔS_m^{rot} , should also play an important role on promoting the melting point.

The melting points increase with the degree of chain branching, which is supported by the melting points of the ILs from $[C_n\text{mim}](\text{Cl}$ and $[\text{PF}_6])$ with $n = 3$ and 4 to $[i\text{-}C_n\text{mim}](\text{Cl}$ and $[\text{PF}_6])$ to $[\text{tert-butylmim}][\text{PF}_6]$. Appending an isopropyl group instead of an n -propyl group in $[\text{R}_3\text{mim}][\text{PF}_6]$ also increases the melting point by 62°C [120, 135]. This increase is attributed to the changes in efficiency of the crystal packing as free rotation volume decreases and atom density increases [135, 155].

The melting points of the ILs can be modified by grafting the functional group(s) into the cationic head ring. $[\text{Ph}(\text{CH}_2)_m\text{mim}][\text{PF}_6]$ and $[\text{Tf}_2\text{N}]$ with $m = 1\text{--}3$ present significantly higher melting points than their $[C_n\text{mim}]^+$ counterparts with $n = m + 6$ [11, 12, 20, 54, 111, 116]. Grafting ethynyl instead of saturated alkyl also significantly promotes the melting points as can be seen from the results from $[\text{C}_3\text{mim}]\text{Cl}$ to $[\text{HC} \equiv \text{CCH}_2\text{mim}]\text{Cl}$ (60 vs 142°C) and from $[\text{C}_3\text{mim}][\text{BF}_4]$ to $[\text{HC} \equiv \text{CCH}_2\text{mim}][\text{BF}_4]$ (-17 vs 67°C) [113, 120, 126–130, 134]. Noting that, the effects of these groups result not only from their positive contributions to the enthalpy of melting (due to the $\pi - \pi$

interactions) but also from their negative contributions to the ΔS_m^{conf} (due to the reduced chain flexibility). The melting point of $[\text{NC}(\text{CH}_2)_3\text{Py}]\text{Cl}$ is also lower by 30°C than that of $[\text{C}_4\text{Py}]\text{Cl}$ [108, 149–153, 156]. One possible reason is due to the formation of the intramolecular “cyclic” structure through the $\text{C} \equiv \text{N} \dots \pi$ interactions (it is well known that the intramolecular cyclic structure through the H-bonding reduces the melting point of the organic compound). This idea is supported by the crystal structure of $[\text{NC}(\text{CH}_2)_3\text{Py}]\text{Cl}$, which shows that the $\text{C} \equiv \text{N}$ group points toward the center of the pyridinium ring and engages in the $\text{C} \equiv \text{N} \dots \pi$ interactions with it [157]. In the case of $[\text{NC}(\text{CH}_2)_n\text{mim}][\text{BF}_4]$ [114], $([\text{NC}(\text{CH}_2)_3\text{mim}]$ and $[\text{NC}(\text{CH}_2)_4\text{mim}])[\text{BF}_4]$ could form intramolecular “cyclic” structures. However, the expansionary force of the three-membered ring is very large so that it is more favorable for $[\text{NCCH}_2\text{-mim}]$ - and $[\text{NC}(\text{CH}_2)_2\text{mim}][\text{BF}_4]$ to form the intermolecular “cyclic” structures (i.e., forming a dimer) through the two head-to-tail $\text{C} \equiv \text{N} \dots \pi$ interactions rather than the intramolecular “cyclic” structures. As a result, the melting points of $[\text{NC}(\text{CH}_2)_n\text{mim}][\text{BF}_4]$ decrease only slightly as n increases from 1 to 2 or from 3 to 4. However, their melting points are considerably lowered as n increases from 2 to 3 (the intermolecular cyclic structure through the H-bonding promotes the melting point of the organic compound). For organic compounds, H-bondings are usually much stronger than the van der Waals interactions in a crystal lattice. However, this effect is not clearly observed for the ILs containing the hydroxyl and carboxyl functional groups. $[\text{CF}_3\text{CH}_2\text{mim}][\text{TfO}]$ has a melting point 54°C higher than that of $[\text{C}_2\text{mim}][\text{TfO}]$ due to the presence CF_3CH_2 group which withdraws the electron density on the imidazolium ring and promotes H-bonding [158].

4.1.3 Effect of Anion Structures

The anion structures are not always symmetrical or simple, so their influences on melting points should rely on their contributions to the melting enthalpy and melting entropy. An inspection of the literature data indeed reveals that, with the shorter cation chains, the melting points of the ILs containing $[\text{C}_n\text{mim}]^+$ increase on changing anion through the series $[\text{DCA}]^-$, $[\text{Tf}_2\text{N}]^-$, $[\text{TA}]^-$, $[\text{BF}_4]^-$, $[\text{TfO}]^-$, $[\text{NfO}]^-$, $[\text{NO}_3]^-$, $[\text{AsF}_6]^-$, and $[\text{PF}_6]^-$ [4, 5, 9–12, 16–18, 20, 23–25, 33, 34, 36, 52, 54, 107, 110, 111, 113, 114, 116, 119–133, 135, 136, 139, 140, 145–147]. This trend correlates neither with the strength of the electrostatic force nor with the ability of the anion to form the H-bonding with the cation. On the other hand, the cation and anion of an IL have their own molar volumes and molar masses. Therefore, the interactions between the cation and the anion should also include the van der Waals interactions. According to the Pitzer’s equation [2], the thermodynamic behavior of the concentrated aqueous electrolyte solutions or the molten salt systems are strongly dependent on the short-range interactions between the inorganic cations and inorganic anions. The molar volumes and molar masses of the

organic cations and anions are in general greater than those of the inorganic ones, and the concentrations of ILs are also very high ($[C_4mim][PF_6]$: $3.52 \text{ mol}\cdot\text{kg}^{-1}$). Therefore, the short-range interactions between the IL-cations and IL-anions should play an important role in determining the phase behavior of the ILs. The values of $\Delta H_m^{\text{ion-ion}}$ and ΔH_m^{sc} of the ILs with $[AsF_6]^-$ or $[PF_6]^-$ are less than those of the ILs with $[BF_4]^-$, and the differences in their entropies of melting should be small because these anions are highly symmetric. The greater value of ΔH_m^{van} due to the short-range interactions between the cation and $[AsF_6]^-$ or between the cation and $[PF_6]^-$ is then the most possible reason behind the above trend. Note that the melting points of $[CB_{11}H_6Cl_6]^-$, $[CB_{11}H_{12}]^-$, and $[CB_{11}H_6Br_6]^-$ produced ILs are apparently higher than those of the ILs based on the above anions [115]. This can also be interpreted only by recalling the effect of the short-range interactions between the cations and the anions, because the H-bondings between C(2)-H of the imidazolium ring and these large anions are regarded as less important (for instance, $[2\text{-Me}C_2mim][CB_{11}H_{12}]$ and $[CB_{11}H_6Cl_6]$ exhibit melting points some 20–30°C higher than those of their $[C_2mim]^+$ -counterparts) [115], and the electrostatic forces between $[C_nmim]^+$ and these larger anions are also less than those between $[C_nmim]^+$ and the above anions. Now $[Tf_2N]^-$ has been recognized as one of the most effective anions in producing low melting points and, in the literature, the reason is attributed to better charge delocalization and its inability to undergo H-bonding[4–9]. However, while $[Tf_2N]^-$ is larger than $[PF_6]^-$ and thus the $\Delta H_m^{\text{ion-ion}}$ in $[C_2mim][Tf_2N]$ should be less than that in $[C_2mim][PF_6]$ (as can be deduced from Fig. 1), the enthalpy of melting of $[C_2mim][Tf_2N]$ is greater than that of $[C_2mim][PF_6]$ [11, 12], which is clearly now a result of the above-mentioned short-range interactions. As noted above, the trends followed by the anions with similar structures ($[TaF_6]^-$, $[SbF_6]^-$, $[AsF_6]^-$, and $[PF_6]^-$; their sizes increase from left to right [144]) and ($[AuCl_4]^-$, $[NiCl_4]^-$, and $[CoCl_4]^-$) are due to the differences in the properties of the central atoms, which may yield the greater charge density, smaller molar volume, and smaller molar mass, all of which tend to increase the $\Delta H_m^{\text{ion-ion}}$.

The melting point of $[C_{12}mim][BPh_4]$ is higher by 142°C than that of $[C_{12}mim][BF_4]$ [18, 110], suggesting that presence of an aromatic ring in an anionic structure can introduce the specific interactions and thus can considerably increase the melting point.

The effect of anion chain length is evident. For example, the melting points of $[C_2mim][C_nBF_3]$ decrease from $n = 3$ to $n = 4$, and then increase as $n \geq 4$ [121]. The melting points of the ILs based on $[PF_6]^-$ are in general higher than those of the ILs based on $[BF_4]^-$. $[C_2mim][1\text{-}C_nCB_{11}H_{11}]$ ($n = 1\text{--}4$) also exhibit considerably lower melting points (ca. 62°C) than $[C_2mim][CB_{11}H_{12}]$ [115]. Hexahalogenation of $[CB_{11}H_{12}]^-$ shows no substantial effect on the melting points. Packing inefficiency was considered to be the dominating factor giving the low melting points to the ILs composed of $[C_nmim]^+$ and carborane anions [115].

4.2 Effect of Ionic Structures on Glass Transition

The tendency of an IL to form glass is related to the interactions between its ions and its ability to resist the configurational changes to a more order state as temperature is lowered. Therefore, the glass transitions of the ILs having the same anion are related to the entropy symbolized by Eq. 17: the ILs with larger conformational entropies, i.e., the ILs based on $[C_n\text{mim}]^+$, $[2\text{-Me}C_n\text{mim}]^+$, $[C_n\text{im}]^+$, $[2\text{-Me}C_n\text{im}]^+$, $[(C_n)_2\text{im}]^+$, and $[C_n(C_2\text{im})_2]^{2+}$ show the noticeable tendency toward glass formation, whereas the ILs having symmetric structures, for example, the ILs with $[C_1\text{mim}]^+$ and $[N_{1,1,1,1}]^+$, are seldom able to form the glass. The glass transitions of the $[C_n\text{mim}][\text{PF}_6]$ series decrease progressively from -74°C for $n = 3$ to the minimum value (-84°C) for $n = 7$, but then increase with further elongating the chain length from $n = 7$ to $n = 10$ [10, 11, 16–18, 159, 160]. The glass transitions of $[(C_n)_2\text{im}][\text{PF}_6]$ also decrease from $n = 4$ to $n = 8$ and increase when $n > 8$ [147].

The directional H-bondings make special contributions to the glass transitions of the ILs, that is, grafting the alcohol groups promotes the glass formation rather than crystallization, presumably because the directional H-bondings restrict the Coulombic restructuring of the liquids into the crystalline lattices. Incorporation of these groups induces the directional H-bondings that dominate the melting process of the organic compounds and thus enhances their melting points. However, the melting process of the ILs with the short tail chains is governed by the Coulombic forces. On the other hand, the presence of the $[X]^+ - \text{H} \cdots [X]^+$ H-bonding requires that the $\text{H} \cdots [X]^+$ distance must be less than the sum of the H and X van der Waals radii, and the $[X]^+ - \text{H} \cdots [X]^+$ angle must be greater than 90° . This means that the presence of the H-bonding resists the structural changes and promotes the ability of the ILs to persist with their liquid structures to the solid states. Furthermore, a comparison of the glass transitions with the viscosities of $[\text{CH}_3\text{CH}(\text{OH})\text{CH}_2\text{mim}][\text{TF}_2\text{N}]$, $[\text{Cl}^-]$, $[\text{NO}_3^-]$, and $[\text{PF}_6^-]$ and $[(\text{CH}_2)_2\text{OHmim}][\text{PF}_6^-]$ and $[\text{BF}_4^-]$, (-67.6 , -68.9 , -79.3 , -88.4°C vs 342, 1,856, 502, 319 cP) [161] and (-72 and -84°C vs 148 and 90 cP) [162, 163], suggests that the glass transitions of the functionalized ILs are related to their viscosities (probably due to the flexibility of $[\text{TF}_2\text{N}]^-$ which promotes the glass formation and the mobility of the anion). However, no such relation is observed when the introduced functional groups can only engage in the nondirectional specific interactions. $[\text{Ph}(\text{CH}_2)_m\text{mim}][\text{TF}_2\text{N}]$ with $m = 2$ and 3 display apparently higher glass transitions than their $[C_n\text{mim}]^+$ counterparts with $n = m + 6$ as supported by the data for $([\text{PhCH}_2\text{mim}]$ and $[C_7\text{mim}][\text{TF}_2\text{N}]$, -56 and -85°C , respectively [11, 12, 24, 25, 145].

The anion effect also involves a complex interplay of the short- and long-range interactions as well as the symmetry and flexibility of the anion. However, their influences are in a quite predictable manner. The glass transitions of $[C_4\text{mim}]^+$ -produced ILs increase in the anion series of $[\text{DCA}]^-$, $[\text{TF}_2\text{N}]^-$, $[\text{BF}_4]^-$, $[\text{PF}_6]^-$, and Cl^- [10–12, 16–18, 110, 159, 164]. $[\text{DCA}]^-$ and $[\text{TF}_2\text{N}]^-$ produce the ILs with lower glass transitions, which may be attributed to the better charge delocalization

and the greater flexibility of their chains. Furthermore, the large differences in glass transitions between [C₄mim][Barf] [11, 12, 16, 18, 20, 53, 54, 164] and [C₄mim][Tf₂N] indicate that the anion's influence on glass transitions may be dramatic.

The results for the ILs based on alkyl- and alkenyltrifluoroborates are very noticeable. The glass transitions of the [C₂mim]⁺-based ILs decrease in the anion order [CH₂ = CHBF₃]⁻ < [C₄BF₃]⁻ < [C₃BF₃]⁻ < [C₂BF₃]⁻ < [C₁BF₃]⁻ = [BF₄]⁻ [121–123, 125–130, 165]. In addition, while fluorination of the alkyl chain of the cation tends to increase the glass transitions of the ILs (see, for example, the glass transitions of ([SF₅(CF₂)₂(CH₂)₄mim] and [SF₅(CF₂)₄(CH₂)₂mim])[Tf₂N] and ([C₃mim] and [CF₃(CH₂)₂mim])[Tf₂N]) due to the enhanced van der Waals interactions [11, 12, 18, 24, 25, 111, 135, 145], fluorination of the alkyl chain in the [R₄BF₃]⁻ significantly decreases the glass transitions, which is clearly seen from the results for [C₂mim]([C₁BF₃] and [CF₃BF₃]), -93 vs -117°C [121], and [C₂mim]([N(CH₃SO₂)₂] and [Tf₂N]), -50 vs -95°C [166]. Because the hyperconjugated structure between the C = C bond and the center boron atom in [CH₂ = CHBF₃]⁻ could produce the better charge delocalization, and the nonfluorinated alkyl group in the examined anions could withdraw the electron density, it seems that the glass transitions of the above ILs are controlled by the negative charge density. Of course, the glass transitions of the [C_nBF₃]⁻ series are dominated by the van der Waals interactions.

4.3 Effect of Ionic Structures on Thermal Stability

The decomposition temperatures, including the onset (T_{onset}) and the start (T_{start}) temperatures for the decomposition, of the ILs, were usually determined by thermogravimetric analysis (TGA) [4, 17, 22, 120, 121, 126–130, 139, 155, 167–176]. The onset temperature is the intersection of the baseline below their decomposition temperature with the tangent to the mass loss vs temperature plots in the TGA experiment [139]. The start temperature is the temperature at which the measurable mass loss is first observed (under which the decomposition can be negligible). Because the start temperature is much lower than the onset temperature, and the higher decomposition temperatures calculated from fast TGA scans under a protective atmosphere do not imply long-term thermal stability below these temperatures, recently the maximum operating temperature, $T_{z'/t}$, the temperature at which the degree of conversion z' ($0 < z' < 1$) occurs over a given amount of time t , is developed to estimate the thermal stability of the ILs [174]. For certain samples, the TGA-determined onset temperatures depend on the type of sample pan (aluminum or alumina) [120], but the experiments under nitrogen or air produce the same results [4].

The thermal stability of the ILs with a given anion is dominated by the charge density, acidic proton, and expansionary force of the cation head group. It is shown that [C₂mim]([BF₄], [Me], and [Tf₂N]) and [C₄mim][Tf₂N] are more stable than

$[N_{2,2,2,2}][BF_4]$, $[Me]$, and $[Tf_2N]$) and $[N_{4,4,4,4}][Tf_2N]$ [4, 119–121, 177] because the charge density of the imidazolium head ring is lower. It is noted that the above results do not mean that the imidazolium ILs are always chemically inert [175]. Methylation on the imidazolium ring increases the thermal stability of the cation [34] and substitution of the C(2)-H has the largest effect because of the greater acidity of this proton. This can be seen by comparing the results for $([C_4mim]$ and $[2-MeC_4mim])[BF_4]$ [16–18, 110, 164, 176], $([C_nmim]$ and $[2-MeC_nmim])Cl$ with $n = 2$ and 3 [120] and $([C_3mim]$ and $[2-MeC_3mim])[PF_6]$ [120]. For $([Tf_2N]^-, [PF_6]^-, \text{ and } Cl^-)$ -based ILs, the thermal stability increases through the series of $[C_nmim]^+$, $[2-MeC_nmim]^+$ ($n = 2$ and 3), and $[M_5I]^+$ [120].

Introduction of the functional groups can significantly change the thermal stability of the ILs. Grafting the ferrocenylmethyl group dramatically reduces the thermal stability of the imidazolium ILs as supported by the results from $[C_2mim]$ (I and $[Tf_2N]$) to $[ferrocenylmethylmim]$ (I and $[Tf_2N]$) [4, 119, 120, 177, 178].

Branching the alkyl chain decreases the thermal stability of the IL as exemplified by the lower thermal stabilities of $[i-C_3mim][PF_6]$ and $[Tf_2N]$ compared to those of $[C_3mim][PF_6]$ and $[Tf_2N]$ [120]. The thermal stabilities generally increase with decreasing chain length and increase from $[C_{18}mim]^+$ to $[M_5I]^+$ [4, 107, 120, 140].

The effect of negative charge density is significant. However, it appears that the influence of increasing the anion's charge density should not be considered in isolation. For the IL with lower cationic charge density, the thermal stability increases if the anion's charge density is lowered or its charge-bearing region is effectively isolated. $[C_2mim][TfO]$ and $[Tf_2N]$ are stable up to $400^\circ C$ [24], but $[C_2mim][TA]$ only to $150^\circ C$ [4–9]. The thermal stabilities of the $[C_2mim]^+$ -based ILs increase in the order $[TA]^- < Cl^- < [PF_6]^- < [BF_4]^- < [AsF_6]^- < [TfO]^- < [Tf_2N]^- < [Me]^-$ [4, 11, 12, 20, 33, 34, 53, 54, 113, 119–121, 174]. It was shown that the thermal decomposition of $[C_2mim][C_nBF_3]$ ($n = 1$ to 5) was initiated from the pyrolysis of $[C_nBF_3]^-$ [121]. Their thermal stabilities increase in the anion orders $[C_1BF_3]^- < [C_3BF_3]^- < [C_5BF_3]^- < [BF_4]^-$ and $[C_4BF_3]^- < [C_2BF_3]^- < [C_1BF_3]^-$ [120, 121].

5 Effect of Ionic Structures on Volume Property

5.1 Molar Volume

The molar volumes are available for $([C_4mim]$ and $[C_8mim])[PF_6]$ and $([C_8mim]$ and $[C_4Py])[BF_4]$ from 298.2 to 343.2 K and between 0.099 and 206.9 MPa [179]. As expected, the molar volumes of $[C_nmim][BF_4]$ and $[PF_6]$ increase progressively as n increases from 6 to 10 and from 4 to 8 [48, 180–182], respectively. The sizes of $[Tf_2N]^-$, $[PF_6]^-$, $[BF_4]^-$, and Cl^- exhibit a clear correlation to the molar volumes of $[C_nmim]^+$ -produced ILs. The molar volumes of the ILs based on the same anion were found to increase almost linearly with increasing cation

alkyl chain length and the addition of two CH₂ units on the chain of [C_{*n*}mim]⁺ at 298.15 K and atmospheric pressure increases the molar volume of the ILs by 34.4 ± 0.5 mL·mol⁻¹ [183, 184].

5.2 Density

5.2.1 Effect of Apparatus and Impurity

As seen in the literature results, the discrepancy between the densities of the different IL samples in general greatly depends on the measurement methodologies used. The largest discrepancy is usually observed between the densities determined with a volumetric flask/pycnometer and those measured using a densimeter. In addition, the pycnometer values were usually more scattered.

The presence of contamination water decreases the densities of the ILs due to the lower densities of water relative to those of the ILs examined. However, the presence of 1,000 ppm contamination water in [C₄mim][BF₄] would cause a 0.00021 decrease in the recommended density value at 298.15 K, suggesting that the effect of contamination water is relatively much less. The ILs composed of [C_{*n*}mim]⁺ in connection with Cl⁻ have smaller densities than in connection with other typical IL anions, indicating that the presence of residual Cl⁻ tends to decrease the densities of the ILs.

5.2.2 Effect of Cation Structures

The density of an IL is a manifestation of the density of the arrangement of its cation and anion and thus strongly depends on the interaction forces between its ions, the symmetry of its ions, and the difference in ionic size between its cation and its anion. The density of the cyclic ring is greater than that of the acyclic structure, and elongating the chain length increases the free volume within the IL so that its density is lowered. Indeed, the densities of [C_{*n*}mim]Cl with *n* = 6 and 8 [17, 176, 185], [C_{*n*}mim][BF₄] with *n* = 4–8 [17–19, 23, 48, 53, 54, 114, 126, 176, 179, 181, 186–189], [C_{*n*}mim][PF₆] with *n* = 4–8 [10, 11, 17, 54, 114, 160, 176, 179, 181, 186–188, 190–196], and [C_{*n*}mim][Tf₂N] with *n* = 2 and 4 [4, 11, 18, 127, 184, 188, 191, 197–200] decrease progressively with increasing cation chain length. This trend is also supported by the observation that, although the water contents of [C_{*n*}Isoq][BETI] decrease progressively from 1.77 wt% for *n* = 4 to 0.41 wt% for *n* = 18, the densities of the ILs diminish gradually from 1.23 g·cm⁻³ for *n* = 4 to 1.05 g·cm⁻³ for *n* = 18 [22].

The densities of functional groups are in general greater than those of *n*-alkyl chains and, thus, grafting the functional group(s) can increase the densities of the ILs. The densities of [NC(CH₂)_{*m*}-mim]([PF₆], Cl, and [BF₄]) (1.61 ≤ ρ ≤

$2.15 \text{ g}\cdot\text{cm}^{-3}$) [114] at 293.15 K were considerably greater than the densities of their $[\text{C}_n\text{-mim}]^+$ counterparts with $n = m + 1$ ($\rho \leq 1.2972 \text{ g}\cdot\text{cm}^{-3}$).

5.2.3 Effect of Anion Structures

The density of an IL depends on the density and symmetry of its anion. The densities of $[\text{C}_n\text{-mim}]^+$ -based ILs combined with different anions increase in the order $\text{Cl}^- < [\text{BF}_4]^- < [\text{TfO}]^- < [\text{PF}_6]^- < [\text{Tf}_2\text{N}]^-$ [4, 11, 16–19, 48, 53, 54, 114, 126, 127, 136, 160, 176, 179, 181, 184, 185, 187, 189–194, 196–199, 201–219]. In addition, the order $\text{Cl}^- < [\text{EtSO}_4]^- < [\text{TA}]^- < [\text{BF}_4]^- < [\text{TfO}]^- < [\text{Tf}_2\text{N}]^-$ [4, 11, 121, 127, 189, 197–199, 220] is followed by the densities of the $[\text{C}_2\text{-mim}]^+$ -produced ILs. These orders suggest that the densities of the ILs formed with halide are noticeably lower than those of the ILs based on other typical IL anions. The order for the densities of $[\text{C}_n\text{-mim}][n\text{-C}_m\text{F}_{2m+1}\text{BF}_3]$ with $n = 1\text{--}6$ and $m = 1\text{--}4$ at 298.15 K [121, 176, 218, 220–225] are $[\text{C}_1\text{F}_3\text{BF}_3]^- < [\text{C}_2\text{F}_5\text{BF}_3]^- < [n\text{-C}_3\text{F}_7\text{BF}_3]^- < [n\text{-C}_4\text{F}_9\text{BF}_3]^-$. The densities increase from $[\text{C}_6\text{-mim}][(\text{C}_2\text{F}_5)_3\text{PF}_3]$ to $[\text{C}_6\text{-mim}][(\text{n-C}_3\text{F}_7)_3\text{PF}_3]$. These results imply that increasing number of CF_2 units in the anion chain increases the densities of the ILs.

6 Effect of Ionic Structures on Viscosity

6.1 Analyses

The Eyring absolute rate theory can be expressed as $\phi_{\text{mixture}} = \phi_{\text{ideal}} \exp\left(\frac{\Delta G^\ddagger}{RT}\right)$ with $\phi_{\text{ideal}} = \exp\left(\sum_i^N x_i \ln \phi_i\right)$, where ΔG^\ddagger is the molar excess activation free energy of flow, and ϕ_{mixture} and ϕ_{ideal} are the kinematic viscosities of a mixed solution and an ideal solution, respectively. In the present analyses the viscosity of a binary system is expressed as $\ln \eta_{\text{mixture}} = (x_{\text{H}_2\text{O}} \ln \eta_{\text{H}_2\text{O}} + x_{\text{IL}} \ln \eta_{\text{IL}}) + f(M_{\text{mixture}})$, where $f(M_{\text{mixture}})$ essentially corrects the contribution from $(\ln \rho_{\text{mixture}} - x_{\text{H}_2\text{O}} \ln \rho_{\text{H}_2\text{O}} - x_{\text{IL}} \ln \rho_{\text{IL}}) + \frac{\Delta G^\ddagger}{RT}$. It is clear that the presence of water in ILs can significantly decrease the viscosity of ILs due to the much lower viscosity of water relative to those of ILs.

6.2 Effect of Cation Structures

Methylation at the C(2)-position of the head group considerably raises the viscosities of $[\text{C}_n\text{-mim}][\text{Tf}_2\text{N}]$ ($n = 2$, from 34.0 to 106.0 cP at 293.15 K [4–9];

$n = 6$, from 68.0 to 131.0 cP at 298.15 K [175]). The viscosities of ($[C_2\text{mim}]$ and $[5\text{-Me}C_2\text{mim}])[\text{Tf}_2\text{N}]$, ($[(C_2)_2\text{im}]$ and $[5\text{-Me}(C_2)_2\text{im}])[\text{Tf}_2\text{N}]$, and ($[C_2\text{mim}]$ and $[5\text{-Me}C_2\text{mim}])[\text{TfO}]$ at 293.15 K are 34.0 vs 37.0 cP, 35.0 vs 36.0 cP, and 45.0 vs 51.0 cP [4–9], respectively, implying that C(5)-position methylation has only a slight effect on the viscosities of the examined ILs.

It is seen that the viscosities of $[C_n\text{mim}]\text{Cl}$ with $n = 6$ and 8 [17, 175, 221], $[C_n\text{mim}][\text{BF}_4]$ with $n = 2\text{--}10$ [10, 16, 17, 35, 114, 119, 121, 125–130, 136, 162, 175, 218, 221–229], $[C_n\text{mim}][\text{PF}_6]$ with $n = 4\text{--}8$ [3, 10, 16, 17, 62, 114, 129, 130, 136, 141, 162, 183, 197, 227, 228, 230, 231], $[C_n\text{mim}][\text{Tf}_2\text{N}]$ with $n = 2\text{--}8$ [4–9, 16, 17, 25, 119, 136, 139, 175, 183, 228], and $[C_n\text{mim}][\text{TA}]$ with $n = 2$ and 4 [4–9, 16, 139, 228] increase progressively with increasing cation chain length. The same is true for the viscosities of $[(C_2)_2\text{im}][\text{Tf}_2\text{N}]$ and $[C_4C_2\text{im}][\text{Tf}_2\text{N}]$ [4–9]. However, it is noteworthy that the viscosity of $[C_2\text{mim}][\text{Tf}_2\text{N}]$ [139] is smaller than the viscosity of $[C_1\text{mim}][\text{Tf}_2\text{N}]$ (32.0 vs 38.4 cP at 298.15 K), probably due to its more sufficient side-chain mobility. Ramifying the alkyl chain reduces the rotational freedom and hence makes the ILs more viscous, which can be clearly seen by comparing the viscosity of $[i\text{-}C_4\text{mim}][\text{Tf}_2\text{N}]$ and $[C_4\text{mim}][\text{Tf}_2\text{N}]$ at 293.15 K, 83.0 vs 52.0 cP [4–9, 136].

Grafting functional groups into $[\text{R}_1\text{mim}]^+$ can modify the viscosities of ILs. The viscosity of $[\text{CF}_3\text{CH}_2\text{mim}][\text{Tf}_2\text{N}]$ at 293.15 K is apparently greater than the viscosity for $[C_2\text{mim}][\text{Tf}_2\text{N}]$ (248.0 vs 34.0 cP) [4–9], implying that fluorination of the alkyl chain dramatically promotes the viscosity of ILs due to the enhanced van der Waals interactions. The nitrile-functionalized ILs, ($[\text{NC}(\text{CH}_2)_2\text{mim}]$ and $[\text{NC}(\text{CH}_2)_4\text{mim}])[\text{BF}_4]$ (65.5 vs 552.9 cP at 298.15 K [114]) and $[\text{NC}(\text{CH}_2)_4\text{mim}][\text{PF}_6]$ (2,181.0 cP at 298.15 K [114]), have considerably higher viscosities than ($[C_2\text{mim}]$ and $[C_4\text{mim}])[\text{BF}_4]$ (the viscosity values at 298.15 K are 38.0 and 103.0 cP [121, 126–130], respectively) and $[C_4\text{mim}][\text{PF}_6]$ (the viscosity at 298.15 K is 289.0 cP [228]). Because water contamination decreases the viscosities of ionic liquids and the chloride ion in the used samples of $[\text{NC}(\text{CH}_2)_4\text{mim}][\text{BF}_4]$ and $[\text{NC}(\text{CH}_2)_4\text{mim}][\text{PF}_6]$ was below the detection limit, these trends should be attributed to the formation of the intermolecular and the intramolecular “cyclic” structures within $[\text{NC}(\text{CH}_2)_n\text{mim}][\text{BF}_4]$ and $[\text{PF}_6]$.

6.3 Effect of Anion Structures

The anion dramatically influences the viscosity of ILs. The results show that the viscosities of the $[C_n\text{mim}]^+$ -based ILs with $n = 4\text{--}8$ increase from $[\text{BF}_4]^-$ to $[\text{PF}_6]^-$ [3, 10, 16, 17, 62, 114, 126–130, 136, 141, 162, 175, 183, 197, 218, 226–231]. A comparison of the viscosities shows that the general order for increasing viscosity of the ILs of $[C_n\text{mim}]^+$ with $n = 2$ and 4 is $[\text{Tf}_2\text{N}]^- < [\text{TA}]^- < [\text{TfO}]^-$ [4–9, 16, 17, 119, 136, 139, 183, 228]. The $[\text{Tf}_2\text{N}]^-$ -based ILs exhibit the lower melting points, glass transitions, and viscosities, presumably because they combine better charge delocalization with greater chain flexibility, which produces larger

melting entropy and increases the chain mobility so that the melting point and viscosity are lowered but the ability of the IL to resist the increase in viscosity as the temperature is lowered is promoted. The anion order for the viscosities of the $[C_n\text{mim}]^+$ -based ILs, $[\text{TF}_2\text{N}]^-$, $[\text{BF}_4]^-$ and Cl^- , are consistent with those for the H-bond basicity of the ILs and thereby of these anions (the H-bond basicity of an IL is governed by that of its anion [59]). The viscosities increase in the anion order $[\text{TF}_2\text{N}]^- < [\text{BF}_4]^- < [\text{PF}_6]^-$, which is also in line with the order observed for the melting points and glass transitions of the ILs. However, the viscosities of $[\text{PEG}_n\text{mim}]^+$ - and $[\text{PEG}_n\text{C}_4\text{im}]^+$ -based ILs with $n = 1-3$ increase through the trend of $[\text{BF}_4]^- < [\text{PF}_6]^- < [\text{TF}_2\text{N}]^-$ [163]. In this case it seems possible that the contributions from the anion size and the van der Waals interactions override those from other factors.

The reported viscosities of the ILs combining $[\text{C}_2\text{mim}]^+$ with different anions increase in the orders $[\text{BF}_4]^- < [\text{CH}_2 = \text{CHBF}_3]^- < [\text{C}_1\text{BF}_3]^- < [\text{C}_3\text{BF}_3]^- < [\text{C}_2\text{BF}_3]^- < [\text{C}_4\text{BF}_3]^- < [\text{C}_5\text{BF}_3]^-$, $[\text{CF}_2 = \text{CFBF}_3]^- < [\text{CF}_3\text{BF}_3]^- < [\text{C}_2\text{F}_5\text{BF}_3]^- < [n\text{-C}_3\text{F}_7\text{BF}_3]^- < [n\text{-C}_4\text{F}_9\text{BF}_3]^- = [\text{BF}_4]^-$ [35, 119, 121, 125–130, 214, 227, 232]. The water contents of these ILs, 100–300 ppm ($0.0011 \leq x_{\text{H}_2\text{O}} \leq 0.0042$), were low, and therefore the water contamination should not change the anion order for the viscosities of the ILs. The fact that the viscosities increase with increasing anion chain length implies that their viscosities are governed by the van der Waals interactions. In addition, the results from $([\text{CH}_2 = \text{CH-BF}_3]^- \text{ and } [\text{CF}_2 = \text{CF-BF}_3]^-)$, $[\text{C}_m\text{F}_{2m-1}\text{BF}_3]^-$, and $[(\text{C}_m\text{F}_{2m-1})_3\text{PF}_3]^-$ to $([\text{C}_1, \text{C}_2\text{BF}_3]^- \text{ and } [\text{C}_2\text{F}_5\text{BF}_3]^-)$, $[\text{BF}_4]^-$, and $[\text{PF}_6]^-$ suggest that the effects of the charge delocalization and the chain flexibility override that of the van der Waals interactions.

These orders indicate that the viscosities increase with increasing anion chain length and that the viscosities of these ILs are governed by the van der Waals interactions. The results from $[\text{CH}_2 = \text{CHBF}_3]^-$ and $[\text{CF}_2 = \text{CFBF}_3]^-$ to $[\text{C}_n\text{BF}_3]^-$ and $[n\text{-C}_m\text{F}_{2m+1}\text{BF}_3]^-$ suggest that the effect of the charge delocalization overrides that of the van der Waals interactions [121].

7 Effect of Ionic Structures on Conductivity

The specific conductivity σ' of a liquid salt can be expressed as [4]

$$\sigma' = \frac{yF^2\rho}{6\pi N_A M \eta} \left[(\zeta_a r_a)^{-1} + (\zeta_c r_c)^{-1} \right] \quad (18)$$

where $0 \leq y \leq 1$ is the degree of dissociation. ζ_a and ζ_c are the “correction” factors taking into account the specific interactions between the mobile ions in the melt, and r_a and r_c are the anion and cation hydrodynamic radii. Equation 18 is based on the relationship

$$\sigma' = \frac{yF\rho}{M} [u_a + u_c] \quad (19)$$

and the modified form of the Stokes–Einstein relationship that correlates ionic mobilities to viscosities of the medium [4], that is,

$$u_a = \frac{F}{6\pi N_A \zeta_a r_a \eta} \quad (20)$$

and

$$u_c = \frac{F}{6\pi N_A \zeta_c r_c \eta} \quad (21)$$

where u_a and u_c are the anion and cation mobilities, respectively, in the liquid. The conductivity relies on the number and mobility of the charge carriers. If the ion–ion interactions are so strong that the ILs move as the ion aggregates, then the conductivity will be low.

In the case of ILs composed of a constant anion in connection with the cations of the same head group, the values of V , η , $(\zeta_a r_a)$, and $(\zeta_c r_c)$ in Eq. 18 increase with increasing cation tail length. Consequently, the conductivity would decrease with increasing cation tail length. The results show that the conductivities of $[C_n\text{mim}][\text{Tf}_2\text{N}]$ decrease from $n = 2$ to $n = 8$ [4–9, 16, 112, 119, 126–130, 150, 175, 233]. The conductivities also decrease from $[C_2\text{mim}][\text{BF}_4]$ to $[C_4\text{mim}][\text{BF}_4]$ [10, 16, 35, 119, 121, 124–130, 155, 233, 234], whilst the conductivities of $[C_n\text{mim}][(\text{C}_2\text{F}_5)_3\text{PF}_3]$ decrease progressively from $n = 2$ to $n = 6$ [175]. Furthermore, methylation at the C(2)-position on $[C_2\text{mim}]^+$ is expected to increase the conductivity through eliminating the specific interactions between the C(2)-H and the anion, but this is not the case. Instead, methylation at the C(2)- and C(5)-positions of $[C_2\text{mim}]^+$ and $[(C_2)_2\text{im}]^+$ rings considerably reduces the conductivities of $[C_2\text{mim}][(\text{TfO})]$ and $[C_2\text{mim}][\text{Tf}_2\text{N}]$ and $[(C_2)_2\text{im}][\text{Tf}_2\text{N}]$ [4–9, 112, 119, 126–130, 150, 175]. However, the dimer salts $[C_n(C_2\text{im})_2][\text{Tf}_2\text{N}]$ ($n = 2–8$) do not conform to the same trend because the salts with $n = 6$ and 8 display much higher conductivities than the rest [173, 235]. Branching the alkyl chain decreases the conductivity as supported by the results for the $[\text{Tf}_2\text{N}]^-$ -based ILs from $[C_4\text{mim}]^+$ to $[i\text{-C}_4\text{mim}]^+$ and from $[2\text{-MePhCH}_2\text{-C}_4\text{im}]^+$ to $[2\text{-MePhCH}_2\text{-}i\text{-C}_4\text{im}]^+$ [4–9, 16, 150, 236]. Trifluoroethylated imidazolium IL, $[\text{CF}_3\text{CH}_2\text{mim}][\text{Tf}_2\text{N}]$, shows a dramatically lower conductivity than its ethylated analogue, $[C_2\text{mim}][\text{Tf}_2\text{N}]$ [4–9, 112, 119, 126–130, 150, 175].

The relationship between the anion size and the conductivity of ILs is usually limited to the anions with similar structures. For example, the conductivities of $[C_2\text{mim}][\text{R-BF}_3]$ decreases in the anion order $[\text{CF}_3\text{BF}_3]^- > [\text{BF}_4]^- > [\text{C}_2\text{F}_5\text{BF}_3]^- > [\text{CH}_2 = \text{CH-BF}_3]^- > [\text{C}_1\text{BF}_3]^- > [\text{C}_3\text{F}_7\text{BF}_3]^- > [\text{C}_2\text{BF}_3]^- > [\text{C}_3\text{BF}_3]^- > [\text{C}_4\text{F}_9\text{BF}_3]^- > [\text{C}_4\text{BF}_3]^- > [\text{C}_5\text{BF}_3]^-$ [35, 119, 121, 124–130, 155, 214, 232–234, 237]. It is evident that the conductivities of $[C_2\text{mim}][(\text{C}_m\text{F}_{2m+1}\text{BF}_3)]$

and $[C_m\text{BF}_3]$ increase with increasing anion chain length [121, 214, 232, 237]. Furthermore, the results from $[\text{CF}_3\text{BF}_3]^-$ to $[\text{BF}_4]^-$, from $[C_m\text{F}_{2m-1}\text{BF}_3]^-$ to $[C_m\text{BF}_3]^-$, and from $[\text{CH}_2 = \text{CH-BF}_3]^-$ to $[C_1\text{BF}_3]^-$ indicate that the charge delocalization plays an important role in determining the conductivity and that the conductivities of these ILs are inversely related to their viscosities. Increasing the anion size from $[\text{Tf}_2\text{N}]^-$ to $[\text{BETI}]^-$ and from $[\text{BF}_4]^-$ to $[\text{PF}_6]^-$ decreases the conductivities from $8.4 \times 10^{-3} \text{ S}\cdot\text{cm}^{-1}$ [4–9] for $[\text{C}_1\text{mim}][\text{Tf}_2\text{N}]$ to $1.0 \times 10^{-3} \text{ S}\cdot\text{cm}^{-1}$ [9] for $[\text{C}_1\text{mim}][\text{BETI}]$ and from $3.5 \times 10^{-3} \text{ S}\cdot\text{cm}^{-1}$ [16] for $[\text{C}_4\text{mim}][\text{BF}_4]$ to $1.49 \times 10^{-3} \text{ S}\cdot\text{cm}^{-1}$ [16] for $[\text{C}_4\text{mim}][\text{PF}_6]$, respectively. However, $[\text{C}_2\text{mim}]^+$ in connection with $[\text{Tf}_2\text{N}]^-$ displays higher conductivity than that connected with the smaller anion, $[\text{AcO}]^-$ [4–9, 112, 119, 126–130, 150, 175]. The reason may be attributed to the stronger specific interactions between $[\text{AcO}]^-$ and the cation, which decreases the conductivity of the IL.

The conductivities of the ILs with $[\text{C}_n\text{mim}]^+$ in general increase through the series of $[\text{NfO}]^-$, $[\text{HB}]^-$, $[\text{PF}_6]^-$, $[\text{AcO}]^-$, $[\text{TfO}]^-$, $[\text{TA}]^-$, $[\text{BF}_4]^-$, $[\text{Tf}_2\text{N}]^-$, $[\text{DCA}]^-$, and $[\text{F}(\text{HF})_n]^-$ [4–10, 16, 35, 112, 119, 121–130, 150, 155, 175, 233, 234], which is inversely related to the anion order for the viscosities of the same ILs. It is noticeable that $[\text{F}(\text{HF})_n]^-$ and $[\text{Barf}]^-$ -based ILs yield the high and the low conductivities, respectively [20, 53, 54, 123].

8 Conclusions

Increasing anion flexibility yields greater melting entropy and promotes the mobility of the anion. Better charge delocalization reduces the melting enthalpy and enhances the degree of ion dissociation that is favorable to lowering the viscosity. As a result, the melting point, glass transition, and viscosity of the ILs are lowered either by delocalizing negative charge or by increasing anion flexibility. Elongating the cation chain length progressively decreases/increases the conductivity/viscosity of the IL. Branching the cation alkyl group increases the melting points but decreases the thermal stabilities of the ILs; it also makes the ILs more viscous and less conductive.

The effect of the functional group is related to its ability to undergo interactions with the anion. Grafting functional groups such as the fluorinated alkyl chain into the cation head group increases van der Waals interactions. Accordingly, the melting point, glass transition, density, and viscosity of ILs are in general promoted, but the conductivities are in general decreased. Introduction of the $\text{NC}(\text{CH}_2)_m$ group is found to induce the formation of the intra- or intermolecular “cyclic” structure through the $\text{C} \equiv \text{N} \cdots \pi$ interactions, which is particularly important for understanding the unusually reduced melting points of $[\text{NC}(\text{CH}_2)_3\text{-Py}](\text{Cl}$ and $[\text{Tf}_2\text{N}])$ relative to those of their $[\text{C}_4\text{Py}]^+$ counterparts. Furthermore, the unusually higher densities and viscosities displayed by $[\text{NC}(\text{CH}_2)_n\text{-mim}](\text{Cl}$, $[\text{BF}_4]$, and $[\text{PF}_6])$ and $[\text{NC}(\text{CH}_2)_3\text{-Py}][\text{Tf}_2\text{N}]$ become understandable, because the cyclic structure is denser

than the acyclic structure and the formation of the cyclic structure makes the cation less mobile.

Glossary of Abbreviations

Abbreviations	Full Names
IL	Ionic liquid
$[C_n\text{mim}]^+$	1-Alkyl-3-methylimidazolium
$[2\text{-Me}C_n\text{mim}]^+$	1-Alkyl-2,3-dimethylimidazolium
$[2\text{-Me}C_n\text{im}]^+$	1-Alkyl-2-methylimidazolium
$[C_{10}C_{10}\text{im}]^+$	1,3-Didecylimidazolium
$[(C_2)_2\text{im}]^+$	1,3-Diethylimidazolium
$[C_n\text{im}]^+$	1-Alkylimidazolium
$[2\text{-Et}C_2\text{mim}]^+$	1,2-Diethyl-3-methylimidazolium
$[C_n(C_2\text{im})_2]^+$	α , ω -Diimidazoliummethylene
$[(C_n)_2\text{im}]^+$	1,3-Dialkylimidazolium
$[C_4C_2\text{im}]^+$	1-Butyl-3-ethylimidazolium
$[i\text{-}C_3\text{mim}]^+$	1-iso-Propyl-3-methylimidazolium
$[C_n\text{Isoq}]^+$	<i>N</i> -Alkyl-isoquinolinium
$[M_5I]^+$	Pentamethylimidazolium
$[P_{1,n}]^+$	<i>n</i> -Alkyl- <i>N</i> -methylpyrrolidinium
$[C_n\text{Py}]^+$	1-Alkyl-pyridinium
$[C_n\text{-}3\text{-MePy}]^+$	1-Alkyl-3-methylpyridinium
$[C_n\text{-}4\text{-MePy}]^+$	1-Alkyl-4-methylpyridinium
$[N_{n_1,n_2,n_3,n_4}]^+$	Quaternary ammonium
$[\text{HC} \equiv \text{CCH}_2\text{mim}]^+$	1-(2-Propynyl)-3-methylimidazolium
$[\text{CH}_3\text{CH}(\text{OH})\text{CH}_2\text{mim}]^+$	1-(2-Hydroxypropyl)-3-methylimidazolium
$[(\text{CH}_2)_2\text{OHmim}]^+$	1-(2-Hydroxyethyl)-3-methylimidazolium
$[\text{CF}_3\text{CH}_2\text{mim}]^+$	1-(2,2,2-Trifluoroethyl)-3-methylimidazolium
$[\text{NC}(\text{CH}_2)_n\text{mim}]^+$	1-Alkyl nitrile-3-methylimidazolium
$[\text{PEG}_n\text{mim}]^+$	1-(2-Hydroxy-ethyl) _{<i>n</i>} -3-methylimidazolium
$[\text{PEG}_n\text{C}_3\text{im}]^+$	1-(2-Hydroxy-ethyl) _{<i>n</i>} -3-propylimidazolium
$[\text{CF}_3(\text{CH}_2)_2\text{mim}]^+$	1-Methyl-3-trifluoropropylimidazolium
$[\text{NC}(\text{CH}_2)_3\text{Py}]^+$	<i>N</i> -Butyronitrile pyridinium
$[\text{Ph}(\text{CH}_2)_n\text{mim}]^+$	1-(ω -Phenylalkyl)-3-methylimidazolium
$[\text{AuCl}_4]^-$	Tetrachloroaurate
$[\text{AlCl}_4]^-$	Tetrachloroaluminate
$[\text{TA}]^-$	Trifluoroacetate
$[\text{HB}]^-$	Heptafluorobutanoates
$[\text{BETI}]^-$	Bis(perfluoroethylsulfonyl)imide

(continued)

Abbreviations	Full Names
[AcO] ⁻	Acetate
[Barf] ⁻	Tetrakis[<i>p</i> -dimethyl(1H,1H,2H,2H-perfluorooctyl)silylphenyl]-borate
[SbF ₆] ⁻	Hexafluoroantimonate
[AsF ₆] ⁻	Hexafluoroarsenate
[BPh ₄] ⁻	Tetraphenylborate
[NfO] ⁻	Nonaflate
[TfO] ⁻	Trifluoromethanesulfonate
[Tf ₂ N] ⁻	Bis(trifluoromethylsulfonyl)imide
[DCA] ⁻	Dicyanamide
[Sac] ⁻	Saccharinate
[Me] ⁻	Tris(trifluoromethylsulfonyl)methide
[N(CH ₃ SO ₂) ₂] ⁻	Bis(methane sulfonyl)amide
[CB ₁₁ H ₁₂] ⁻	Carborane
[1-C _n CB ₁₁ H ₁₁] ⁻	1-Alkylcarborane
[(C ₂ F ₅) ₃ PF ₃] ⁻	Tris(pentafluoroethyl)trifluorophosphate
[(<i>n</i> -C ₃ F ₇) ₃ PF ₃] ⁻	Tris(heptafluoropropyl)trifluorophosphate
[C _n BF ₃] ⁻	Alkyltrifluoroborate
[CH ₂ = CHBF ₃] ⁻	Vinyltrifluoroborate
[C ₁ F ₃ -BF ₃] ⁻	Trifluoromethyltrifluoroborate
[C ₂ F ₅ -BF ₃] ⁻	Pentafluoroethyltrifluoroborate
[C ₃ F ₇ -BF ₃] ⁻	Heptafluoropropyltrifluoroborate
[C ₄ F ₉ -BF ₃] ⁻	Nonafluorobutyltrifluoroborate
[CF ₂ = CFBF ₃] ⁻	Trifluorovinyltrifluoroborate
[C(CN) ₃] ⁻	Tricyanomethanide

References

1. Visser AE, Swatloski RP, Reichert WM et al (2001) Task-specific ionic liquids for the extraction of metal ions from aqueous solutions. *Chem Commun* 1:135–136
2. Pitzer KS (1980) Electrolytes. From dilute solutions to fused salts. *J Am Chem Soc* 102:2902–2906
3. Baker SN, Baker GA, Kane MA et al (2001) The cybotactic region surrounding fluorescent probes dissolved in 1-butyl-3-methylimidazolium hexafluorophosphate: effects of temperature and added carbon dioxide. *J Phys Chem B* 105:9663–9668
4. Bonhôte P, Dias AP, Papageorgiou K et al (1996) Hydrophobic, highly conductive ambient-temperature molten salts. *Inorg Chem* 35:1168–1178
5. Geetha S, Trivedi DC (2003) Properties and applications of chloroaluminate as room temperature ionic liquid. *Bull Electrochem* 19:37–48
6. Dupont J, Spencer J (2004) On the noninnocent nature of 1, 3-dialkylimidazolium ionic liquids. *Angew Chem Int Ed* 43:5296–5297
7. Chauvin Y, Musmann L, Olivier H (1996) A novel class of versatile solvents for two-phase catalysis: hydrogenation, isomerization, and hydroformylation of alkenes catalyzed by rhodium complexes in liquid 1,3-dialkylimidazolium salts. *Angew Chem Int Ed* 34:2698–2700

8. Suarez PAZ, Dullius JEL, Einloft S et al (1996) The use of new ionic liquids in two-phase catalytic hydrogenation reaction by rhodium complexes. *Polyhedron* 15:1217–1219
9. Singh B, Sekhon SS (2005) Polymer electrolytes based on room temperature ionic liquid: 2,3-dimethyl-1-octylimidazolium triflate. *J Phys Chem B* 109:16539–16543
10. Suarez PAZ, Einloft S, Dullius JEL et al (1998) Synthesis and physical-chemical properties of ionic liquids based on 1-n-butyl-3-methylimidazolium cation. *J Chim Phys Chim Biol* 95:1626–1639
11. Dzyuba SV, Bartsch RA (2002) Influence of structural variations in 1-alkyl (aralkyl)-3-methylimidazolium hexafluorophosphates and bis(trifluoromethyl sulfonyl) imides on physical properties of the ionic liquids. *Chemphyschem* 3:161–166
12. Arce A, Rodriguez O, Soto (2004) Experimental determination of liquid-liquid equilibrium using ionic liquids: *tert*-amyl ethyl ether + ethanol + 1-octyl-3-methylimidazolium chloride system at 298.15 K. *J Chem Eng Data* 49:514–517
13. Sun J, Forsyth M, MacFarlane DR (1998) Room-temperature molten salts based on the quaternary ammonium ion. *J Phys Chem B* 102:8858–8864
14. Abbott AP, Capper G, Davies DL et al (2004) Ionic liquids based upon metal halide/substituted quaternary ammonium salt mixtures. *Inorg Chem* 43:3447–3452
15. Gordon JE, SubbaRao GN (1978) Fused organic salts. 8. Properties of molten straight-chain isomers of tetra-n-pentylammonium salts. *J Am Chem Soc* 100:7445–7454
16. Tokuda H, Hayamizu K, Ishii K et al (2004) Physicochemical properties and structures of room temperature ionic liquids. 1. Variation of anionic species. *J Phys Chem B* 108:16593–16600
17. Huddleston JG, Visser AE, Reichert WM et al (2001) Characterization and comparison of hydrophilic and hydrophobic room temperature ionic liquids incorporating the imidazolium cation. *Green Chem* 3:156–164
18. Fredlake CP, Crosthwaite JM, Hert DG et al (2004) Thermophysical properties of imidazolium-based ionic liquids. *J Chem Eng Data* 49:954–964
19. Dyson PJ, Laurency G, Ohlin CA et al (2003) Determination of hydrogen concentration in ionic liquids and the effect (or lack of) on rates of hydrogenation. *Chem Commun* 19:2418–2419
20. Gupta OD, Armstrong PD, Shreeve JM (2003) Quaternary trialkyl(polyfluoroalkyl)ammonium salts including liquid iodides. *Tetrahedron Lett* 44:9367–9370
21. MacFarlane DR, Meakin P, Sun J et al (1999) Pyrrolidinium imides: a new family of molten salts and conductive plastic crystal phases. *J Phys Chem B* 103:4164–4170
22. Visser AE, Holbrey JD, Rogers RD (2001) Hydrophobic ionic liquids incorporating N-alkylisoquinolinium cations and their utilization in liquid-liquid separations. *Chem Commun* 23:2484–2485
23. Solvent Innovations Technical Product List (2005) <http://www.solventinnovation.com/index-overview.htm>. Consulted March 2005
24. Dzyuba SV, Bartsch RA (2002) Expanding the polarity range of ionic liquids. *Tetrahedron Lett* 43:4657–4659
25. Aggarwal A, Lancaster NL, Sethi AR et al (2002) The role of hydrogen bonding in controlling the selectivity of Diels–Alder reactions in room-temperature ionic liquids. *Green Chem* 4:517–520
26. Ross J, Xiao J (2003) The effect of hydrogen bonding on allylic alkylation and isomerization reactions in ionic liquids. *Chem Eur J* 9:4900–4906
27. Chiappe C, Pieraccini DJ (2004) Kinetic study of the addition of trihalides to unsaturated compounds in ionic liquids. Evidence of a remarkable solvent effect in the reaction of ICl_2^- . *Org Chem* 69:6059–6064
28. Abdul-Sada AK, Greenway AM, Hitchcock PB et al (1986) Upon the structure of room temperature halogenoaluminate ionic liquids. *J Chem Soc Chem Commun* 1753–1754
29. Dieter KM, Dymek CJ, Heimer NE et al (1988) Ionic structure and interactions in 1-methyl-3-ethylimidazolium chloride- AlCl_3 molten salts. *J Am Chem Soc* 110:2722–2726

30. Avent AG, Chaloner PA, Day MP et al (1994) Evidence for hydrogen bonding in solutions of 1-ethyl-3-methylimidazolium halides, and its implications for room-temperature halogenoaluminate(III) ionic liquids. *J Chem Soc Dalton Trans* 3405–3413
31. Fuller J, Carlin RT, De Long HC et al (1994) Structure of 1-ethyl-3-methylimidazolium hexafluorophosphate: model for room temperature molten salts. *J Chem Soc Chem Commun* 299–300
32. Tait S, Osteryoung RA (1984) Infrared study of ambient-temperature chloroaluminates as a function of melt acidity. *Inorg Chem* 23:4352–4360
33. Kolle P, Dronsowski R (2004) Hydrogen bonding in the crystal structures of the ionic liquid compounds butyldimethylimidazolium hydrogen sulfate, chloride, and chloroferrate(II, III). *Inorg Chem* 43:2803–2809
34. Wilkes JS, Zaworotko MJ (1992) Air and water stable 1-ethyl-3-methylimidazolium based ionic liquids. *J Chem Soc Chem Commun* 965–967
35. Hayamizu K, Aihara Y, Nakagawa H (2004) Price, ionic conduction and ion diffusion in binary room-temperature ionic liquids composed of [emim][BF₄] and LiBF₄. *J Phys Chem B* 108:19527–19532
36. Crowhurst L, Mawdsley PR, Perez-Arlandis JM et al (2003) Solvent–solute interactions in ionic liquids. *Phys Chem Chem Phys* 5:2790–2794
37. Moret ME, Chaplin AB, Lawrence AK et al (2005) Synthesis and characterization of organometallic ionic liquids and a heterometallic carbene complex containing the chromium tricarbonyl fragment. *Organometallics* 24:4039–4048
38. Elaiwi A, Hitchcock PB, Seddon KR et al (1995) Hydrogen bonding in imidazolium salts and its implications for ambient-temperature halogenoaluminate(III) ionic liquids. *J Chem Soc Dalton Trans* 3467–3472
39. Hitchcock PB, Seddon KR, Welton T (1993) Hydrogen-bond acceptor abilities of tetrachlorometalate(II) complexes in ionic liquids. *J Chem Soc Dalton Trans* 2639–2643
40. Abdul-Sada AK, Al-Juaid S, Greenway AM et al (1990) Upon the hydrogen-bonding ability of the H4 and H5 protons of the imidazolium cation. *Struct Chem* 1:391–394
41. Amyes TN, Diver ST, Richard JP et al (2004) Formation and stability of N-heterocyclic carbenes in water: the carbon acid pK_a of imidazolium cations in aqueous solution. *J Am Chem Soc* 126:4366–4374
42. Wasserscheid P, Hal R, Bösmann A (2002) 1-n-Butyl-3-methylimidazolium ([bmim]) octylsulfate—an even ‘greener’ ionic liquid. *Green Chem* 4:400–404
43. Cole AC, Jensen JL, Ntai I et al (2002) Novel Brønsted acidic ionic liquids and their use as dual solvent-catalysts. *J Am Chem Soc* 124:5962–5963
44. Bondi A (1968) *Physical properties of molecular crystals, liquids and glasses*. Wiley, New York
45. Dannenfelser RM, Yalkowsky SH (1996) Estimation of entropy of melting from molecular structure: a non-group contribution method. *Ind Eng Chem Res* 35:1483–1486
46. Zhao LW, Yalkowsky SH et al (1999) A combined group contribution and molecular geometry approach for predicting melting points of aliphatic compounds. *Ind Eng Chem Res* 38:3581–3584
47. Branco LC, Crespo JG, Afonso CAM (2002) Studies on the selective transport of organic compounds by using ionic liquids as novel supported liquid membranes. *Chem Eur J* 8:3865–3871
48. Przybysz K, Drzewinska E, Stanisławska A et al (2005) Ionic liquids and paper. *Ind Eng Chem Res* 44:4599–4604
49. Branco LC, Crespo JG, Afonso CAM (2002) Highly selective transport of organic compounds by using supported liquid membranes based on ionic liquids. *Angew Chem Int Ed* 41:2771–2773
50. Dupont J, Suarez PAZ, De Souza RF et al (2000) C-H- π interactions in 1-n-butyl-3-methylimidazolium tetraphenylborate molten salt: solid and solution structures. *Chem Eur J* 6:2377–2381

51. Muldoon MJ, Gordon CM, Dunkin (2001) IR Investigations of solvent–solute interactions in room temperature ionic liquids using solvatochromic dyes. *J Chem Soc Perkin Trans* 2:433–435
52. Gozzo FC, Santos LS, Augusti R et al (2004) Gaseous supramolecules of imidazolium ionic liquids: “magic” numbers and intrinsic strengths of hydrogen bonds. *Chem Eur J* 10:6187–6193
53. Van den Broeke J, Winter F, Deelman BJ et al (2002) A highly fluorous room-temperature ionic liquid exhibiting fluorous biphasic behavior and its use in catalyst recycling. *Org Lett* 4:3851–3854
54. Berthod A, Ruiz-Angel MJ, Huguet S (2005) Nonmolecular solvents in separation methods: dual nature of room temperature ionic liquids. *Anal Chem* 77:4071–4080
55. Morrow TI, Maginn EJ (2002) Molecular dynamics study of the ionic liquid 1-n-butyl-3-methylimidazolium hexafluorophosphate. *J Phys Chem B* 106:12807–12813
56. Hardacre C, McMath SEJ, Nieuwenhuyzen M et al (2003) Liquid structure of 1, 3-dimethylimidazolium salts. *J Phys Condens Matter* 15:S159–S166
57. Lee KM, Lee CK, Lin IJB (1997) First example of interdigitated U-shape benzimidazolium ionic liquid crystals. *Chem Commun* 899–900
58. Mayr H, Ofial AR, Wurthwein EU et al (1997) NMR spectroscopic evidence for the structure of iminium ion pairs. *J Am Chem Soc* 119:12727–12733
59. Anderson JL, Ding J, Welton T et al (2002) Characterizing ionic liquids on the basis of multiple solvation interactions. *J Am Chem Soc* 124:14247–14254
60. Ronig B, Pantenburg I, Wesemann L (2002) Melttable stannaborate salts. *Eur J Inorg Chem* 2:319–322
61. Golding JJ, MacFarlane DR, Spiccia L et al (1998) Weak intermolecular interactions in sulfonamide salts: structure of 1-ethyl-2-methyl-3-benzyl imidazolium bis[(trifluoromethyl)sulfonyl]amide. *Chem Commun* 1593–1594
62. Koel M (2000) Physical and chemical properties of ionic liquids based on the dialkylimidazolium cation. *Proc Estonian Acad Sci Chem* 49:145–155
63. Kato T (2002) Self-assembly of phase-segregated liquid crystal structures. *Science* 295:2414–2418
64. Kishimoto K, Suzawa T, Yokota T et al (2005) Nano-segregated polymeric film exhibiting high ionic conductivities. *J Am Chem Soc* 127:15618–15623 and references 1–19 cited therein
65. Abdallah DJ, Robertson A, Hsu H-F et al (2000) Smectic liquid-crystalline phases of quaternary group VA (especially phosphonium) salts with three equivalent long n-alkyl chains. How do layered assemblies form in liquid-crystalline and crystalline phases? *J Am Chem Soc* 122:3053–3062
66. Zhou GP, Zhang Y, Huang XR et al (2008) Catalytic activities of fungal oxidases in hydrophobic ionic liquid 1-butyl-3-methylimidazolium hexafluorophosphate-based microemulsion. *J Colloids Surf B-Biointerfaces* 66:146–149
67. Pott T, Méléard P (2009) New insight into the nanostructure of ionic liquids: a small angle X-ray scattering (SAXS) study on liquid tri-alkyl-methyl-ammonium bis(trifluoromethanesulfonyl)amides and their mixtures. *Phys Chem Chem Phys* 11:5469–5475
68. Yollner K, Popovitz-Biro R, Lahau M et al (1997) Impact of molecular order in Langmuir–Blodgett films on catalysis. *Science* 278:2100–2102
69. Jervis H, Raimondi ME, Raja R et al (1999) Templating mesoporous silicates on surfactant ruthenium complexes: a direct approach to heterogeneous catalysts. *J Chem Soc Chem Commun* 2031–2032
70. Antonietti M, Kuang D, Smarsly B et al (2004) Ionic liquids for the convenient synthesis of functional nanoparticles and other inorganic nanostructures. *Angew Chem Int Ed* 43:4988–4992
71. Ding K, Miao Z, Liu Z et al (2007) Facile synthesis of high quality TiO₂ nanocrystals in ionic liquid via a microwave-assisted process. *J Am Chem Soc* 129:6362–6363

72. Xie Y, Ding K, Liu Z et al (2009) In situ controllable loading of ultrafine noble metal particles on titania. *J Am Chem Soc* 131:6648–6649
73. Hu Y-F, Liu Z-C, Xu C-M et al (2011) The molecular characteristics dominating the solubility of gases in ionic liquids. *Chem Soc Rev* 40:3802–3823
74. Rebelo LPN, Canongia Lopes JN, Esperança JMSS et al (2007) Accounting for the unique, doubly dual nature of ionic liquids from a molecular thermodynamic and modeling standpoint. *Acc Chem Res* 40:1114–1121
75. Shigeto S, Hamaguchi H (2006) Evidence for mesoscopic local structures in ionic liquids: CARS signal spatial distribution of $C_n\text{mim}[\text{PF}_6]$ ($n = 4, 6, 8$). *Chem Phys Lett* 427:329–332
76. Triolo A, Russina O, Fazio B et al (2008) Morphology of 1-alkyl-3-methylimidazolium hexafluorophosphate room temperature ionic liquids. *Chem Phys Lett* 457:362–365
77. Russina O, Triolo A, Gontrani L et al (2009) Morphology and intermolecular dynamics of 1-alkyl-3-methylimidazolium bis{(trifluoromethane)sulfonyl}amide ionic liquids: structural and dynamic evidence of nanoscale segregation. *J Phys Condens Matter* 21:424121-1–424121-9
78. Russina O, Beiner M, Pappas C et al (2009) Temperature dependence of the primary relaxation in 1-hexyl-3-methylimidazolium bis{(trifluoromethyl)sulfonyl}imide. *J Phys Chem B* 113:8469–8474
79. Wang Y, Voth GA (2005) Unique spatial heterogeneity in ionic liquids. *J Am Chem Soc* 127:12192–12193
80. Canongia Lopes JNA, Gomes MFC, Pádua AAH (2006) Nonpolar, polar, and associating solutes in ionic liquids. *J Phys Chem B* 110:16816–16818
81. Seduraman A, Klähn M, Wu P (2009) Characterization of nano-domains in ionic liquids with molecular simulations. *Calphad* 33:605–613
82. Wang Y, Voth GA (2006) Tail aggregation and domain diffusion in ionic liquids. *J Phys Chem B* 110:18601–18608
83. Raju SG, Balasubramanian S (2009) Emergence of nanoscale order in room temperature ionic liquids: simulation of symmetric 1,3-didecylimidazolium hexafluorophosphate. *J Mater Chem* 19:4343–4347
84. Sarangi SS, Bhargava BL, Balasubramanian S (2009) Nanoclusters of room temperature ionic liquids: a molecular dynamics simulation study. *Phys Chem Chem Phys* 11:8745–8751
85. Iwata K, Okajima H, Saha S et al (2007) Local structure formation in alkyl-imidazolium-based ionic liquids as revealed by linear and nonlinear Raman spectroscopy. *Acc Chem Res* 40:1174–1181
86. Xiao D, Hines LG Jr, Li S et al (2009) Effect of cation symmetry and alkyl chain length on the structure and intermolecular dynamics of 1, 3-dialkylimidazolium bis{(trifluoromethane)sulfonyl}amide ionic liquids. *J Phys Chem B* 113:6426–6433
87. Margulis C (2004) Computational study of imidazolium-based ionic solvents with alkyl substituents of different lengths. *J Mol Phys* 102:829–838
88. Shimizu K, Tariq M, Rebelo LPN et al (2010) Binary mixtures of ionic liquids with a common ion revisited: a molecular dynamics simulation study. *J Mol Liq* 153:52–56
89. Wang YT, Jiang W, Yan TY et al (2007) Understanding ionic liquids through atomistic and coarse-grained molecular dynamics simulations. *Acc Chem Res* 40:1193–1199
90. Pádua AAH, Costa Gomes MF, Canongia Lopes JNA (2007) Molecular solutes in ionic liquids: a structural perspective. *Acc Chem Res* 40:1087–1096
91. Hu Z, Margulis CJ (2007) Room-temperature ionic liquids: slow dynamics, viscosity, and the red edge effect. *Acc Chem Res* 40:1097–1105
92. Pópolo MGD, Kohanoff J, Lynden-bell RM et al (2007) Clusters, liquids, and crystals of dialkylimidazolium salts. A combined perspective from ab initio and classical computer simulations. *Acc Chem Res* 40:1156–1164
93. Urahata SM, Ribeiro MCC (2004) Structure of ionic liquids of 1-alkyl-3-methylimidazolium cations: a systematic computer simulation study. *J Chem Phys* 120:1855–1863

94. Canongia Lopes JNA, Pádua AAH (2006) Nanostructural organization in ionic liquids. *J Phys Chem B* 110:3330–3335
95. Wakasa M, Yago T, Hamasaki A (2009) Nanoscale heterogeneous structure of ionic liquid as revealed by magnetic field effects. *J Phys Chem B* 113:10559–10561
96. Mandal PK, Sarkar M, Samanta A (2004) Excitation-wavelength-dependent fluorescence behavior of some dipolar molecules in room-temperature ionic liquids. *J Phys Chem A* 108:9048–9053
97. Santos LMNBF, Lopes JNC, Coutinho JAP et al (2007) Ionic liquids: first direct determination of their cohesive energy. *J Am Chem Soc* 129:284–285
98. Paul A, Mandal PK, Samanta A (2005) On the optical properties of the imidazolium ionic liquids. *J Phys Chem B* 109:9148–9153
99. Tokuda H, Hayamizu K, Ishii K et al (2005) Physicochemical properties and structures of room temperature ionic liquids. 2. Variation of alkyl chain length in imidazolium cation. *J Phys Chem B* 109:6103–6110
100. Hamaguchi H-O, Ozawa R (2005) Structure of ionic liquids and ionic liquid compounds are ionic liquids genuine liquids in the conventional sense? *Adv Chem Phys* 131:85–104
101. Berg RW (2007) Raman spectroscopy and ab-initio model calculations on ionic liquids. *Monatshefte für Chemie* 138:1045–1075
102. Hu ZH, Margulis C (2006) Heterogeneity in a room-temperature ionic liquid: persistent local environments and the red-edge effect. *J Proc Natl Acad Sci* 103:831–836
103. Bhargava BL, Devane R, Klein ML et al (2007) Nanoscale organization in room temperature ionic liquids: a coarse grained molecular dynamics simulation study. *Soft Matter* 3:1395–1400
104. Triolo A, Russina O, Bleif H-J et al (2007) Nanoscale segregation in room temperature ionic liquids. *J Phys Chem B* 111:4641–4644
105. Xiao D, Rajian JR, Cady A et al (2007) Nanostructural organization and anion effects on the temperature dependence of the optical Kerr effect spectra of ionic liquids. *J Phys Chem B* 111:4669–4677
106. De Andrade J, Böes ES, Stassen H (2002) Computational study of room temperature molten salts composed by 1-alkyl-3-methylimidazolium cations–force-field proposal and validation. *J Phys Chem B* 106:13344–13351
107. Gordon CM, Holbrey JD, Kennedy A et al (1998) Ionic liquid crystals: hexafluorophosphate salts. *J Mater Chem* 8:2627–2636
108. Bowlas CJ, Bruce DW, Seddon KR (1996) Liquid-crystalline ionic liquids. *J Chem Soc Chem Commun* 14:1625–1626
109. Holbrey JD, Seddon KR (1999) The phase behaviour of 1-alkyl-3-methylimidazolium tetrafluoroborates; ionic liquids and ionic liquid crystals. *J Chem Soc Dalton Trans* 2133–2139
110. Hardacre C, Holbrey JD, McCormac PB et al (2001) Crystal and liquid crystalline polymorphism in 1-alkyl-3-methylimidazolium tetrachloropalladate(II) salts. *J Mater Chem* 11:346–350
111. Bradley AE, Hardacre C, Holbrey JD et al (2002) Small-angle X-ray scattering studies of liquid crystalline 1-alkyl-3-methylimidazolium salts. *Chem Mater* 14:629–635
112. Welton T (1999) Room-temperature ionic liquids. Solvents for synthesis and catalysis. *Chem Rev* 99:2071–2083
113. Sheldon R (2001) Catalytic reactions in ionic liquids. *Chem Commun* 23:2399–2407
114. Zhao DB, Zhao FF, Scopelliti R et al (2004) Synthesis and characterization of ionic liquids incorporating the nitrile functionality. *Inorg Chem* 43:2197–2205
115. Larsen AS, Holbrey JD, Tham FS et al (2000) Designing ionic liquids: imidazolium melts with inert carborane anions. *J Am Chem Soc* 122:7264–7272
116. Law G, Watson PR (2001) Surface tension measurements of n-alkylimidazolium ionic liquids. *Langmuir* 17:6138–6141

117. Carter EB, Culver SL, Fox PA et al (2004) Sweet success: ionic liquids derived from non-nutritive sweeteners. *Chem Commun* 630–631
118. Ohno H, Yoshizawa M (2002) Ion conductive characteristics of ionic liquids prepared by neutralization of alkylimidazoles. *Solid State Ion* 154:303–309
119. McEwen AB, Ngo HL, LeCompte K et al (1999) Electrochemical properties of imidazolium salt electrolytes for electrochemical capacitor applications. *J Electrochem Soc* 146:1687–1695
120. Ngo HL, LeCompte K, Hargens L et al (2000) Thermal properties of imidazolium ionic liquids. *Thermochim Acta* 357:97–102
121. Zhou ZB, Matsumoto H, Tatsumi K (2005) Structure and properties of new ionic liquids based on alkyl- and alkenyltrifluoroborates. *Chemphyschem* 6:1324–1332
122. Yoshida Y, Muroi K, Otsuka A et al (2004) 1-Ethyl-3-methylimidazolium based ionic liquids containing cyano groups: synthesis, characterization, and crystal structure. *Inorg Chem* 43:1458–1462
123. Hagiwara R, Hirashige T, Tsuda T et al (1999) Acidic 1-ethyl-3-methylimidazolium fluoride: a new room temperature ionic liquid. *J Fluorine Chem* 99:1–3
124. Fuller J, Carlin RT, Osteryoung RA et al (1997) The room temperature ionic liquid 1-ethyl-3-methylimidazolium tetrafluoroborate: electrochemical couples and physical properties. *J Electrochem Soc* 144:3881–3885
125. Matsumoto K, Hagiwara R, Yoshida R et al (2004) Syntheses, structures and properties of 1-ethyl-3-methylimidazolium salts of fluoro-complex anions. *Dalton Trans* 1:144–149
126. Nishida T, Tashiro Y, Yamamoto M (2003) Physical and electrochemical properties of 1-alkyl-3-methylimidazolium tetrafluoroborate for electrolyte. *J Fluorine Chem* 120:135–141
127. Noda A, Hayamizu K, Watanabe M (2001) Pulsed-gradient spin-echo 1H and 19F NMR ionic diffusion coefficient, viscosity, and ionic conductivity of non-chloroaluminate room-temperature ionic liquids. *J Phys Chem B* 105:4603–4016
128. Matsumoto H, Yanagida M, Tanimoto K et al (2000) Highly conductive room temperature molten salts based on small trimethylalkylammonium cations and bis(trifluoromethylsulfonyl)imide. *Chem Lett* 29:922–923
129. Zhang J, Wu W, Jiang T et al (2003) Conductivities and viscosities of the ionic liquid [bmim][PF₆] + water + ethanol and [bmim][PF₆] + water + acetone ternary mixtures. *J Chem Eng Data* 48:1315–1317
130. Okoturo OO, VanderNoot TJ (2004) Temperature dependence of viscosity for room temperature ionic liquids. *J Electroanal Chem* 568:167–181
131. Noda A, Watanabe M (2000) Highly conductive polymer electrolytes prepared by in situ polymerization of vinyl monomers in room temperature molten salts. *Electrochim Acta* 45:1265–1270
132. Domanska U, Marciniak A (2005) Liquid phase behaviour of 1-hexyloxymethyl-3-methylimidazolium-based ionic liquids with hydrocarbons: the influence of anion. *J Chem Thermodyn* 37:577–585
133. Suarez PAZ, Selbach VM, Dullius JEL et al (1997) Enlarged electrochemical window in dialkyl-imidazolium cation based room-temperature air and water-stable molten salts. *Electrochim Acta* 42:2533–2535
134. Wilkes JS, Levisky JA, Wilson RA et al (1982) Dialkylimidazolium chloroaluminate melts: a new class of room-temperature ionic liquids for electrochemistry spectroscopy, and synthesis. *Inorg Chem* 21:1263–1264
135. Carmichael AJ, Hardacre C, Holbrey JD et al (1999) In: Truelove PC, De Long HC, Stafford GR et al (eds) Eleventh international symposium on molten salts. The Electrochemical Society, Pennington
136. Fannin AA Jr, Floreani DA, King LA et al (1984) Properties of 1, 3-dialkylimidazolium chloride-aluminum chloride ionic liquids. 2. Phase transitions, densities, electrical conductivities, and viscosities. *J Phys Chem* 88:2614–2621

137. Ye C, Shreeve JM (2004) Syntheses of very dense halogenated liquids. *J Org Chem* 69:6511–6513
138. Crosthwaite JM, Muldoon MJ, Dixon JK et al (2005) Phase transition and decomposition temperatures, heat capacities and viscosities of pyridinium ionic liquids. *J Chem Thermodyn* 37:559–568
139. Singh RP, Winter RW, Gard GL et al (2003) Quaternary salts containing the pentafluoro-sulfanyl (SF₅) group. *Inorg Chem* 42:6142–6146
140. Hasan M, Ivan V, Kozhevnikov M et al (1999) Gold compounds as ionic liquids. synthesis, structures, and thermal properties of N, N-dialkylimidazolium tetrachloroaurate salts. *Inorg Chem* 38:5637–5638
141. Cooper EI, O'Sullivan EJM (2000) In: Gale RJ, Blomgren G (eds) Proceedings of the eighth international symposium on molten salts. The Electrochemical Society, Pennington
142. Ma M, Johnson KE (1994) In: Hussey CL, Newman DS, Mamantov G et al (eds) Proceedings of the ninth international symposium on molten salts. The Electrochemical Society, Pennington
143. Matsumoto K, Hagiwara R (2005) A new room temperature ionic liquid of oxyfluoro-metallate anion: 1-ethyl-3-methylimidazolium oxypentafluorotungstate (EMImWOF₅). *J Fluorine Chem* 126:1095–1100
144. Mu ZG, Zhou F, Zhang SX et al (2005) Effect of the functional groups in ionic liquid molecules on the friction and wear behavior of aluminum alloy in lubricated aluminum-on-steel contact. *Tribol Int* 38:725–731
145. Guillet E, Imbert D, Scopelliti R et al (2004) Tuning the emission color of europium-containing ionic liquid-crystalline phases. *Mater Chem* 16:4063–4073
146. Dzyuba SV, Bartsch RA (2001) New room-temperature ionic liquids with C₂-symmetrical imidazolium cations. *Chem Commun* 1466–1467
147. Sun J, MacFarlane DR, Forsyth M (2003) A new family of ionic liquids based on the 1-alkyl-2-methyl pyrrolinium cation. *Electrochim Acta* 48:1707–1711
148. Carpio RA, King LA, Lindstrom RE et al (1979) Density, electric conductivity, and viscosity of several N-alkylpyridinium halides and their mixtures with aluminum chloride. *J Electrochem Soc* 126:1644–1650
149. Widegren JA, Saurer EM, Marsh KN et al (2005) Electrolytic conductivity of four imidazolium-based room-temperature ionic liquids and the effect of a water impurity. *J Chem Thermodyn* 37:569–575
150. Neve F, Imperor-Clerc M (2004) An I_{a3}d thermotropic cubic phase from N-alkylpyridinium tetrahalocuprates. *Liq Cryst* 31:907–912
151. Taubert A, Steiner P, Manton A (2005) Ionic liquid crystal precursors for inorganic particles: phase diagram and thermal properties of a CuCl nanoplatelet precursor. *J Phys Chem B* 109:15542–15547
152. Taubert A (2004) CuCl nanoplatelets from an ionic liquid-crystal precursor. *Angew Int Ed Chem* 43:5380–5382
153. Egashira M, Okadab S, Yamaki J et al (2005) Effect of small cation addition on the conductivity of quaternary ammonium ionic liquids. *Electrochim Acta* 50:3708–3712
154. Wasserscheid P, Welton T (2003) Ionic liquids in synthesis. Wiley-VCH, Weinheim
155. Fei ZF, Zhao DB, Scopelliti R et al (2004) Organometallic complexes derived from alkyne-functionalized imidazolium salts. *Organometallics* 23:1622–1628
156. Zhao DB, Fei ZF, Geldbach TJ et al (2004) Nitrile-functionalized pyridinium ionic liquids: synthesis, characterization, and their application in carbon-carbon coupling reactions. *J Am Chem Soc* 126:15876–15882
157. Pringle JM, Golding J, Forsyth CM et al (2002) Physical trends and structural features in organic salts of the thiocyanate anion. *J Mater Chem* 15:3475–3480
158. Yoshizawa M, Ogihara M, Ohno H (2001) Design of new ionic liquids by neutralization of imidazole derivatives with imide-type acids. *Electrochem Solid Lett* 4:E25–E27

159. Kim KS, Choi S, DembereNyamba D et al (2004) Ionic liquids based on N-alkyl-N-methylmorpholinium salts as potential electrolytes. *Chem Commun* 828–829
160. Chun S, Dzyuba SV, Bartsch RA (2001) Influence of structural variation in room-temperature ionic liquids on the selectivity and efficiency of competitive alkali metal salt extraction by a crown ether. *Anal Chem* 73:3737–3741
161. Holbrey JD, Turner MB, Reichert WM et al (2003) New ionic liquids containing an appended hydroxyl functionality from the atom-efficient, one-pot reaction of 1-methylimidazole and acid with propylene oxide. *Green Chem* 5:731–736
162. Branco LC, Rosa JN, Moura Ramos JJ et al (2002) Preparation and characterization of new room temperature ionic liquids. *Chem Eur J* 8:3671–3677
163. Fraga-Dubreuil J, Famelart MH, Bazureau JP (2002) Ecofriendly fast synthesis of hydrophilic poly (ethyleneglycol)-ionic liquid matrices for liquid-phase organic synthesis. *Org Process Res Dev* 6:374–378
164. Xu W, Cooper EI, Angell CA (2003) Ionic liquids: ion mobilities, glass temperatures, and fragilities. *J Phys Chem B* 107:6170–6178
165. Ohno H, Nishimura N (2001) Ion conductive characteristics of DNA film containing ionic liquids. *J Electrochem Soc* 148:E168–E170
166. Pringle JM, Golding J, Baranyai K et al (2003) The effect of anion fluorination in ionic liquids—physical properties of a range of bis(methanesulfonyl)amide salts. *New J Chem* 27:1504–1510
167. Del Sesto RE, Corley C, Robertson A et al (2005) Tetraalkylphosphonium-based ionic liquids. *J Organometallic Chem* 690:2536–2542
168. Xue H, Arritt SW, Twamley B et al (2004) Energetic salts from N-aminoazoles. *Inorg Chem* 43:7972–7977
169. Katritzky AR, Singh S, Kirichenko K et al (2005) 1-Butyl-3-methylimidazolium 3,5-dinitro-1,2,4-triazolate: a novel ionic liquid containing a rigid, planar energetic anion. *Chem Commun* 868–870
170. Kim JW, Singh RP, Shreeve JM (2004) Low melting inorganic salts of alkyl-, fluoroalkyl-, alkyl ether-, and fluoroalkyl ether-substituted oxazolidine and morpholine. *Inorg Chem* 43:2960–2966
171. Tao G, He L, Sun N et al (2005) New generation ionic liquids: cations derived from amino acids. *Chem Commun* 3562–3564
172. Pernak J, Feder-Kubis J (2005) Synthesis and properties of chiral ammonium-based ionic liquids. *Chem Eur J* 11:4441–4449
173. Jin CM, Twamley B, Shreeve JM (2005) Low-melting dialkyl- and bis(polyfluoroalkyl)-substituted 1,1'-methylenebis(imidazolium) and 1,1'-methylenebis(1,2,4-triazolium) bis(trifluoromethanesulfonyl)amides: ionic liquids leading to bis(N-heterocyclic carbene) complexes of palladium. *Organometallics* 24:3020–3023
174. Baranyai KJ, Deacon GB, MacFarlane DR et al (2004) Thermal degradation of ionic liquids at elevated temperatures. *Aust J Chem* 57:145–147
175. Ignatev NV, Welz-Biermann U, Kucheryna A et al (2005) New ionic liquids with tris(perfluoroalkyl)trifluorophosphate (FAP) anions. *J Fluorine Chem* 126:1150–1159
176. Zhang SM, Hou YM, Huang WG et al (2005) Preparation and characterization of novel ionic liquid based on benzotriazolium cation. *Electrochim Acta* 50:4097–4103
177. Oxley JD, Prozorov T, Suslick KS (2003) Sonochemistry and sonoluminescence of room-temperature ionic liquids. *J Am Chem Soc* 125:11138–11139
178. Gao Y, Twamley B, Shreeve JM (2004) The first (ferrocenylmethyl) imidazolium and (ferrocenylmethyl)triazolium room temperature ionic liquids. *Inorg Chem* 43:3406–3412
179. Gu Z, Brennecke JF (2002) Volume expansivities and isothermal compressibilities of imidazolium and pyridinium-based ionic liquids. *J Chem Eng Data* 47:339–345
180. Domańska U, Marciniak A (2003) Solubility of 1-alkyl-3-methylimidazolium hexafluorophosphate in hydrocarbons. *J Chem Eng Data* 48:451–456

181. Letcher TM, Reddy P (2004) Ternary liquid–liquid equilibria for mixtures of 1-hexyl-3-methylimidazolium (tetrafluoroborate or hexafluorophosphate) + ethanol + an alkene at $T = 298.2\text{K}$. *Fluid Phase Equilib* 219:107–112
182. Morgan D, Ferguson L, Scovazzo P et al (2005) Diffusivities of gases in room-temperature ionic liquids: data and correlations obtained using a lag-time technique. *Ind Eng Chem Res* 44:4815–4823
183. Rebelo LPN, Najdanovic-Visak V, Gomes de Azevedo R et al (2005) Phase behavior and thermodynamic properties of ionic liquids, ionic liquid mixtures, and ionic liquid solutions. In: Rogers RD, Seddon KR (eds) *Ionic liquids IIIA: fundamentals, progress, challenges, and opportunities—properties and structure*, ACS Symp Ser 901. American Chemical Society, Washington, DC
184. Gomes de Azevedo R, Esperança JMSS, Szydłowski J et al (2005) Thermophysical and thermodynamic properties of ionic liquids over an extended pressure range: [bmim][NTf₂] and [hmim][NTf₂]. *J Chem Thermodyn* 37:888–899
185. Letcher TM, Deenadayalu N, Soko B et al (2003) Ternary liquid-liquid equilibria for mixtures of 1-methyl-3-octylimidazolium chloride + an alkanol + an alkane at 298.2 K and 1 bar. *J Chem Eng Data* 48:904–907
186. Soriano AN, Doma BT Jr, Li MH (2009) Measurements of the density and refractive index for 1-n-butyl-3-methylimidazolium-based ionic liquids. *J Chem Thermodyn* 41:301–307
187. Gomes de Azevedo R, Esperança JMSS, Najdanovic-Visak V et al (2005) Thermophysical and thermodynamic properties of 1-butyl-3-methylimidazolium tetrafluoroborate and 1-butyl-3-methylimidazolium hexafluorophosphate over an extended pressure range. *J Chem Eng Data* 50:997–1008
188. Carda-Broch S, Berthod A, Armstrong DW (2003) Solvent properties of the 1-butyl-3-methylimidazolium hexafluorophosphate ionic liquid. *Anal Bioanal Chem* 375:191–199
189. Wang J, Tian Y, Zhao Y et al (2003) A volumetric and viscosity study for the mixtures of 1-n-butyl-3-methylimidazolium tetrafluoroborate ionic liquid with acetonitrile, dichloromethane, 2-butanone and n, n –dimethylformamide. *Green Chem* 5:618–622
190. Kabo GJ, Blokhin AV, Paulechka YU et al (2004) Thermodynamic properties of 1-butyl-3-methylimidazolium hexafluorophosphate in the condensed state. *J Chem Eng Data* 49:453–461
191. Lee SH, Lee SB (2005) The Hildebrand solubility parameters, cohesive energy densities and internal energies of 1-alkyl-3-methylimidazolium-based room temperature ionic liquids. *Chem Commun* 3469–3471
192. Harris KR, Woolf LA, Kanakubo M (2005) Temperature and pressure dependence of the viscosity of the ionic liquid 1-butyl-3-methylimidazolium hexafluorophosphate. *J Chem Eng Data* 50:1777–1782
193. Zafarani-Moattar MT, Shekaari H (2005) Volumetric and speed of sound of ionic liquid, 1-butyl-3-methylimidazolium hexafluorophosphate with acetonitrile and methanol at $T = (298.15–318.15)\text{K}$. *J Chem Eng Data* 50:1694–1699
194. Fadeev AG, Meagher MM (2001) Opportunities for ionic liquids in recovery of biofuels. *Chem Commun* 295–296
195. Huo Y, Xia S, Ma P (2007) Densities of ionic liquids, 1-butyl-3-methylimidazolium hexafluorophosphate and 1-butyl-3-methylimidazolium tetrafluoroborate, with benzene, acetonitrile, and 1-propanol at $T = (293.15\text{ to }343.15)\text{K}$. *J Chem Eng Data* 52:2077–2082
196. Liu JF, Jiang GB, Yg C et al (2003) Use of ionic liquids for liquid-phase microextraction of polycyclic aromatic hydrocarbons. *Anal Chem* 75:5870–5876
197. Hyun BR, Dzyuba SV, Bartsch RA et al (2002) Intermolecular dynamics of room-temperature ionic liquids: femtosecond optical Kerr effect measurements on 1-alkyl-3-methylimidazolium bis((trifluoromethyl)sulfonyl)imides. *J Phys Chem A* 106:7579–7585
198. Krummen M, Wasserscheid P, Gmehling J (2002) Measurement of activity coefficients at infinite dilution in ionic liquids using the dilutor technique. *J Chem Eng Data* 47:1411–1417

199. Luo H, Dai S, Bonnesen PV (2004) Solvent extraction of Sr^{2+} and Cs^+ based on room-temperature ionic liquids containing monoaza-substituted crown ethers. *Anal Chem* 76:2773–2779
200. Paulechka YU, Blokhin AV, Kabo GJ et al (2007) Thermodynamic properties and polymorphism of 1-alkyl-3-methylimidazolium bis(triflamides). *J Chem Thermodyn* 39:866–877
201. Rebelo LPN, Najdanovic-Visak V, Visak ZP et al (2004) A detailed thermodynamic analysis of $[\text{C}_4\text{mim}][\text{BF}_4]$ + water as a case study to model ionic liquid aqueous solutions. *Green Chem* 6:369–381
202. Triolo A, Russina O, Hardacre C et al (2005) Relaxation processes in room temperature ionic liquids: the case of 1-butyl-3-methyl imidazolium hexafluorophosphate. *J Phys Chem B* 109:22061–22066
203. Pereiro AB, Rodríguez A (2007) Thermodynamic properties of ionic liquids in organic solvents from (293.15 to 303.15) K. *J Chem Eng Data* 52:600–608
204. Troncoso J, Cerdeiriña CA, Sanmamed YA et al (2006) Thermodynamic properties of imidazolium-based ionic liquids: densities, heat capacities, and enthalpies of fusion of $[\text{bmim}][\text{PF}_6]$ and $[\text{bmim}][\text{NTf}_2]$. *J Chem Eng Data* 51:1856–1859
205. Li W, Zhang Z, Han B et al (2007) Effect of water and organic solvents on the ionic dissociation of ionic liquids. *J Phys Chem B* 111:6452–6456
206. Heintz A, Klasen D, Lehmann JK et al (2005) Excess molar volumes and liquid–liquid equilibria of the ionic liquid 1-methyl-3-octyl-imidazolium tetrafluoroborate mixed with butan-1-ol and pentan-1-ol. *J Solut Chem* 34:1135–1144
207. Fu D, Sun X, Pu J et al (2006) Effect of water content on the solubility of CO_2 in the ionic liquid $[\text{bmim}][\text{PF}_6]$. *J Chem Eng Data* 51:371–375
208. Gardas RL, Freire MG, Carvalho PJ et al (2007) High-pressure densities and derived thermodynamic properties of imidazolium-based ionic liquids. *J Chem Eng Data* 52:80–88
209. Pereiro AB, Tojo E, Rodríguez A et al (2006) Properties of ionic liquid HMIMPF₆ with carbonates, ketones and alkyl acetates. *J Chem Thermodyn* 38:651–661
210. Rebelo LPN, Canongia Lopes JN, Esperança JMSS et al (2005) On the critical temperature, normal boiling point, and vapour pressure of ionic liquids. *J Phys Chem B* 109:6040–6044
211. Canongia Lopes JN, Cordeiro TC, Esperança JMSS et al (2005) Deviations from ideality in mixtures of two ionic liquids containing a common ion. *J Phys Chem B* 109:3519–3525
212. Sanmamed YA, González-Salgado D, Troncoso J et al (2007) Viscosity-induced errors in the density determination of room temperature ionic liquids using vibrating tube densitometry. *Fluid Phase Equilib* 252:96–102
213. Zhou ZB, Matsumoto H, Tatsumi K (2004) Low-melting, low-viscous, hydrophobic ionic liquids: 1-alkyl(alkyl ether)-3-methylimidazolium perfluoroalkyltrifluoroborate. *Chem Eur J* 10:6581–6591
214. Tomida D, Kumagai A, Qiao K et al (2006) Viscosity of $[\text{bmim}][\text{PF}_6]$ and $[\text{bmim}][\text{BF}_4]$ at high pressure. *Int J Thermophys* 27:39–47
215. Harris KR, Kanakubo M, Woolf LA (2007) Temperature and pressure dependence of the viscosity of the ionic liquids 1-hexyl-3-methylimidazolium hexafluorophosphate and 1-butyl-3-methylimidazolium bis(trifluoromethylsulfonyl)imide. *J Chem Eng Data* 52:1080–1085
216. Harris KR, Kanakubo M, Woolf LA (2006) Temperature and pressure dependence of the viscosity of the ionic liquids 1-methyl-3-octylimidazolium hexafluorophosphate and 1-methyl-3-octylimidazolium tetrafluoroborate. *J Chem Eng Data* 51:1161–1167
217. Seddon KR, Stark A, Torres MJ (2002) Viscosity and density of 1-alkyl-3-methylimidazolium ionic liquids. In: Abraham M, Moens L (eds) *Clean solvents: alternative media for chemical reactions and processing*. ACS Symp Ser, American Chemical Society, Washington, DC
218. Jacquemin J, Husson P, Padua AAH et al (2006) Density and viscosity of several pure and water-saturated ionic liquids. *Green Chem* 8:172–180
219. Arce A, Rodríguez O, Soto A (2004) *tert*-Amyl ethyl ether separation from its mixtures with ethanol using the 1-butyl-3-methylimidazolium trifluoromethanesulfonate ionic liquid: liquid-liquid equilibrium. *Ind Eng Chem Res* 43:8323–8327

220. Yang JZ, Lu XM, Gui JS et al (2004) A new theory for ionic liquids—the Interstice Model Part 1. The density and surface tension of ionic liquid EMISE. *Green Chem* 6:541–543
221. Yang JZ, Lu XM, Gui JS et al (2005) Volumetric properties of room temperature ionic liquid. 2. The concentrated aqueous solutions of 1-methyl-3-ethylimidazolium ethyl sulfate + water in a temperature range of 278.2 K to 338.2 K. *J Chem Thermodyn* 37:1250–1255
222. Arce A, Rodil E, Soto A (2006) Volumetric and viscosity study for the mixtures of 2-ethoxy-2-methylpropane, ethanol, and 1-ethyl-3-methylimidazolium ethyl sulfate ionic liquid. *J Chem Eng Data* 51:1453–1457
223. Comminges C, Barhdadi R, Laurent M et al (2006) Determination of viscosity, ionic conductivity, and diffusion coefficients in some binary systems: ionic liquids + molecular solvents. *J Chem Eng Data* 51:680–685
224. Gómez E, González B, Calvar N et al (2006) Physical properties of pure 1-ethyl-3-methylimidazolium ethylsulfate and its binary mixtures with ethanol and water at several temperatures. *J Chem Eng Data* 51:2096–2102
225. Scopigno T, Ruocco G, Sette F et al (2003) Is the fragility of a liquid embedded in the properties of its glass? *Science* 302:849–852
226. Abraham MA, Moens L (2002) Clean solvents. Alternative media for chemical reactions and processing. American Chemical Society, Washington, DC
227. Seddon KR, Stark A, Torres M (2000) Influence of chloride, water, and organic solvents on the physical properties of ionic liquids. *J Pure Appl Chem* 72:2275–2287
228. Kitaoka S, Nobuoka K, Ishikawa Y (2005) Ionic liquids for tetraarylporphyrin preparation. *Tetrahedron* 61:7678–7685
229. McFarlane DR, Sun AJ, Golding J et al (2000) High conductivity molten salts based on the imide ion. *Electrochim Acta* 45:1271–1278
230. Sudhir NVKA, Brennecke JF, Samanta A (2001) How polar are room-temperature ionic liquids? *Chem Commun* 413–414
231. Marsh KN, Boxall JA, Lichtenthaler R (2004) Room temperature ionic liquids and their mixtures—a review. *Fluid Phase Equilib* 219:93–98
232. Zhou ZB, Matsumoto H, Tatsumi K (2004) Low-viscous, low-melting, hydrophobic ionic liquids: 1-alkyl-3-methylimidazolium trifluoromethyltrifluoroborate. *Chem Lett* 33:680–681
233. Nanjundiah C, McDevitt F, Koch VR (1997) Differential capacitance measurements in solvent-free ionic liquids at Hg and C interfaces. *J Electrochem Soc* 144:3392–3397
234. Noda A, Watanabe M (1999) Abstracts of annual meeting of the Electrochemical Society of Japan, p 309
235. Ito K, Nishina N, Ohno H (2000) Enhanced ion conduction in imidazolium-type molten salts. *Electrochim Acta* 45:1295–1298
236. Golding J, MacFarlane DR, Forsyth M (1998) Imidazolium room temperature molten salt systems. *Molten Salt Forum* 5–6:589–592
237. Zhou ZB, Takeda M, Ue M (2004) New hydrophobic ionic liquids based on perfluoroalkyltrifluoroborate anions. *J Fluorine Chem* 125:471–476

Microstructure Study of Ionic Liquids by Spectroscopy

Haoran Li

Abstract The relationship between the structures and properties of the ionic liquids (ILs) is the foundation for designing novel ionic liquids and developing ILs-based applications, which is very important. Spectroscopic methods have been developed as an important tool to study the structures and interactions of the solutions. Recently, spectroscopic methods have played a key role in the study of the structures and the interactions of the ILs or the solutions containing them. Herein, the applications and progress of different spectroscopic methods including IR, Raman, NMR, and ESR methods in the study on the structures and properties of pure ionic liquids and ionic liquids/solvent mixtures are reviewed, indicating the importance of the spectroscopic methods.

Keywords Ionic liquids • Spectroscopy • Infrared • Raman • NMR • ESR • UV • Structure • Interaction

Information on structures and interactions between cations and anions of ionic liquids (ILs) can be provided by various spectroscopies, which play a more and more important role in the investigation of the properties related to the microstructure of ILs. All types of spectra have some features in common, and all the spectra are related to the frequency, ν , and wavelength, λ , of electromagnetic radiation. Figure 1 summarizes the frequencies, wavelengths, and wavenumbers of the various regions of the electromagnetic spectrum and anticipates the type of transition, which provides us with important information to explore the microstructure of the ILs from the viewpoint of the molecule and atom. Spectrometers are instruments that detect the frequency composition of electromagnetic radiation scattered, emitted, or absorbed by atoms and molecules. As we know, the special properties of the ILs depend on their microstructures, and the more information we get from the

H. Li (✉)

Department of Chemistry, Zhejiang University, Hangzhou 310027, P. R. China
e-mail: lihr@zju.edu.cn

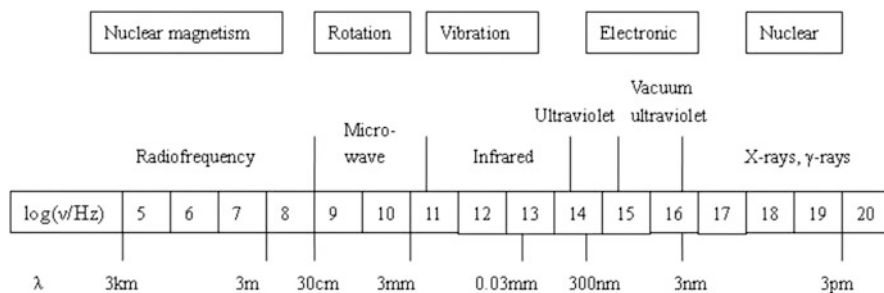


Fig. 1 The electromagnetic spectrum and the classification of the spectral regions [1]

various spectroscopies the more effect on the molecule design and application of the ILs we can have.

1 Microstructure of ILs Investigated by Rotational and Vibrational Spectra

The rotation and vibration of molecules produce IR and Raman spectra, the former depending on the change of dipole moment during the energy level transition and the latter on the change of polarizability.

1.1 Infrared Spectroscopy

The most common range for infrared spectroscopy is the mid-infrared ($400\text{--}4,000\text{ cm}^{-1}$) and near-infrared spectroscopy is in the range $4,000\text{--}11,000\text{ cm}^{-1}$, while that of $10\text{--}400\text{ cm}^{-1}$ is called far infrared spectroscopy. Operating in the infrared almost always involves the use of Fourier transform techniques of spectral detection and analysis. An actual signal consists of radiation spanning a larger number of wavenumbers, and the total intensity at the detector. Using frequency shift of intensity change, or peak area change, the microstructures of the ILs could be explored, and IR spectra have an advantage in the investigation of the structure of hydrogen bonds, ionic pairs, and aggregation of the ions.

1.1.1 The Microstructure of ILs Related to Hydrogen Bonds, Aggregation by Frequency Shift, Intensity Change, and Peak Area Change in IR Spectroscopy

Vibrational spectroscopy is a versatile tool in probing H-bonding of both liquid and solid compounds or their solutions, and information is provided which may assist in an understanding at molecular level of the general interactions that exist in ILs and ILs' solutions.

So far, the hydrogen bond which exists in the imidazolium-based ILs has been widely investigated, with the questions on the H-bond including the following. Is there ion-pair formation in the ILs? Are there specific points on the imidazolium cation where interactions with various anions occur? Where does the H-bond locate? As reported by Katsyuba et al. [2], ion-pair formation is the H-bonding between H-C(2) and $[\text{BF}_4]^-$ in $[\text{EMIM}][\text{BF}_4]$, and the results are in good agreement with computations. It was found that the red shift of the ν (H-C(2)) band, caused by the interaction with the anion, suggests that the $[\text{EMIM}]^+$ and $[\text{BF}_4]^-$ ions are held together mainly by powerful Coulomb attractions that keep them closely associated even in dilute CD_2Cl_2 solutions, and that H-bonding plays only a minor role. The main point regarding the position of H-bond in imidazolium-based ILs is the suggestion that the C2-H play the most important role. The correlations between calculated and experimental spectra were based primarily on peak intensities and secondarily on peak frequencies for both Raman and infrared spectra of $[\text{C}_{2-4}\text{MIM}][\text{PF}_6]$, indicating hydrogen-bonding interactions between the fluorine atoms of the $[\text{PF}_6]^-$ anion and the C2 hydrogen on the imidazolium ring [3]. In particular, the gas phase molecular structures of the $[\text{C}_{2-4}\text{MIM}][\text{BF}_4]$ ion pairs suggest hydrogen-bonding interactions between the fluorine atoms of the $[\text{BF}_4]^-$ anion and the C2 hydrogen on the imidazolium ring [4]. Additional interactions are observed between $[\text{BF}_4]^-$ and H atoms on the adjacent alkyl side chains in all polymorphic structures. In order to explore the C2-H, the replacement of the C-2 hydrogen with methyl was examined by Diete et al.

The presence of water in room temperature ionic liquids (RTILs) may affect many of their solvent properties such as polarity, viscosity, and conductivity. Infrared spectroscopy, arguably, is the most powerful method to probe the molecular state of water present in various solvents. It is known that water molecules absorbed from the air are present mostly in the “free” (not self-associated) state; as seen in Fig. 2, there is no change in the frequency and the water via H-bonding with anions such as symmetric 1: 2 type complexes: anion...H-O-H...anion. Kazarian et al. [5] used ATR and transmission IR spectroscopy to study the molecular state of dissolved water in several ionic liquids based on $[\text{BMIM}]^+$ with several anions. The strength of H-bonding between water molecules and anions was shown to increase in the order $[\text{PF}_6]^- < [\text{SbF}_6]^- < [\text{BF}_4]^- < [(\text{CF}_3\text{SO}_2)_2\text{N}]^- < [\text{ClO}_4]^- < [\text{CF}_3\text{SO}_3]^- < [\text{NO}_3]^- < [\text{CF}_3\text{CO}_2]^-$. However, H-bond interactions of water diluted in 1-alkyl-3-methyl imidazolium ILs with $[\text{PF}_6]^-$ and $[\text{BF}_4]^-$ involves a more noticeable electrostatic character through polarization of water due to the local electrostatic fields induced by surrounding ions rather than H-bond interactions of water in normal molecular solvents [6].

The structure change of water in a solution of ionic salts is also an interesting issue focusing on the overlapping OH peaks in the spectrum, both fundamentally and practically. The vibrational modes of water that result in bands in the OH-stretching region ($3,000\text{--}3,800\text{ cm}^{-1}$) are sensitive to the environment and intermolecular interactions.

The state of water in $[\text{EMIM}]^+[\text{BF}_4]^-$ has been investigated by ATR-IR spectroscopy by Takamuku et al., revealing that individual water molecules hydrogen-

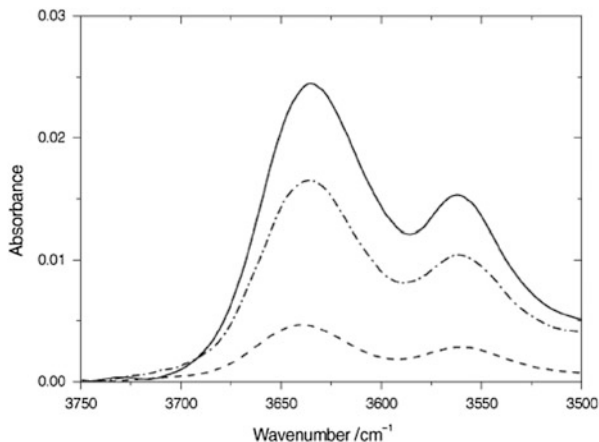


Fig. 2 ATR-IR spectra of [BMIM][BF₄] in the $\nu(\text{O-H})$ region showing the uptake of water from air as a function of time: spectrum of [BMIM][BF₄] after it has been placed on the diamond ATR crystal [5]

bonded to the anions predominate in the solutions at $\chi_w \leq \sim 0.2$, while $\sim 30\%$ of water molecules are hydrogen-bonded among them in the solutions at $\chi_w > \sim 0.3$, suggesting the state of water molecules in [EMIM]⁺[BF₄]⁻ change significantly at 0.30. The interactions between the C2 atom within the imidazolium ring of [EMIM]⁺ and [BF₄]⁻ are strengthened with increasing water content while those at the C4 and C5 atoms weaken [7]. As in [EMIM][NTf₂] and [EMIM][EtSO₄], protonated and deuterated water molecules are presumed to have completely different polarities, but anions are still responsible for the interaction of ILs and water with water molecules mainly H-bonded to the IL anions [8].

During the investigation of the ion pairs of several imidazolium-based ILs, it is reported that the vibrations of the cations depend on both the conformational changes and the association with the anions [9]. In addition, chloride and bromide anions in vacuum also occupy positions above or below the imidazolium ring, but in the condensed state these positions are destabilized, and the position and type of the anion influence the conformation of the side chains bound to the imidazolium N1 atom.

The change of peak area in the IR spectra could also provide information on the structure change in the ILs [10]. Kim et al. studied the CH and OH band positions and intensities for all concentrations of [EMIM][BF₄] and water by examining ATR-IR absorption spectra at several concentrations. Change in the spectral shape in the OH stretch vibration region shows a hydrogen-bonding network of water molecules breaking down rapidly as the IL is added, while those from the terminal methyl group of the butyl chain are blue-shifted by $\sim 10 \text{ cm}^{-1}$ with the addition of water. Trends in the change of the peak positions and the peak intensities suggest qualitative change of the intermolecular structure in the [EMIM][BF₄] + H₂O mixture at 32 ± 2 and 45 ± 2 mol/L of water concentration as shown in Figs. 3 and 4.

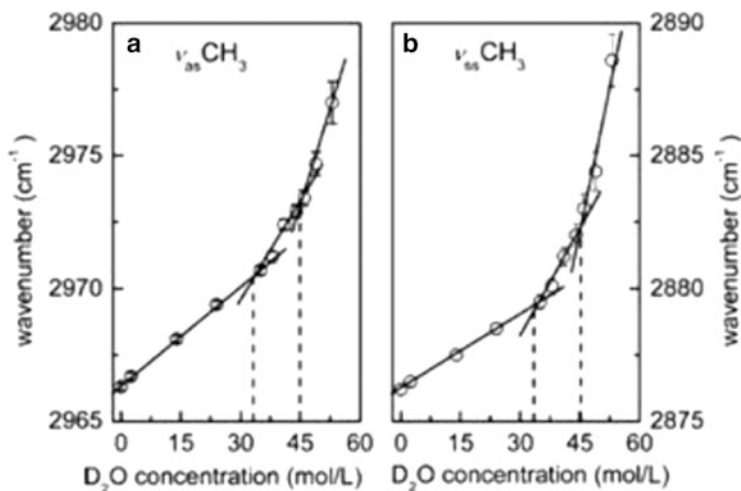


Fig. 3 (a) Peak shift of ν_{ASCH_3} . (b) Peak shift of ν_{SSCH_3} with increasing the D_2O concentration in the $[BMIM][BF_4] + D_2O$ mixture. *Open circles* represent the deconvoluted data. *Solid lines* are the guide lines following the peak shift, and *dashed lines* indicate the concentration where the slope changes discontinuously [10]

1.1.2 The Hydrogen Bond in ILs/Water by High-Pressure IR and Temperature-Dependent IR Spectroscopy

Water molecules seem to be separated from each other at low content, while self-association appears at higher concentration. At high ionic liquid concentrations ionic liquids seem to form clusters as in the pure state and water molecules interact with the clusters without interacting among themselves. Cation–solvent interactions play a non-negligible role in ionic liquid mixtures. Several studies have shown that C–H...O and C–H...X hydrogen bonds play an important role in the structure of ionic liquids, especially those derived from the 1-alkyl-3-methylimidazolium cation. Thus the study of C–H...O and C–H...X hydrogen bonds is significant.

The microscopic features of binary mixtures formed by $[EMIM][TFSA]^-$ or $[EMI][FSA]^-$ and a molecular liquid (acetonitrile or methanol) have been investigated using high-pressure infrared spectroscopy by Umebayashi et al. [11]. Two different forms, i.e., isolated and associated structures of the imidazolium C–H, were proposed on the basis of responses to changes in pressure and concentration in order to gain an insight of isolated and associated structure. The associated configuration is favored with increasing pressure by debiting the isolated form for $[EMIM][FSA]^-/CD_3CN$ mixtures. The increase in the alkyl chain length may not significantly perturb the isolated-associated structural equilibrium in CD_3CN mixtures. In O–H...O hydrogen-bonding, methanol molecules can act as both proton donors and acceptors and aggregate with themselves. In the $[EMIM][TFSA]/CD_3OD$ and $[BMIM][TFSA]/CD_3OD$ mixtures, CD_3OD molecules may

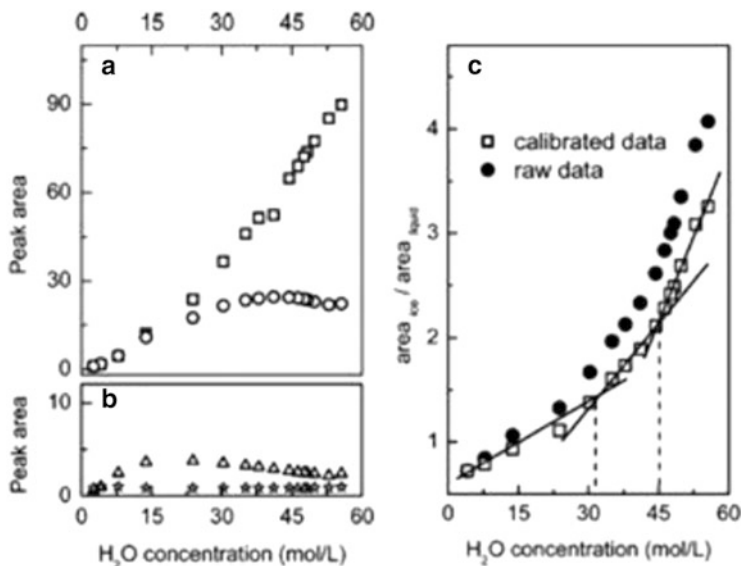


Fig. 4 Peak areas of OH vibrational peaks of water molecule in the [BMIM][BF₄] + H₂O mixtures by Gaussian fitting with increasing water concentration. (a) *Open squares* and *open circles* represent the area of the icelike and liquidlike OH stretch mode peaks, respectively. (b) *Open triangles* and *open stars* represent the area of the symmetric and antisymmetric stretch mode of weakly bonded OH peak. (c) Ratios of the peak areas of the icelike and liquidlike peaks. *Filled circles* represent the raw data, and *open squares* represent the ratios after the correction. *Solid lines* are guides to the eye, and *dashed lines* indicate the concentration where the slope changes discontinuously [10]

prefer to aggregate with themselves by hydrogen-bonding, and TFSA⁻ interacts with the cations to form associated configurations. As an [EMIM][FSA]/CD₃CN mixture was compressed, the increase in the isolated C–H band intensity was observed and some associated species are switched to the isolated form. A clustering of the alkyl groups at high concentration and the formation of a certain water structure around alkyl C–H groups in the water-rich region was found by high-pressure infrared spectroscopy during the study of hydrogen-bonding structures of 1-butyl-3-methylimidazolium halides/D₂O mixtures [12]. Water can be added to change the structural organization of 1-butyl-3-methylimidazolium chloride in the ionic liquid-rich composition region by introducing water-imidazolium C–H interactions. The presence of water significantly perturbs the ionic liquid–ionic liquid associations in the polar region. The hydrogen-bonding patterns in diluted aqueous ionic liquid solution are mainly determined by imidazolium cation–water cluster interactions instead of the relative hydrogen-bonding acceptor strength of Br⁻ and Cl⁻ [13]. Both methyl C–H and imidazolium C–H groups are favorable sites for C–H...O hydrogen-bonding in a dilute dimethylimidazolium methyl sulfate/D₂O mixture, which, due to the hydrogen bond energy, is the Columbic interaction between the positive and negative partial charges on the hydrogen atom

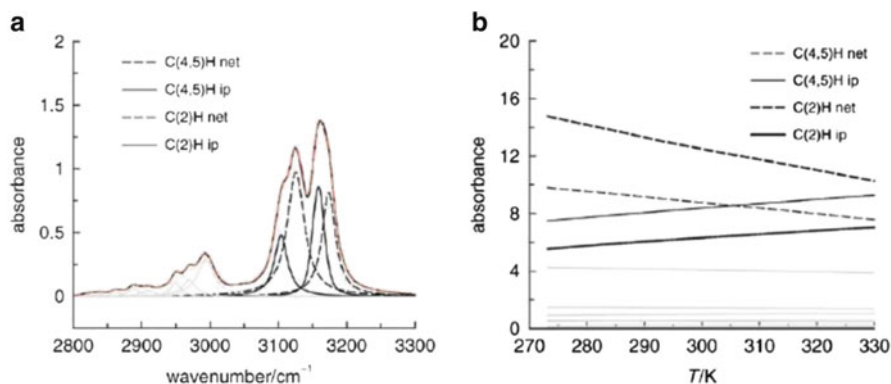


Fig. 5 (a) Deconvoluted infrared spectrum of the CH stretching region of neat $[C_2MIM][NTf_2]$ at 273 K; the network structure as well as ionic pairs conformations were assigned. (b) Structure (*net*, *dashed lines*) decrease with increasing temperature, whereas those attributed to ion pairs (*ip*, *solid lines*) continuously increase [16]

and the acceptor atom. Hydrogen bond interactions like C–H...F were observed between $[PF_6]^-$ and H atoms on the alkyl side chains and imidazolium ring for 1-butyl-3-methylimidazolium hexafluorophosphate. Two types of O–H species, i.e., free O–H and bonded O–H. non-negligible roles of weak hydrogen bonds in the structure of ionic liquids, were reported by using high-pressure infrared measurements to observe the microscopic structures of $[EMIM][(CF_3SO_2)_2N]$, $[EMIM][TFSA]$, $[EMIM][(FSO_2)_2N]$, and $[EMIM][FSA]$ [14]. Umabayashi et al. studied the aggregation behaviors and hydrogen-bond network in $[BMIM][BF_4]$ /water or methanol mixtures by high-pressure IR spectroscopy.

Temperature-dependent IR spectra as a useful tool can be used to explore the H-bond in ILs because the H-bond between molecules depends on the temperature. Yokozeki et al. applied temperature-dependent IR spectra to study the C–H stretching modes of the imidazolium ring in $[BMIM][PF_6]$, $[BMIM][Tf_2N]$, $[EMIM][Tf_2N]$, $[HMIM][Tf_2N]$, and $[BMIM][BF_4]$ [15]. Koddermann et al. reported that ion-pair formation already occurs in the neat IL and increases with temperature. Ion pairs H-bonded via C2–H are strongly favored over those H-bonded via C4,5–H; in Fig. 5 the two lower frequency were assigned to the C2–H with a stronger positive charge leading to the H-bonding via C2–H, and this finding was in agreement with DFT (gas phase) calculations, which show a preference for ion pairs H-bonded via C2–H as a result of the acidic C2–H bond [16].

1.1.3 The Interaction Between ILs and Water by Two-Dimensional IR Spectroscopy

Two-dimensional infrared (2D IR) spectroscopy is a novel analytical technique based on time-resolved detection of IR signals to study molecular interactions. In 2D IR, a spectrum is obtained as a function of two independent wavenumbers. Introduction of the second spectral dimension provides a new opportunity for

analyzing vibrational spectra. Some notable features of the two-dimensional approach are the simplification of complex spectra consisting of many overlapped peaks, enhancement of spectral resolution by spreading peaks over the second dimension, and identification of various inter- and intramolecular interactions through selective correlation of IR peaks.

Two-dimensional correlation analysis infrared spectroscopy was first proposed by Dr. Noda as it can distinguish the overlapped bands, and can provide information when there is an outside perturbation. Lendl et al. applied 2D IR spectroscopy to study the state of water and methanol molecule in three different imidazolium-based ILs. It was found that the methyl alcohol was in favor of forming dimer when the concentration of methyl alcohol was above 0.8 wt%.

In Li's group, two-dimensional vibrational spectroscopy was applied to investigate the dilution process of [EMIM][BF₄] in water. With increasing water content in ionic liquid (IL)/water mixtures, the C–H stretching vibration of the imidazolium cation showed systematic blue-shifts, which reflect the weakening of the cohesion between the cation and anion of ILs. The three-dimensional network structure of pure ILs was gradually broken down into ionic clusters, then the clusters were further dissociated into ionic pairs surrounded by water molecules, and finally the latter became the dominant form in bulk water [17].

1.1.4 The Hydrogen Bond in ILs/Water by Near IR Spectroscopy

Wu et al. used the near-infrared (NIR) technique and two-dimensional (2D) correlation spectra for [AMIM]Cl/H₂O to explore the effect of ethanol on the structural organization of aqueous solution of [BMIM][BF₄] and [AMIM]Cl [18]. It was deduced that ethanol molecules prefer to compete with water by interacting with imidazolium C2–H rather than C4,5–H groups, accompanied by the formation of C2–H...O interactions with ethanol molecules, while ethanol molecules do not interact specially with any imidazolium C–H groups for [BMIM][BF₄]. For both ILs, ethanol molecules were capable of changing the interaction between cations and water and between anions and water by introduction of C–H...O interactions with cations.

1.1.5 The Microstructure of ILs by Far IR Spectroscopy

So far there is no direct evidence for cation–anion interaction in ionic liquids. FTIR and Raman studies on ionic liquids have focused on the mid-infrared range and on the investigations of intermolecular stretching and bending modes. H bonds introduce “defects” into the Coulomb network of ILs and increase the dynamics of the cations and anions, resulting in decreased melting points and reduced viscosities. Far IR spectroscopy could provide the information to explore the interaction between anion and cations, and hydrogen bonds in the low-frequency vibrational spectra of a range between 30 and 300 cm⁻¹. Fumino et al. presented FTIR measurements of imidazolium-based ionic liquids [EMIM][SCN], [C₂mim]

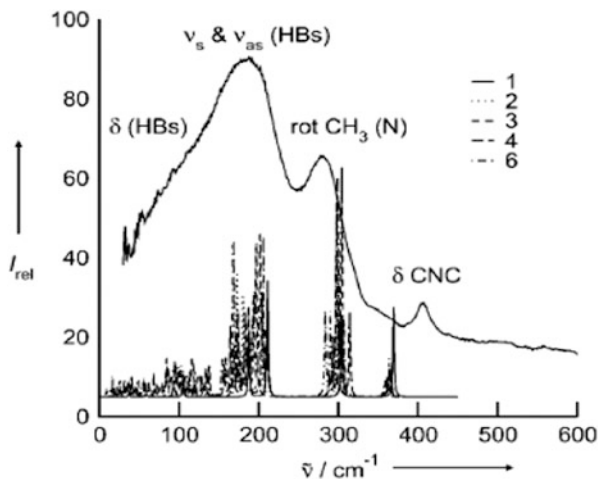


Fig. 6 Measured low-frequency vibrational FTIR spectrum of dimethylammonium nitrate (DMAN) at 353 K compared to the vibrational modes of the corresponding PIL clusters $[(DMA)(NO_3)]_x$ with $x = 1, 2, 3, 4,$ and 6 calculated by DFT at the B3LYP/6-31 + G* level of theory. The major vibrational bands are in agreement with the calculated frequencies, which are corrected for the harmonic approximation

$[N(CN)_2]$, $[C_2mim][EtSO_4]$, and $[C_2mim][NTf_2]$ in the far infrared spectral region to study the cohesion energies between cations and anions in imidazolium-based ionic liquids [19]. It was found that the intermolecular stretching modes were shifted to higher wavenumbers with increasing ionic strength of the used anion and can be correlated to the calculated average binding energies of the ionic liquid. They also measured both the mid- and far-FTIR spectra of imidazolium-based ILs as a function of temperature in order to determine whether the spectra are significantly affected by suppression of the C(2)–H...A–H bond upon methylation. Ludwig et al. [20] presented the first far-IR spectra of the PILs EAN, PAN, and DMAN. Intermolecular bending and stretching modes of the hydrogen bonds + NH...O- are shown in Fig. 6. Only water exhibits a tetrahedral H-bond network. For EAN such a network is impossible, owing to the different structures and donor/acceptor abilities of the ions [21]. Strong C2–H-anion interactions in $[EMIM][NTf_2]$ in the far-FTIR spectra were studied by Koddermann et al. by substituting the C2–H hydrogen in $[EMIM][NTf_2]$ by the methyl group in $[EMMIM][NTf_2]$.

1.2 Raman Spectroscopy

In Raman spectroscopy, molecular energy levels are explored by examining the frequencies present in the radiation scattered by molecules. Raman spectroscopy is often complementary to infrared spectroscopy because, as we shall see, different selection rules are obeyed. And there are many advantages of Raman spectroscopy,

such as that Raman spectroscopy provides vibrational Raman spectra that are often called “molecular fingerprints,” which can show the structure and dynamics of molecules (ions), and the versatility of Raman spectroscopy enables us to measure Raman spectra and hence to study molecules comparatively in different phases or states.

1.2.1 The Conformation of Cations and Anions by Raman Spectroscopy

Over the large range of possible cation and anion variations in ILs, the imidazolium-based ILs are the most studied today both experimentally and computationally. Columbic, van der Waals, and hydrogen-bonding effects can all take place in ILs and determine the ILs structural and physicochemical properties, and can also influence and thus be detected in their vibrational spectra.

Katayanagi et al. [22] reported that the Raman spectrum of liquid [BMIM]I tied in with those of [BMIM]Cl which has two crystal forms, monoclinic crystal and orthorhombic crystal and [BMIM]Br in the molten phase and in crystals. The Raman spectrum shows that the *trans* and *gauche* conformations also coexist in [BMIM]I liquid, and contribution of the *trans* conformation is found to be higher in [BMIM]I liquid than in molten [BMIM]Cl and [BMIM]Br. The specific conformers, the two most stable [BMIM]⁺ conformers, GA, AA, according to the ab initio calculations of [BMIM][BF₄], have been studied by IR and Raman spectroscopy, with ab initio calculation [23] indicating the existence of unique [BMIM]⁺ conformers. The IL is considered to be a mix of cation conformers as well as a mix of ion pairs. From the results, we know Raman spectroscopy can be extremely useful for identification of different [BMIM]⁺ conformers. Berg et al. [24] also used the Raman bands to characterize the conformers of the 1-hexyl-3-methylimidazolium cation. The vibrational analysis of the binary system reveals that neither the changes in hydrogen-bonding to the ring hydrogen atoms nor the change in the Columbic environment has any detectable effect upon the essentially 50:50 distribution of the two conformers. Meanwhile, a conformational equilibrium was reported to be established between the C1 and C2 conformers of [TFSI]⁻ in the liquid [EMI][FTSI], and the C2 conformer is more favorable than the C1 one [25]. Jeon et al. [26] explored the structures of [BMIM]I and [BMIM][BF₄] and their aqueous mixtures were investigated by using ATR IR and Raman spectroscopy with the finding that I⁻ is expected to be closer to the C2 hydrogen of the imidazolium cation and to interact more specifically as compared to BF₄⁻. Raman spectra around 600 cm⁻¹, indicative of the butyl chain conformation, changed differently as the water concentration was increased between [BMIM]I and [BMIM][BF₄], the former being linked to the *trans* conformation while the latter belonged to the *cis* form conformation, as shown in Figs. 7 and 8.

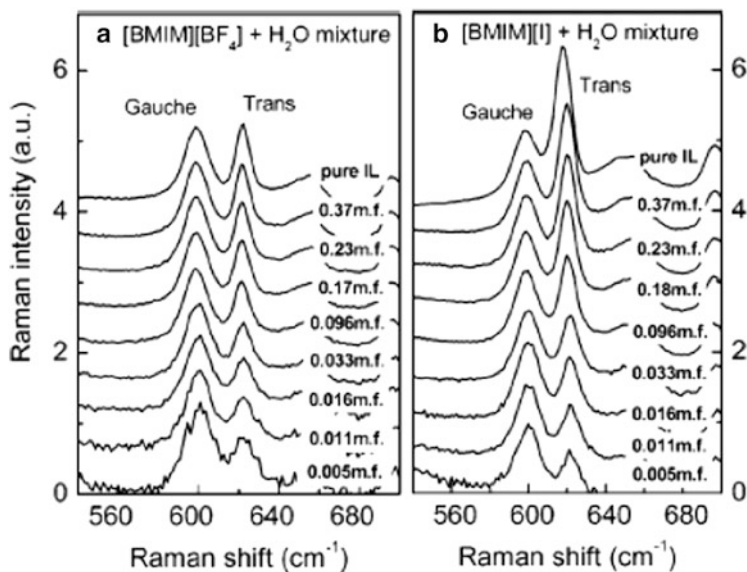


Fig. 7 Normalized Raman spectra between 540 and 700 cm^{-1} with varying water content: (a) [BMIM][BF₄] + water mixture and (b) [BMIM][I] + water mixture [26]

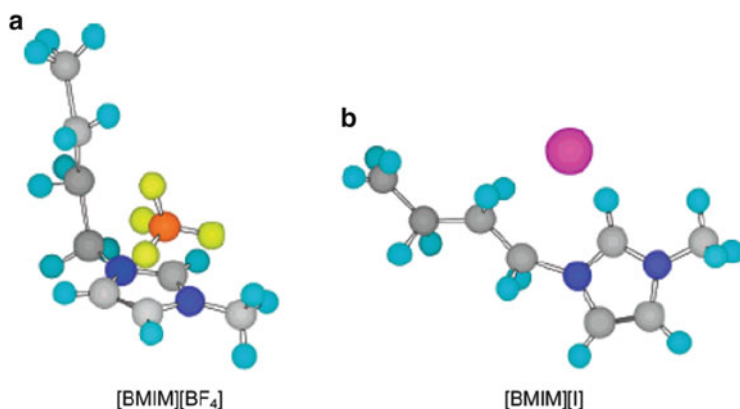


Fig. 8 Proposed anion positions of (a) [BF₄]⁻ around [BMIM]⁺ and (b) I⁻ around [BMIM]⁺

1.2.2 Study of the Interaction Between ILs and Water by Raman Spectroscopy

As we know, regarding the presence of water, the IL's structural organization ability depends on the anion-cation interaction strengths.

Sasa et al. [27] explored the molecular structure and arrangement of 1-butyl nitrile-3-methylimidazolium halide, in the presence and absence of the

intruded water molecule, by single crystal X-ray crystallography and near-infrared Raman spectroscopy. Water molecules are found to change the conformation of the *n*-butylnitrile chain of the cation, and the hydrogen-bonding interaction between the anion and water molecule, leading to loose molecular packing, is most likely to be responsible for the change. Among the three C–H...Cl hydrogen bonds, the strongest one is found between C2–H and the chloride anion. The water molecule changes the position of the chloride anion and takes it away from the imidazolium ring, and that may be one possible reason why hydrogen-bonding involving C4–H, C5–H, and the chloride anion are absent in the system.

FT IR and Raman spectroscopies have been used to investigate the role played by water on the structural organization of 1-butyl-3-methyl-imidazolium tetrafluoroborate and H₂O mixtures by Fazio et al. [28]. It was found that the water clusters favor the organization of IL in the polar network, where they are embedded, and the aggregation of hydrophobic alkyl tails in a micelle like structure. The organization starts to weaken owing to the gradual breakup of the ion-pair interactions when mixtures with the water molar fraction exceeding 0.7.

1.2.3 The Microstructure of the Metal-Containing ILs

Sitze et al. [29] reported that both Raman scattering and ab initio calculations indicated that $[\text{FeCl}_4]^{2-}$ were the predominant iron-containing species in the ionic liquids from a mole ratio of 1 FeCl₂/3 [BMIM]Cl to 1 FeCl₂/1 [BMIM]Cl. Anionic species formed in the mixture of 1-*n*-butyl-3-methylimidazolium chloride ([BMIM]Cl) with different amounts of niobium pentachloride (NbCl₅) or zinc dichloride (ZnCl₂) were investigated by Raman spectroscopy, suggesting that the formation of larger anions causes a shift of the C–H stretching modes to higher wavenumbers as the result of a decrease in the hydrogen bond between Cl[−] and the hydrogen from the cation [30]. The exchange of Cl[−] by larger anions such as $[\text{NbCl}_6]^-$, $[\text{ZnCl}_4]^{2-}$, $[\text{ZnCl}_6]^{2-}$, etc., causes a decrease in the H–Cl hydrogen-bonding, resulting in a shift of the C–H stretching modes to higher values. A preliminary Raman investigation of the ionic liquid *N*-methyl-*N*-propylpyrrolidinium bis(trifluoromethanesulfonyl)imide ([PYR₁₃][TFSI]) and its 2/1 complex with the lithium salt LiN(SO₂CF₃)₂ is reported by Castriota et al. [31]. The interaction between the [TFSI][−] anion and [PYR₁₃]⁺ and Li⁺ cations suggests that the anion has only a very weak interaction with the organic, sterically shielded cations, but strong coordination to the Li⁺ cations.

2 Microstructure of ILs Investigated by Magnetic Resonance Spectra

We can expect that the application of a magnetic field should affect atoms and molecules. One of the most widely used spectroscopic procedures in chemistry makes use of the classical concept of resonance, and the resonance frequency of a magnetic nucleus is affected by its electronic environment. The magnetic resonance experiment is the resonant absorption of radiation by nuclei or unpaired electrons exposed to a magnetic field. The effect of magnetic fields in electrons and nuclei produce the nuclear magnetic resonance (NMR) and electron spin resonance (ESR) spectroscopy, respectively.

2.1 Nuclear Magnetic Resonance Spectroscopy (NMR)

Nuclear magnetic resonance is the study of the properties of molecules containing magnetic nuclei by applying a magnetic field and observing the frequency of the resonant electromagnetic field.

2.1.1 Study of the Microstructure of ILs by Chemical Shift Change in NMR Spectra

It is conventional to express resonance frequencies in terms of an empirical quantity called the chemical shift, which is related to the difference between the resonance frequency of the nucleus in question and that of a reference standard. The most widely used methods for probing H-bonding are IR and NMR spectroscopic techniques, in which the C2–H stretching frequencies and chemical shifts of this H-bonding are examined.

The microscopic structure of the aggregates has not been well defined. Considering the fact that NMR is a very sensitive technique for the study of the aggregation behavior of classical surfactants, the structure of ILs can be studied by NMR.

NMR spectra show all the peaks affected by the interaction between the protons of the imidazolium cation and those of the anion. As reported, the imidazolium ring is surrounded by three tetraphenylborate anions that are connected to the same cation by C–H- π (phenyl rings) interactions [32]. Katsyuba et al. used DFT methods in combination with NMR spectroscopy to investigate possible variants of the molecular structure of the ion pairs of the ionic liquid [EMIM][BF₄] in dichloromethane [33]. They found an equilibrium between ca. 70 % and 80 % of structures with the anion positioned near the C2 atom of the imidazolium ring and ca. 20–30 % of structures with the anion close to the C5 and/or C4 atoms. Both computations and experimental NMR data suggest that the ratio of the two above-mentioned types of structures of the imidazolium-based ILs is influenced by the

concentration/polarity of their dichloromethane solutions. Besides the H-bond, aggregation of ILs can also be investigated by NMR. It was suggested that the self-association of EmimBF₄ and N₄NO₃ plays the leading role, and water prefers to interact with IL rather than self-association in IL-rich regions [34]. Remsing et al. [35] studied the self aggregation of the ILs, [C₄mim]Cl, [C₈mim]Cl, [C₄mim][BF₄], [C₄mim]Cl, in aqueous solution through ¹H NMR and steady-state fluorescence spectroscopy, suggesting aggregation induced conformational changes in different ILs are shown to depend on the aromatic ring, alkyl chain, counterions, and their interactions with water. Critical aggregation concentration of different ILs determined by using various techniques is in fairly good agreement. What's more, the imidazolium rings in the aggregates were exposed to water and the molecular motion of the aggregates is more restricted than that of the monomers of the ILs. Furthermore, a stair-like microscopic aggregation structure is suggested for the [C_nmim]Br/D₂O (n = 6, 8, 10) systems from 2D ¹H-¹H NOESY measurements. The aggregation number of the ILs was found to increase with increasing length of the alkyl chain. The microscopic structure π - π stacking interactions between the imidazolium rings of cations, H-bonding interactions between cations of the ILs and Br⁻, and those between water and Br⁻ were considered [36].

2.1.2 Microstructure of ILs by Relaxation Time Change and Self-Diffusion Coefficient

Huang et al. explored the [EMIM][BF₄] by NMR techniques, and the diffusion coefficients measured at temperatures ranging from 300 to 360 K indicate that phase change occurred in the vicinity of 333 K [37]. It was found that the phase change was ascribed to the transformation of the diffusion particle from "discrete ion-pair" to "individual ion" at temperatures above 335 K, due to the decomposition of the [EMIM]⁺-[BF₄]⁻ ion pair. The analysis of the ¹³C dipole-dipole relaxation rates identifies the formation of the hydrogen bond C2-H...F between the counterions, [EMIM]⁺ and [BF₄]⁻. Judeinstein et al. proposed that PFG NMR yield the self-diffusion coefficients of the proton-conducting ionic liquid components, while, on the other hand, ¹³C, ¹H, and ¹⁵N, ¹H correlation and intermolecular Overhauser experiments gave insight into the nature of protonic species and ion-pairing behavior [38]. The self-diffusion properties of the butyl-methylimidazolium bis(trifluoromethylsulfonyl)imide ([BMIM][TFSI]) + water system were studied by Rollet et al. using pulsed field gradient NMR [39]. Miscibility of water is not complete at the microscale and the [BMIM][TFSI] + water system shows a partial segregation between [BMIM][TFSI] + some water molecules phase and water + some [BMIM][TFSI] ions phase. Menjoge et al. found an increase in the ion diffusivities with increasing water concentration, and decrease in the difference between the diffusion coefficient of the cation and that of the anion as water concentration increases during the investigation of anions, cations, and water in two 1-ethyl-3-methylimidazolium-based ionic liquids by novel pulsed field gradient NMR option [40].

2.1.3 The Microstructure of ILs by 2D NOESY Spectra

The nuclear Overhauser effect (NOE) is a powerful investigative tool, as it originates from dipolar interaction between pairs of nuclei and thus provides information on the molecular sites involved in the interaction.

Mele et al. successfully measured the cation and anion distances in neat liquid [BMIM][BF₄] and [BDMIM][BF₄] by NMR spectroscopy, suggesting that the butyl chain of [BMIM][BF₄] and [BDMIM][BF₄] might act on the polar imidazolium ring, which would prevent the aggregation of ILs. However, there was no interaction between the molecules in [BMIM][Tf₂N] and [BDMIM][Tf₂N] [41]. Mele et al. applied the NOE effect of NMR to [BMIM][BF₄] to study the effect of the quantity of water on the structure of the IL. Along with the quantity of water increasing, the intensity of the C2, 4, and the 5-H of the imidazolium ring was reducing, while that of methyl and the butyl on the imidazolium ring was strengthening, suggesting that the water molecule interacted with the C2, 4, the 5-H first, and then that would occur with the proton of methyl and the butyl on the imidazolium ring as the concentration of water increased. The structure of ILs would get looser when the water was added to the solution, as a result of the water impairing the interaction between the anion and C–H of imidazolium. The cation and anion would not be disassembled completely even if there existed little water or polar solvent (for example DMSO), and we could study the O–H...F interaction between the anion and cation directly by a different nucleus ¹H{¹⁹F}NOE effect, as well as the O–H...F interaction between the water and anion [42]. Santini and Pádua et al. studied the interaction between [BDMIM][Tf₂N], [BMIM][Tf₂N], and toluene in different concentrations by 1DNMR and ROESY. It was found that the hydrogen bond forming between C2–H of [BMIM][Tf₂N] and toluene, causing the bonding energy between toluene and [BMIM][Tf₂N], would be bigger than that in [BDMIM][Tf₂N] solution [43].

The ionic pairs and the micelles could be investigated by the two-dimensional NMR. Dupont et al. reported the chemical shift of hydrogen atoms that moved in high field migration in the [BMIM][BPh₄] and chloroform-d solution. In addition, ¹H NOESY spectra presented the cross peak, suggesting that the [BMIM][BPh₄] turns to ([BMIM][BPh₄])_n in the form of ionic aggregation by weak C–H...π interaction in chloroform-d, but an isolated ion pair was found in [D6]DMSO [32].

2.2 Electron Spin Resonance Spectroscopy (ESR)

Electron spin resonance is the study of molecules and ions containing unpaired electrons by observing the magnetic fields at which they come into resonance with monochromatic radiation, usually using TEMPO, TEMPOL, and CAT-1 as the free probe molecule. ESR spectroscopy is less widely applicable than NMR because it cannot be detected in normal, spin-paired molecules and the sample must possess

unpaired electron spins. It is used to study radicals formed during chemical reactions or by radiation, radicals that act as probes of biological structure, many d-metal complexes, and molecules in triplet states. Herrmann et al. reported that the above three kinds of free radical probe molecules had different correlation times in the ESR spectra of ILs, indicating that the IL may have a fluctuating character, with the borderline case of a microphase separation (in the ionic liquid, to have one kind of specific change structure is a phenomenon which will make it separable). This suspicion of specific structure change in ILs was also supported by the magnetic lag phenomenon of the probe effected by the different lengths of alkyl chain and anions [44]. It was found that specific interactions in the ionic liquids, as well as between the spin-probe molecules and the constituents of the ionic liquids, are reflected in the spectra of the spin probes, depending on their molecular structure.

ESR was also used to study the interaction between the ILs and SO_2 . The rotational active energy of the TEMPO probe decreased greatly in the SO_2 saturated ionic liquid, as a result of the SO_2 shielding the electrostatic force between the anion and cation [45].

3 Microstructure of ILs Investigated by Electronic Transitions–Ultraviolet and Visible Spectroscopy

Ultraviolet/visible spectroscopy can be used to investigate the properties and structures of the ILs, where organic anions and cations exist, such as the imidazolium, which have an absorptive band in the UV/visible spectrum. Gilbert et al. measured the range of the acidity of the non-chlorine aluminic acid ionic liquid by UV/visible spectroscopy, using 4-nitrophenylamine as the indicator. It was reported that in non-chloroaluminate ionic liquids based on the $[\text{Tf}_2\text{N}]^-$ and $[\text{BF}_4]^-$ anions, to which an acid has been added, it is possible to reach acidity levels ranging from -3.35 to -7.00 , depending on the ionic liquid and the acid [46].

Acknowledgments This work was supported by the National Natural Science Foundation of China (20990221).

References

1. Malacara-Hernandez D (2002) Color vision and colorimetry: theory and applications. SPIE Press, Bellingham
2. Katsyuba SA, Dyson PJ, Vandyukova EE et al (2004) Molecular structure, vibrational spectra, and hydrogen bonding of the ionic liquid 1-ethyl-3-methyl-1H-imidazolium tetrafluoroborate. *Helv Chim Acta* 87:2556
3. Talaty ER, Raja S, Storhaug VJ et al (2004) Raman and infrared spectra and a initio calculations of C2-4MIM imidazolium hexafluorophosphate ionic liquids. *J Phys Chem B* 108:13177

4. Heimer NE, Del Sesto RE, Meng ZZ et al (2006) Vibrational spectra of imidazolium tetrafluoroborate ionic liquids. *J Mol Liq* 124:84
5. Cammarata L, Kazarian SG, Salter PA et al (2001) Molecular states of water in room temperature ionic liquids. *Phys Chem Chem Phys* 3:5192
6. Danten Y, Cabaco MI, Besnard M (2009) Interaction of water highly diluted in 1-alkyl-3-methyl imidazolium ionic liquids with the PF₆⁻ and BF₄⁻ anions. *J Phys Chem A* 113:2873
7. Takamuku T, Kyoshoin Y, Shimomura T et al (2009) Effect of water on structure of hydrophilic imidazolium-based ionic liquid. *J Phys Chem B* 113:10817
8. Koddermann T, Wertz C, Heintz A et al (2006) The association of water in ionic liquids: a reliable measure of polarity. *Angew Chem Int Edit* 45:3697
9. Katsyuba SA, Zvereva EE, Vidis A et al (2007) Application of density functional theory and vibrational spectroscopy toward the rational design of ionic liquids. *J Phys Chem A* 111:352
10. Jeon Y, Sung J, Kim D et al (2008) Structural change of 1-butyl-3-methylimidazolium tetrafluoroborate plus water mixtures studied by infrared vibrational spectroscopy. *J Phys Chem B* 112:923
11. Umebayashi Y, Jiang JC, Lin KH et al (2009) Solvation and microscopic properties of ionic liquid/acetonitrile mixtures probed by high-pressure infrared spectroscopy. *J Chem Phys* 131:234502
12. Chang HC, Jiang JC, Chang CY et al (2008) Structural organization in aqueous solutions of 1-butyl-3-methylimidazolium halides: a high-pressure infrared spectroscopic study on ionic liquids. *J Phys Chem B* 112:4351
13. Chang HC, Jiang JC, Tsai WC et al (2006) Hydrogen bond stabilization in 1,3-dimethylimidazolium methyl sulfate and 1-butyl-3-methylimidazolium hexafluorophosphate probed by high pressure: the role of charge-enhanced C-H center dot center dot center dot O interactions in the room-temperature ionic liquid. *J Phys Chem B* 110:3302
14. Umebayashi Y, Jiang JC, Shan YL et al (2009) Structural change of ionic association in ionic liquid/water mixtures: a high-pressure infrared spectroscopic study. *J Chem Phys* 130:12450
15. Yokozeki A, Kasprzak DJ, Shiflett MB (2007) Thermal effect on C-H stretching vibrations of the imidazolium ring in ionic liquids. *Phys Chem Chem Phys* 9:5018
16. Koddermann T, Wertz C, Heintz A et al (2006) Ion-pair formation in the ionic liquid 1-ethyl-3-methylimidazolium bis(triflyl)imide as a function of temperature and concentration. *Chemphyschem* 7:1944
17. Zhang LQ, Wang Y, Xu Z et al (2009) Comparison of the blue-shifted C-D stretching vibrations for DMSO-d(6) in imidazolium-based room temperature ionic liquids and in water. *J Phys Chem B* 113:5978
18. Wu B, Zhang YM, Wang HP (2009) Insight into the intermolecular interactions in [Bmim]BF₄/[Amim]Cl-ethanol-water mixtures by near-infrared spectroscopy. *J Phys Chem B* 113:12332
19. Fumino K, Wulf A, Ludwig R (2008) The cation-anion interaction in ionic liquids probed by far-infrared spectroscopy. *Angew Chem Int Edit* 47:3830
20. Fumino K, Wulf A, Ludwig R (2009) Hydrogen bonding in protic ionic liquids: reminiscent of water. *Angew Chem Int Edit* 48:3184
21. Koddermann T, Fumino K, Ludwig R et al (2009) What far-infrared spectra can contribute to the development of force fields for ionic liquids used in molecular dynamics simulations. *Chemphyschem* 10:1181
22. Katayanagi H, Hayashi S, Hamaguchi HO et al (2004) Structure of an ionic liquid, 1-n-butyl-3-methylimidazolium iodide, studied by wide-angle X-ray scattering and Raman spectroscopy. *Chem Phys Lett* 392:460
23. Holomb R, Martinelli A, Albinsson I et al (2008) Ionic liquid structure: the conformational isomerism in 1-butyl-3-methyl-imidazolium tetrafluoroborate ([bmim][BF₄]). *J Raman Spectr* 39:793
24. Berg RW, Deetlefs M, Seddon KR et al (2005) Raman and ab initio studies of simple and binary 1-alkyl-3-methylimidazolium ionic liquids. *J Phys Chem B* 109:19018

25. Fujii K, Fujimori T, Takamuku T et al (2006) Conformational equilibrium of bis(trifluoromethanesulfonyl) imide anion of a room-temperature ionic liquid: Raman spectroscopic study and DFT calculations. *J Phys Chem B* 110:8179
26. Jeon Y, Sung J, Seo C et al (2008) Structures of ionic liquids with different anions studied by infrared vibration spectroscopy. *J Phys Chem B* 112:4735
27. Saha S, Hamaguchi HO (2006) Effect of water on the molecular structure and arrangement of nitrile-functionalized ionic liquids. *J Phys Chem B* 110:2777
28. Fazio B, Triolo A, Di Marco G (2008) Local organization of water and its effect on the structural heterogeneities in room-temperature ionic liquid/H₂O mixtures. *J Raman Spectr* 39:233
29. Sitze MS, Schreiter ER, Patterson EV et al (2001) Ionic liquids based on FeCl₃ and FeCl₂. Raman scattering and ab initio calculations. *Inorg Chem* 40:2298
30. Alves MB, Santos VO, Soares VCD et al (2008) Raman spectroscopy of ionic liquids derived from 1-n-butyl-3-methylimidazolium chloride and niobium chloride or zinc chloride mixtures. *J Raman Spectr* 39:1388
31. Castriota M, Caruso T, Agostino RG et al (2005) Raman investigation of the ionic liquid N-methyl-N-propylpyrrolidinium bis(trifluoromethanesulfonyl)imide and its mixture with LiN(SO₂CF₃)₂. *J Phys Chem A* 109:92
32. Dupont J, Suarez PAZ, De Souza RF et al (2000) C-H- π interactions in 1-n-butyl-3-methylimidazolium tetraphenylborate molten salt: solid and solution structures. *Chem Eur J* 6:2377
33. Katsyuba SA, Griaznova TP, Vidis A et al (2009) Structural studies of the ionic liquid 1-ethyl-3-methylimidazolium tetrafluoroborate in dichloromethane using a combined DFT-NMR spectroscopic approach. *J Phys Chem B* 113:5046
34. Zhu X, Wang Y, Li HR (2009) The structural organization in aqueous solutions of ionic liquids. *Aiche J* 55:198
35. Remsing RC, Wildin JL, Rapp AL et al (2007) Hydrogen bonds in ionic liquids revisited: 35/37Cl NMR studies of deuterium isotope effects in 1-n-butyl-3-methylimidazolium chloride. *J Phys Chem B* 111:11619
36. Remsing RC, Liu ZW, Sergeyev I et al (2008) Solvation and aggregation of N,N'-Dialkylimidazolium ionic liquids: a multinuclear NMR spectroscopy and molecular dynamics simulation study. *J Phys Chem B* 112:7363
37. Huang JF, Chen PY, Sun IW et al (2001) NMR evidence of hydrogen bonding in 1-ethyl-3-methylimidazolium-tetrafluoroborate room temperature ionic liquid. *Inorg Chim Acta* 320:7
38. Judeinstein P, Iojoiu C, Sanchez JY et al (2008) Proton conducting ionic liquid organization as probed by NMR: self-diffusion coefficients and heteronuclear correlations. *J Phys Chem B* 112:3680
39. Rollet AL, Porion P, Vaultier M et al (2007) Anomalous diffusion of water in [BMIM][TFSI] room-temperature ionic liquid. *J Phys Chem B* 111:11888
40. Menjoge A, Dixon J, Brennecke JF et al (2009) Influence of water on diffusion in imidazolium-based ionic liquids: a pulsed field gradient NMR study. *J Phys Chem B* 113:6353
41. Mele A, Romano G, Giannone M et al (2006) The local structure of ionic liquids: cation-cation NOE interactions and internuclear distances in neat [BMIM][BF₄] and [BDMIM]-[BF₄]. *Angew Chem Int Edit* 45:1123
42. Mele A, Tran CD, Lacerda SHD (2003) The structure of a room-temperature ionic liquid with and without trace amounts of water: the role of C-H center dot center dot center dot O and C-H center dot center dot center dot F interactions in 1-n-butyl-3-methylimidazolium tetrafluoroborate. *Angew Chem Int Edit* 42:4364
43. Gutel T, Santini CC, Padua AAH et al (2009) Interaction between the π -system of toluene and the imidazolium ring of ionic liquids: a combined NMR and molecular simulation study. *J Phys Chem B* 113:170
44. Stoesser R, Herrmann W, Zehl A et al (2006) ESR spin probes in ionic liquids. *Chemphyschem* 7:1106

45. Barrosse-Antlle LE, Hardacre C, Compton RG (2009) SO₂ saturation of the room temperature ionic liquid [C₂mim][NTf₂] much reduces the activation energy for diffusion. *J Phys Chem B* 113:1007
46. Thornazeau C, Olivier-Bourbigou H, Magna L (2003) Determination of an acidic scale in room temperature ionic liquids. *J Am Chem Soc* 125:5264

Index

- A**
Activity coefficients, infinite dilution, 123
Agarose, 80, 88
 dissolution, 99
Aggregates, formation, 44
 microscopic structure, 62
Aggregation, anionic type, 56
 application, 68
 cationic structure, 52
 microstructure, 39
 numbers, 45
 organic additives, 59
 salts, 57
 self-, 61
 in solution, 39
 surfactant, 61
 thermodynamics, 48
Alcohols, 121
Alkylimidazolium, 40
1-Alkyl-3-methylimidazolium bromide, 44
Alkylpyridinium, 40
Ammonium nitrate IL (ANILs), 27
Anions, 56
 structures, 158
- B**
Binding energies, 22
Biodegradation, 68
Biopolymers, 79
 dissolution, 83
Bis(trifluoromethanesulfonyl)amide, 40
Bombyx mori, 96
Bovine serum albumin (BSA), 71
1-Butyl-3-methylimidazolium dicyanamide, 70
1-Butyl-3-methylimidazolium halides, 7, 80
1-Butyl-3-methylimidazolium octylsulfate, 44
1-Butyl-3-methylimidazolium
 tetrafluoroborate, 44, 186
- C**
Carbon dioxide, absorption, 31
 solubility/dissolution, 116
Catalysts, 31
Cation structures, 157
 head/tail groups, 147
Cellulose, dissolution, 29, 83
Chitin, 80
 dissolution, 94
Choline chloride, 118
Color fastness, 98
Conductivity, 4, 159
Critical aggregation concentration (CAC), 44
- D**
Daidzein, 29
Deacetylation (DA), 95
Density, 107, 109, 156
Dextrin, 80
 dissolution, 99
Dialkylimidazolium haloaluminates, 2, 7
Diels–Alder cycloaddition, 31, 144
Diesel, 29
Diethylene glycol, 60
Dimethylsulfoxide, 60
Disposal, 68
Dissolution, 79
1-Dodecyl-3-methylpyridinium bromide, 55

E

- Electromagnetic spectrum, 176
- Electron spin resonance spectroscopy (ESR), 175, 189
- Enthalpy of vaporization, 5, 107, 124
- Ethylene glycol, 60
- 1-Ethyl-3-methylimidazolium halides, 7

F

- Ferrocenylmethyl group, 155
- Fibroin, 80, 96
- Fluoro-anion-based ILs, 10
- Formamide, 60

G

- Gas absorption, 31
- Gasoline, 29
- Genistein, 29
- Glass transition, 153
- Glycitein, 29

H

- Haloaluminate salts, 2
- Heat capacity, 107, 125
- Hemicellulose, 80
 - dissolution, 93
- Henry's constants, 116
- 1-Hexadecyl-3-butylimidazolium bromide, 60
- Hexafluorophosphate, 2, 40
- Hydrogen bonding, 1, 25, 99, 141, 144

I

- Imidazonium hexafluorophosphat, 11
- Infrared spectroscopy, 175, 176
- Interactions, 141
- Ion cluster, 14
- Ion-ion interactions, 142
- Ion pairs, 14
 - binding energy, 22
- Ionic liquids, 1, 39, 79, 107, 141, 175
- Isothermal titration calorimetry (ITC), 44

K

- Keratin, 80, 98
- Kraft lignin (Indulin AT), 92

L

- Lignin, 80
 - dissolution, 91
- Lignocellulosic biomass, 80
- Liquid-liquid equilibria (LLE), 120
- Local H-bonded network, 27

M

- Melting points, 3, 22, 147
- Membrane separations, 39, 68
- Methane, 40
- Methylation, 6, 143, 147, 155, 157, 160, 183
- N*-Methyl-*N*-propylpyrrolidinium bis(trifluoromethanesulfonyl)imide, 186
- 1-Methyl-3-octylimidazoliumchloride, 44
- Micellar liquid chromatography (MLC), 59
- Micelle collapse, 68
- Microstructure, 176
- Molar conductivity, 23
- Molar volume, 155
- Molten salts, 60

N

- Nanostructures, 141, 146
- Nile Red, 70
- Nitrate, 40
- Nitrides, 29
- NMR, 44, 62, 175, 187
- NOESY, 189
- Noncovalent interactions, 22
- Nuclear Overhauser effect (NOE), 189

P

- Pectin, 80
 - dissolution, 99
- PEG200, 119
- Phase behavior, 116
- Phosphonium-based ILs, 109
- Polyethylene glycol (PEG), 119
- PVT behavior, 107
- Pyridinium halides, 2

R

- Raman spectroscopy, 175, 183
- Recycling, 68
- Room temperature ionic liquids (RTILs), 2

S

Saccharides, 71
SDS, 61
Self-aggregation, 61
Silk, 80
 dissolution, 96
Small angle neutron scattering (SANS), 4, 62
Soybean isoflavone aglycone homologues, 29
Starch, 80
 dissolution, 99
Stauff-Klebens equation, 53
Sulfides, 29
Sulfonate (mesylate), 40
Sulfur dioxide, absorption, 31
Surfactants, 61
Symmetry-adapted perturbation theory (SAPT), 22

T

Tetraalkylammonium, 40
Tetraalkylphosphonium, 40
Tetrafluoroborate, 2, 40
Thermal properties, 141
 stability, 154
Tocopherol, 29
Toxicity, 40, 68, 83, 94, 100

Transport property, 141
Triethylene glycol, 60
Trifluoromethane sulfonate (triflate), 40

U

Ultraviolet (UV), 175
Ultraviolet/visible (UV/VIS) spectroscopy, 190
Urea, 118

V

Vaporization, enthalpy, 5, 107, 124
Vapor–liquid equilibria (VLE), 116
Viscosity, 3, 157
Volatile organic compounds (VOCs), 40
Volume property, 141

W

Wool, dissolution, 97
 keratin, 80

Z

Zeolitic materials, 146